




5-2016

Mining Uranium from Seawater: A Coordination Chemistry Approach

Nada Mehio

University of Tennessee - Knoxville, nmehio@vols.utk.edu

Follow this and additional works at: https://trace.tennessee.edu/utk_graddiss

 Part of the [Inorganic Chemistry Commons](#), and the [Physical Chemistry Commons](#)

Recommended Citation

Mehio, Nada, "Mining Uranium from Seawater: A Coordination Chemistry Approach. " PhD diss., University of Tennessee, 2016.
https://trace.tennessee.edu/utk_graddiss/3726

This Dissertation is brought to you for free and open access by the Graduate School at TRACE: Tennessee Research and Creative Exchange. It has been accepted for inclusion in Doctoral Dissertations by an authorized administrator of TRACE: Tennessee Research and Creative Exchange. For more information, please contact trace@utk.edu.

To the Graduate Council:

I am submitting herewith a dissertation written by Nada Mehio entitled "Mining Uranium from Seawater: A Coordination Chemistry Approach." I have examined the final electronic copy of this dissertation for form and content and recommend that it be accepted in partial fulfillment of the requirements for the degree of Doctor of Philosophy, with a major in Chemistry.

Sheng Dai, Major Professor

We have read this dissertation and recommend its acceptance:

Brian J. Edwards, Mark D. Dadmun, David M. Jenkins

Accepted for the Council:

Carolyn R. Hodges

Vice Provost and Dean of the Graduate School

(Original signatures are on file with official student records.)

**Mining Uranium from Seawater:
A Coordination Chemistry Approach**

A Dissertation Presented for
Doctor of Philosophy
Degree
The University of Tennessee, Knoxville

Nada Mehio
May 2016

Copyright © 2016 by Nada Mehio
All rights reserved.

DEDICATION

This dedication is dedicated to my mother, Rola, my father, Mohamad, and my brother, Omar,
for their continual and dedicated support during the course of my studies.

ACKNOWLEDGMENTS

I'd like to express my deepest gratitude to Prof. Sheng Dai for all his support and guidance during my tenure in graduate school. I thank him for instilling me with the value of rigorous scientific research and analysis and for giving me the opportunity to work on a variety of challenging and interesting projects. I would like to thank Prof. Mark Dadmun, Prof. Brian Edwards, and Prof. David Jenkins for serving on my committee; I have benefited tremendously from their academic guidance and support. I would also like to thank Dr. Vyacheslav S. Bryantsev, Prof. De-en Jiang, and Prof. Robert D. Hancock for their mentorship and outstanding scientific guidance throughout the entirety of my graduate studies. In addition, I would like to thank all the past and current members of Prof. Dai's research group. In particular, I would like to thank Drs. Suree Brown, Chi-Linh Do-Thanh, Sinisa Vukovic, Alexander S. Ivanov, J. Casey Johnson, Chenxi Zhang, and Richard T. Mayes for working with me on the Uranium project. I have thoroughly enjoyed working with all of them and I have learned a lot about chemistry and scientific research from all of them.

I would like to express my appreciation to the US Department of Energy, Office of Nuclear Energy, for providing funding for my work under contract DE-AC05-00OR22725 and to the National Energy Research Scientific Computing Center, a DOE Office of Science User Facility supported by the Office of Science of the U.S. Department of Energy under contract DE-AC02-05CH11231, for providing me with the computational resources I needed to complete my research. Finally, I would like to thank the Chemistry Department for supporting me with teaching assistantships and for providing access to a number of instruments and resources that were used to carry out this research.

ABSTRACT

Poly(acrylamidoxime) fibers are the current state-of-the-art adsorbent for mining uranium from seawater. However, the amidoxime group is not perfectly selective towards the uranyl cation, in particular, competition with transition metal cations remains a major challenge. In order for subsequent generations of chelating polymer adsorbents to be improved, the coordination chemistry of amidoxime-uranyl and -transition metal cation complexes needs to be better understood. While the coordination mode of amidoxime-uranyl complexes has been established in the literature, a number of amidoxime-transition metal cation complex binding motifs can be observed on the Cambridge Structural Database. Likewise, the formation constants, or log K values, of a number of essential amidoxime-uranyl and -transition metal cation complexes remain largely unresolved due to the wide range of conflicting acid dissociation constants, or pK_a [pK_a] values, that have been reported for representative acyclic amidoxime ligands in the literature. Therefore, in **Chapter 2** we use spectroscopic titrations to resolve the pK_a values of acetamidoxime and benzamidoxime. Subsequently, we use those pK_a values to develop computational protocols for predicting the pK_a values of aqueous oxoacid ligands. In **Chapters 3** and **4**, we computationally investigate the binding motif of formamidoximate-dioxovanadium(V) and –oxovanadium(IV) complexes, major competing ions in seawater by utilizing density functional theory and wave-function methods in conjunction with continuum solvation calculations. Our investigations of these formamidoximate complexes universally identified the most stable binding motif to be a tautomericallly rearranged imino hydroxylamine chelate formed via coordination of the imino nitrogen and hydroxylamine oxygen. In **Chapter 5**, we build on the design principles acquired in **Chapters 2-4** to design a ligand, salicylaldoxime that is more selective towards uranyl than competing transition metal cations. Finally, in **Chapter 6** we potentiometrically determine the proton affinity distribution of

the classical poly(acrylamidoxime) fiber between pH 2 and pH 10 via the Stable Numerical Solution of the Adsorption Integral Equation Using Splines (SAIUS) algorithm. This work lays the foundation for resolving the metal cation affinity distribution of the poly(acrylamidoxime) fibers, which can aid in improving the uranium selectivity of subsequent generations of chelating polymers.

TABLE OF CONTENTS

Chapter 1 : Introduction	1
References	10
Chapter 2 : Acidity of the Amidoxime Functional Group in Aqueous Solution: A Combined Experimental and Computational Study	16
Abstract	17
2.1. Introduction	18
2.2. Experimental Methods	20
2.3. Computational Methods	22
2.4. Results and Discussion.....	25
2.5. Conclusion.....	38
References	40
Chapter 3 : Theoretical Study of the Coordination Behavior of Formate and Formamidoximate with Dioxovanadium (V) Cation: Implications for Selectivity towards Uranyl.....	48
Abstract	49
3.1 Introduction	50
3.2. Methods.....	53
3.3. Results and Discussion.....	55
3.3.1. VO_2^+ Cation in the Gas Phase	56
3.3.2. Hydrolyzed VO_2^+ Complexes.....	59

3.3.3. Hydrated VO_2^+ Complexes.....	61
3.3.4. Formate- VO_2^+ Complexes	62
3.3.5. Formamidoximate- VO_2^+ Complexes.....	67
3.3.6. Implications for Ligand Design	70
3.4. Conclusion.....	77
References	80
Chapter 4 : Theoretical Study of Oxovanadium(IV) Complexation with Formamidoximate: Implications for the Design of Uranyl-Selective Adsorbents	
Abstract	89
4.1. Introduction	90
4.2. Methods.....	92
4.3. Results and Discussion.....	95
4.3.1. VO^{2+} Cation in the Gas Phase	96
4.3.2. Hydrated VO^{2+} Complexes.....	97
4.3.3. Formamidoximate- VO^{2+} Complexes.....	101
4.3.4. Implications for Ligand Design	108
4.4 Conclusion.....	111
References	115

Chapter 5 : Quantifying the Binding Strength of Salicylaldoxime-Uranyl Complexes Relative to Competing Salicylaldoxime-Transition Metal Ion Complexes in Aqueous Solution: A Combined Experimental and Computational Study	123
Abstract	124
5.1 Introduction	125
5.2 Experimental Methods	128
5.2.1 Materials and Methods	128
5.2.2 pH Measurements	128
5.2.3 UV/Vis Titrations	129
5.3 Computational Methods	130
5.3.1 Electronic Structure Calculations	130
5.3.2. Calculation of the Complexation Free Energies and Stability Constants.....	132
5.3.3 Natural Bond Orbital (NBO) Analysis	133
5.4 Results and Discussion.....	134
5.4.1 Acidity of Salicylaldoxime.....	134
5.4.2 Comparison of the Acid Dissociation Constants of Salicylaldoxime to Salicylic Acid and Representative Amidoxime Ligands.....	135
5.4.3 Formation of UO_2^{2+} -Salicylaldoxime Complexes	136
5.4.4 Structures and Stabilities of UO_2^{2+} -Salicylaldoxime Complexes from Theoretical Calculations	138
5.4.5 Chemical Bonding Analysis of the UO_2^{2+} -Salicylaldoxime Complex.....	148

5.4.6 Comparison of the Formation Constants of Salicylaldoxime- UO_2^{2+} , Salicylic Acid- UO_2^{2+} , and Representative Amidoxime- UO_2^{2+} Complexes	150
5.4.7 Comparison of the UO_2^{2+} Selectivity of Salicylaldoxime, Salicylic Acid, and Representative Amidoxime Ligands	152
5.5 Conclusion.....	156
References	158
Chapter 6 : Acidity of the Poly(acrylamidoxime) Adsorbent in Aqueous Solution: Determination of the Proton Affinity Distribution via Potentiometric Titrations	165
Abstract	166
6.1. Introduction	167
6.2. Methods.....	169
6.2.1. Synthesis	169
6.2.2. Materials and Characterization Methods	170
6.2.3. Potentiometric Titrations	170
6.2.4. SAIUS Algorithm	171
6.3. Results and Discussion.....	172
6.4. Conclusion.....	179
References	181
Chapter 7 : Conclusion.....	188
References	194

Appendix.....	198
Appendix A: Supporting Information for Acidity of the Amidoxime Functional Group in Aqueous Solution: A Combined Experimental and Computational Study	199
Appendix B: Electronic Supplementary Information for Theoretical Study of the Coordination Behavior of Formate and Formamidoximate with Dioxovanadium (V) Cation: Implications for Selectivity towards Uranyl	251
Appendix C: Supporting Information for Theoretical Study of Oxovanadium(IV) Complexation with Formamidoximate: Implications for the Design of Uranyl-Selective Adsorbents.....	298
Appendix D: Electronic Supplementary Information for Quantifying the Binding Strength of Salicylaldoxime-Uranyl Complexes Relative to Competing Salicylaldoxime-Transition Metal Ion Complexes in Aqueous Solution: A Combined Experimental and Computational Study	326
Vita.....	345

LIST OF TABLES

Table 2.1. Acetamidoxime pK_a values at 25 °C. The pK_{a1} values was obtained at 0.0 M ionic strength and the pK_{a2} value was obtained at 0.3 M ionic strength.....	29
Table 2.2. Benzamidoxime pK_a values at 25 °C. The pK_{a1} value was obtained at 0.0 M ionic strength and the pK_{a2} was obtained at 0.3 M ionic strength.	30
Table 2.3. The computed and experimental gas phase acidities (deprotonation energies) of 16 oxoacids (kcal/mol). ^a	33
Table 2.4. Comparison of the accuracy of the pK_a calculations in water for the training set of 16 oxoacids using a combination of five gas phase and four implicit solvation methods. The mean absolute error and the root mean square deviation (in parentheses) of the pK_a values obtained by the least square fitting of each method are listed below. ^a	34
Table 2.5. Comparison of the free energies of solvation of five conjugate base species to literature values derived applying the cluster pair approximation.....	34
Table 2.6. The computed, predicted, and experimental aqueous pK_a values of 16 oxoacids. ^a	36
Table 3.1. Geometrical parameters of VO_2^+ in the gas phase. ^a	57
Table 3.2. Relative gas phase electronic energies of five- and six-coordinate $VO_2(H_2O)_4^+$ clusters in kcal/mol. ^a	63
Table 3.3. Relative gas phase electronic energies of five- and six-coordinate $VO_2(HCOO)(H_2O)$ in kcal/mol. ^a	66
Table 3.4. Relative gas phase electronic energies of $VO_2(HCOO)(H_2O)_2$ complexes in kcal/mol. ^a	
All energies are given relative to the five-coordinate complex 5 in Figure 7.....	67

Table 3.5. Relative gas phase electronic energies of four- and five-coordinate $\text{VO}_2(\text{HAO})(\text{H}_2\text{O})$ complexes in kcal/mol. ^a All energies are given relative to five-coordinate complex 9 in Figure 8.	73
Table 3.6. Relative gas phase electronic energies of five-coordinate $\text{VO}_2(\text{HAO})(\text{H}_2\text{O})_2$ complexes in kcal/mol. ^a All energies are given relative to five-coordinate complex 16 in Figure 3.9.	74
Table 3.7. Relative gas phase electronic energies of five- and six-coordinate $\text{VO}_2(\text{HAO})(\text{H}_2\text{O})_3$ complexes in kcal/mol. ^a All energies are given relative to five-coordinate complex 21 in Figure 10.	75
Table 4.1. Relative electronic energies (gas phase) of five- and six-coordinate $\text{VO}(\text{H}_2\text{O})_5^{2+}$ clusters in kcal/mol. ^{a,b}	99
Table 4.2. Comparison of experimental and calculated geometrical parameters and $\text{V}\equiv\text{O}$ stretching frequencies of the hydrated VO^{2+} cation ^a	99
Table 4.3. Significant donor-acceptor natural bond orbital interactions and their second-order stabilization energies $E^{(2)}$ (kcal/mol). The starred and unstarred labels correspond to Lewis (donor) and non-Lewis (acceptor) NBOs, respectively. Ligands contributing to the particular interaction are shown in parentheses. LP denotes an occupied lone pair; RY^* denotes a Rydberg orbital; CR denotes a one-center core pair.	105
Table 4.4. Relative electronic energies (gas phase) of five-coordinate $\text{VO}(\text{AO})(\text{H}_2\text{O})_2^+$ complexes in kcal/mol. ^{a,b}	106
Table 4.5. Relative electronic energies (gas phase) of five- and six-coordinate $\text{VO}(\text{AO})(\text{H}_2\text{O})_3^+$ complexes in kcal/mol. ^{a,b}	107

Table 5.1. Salicylaldehyde dissociation and UO_2^{2+} formation constants at 25 °C by ionic strength.....	142
Table 5.2. Calculated free energy changes, ΔG_{aq} (kcal/mol), for reactions (1 – 4) and $\log \beta_1$ ($\log \beta_2$) values for 1:1 (2:1) uranyl complexes with salicylaldehyde ligands.....	148
Table 5.3. Significant donor-acceptor natural bond orbital interactions and their second-order stabilization energies $E^{(2)}$ (kcal/mol). The starred and unstarred labels correspond to Lewis (donor) and non-Lewis (acceptor) NBOs, respectively. Functional groups of ligands contributing to the particular interaction are shown in parentheses. LP denotes an occupied lone pair; CR denotes a one-center core pair; n* denotes vacant UO_2^{2+} orbitals; RY* denotes a Rydberg orbital.	152
Table 6.1. Dissociation constants of acetic acid, ¹³ acetamidoxime, ¹¹ and glutarimidoxime ¹¹ at 25 °C in aqueous solution. Ionic strength corrections were applied with the Davies equation.....	175
Table 6.2. Proton affinities of the carboxylate and amidoxime monomers and their corresponding small molecule pK_a values.	178
Table A. 1. pK_a values obtained by computing the solvation energies with the IEFPCM solvation model. ^{a,b}	201
Table A.2. pK_a values obtained by computing the solvation energies with the CPCM solvation model. ^{a,b}	202
Table A.3. pK_a values obtained by computing the solvation energies with the SMD solvation model. ^{a,b}	203
Table A.4. pK_a values obtained by computing the solvation energies with the COSMO solvation model. ^{a,b}	204

Table A.5. pK_a values obtained by computing the solvation energies with the SVPE2 solvation model. ^{a,b}	205
Table A.6. Relative gas phase electronic energies of five- and six-coordinate $VO_2(HCOO)(H_2O)_3$ in kcal/mol. ^{a,b} All energies are given relative to complex S1 in Figure 9.1.	251
Table A.7. The absolute electronic energies and relative electronic energies of R/R-CCSD(T)/aug-cc-pVDZ//B3LYP/aug-cc-pVDZ (R/R-CCSD(T)//B3LYP) calculations carried out in the restricted formalism in which only valence and valence together with sub-valence 3s and 3p electrons on vanadium are correlated.....	298
Table A.8. The relative Gibbs free energies of 1-15 in aqueous solution computed at the R/R-CCSD(T)//B3LYP level of theory using the IEF-PCM and SMD solvation models in units of kcal/mol. ^a	299
Table A.9. The zero-point energies (ZPE) with thermal corrections and the solvation free energies obtained with the IEF-PCM and SMD solvation models for all 15 VO^{2+} complexes discussed in the manuscript. ^a	302
Table A.10. The complexation free energies for reactions (1) UO_2^{2+} and (2) UO_2^{2+} obtained with the B3LYP//B3LYP//IEF-PCM(UFF), MO6//B3LYP//IEF-PCM(UFF) , and CCSD(T)//B3LYP//IEF-PCM(UFF) levels of theory.....	302
Table A.11. The complexation free energies for reactions (1) VO^{2+} , (2) VO^{2+} , (3) VO^{2+} , and (4) VO^{2+} obtained with the B3LYP//B3LYP//IEF-PCM(UFF), MO6//B3LYP//IEF-PCM(UFF) , and R/R-CCSD(T)//B3LYP//IEF-PCM(UFF) levels of theory.	303
Table A.12. The complexation free energies for reactions (1) VO_2^+ , (2) VO_2^+ , (3) VO_2^+ , and (4) VO_2^+ obtained with the B3LYP//B3LYP//IEF-PCM(UFF), MO6//B3LYP//IEF-PCM(UFF) , and CCSD(T)//B3LYP//IEF-PCM(UFF) levels of theory.....	303

Table A.13. Acid dissociation and formation constants of the ligands and complexes discussed in this manuscript. The ligands ($L^{()}$) tabulated correspond to the ligands illustrated in Figure 5.2. The constants were obtained in aqueous solution at 25 °C and, unless otherwise noted, $I = 0.0$ M ionic strength.....	326
Table A.14. Comparison of experimental, calculated, and predicted stability constant ($\log \beta$) values for UO_2^{2+} -ligand complexes.	328
Table A.15. Full chemical formulas of the CSD crystal structures depicted in Figures 5.1, A.11, and A.12 by CSD reference code.....	330

LIST OF FIGURES

Figure 1.1. Schematic depiction of a small subsection of the poly(acrylamidoxime) fiber and the small ligands that correspond to its acyclic and cyclic amidoxime monomers.	2
Figure 1.2. Representative acyclic amidoxime- UO_2^{2+} and -transition metal cation complexes adapted from the CSD.....	7
Figure 1.3. Representative cyclic amidoxime- UO_2^{2+} and -transition metal cation complexes and analogous unsaturated-transition metal cation complexes adapted from the CSD.....	8
Figure 2.1. The strength of a metal-ligand interaction is conveyed in the form of a complexation constant, $\log K_1$. The amidoxime functional group (HAO) releases a proton to bind to UO_2^{2+} ; therefore, one needs to know the pK_a of HAO to determine the $\log K_1$ value.	19
Figure 2.2. Thermodynamic cycle used to predict pK_a values.	23
Figure 2.3. ^1H -NMR shifts of aqueous acetamidoxime (2×10^{-3} M) versus pH at 25°C and 0.0 M ionic strength. The corresponding spectra can be found in Appendix A, (Figure A.2).....	27
Figure 2.4. (<i>Top</i>) Spectra of benzamidoxime (10^{-4} M) in aqueous solution at 25°C and 0.0 M ionic strength. (<i>Bottom</i>) Variation of absorbance at six different wavelengths of 10^{-4} M benzamidoxime in aqueous solution as a function of pH. The points are experimental values, whereas the solid lines are theoretical curves fitted to the experimental data using Solver. ⁵¹	32
Figure 2.5. A comparison of the computed and experimental pK_a values of 16 oxoacids in water. The computed pK_a values were obtained at the MP2/aug-cc-pVTZ (<i>top</i>) and M06-2X/6-311++G** (<i>bottom</i>) levels of theory with solvent corrections obtained using the SMD solvation models. ZPE and thermal corrections were calculated in the gas phase at the B3LYP/6-311++G** level of theory.....	35

Figure 2.6. The pK_a values in water computed at the MP2/aug-cc-pVTZ and the M06-2X/6-311++G** (in parentheses) level of theory with solvent corrections obtained using the SMD solvation model. ZPE and thermal corrections were obtained at the B3LYP/6-311++G** level of theory.	39
Figure 3.1. Crystal structures of amidoximate- VO_2^+ and carboxylate- VO_2^+ complexes. The DAQSET complex and the DAQSAP complex are representative of the two carboxylate- VO_2^+ binding modes observed in the CSD. The HORWIW complex is the only reported amidoximate- VO_2^+ crystal structure.	51
Figure 3.2. Several occupied molecular orbitals (MOs) illustrating the bonding in the VO_2^+ cation. Dominant atomic contributions to each MO are shown. The MOs were obtained at the B3LYP/aug-cc-pVDZ level of theory with an MO isovalue surface of $0.04 (e/\text{\AA}^3)^{1/2}$	58
Figure 3.3. Structures of hydrated and hydrolyzed $VO_2(H_2O)_3^+$ complexes and relative energies in the gas phase and in aqueous solution (in parentheses) in units of kcal/mol.	59
Figure 3.4. Structures of hydrated and hydrolyzed $VO_2(AO)(H_2O)_3$ complexes and relative energies in the gas phase and in aqueous solution (in parentheses) in units of kcal/mol.	60
Figure 3.5. Structures of $VO_2(H_2O)_4^+$ complexes and relative energies in the gas phase and in aqueous solution (in parentheses) in units of kcal/mol.	61
Figure 3.6. Structures of $VO_2(HCOO)(H_2O)$ complexes and relative energies in the gas phase and in aqueous solution (in parentheses) in units of kcal/mol.	63
Figure 3.7. Structures of $VO_2(HCOO)(H_2O)_2$ complexes and relative energies in the gas phase and in aqueous solution (in parentheses) in units of kcal/mol.	66
Figure 3.8. Structures of $VO_2(AO)(H_2O)$ complexes (AO=formamidoximate) and relative energies in the gas phase and in aqueous solution (in parentheses) in units of kcal/mol.	72

Figure 3.9. Structures of $\text{VO}_2(\text{AO})(\text{H}_2\text{O})_2$ complexes (AO=formamidoximate) and relative energies in the gas phase and in aqueous solution (in parentheses) in units of kcal/mol.	74
Figure 3.10. Structures of $\text{VO}_2(\text{AO})(\text{H}_2\text{O})_3$ complexes (AO=formamidoximate) and relative energies in the gas phase and in aqueous solution (in parentheses) in units of kcal/mol.	74
Figure 3.11. Reaction free-energy profile for tautomerization of formamidoxime calculated in the presence of three solvent (water) molecules (kcal/mol). Implicit solvation corrections are obtained using the IEF-PCM solvation model. DFT-optimized O–H bond lengths in the transition state are shown (Å).	75
Figure 3.12. Reaction free-energy profile for tautomerization of formamidoximate coordinated to VO_2^+ in the presence of five solvent (water) molecules (kcal/mol). Implicit solvation corrections are obtained using the IEF-PCM solvation model. DFT-optimized O–H bond lengths in the transition and intermediate states are shown (Å).	76
Figure 3.13. Crystal structures of amidoximate-transition metal complexes from the CSD. The Type 1 complexes are representative of the tautomericly rearranged binding mode observed in complexes 9, 16, and 21. The Type 2 complexes are representative of the monodentate oxime nitrogen binding mode observed in complexes 10, 17, and 22. The Type 3 complex is representative of the η^2 binding mode observed in complexes 11, 18, and 23. The Type 4 complex is representative of the unrearranged binding motif observed in complexes 12, 19, and 24.	79
Figure 4.1. Crystal structures of carboxylate- VO_2^{2+} complexes. The XUTLON complex, (acetato-O,O')-chloro-bis(4-methylpyridine-N)-oxo-vanadium(IV), and the LOPHIJ complex, aqua-bis(5-cyanopyridine-2-carboxylato-N,O)-oxido-vanadium(IV) dihydrate, are representative of the two carboxylate- VO_2^+ binding modes observed in the CSD.	92

Figure 4.2. Thermodynamic cycle used to calculate ΔG_{aq}	95
Figure 4.3. NBO chemical bonding pattern for the VO^{2+} cation (the isodensity value is 0.15 au). ON stands for occupation numbers.....	96
Figure 4.4. Singly-occupied molecular orbitals (SOMOs) of the representative water and formamidoximate VO^{2+} complexes. Dominant atomic contributions to each SOMO are shown with the VO^{2+} oxygen perpendicular to the plane. The SOMOs were obtained at the B3LYP/aug- cc-pVDZ level of theory.	97
Figure 4.5. Structures and relative Gibbs free energies (kcal/mol) of $\text{VO}(\text{H}_2\text{O})_5^{2+}$ complexes in aqueous solution and in the gas phase (in parentheses). The electronic energies were obtained at the R/R-CCSD(T)//B3LYP level of theory.....	98
Figure 4.6. Structures and relative Gibbs free energies (kcal/mol) of $\text{VO}(\text{AO})(\text{H}_2\text{O})_2^+$ complexes in aqueous solution and in the gas phase (in parentheses). The electronic energies were obtained at the R/R-CCSD(T)//B3LYP level of theory.....	106
Figure 4.7. Structures and relative Gibbs free energies (kcal/mol) of $\text{VO}(\text{AO})(\text{H}_2\text{O})_3^+$ complexes in aqueous solution and in the gas phase (in parentheses). The electronic energies were obtained at the R/R-CCSD(T)//B3LYP level of theory.....	107
Figure 4.8. Strong π -type $\text{LP}_{\text{N}} \rightarrow \text{BD}^*_{\text{CN}}$ interaction with associated second-order stabilization energy shown in parentheses. I and II – resonance structures for the most stable $\text{VO}(\text{AO})(\text{H}_2\text{O})_2^+$ complex.....	108
Figure 4.9. Reaction energy (electronic energy with solution correction) profile for tautomerization of formamidoximate coordinated to VO^{2+} in the presence of four additional solvent (water) molecules (kcal/mol). Implicit solvation corrections are obtained using the IEF-	

PCM solvation model. DFT-optimized O-H bond lengths in the transition and intermediate states are shown (Å)..... 109

Figure 4.10. CSD crystal structures of oximate-VO²⁺ complexes. The DEYMIE (oxo-tris(2-acetylfuranoximato)-vanadium(IV)), DEYMOK (oxo-tris(2-acetylthiopheneoximato)-vanadium(IV) benzene solvate), and WIDRIL (chloro-methanol-oxo-bis(1-(2-thienyl)ethanone oximato)-vanadium(IV)) complexes are representative of the η^2 binding mode observed in complexes 6, 12, and 14. The BEGDOI ((4-(((2-(Dimethylamino)ethyl)imino)methyl)-5-(hydroxymethyl)-2-methylpyridin-3-olato)-(N-(hydroxy)benzenecarboximidato)-oxo-vanadium), NEYVIY((2-Hydroxy-N-(3-((hydroxy)imino)butan-2-ylidene)benzenecarbohydrazonato)(oxo)(quinolin-8-olato)vanadium), and PAVHIE ((Benzhydroxamato)-(N-salicylidene-2-(benzimidazole-2-yl)ethylamine)-oxo-vanadium(IV)) complexes are representative of the monodentate oxygen binding mode observed in complex 10. 114

Figure 5.1. Crystal structures of amidoximate-transition metal complexes from the CSD. The Type1 complexes are representative of complexes in which an amine is directly involved in coordination. The Type 2 complexes are representative of complexes in which an amine is not directly involved in coordination. The full chemical formulas of the crystal structures are provided in Table A.13 of Appendix D by CSD reference code. Color legend: O, red; N, blue; C, grey; H, white; S, yellow; metal ion, purple. 131

Figure 5.2. Ligands discussed in this paper. 132

Figure 5.3. (*Top*) Spectra of salicylaldoxime (5×10^{-5} M) in aqueous solution at 25 °C. The pK_{a1} and pK_{a2} values were obtained at 0.0 M ionic strength. (*Bottom*) Variation of absorbance at six different wavelengths of 5×10^{-5} M salicylaldoxime in aqueous solution as a function of pH. The

points are experimental values, whereas the solid lines are theoretical curves fitted to the experimental data using Solver. 141

Figure 5.4. (*Top*) Spectra of salicylaldoxime (4.8×10^{-5} M) and uranyl (4.8×10^{-5} M) in aqueous solution at 25 °C. The $\log \beta_1$ value was obtained at 0.0 M ionic strength. (*Bottom*) Variation of absorbance at six different wavelengths 4.8×10^{-5} M salicylaldoxime and uranyl in aqueous solution as a function of pH. The points are experimental values, whereas the solid lines are theoretical curves fitted to the experimental data using Solver. 143

Figure 5.5. (*Top*) Spectra of salicylaldoxime (4.8×10^{-5} M) and uranyl (4.8×10^{-6} M) in aqueous solution at 25 °C. The $\log \beta_1$ and $\log \beta_2$ values were obtained at 0.0 M ionic strength. (*Bottom*) Variation of absorbance at five different wavelengths 4.8×10^{-5} M salicylaldoxime and uranyl in aqueous solution as a function of pH. The points are experimental values, whereas the solid lines are theoretical curves fitted to the experimental data using Solver. 144

Figure 5.6. Optimized structures (M06/SSC/6-311++G**) of $[\text{UO}_2(\text{HL}^{(1)})(\text{H}_2\text{O})_3]^+$ complex and their relative Gibbs free energies (kcal/mol) in aqueous solution and in the gas phase (in parentheses). Color legend: O, red; N, blue; C, grey; H, white; U, yellow. 145

Figure 5.7. Optimized structures (M06/SSC/6-311++G**) of $[\text{UO}_2(\text{L}^{(1)})(\text{H}_2\text{O})_2]$ complex and their relative Gibbs free energies (kcal/mol) in aqueous solution and in the gas phase (in parentheses). Color legend: O, red; N, blue; C, grey; H, white; U, yellow. 145

Figure 5.8. The most stable structures of 1:1 and 2:1 uranyl complexes with salicylaldoxime ($\text{HL}^{(1)-}$ and $\text{L}^{(1)2-}$) and obtained at the M06/SSC/6-311++G** level of theory. Uranyl-ligand bond lengths are shown in Å. Color legend: red represents oxygen, blue represents nitrogen, grey represents carbon, white represents hydrogen, and yellow represents uranium. 146

Figure 5.9. Plot of experimental versus calculated stability constants ($\log \beta$) for uranyl complexes with mono- and divalent negative oxygen, imide dioxime, and amidoxime donor ligands. The computed values were obtained at the M06/6-311++G** level of theory with the SMD solvent corrections. The $\log \beta_1$ data for monovalent (blue circles) and divalent (green squares) negative oxygen and imide dioxime donor ligands were taken from ref 41 and 40. The $\log \beta_1$ ($\log \beta_2$) data for 1:1 and 2:1 acet- and benzamidoxime/uranyl complexes (red triangles) were obtained from ref 31. Comparison of experimental, calculated, and predicted $\log \beta$ values is shown in Table A.14 of Appendix D. 147

Figure 5.10. Donor-acceptor interactions with leading contributions to second-order stabilization energies of a) uranyl phenolate $[\text{UO}_2(\text{L}^{\text{IV}})(\text{H}_2\text{O})_4]^+$, b) uranyl benzaldoximate $[\text{UO}_2(\text{L}^{\text{III}})(\text{H}_2\text{O})_3]^+$, and c) uranyl salicylaldoximate $[\text{UO}_2(\text{L}^{\text{I}})(\text{H}_2\text{O})_2]$ complexes. Uranyl-ligand bond lengths are shown in Å. 151

Figure 5.11. The most stable structures of 1:1 and 2:1 Cu^{2+} complexes with salicylaldoxime (HL^{I}) obtained at the M06/SSC/6-311++G** level of theory. Uranyl-ligand bond lengths are shown in Å. Color legend: red represents oxygen, blue represents nitrogen, grey represents carbon, white represents hydrogen, and turquoise represents copper. 155

Figure 6.1. Schematic depiction of a small subsection of the poly(acrylamidoxime) fiber. 168

Figure 6.2. 100-MHz ^{13}C CP/MAS NMR spectra of (a) grafted and (b) amidoximated fibers. (* denotes spinning sideband, spinning speed 8.0 kHz). 173

Figure 6.3. Schematic representing the dissociation of acetic acid,¹³ acetamidoxime,¹¹ and glutarimidoxime¹² in aqueous solution. The following ligands are representative of poly(acrylamidoxime) monomer. 174

Figure 6.4. Titration of 0.049 g of poly(acrylamidoxime) in 100 mL of 0.1 M NaClO ₄ and 0.0100 M HClO ₄ with 0.100 M NaOH at 25 °C.....	176
Figure 6.5. (<i>Left</i>) The normalized proton affinity distribution of poly(acrylamidoxime). (<i>Top Right</i>) Theoretical and experimental adsorption isotherm of poly(acrylamidoxime).....	177
Figure A.1. (<i>Top</i>) Strong acid (0.01 M HClO ₄) versus strong base (0.01 M NaOH) titration used to standardize the pH electrode. The initial solution contained 25 mL of 0.01 M HClO ₄ . (<i>Bottom</i>) Calibration plot used to determine the Nernst slope (-59.08) and the E° correction factor (400.12).....	199
Figure A.2. ¹ H-NMR spectra of aqueous acetamidoxime (2 x 10 ⁻³ M) at 25 °C and 0.0 M ionic strength by pH.....	200
Figure A.3. Structures of VO ₂ (HCOO)(H ₂ O) ₃ complexes and relative energies in the gas phase and in aqueous solution (in parentheses) in units of kcal/mol.	251
Figure A.4. Natural charge distribution in complexes 1, 2, and 3 obtained via natural population analysis (NPA) at the B3LYP/6-31G(d) level of theory.....	300
Figure A.5. Natural charge distribution in complexes 4, 5, 6, and 7 obtained via natural population analysis (NPA) at the B3LYP/6-31G(d) level of theory.....	300
Figure A.6. Natural charge distribution in complexes 8, 10, 11, and 12 obtained via natural population analysis (NPA) at the B3LYP/6-31G(d) level of theory.....	301
Figure A.7. Thermodynamic cycle used to calculate ΔΔG _{aq}	331
Figure A.8. Stepwise dissociation of salicylaldoxime used to fit UV/Vis titration data. Color legend: red represents oxygen, blue represents nitrogen, grey represents carbon, and white represents hydrogen.	331

Figure A.9. Species distribution diagrams of the 1:1 (*top*) and the 10:1 (*bottom*) salicylaldoxime to uranyl titration solutions as a function of pH. Distribution diagrams were generated with the HYSS⁵² software using the uranyl hydrolysis constants in ref. 51 and the uranyl-salicylaldoxime formation constants from this work. 332

Figure A.10. Species distribution diagrams of 0.001 M salicylaldoxime, 1.3×10^{-8} M uranyl, and 0.0025 M carbonate calculated using the HYSS⁵² software. The uranyl carbonate constants were taken from ref. 53 and the uranyl-salicylaldoxime formation constants from this work. 333

Figure A.11. Crystal structures of salicylic acid and glutarimidedioxime complexes. GIQBUE⁵⁹ ($C_{30}H_{32}Cu_2N_4O_{10} \cdot 2(H_3BO_3 \cdot 4(H_2O))$): phenolate- UO_2^{2+} bond = 2.23(1) Å and carboxylate- UO_2^{2+} bond = 2.42(1) Å. BIDVUF⁶⁰ ($C_{14}H_8CuO_6^{2-} \cdot C_8H_{22}CuN_2O_2^{2+} \cdot 4(C_3H_8O)$): phenolate- Cu^{2+} bond = 1.900 Å and carboxylate- Cu^{2+} bond = 1.903 Å. PIMSUB⁶¹ ($C_{14}H_{10}FeN_2O_{12}^{-} \cdot 2(H_3O^+) \cdot Cl^-$): phenolate- Fe^{3+} bond = 1.973 Å and carboxylate- Fe^{3+} bond = 1.944 Å. TEVWAU⁴⁹ ($C_{10}H_{16}N_6O_6U \cdot H_2O$): oximate- UO_2^{2+} bond 1 = 2.430 Å, oximate- UO_2^{2+} bond 2 = 2.535 Å, and piperidine- UO_2^{2+} bond = 2.563 Å. Ref. 15 ($C_{10}H_{16}N_6O_6FeCl_2^+$): oximate- UO_2^{2+} bond 1 = 2.019(7) Å, oximate- UO_2^{2+} bond 1 = 2.027(7) Å, and piperidine- UO_2^{2+} bond = 2.009(8) Å. Color legend: O, red; N, blue; C, grey; H, white; S, yellow; metal ion, purple. 334

Figure A.12. Crystal structures of salicylaldoxime- Fe^{3+} and - Cu^{2+} complexes. BOCCOL⁶⁵ ($C_{56}H_{44}Fe_4N_8O_{16} \cdot C_7H_7NO_2 \cdot C_8H_{10} \cdot C_8H_{10}$): phenolate- Fe^{3+} bond = 1.889(8) Å and oximate- Fe^{3+} bond = 2.14(1) Å. CSALCU⁶⁴ ($C_{14}H_{10}Cl_2CuN_2O_4$): phenolate- Cu^{2+} bond = 1.9082 Å and oximate- Cu^{2+} bond = 1.9579 Å. Color legend: O, red; N, blue; C, grey; H, white; S, yellow; metal ion, purple. 335

Chapter 1 : Introduction

In recent years, there has been great interest in developing low-carbon emission energy sources as an alternative to the widely utilized, high-carbon emission fossil fuels. Nuclear energy is a promising alternative as there is an estimated 4.5 billion tons of uranium,¹ the primary fuel source in nuclear fission, dissolved in seawater, while only 61,600 metric tons are needed annually to meet current global energy demands.² The dominant form of the uranyl ion in seawater is the tricarbonato complex, $\text{UO}_2(\text{CO}_3)_3^{4-}$,^{1, 3-4} which associates with Ca^{2+} , a major cation in seawater, to form a $\text{Ca}_2\text{UO}_2(\text{CO}_3)_3^0$ ternary complex, the dominant uranyl species in seawater.⁵ However, there are a number of challenges associated with developing an adsorbent capable of extracting uranium from seawater that primarily stem from the fact that UO_2^{2+} is present in very low concentrations, 3.3 ppb,⁶ in the presence of competing metal cations.⁴ Therefore, the development of extremely efficient and selective adsorbents is instrumental to making this process industrially viable. Although a number of materials have been investigated over the last six decades, the leading approach for extracting uranium from seawater is the selective adsorption of UO_2^{2+} via a chelating polymer adsorbent.⁶ Chelating polymer adsorbents are widely utilized because they hold four strategic advantages over other classes of materials: (1) selective functional groups capable of high-uranium adsorption capacity and affinity are readily adhered to polymer chains,⁶ (2) there are a number of robust and ductile polymer materials that are capable of adsorbing uranium to be chosen from,⁶ (3) a number of procedures for synthesizing polymeric adsorbents of various shapes at a large scale can be found in the literature,⁶⁻⁸ and (4) the deployment of polymeric adsorbents into seawater is easily facilitated by the close proximity of polymer and seawater densities.⁶⁻⁷ The current state of the art chelating polymer adsorbent is the poly(acrylamidoxime) fiber (**Figure 1.1**),⁹⁻¹⁰ which is a random

copolymer of carboxylate and amidoxime monomers at a 40 to 60 monomer weight ratio, respectively.¹¹⁻¹² The poly(acrylamidoxime) fiber was first identified in a screening of 200 organic polymers as the only adsorbent capable of extracting UO_2^{2+} from pH 8.3 aqueous solution, the approximate pH of seawater.⁹⁻¹⁰ However, the amidoxime functional group is not perfectly selective towards the UO_2^{2+} cation, in particular, competition with transition metal cations, such as Fe^{3+} (3.4 ppb),¹³ Cu^{2+} (0.9 ppb),¹³ VO^{2+} , and VO_2^+ (1.9 ppb),¹³ remains a major challenge.^{6, 14-16}

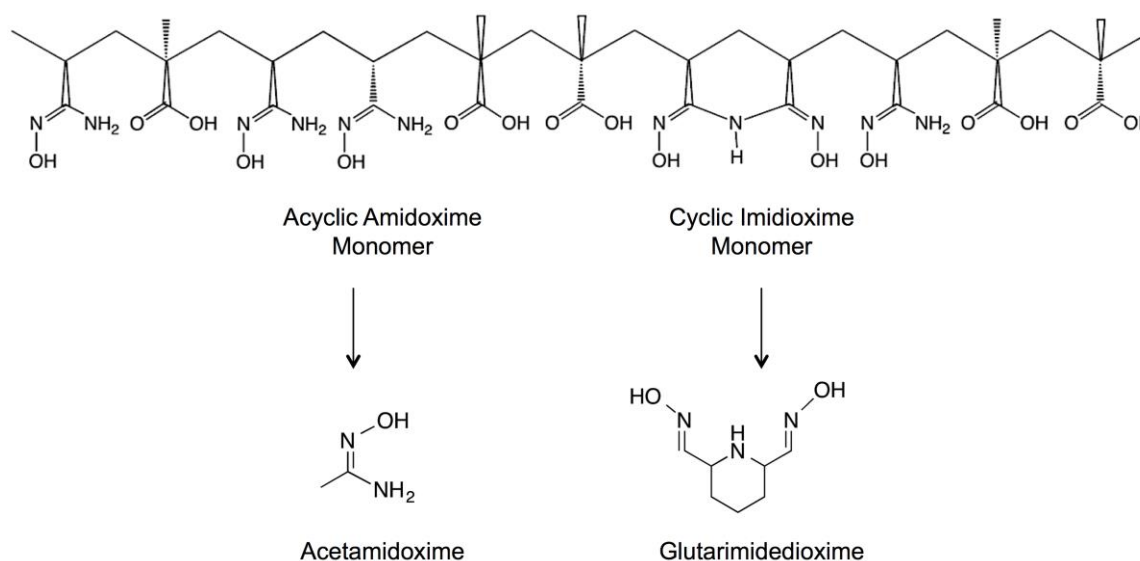


Figure 1.1. Schematic depiction of a small subsection of the poly(acrylamidoxime) fiber and the small ligands that correspond to its acyclic and cyclic amidoxime monomers.

In order for subsequent generations of chelating polymer adsorbents to be improved, the coordination chemistry of amidoxime- UO_2^{2+} and amidoxime-transition metal cation complexes needs to be better understood. As illustrated in **Figure 1.1**, the poly(acrylamidoxime) fiber is composed of two types of amidoxime monomers: an acyclic amidoxime monomer and a cyclic imidioxime monomer. The cyclic imidioxime- and acyclic amidoxime- UO_2^{2+} binding motifs

have been computationally¹⁷⁻¹⁸ and crystallographically¹⁷⁻²⁰ elucidated in the literature. Acyclic amidoximes η^2 coordinate to UO_2^{2+} via the oxime functional group as depicted in the BARYOK,¹⁷ BARYUQ,¹⁷ HORWOC,²⁰ and QEBPOE¹⁹ crystal structures adapted in **Figure 1.2**. Alternatively, as indicated in the TEVWAU¹⁸ crystal structure adapted in **Figure 1.3**, cyclic imidioximes chelate to UO_2^{2+} via a tridentate chelate formed by the oxime oxygen atoms and the amine nitrogen atom. Likewise, crystal structures reported by Rao et al.^{16, 21} (**Figure 1.3**) demonstrate that cyclic imidioximes coordinate to Fe^{3+} , VO_2^+ , and V^{5+} with the UO_2^{2+} binding motif. While no additional cyclic imidioxime-transition metal cation complexes have been reported, there is consensus in the literature that cyclic amidoximes coordinate to transition metals with the UO_2^{2+} binding motif or via a similar binding motif that entails tridentate chelation of the oxime nitrogen atoms and the amine nitrogen atom. This is supported by analogous unsaturated cyclic imidioxime crystal structures that have been reported in the literature; a substantial number of unsaturated cyclic-amidoxime crystal structures with the oxime nitrogen atoms and the amine nitrogen atom chelation motif can be found on the Cambridge Structural Database search (CSD), such as BOBHAB,²² BOBHEF,²² DEYYUC,²³ GEYNOP,²⁴ LUMMOV,²⁵ LUMMUB,²⁵ NIMVEK,²⁶ and SEDJIU²⁷ in **Figure 1.3**. In contrast, as conveyed in **Figure 1.2**, a number acyclic amidoxime-transition metal cation binding motifs can be observed on the CSD: a bidentate chelate formed between an oxime nitrogen atom and a nearby nitrogen functionality atom or an oxime nitrogen (AICOCU10,²⁸ CIMMIW,²⁹ YOHFEI,³⁰ and HORWIW²⁰), monodentate coordination of the oxime oxygen atom (HORWIW²⁰), η^2 coordination of the oxime group (FOWJAC,³¹ RASBOC,³² and RASBIW³²), and a bidentate chelate formed between the amine nitrogen atom and the oxime oxygen atom of the acyclic amidoxime and its imino hydroxylamine tautomer (RASBIW³² and SAFSUN³³, respectively).

Moreover, while Rao and co-workers have reported the binding constants, or log K values, of cyclic imidioxime- UO_2^{2+} complexes and a number of essential cyclic imidioxime-transition metal cation complexes, the UO_2^{2+} and transition metal cation log K values of acyclic amidoxime complexes remain largely unresolved due to the wide range of conflicting acid dissociation constants, or pK_a values, that have been reported for representative acyclic amidoxime ligands in the literature.³⁴⁻³⁸

Thus, in order for the selectivity and capacity of subsequent generations of chelating polymers to be understood, the coordination chemistry of the acyclic amidoxime monomer that occurs on poly(acrylamidoxime) fibers needs to be better understood. Consequentially, a major aim of our group research efforts was to further develop our understanding of the strength of acyclic amidoxime- UO_2^{2+} and -transition metal cation complexes by resolving the pK_a values of representative amidoxime ligands, acetamidoxime and benzamidoxime. As stated previously, the pK_a values of oxoacids, such as cyclic and acyclic amidoxime ligands, are used to determine the log K values of amidoxime-metal complexes, which facilitates the comparison of the strength of amidoxime- UO_2^{2+} relative to competing amidoxime-transition metal cation complexes.³⁹ Moreover, the pK_a and log K values of oxoacids are correlated by linear free energy relationships;⁴⁰ thus, when coupled with binding motif information, methods for predicting the pK_a values of oxoacid ligands, such as amidoximes, can be used to design ligands that further improve the UO_2^{2+} affinity and selectivity of subsequent generations of chelating polymer adsorbents. Therefore, in **Chapter 2** we use ^1H -NMR and UV/Vis spectroscopic titrations to resolve the pK_a values of acetamidoxime and benzamidoxime. Subsequently, we use pK_a those values to develop computational protocols for predicting the pK_a values of aqueous oxoacid ligands. Density functional theory and wave-function methods were utilized in conjunction with

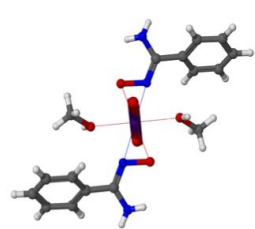
continuum solvation calculations to develop computational protocols for predicting the pK_a values of aqueous oxoacid ligands within < 0.5 pK_a units of their experimental value.

While the computational protocols for predicting the pK_a values of oxoacids aid in the design of ligands that form more stable UO_2^{2+} complexes, they do not facilitate the design of ligands that are more selective to UO_2^{2+} than competing transition metal cations on their own because the $\log K$ value of any oxoacid-metal cation complex is related to the pK_a value of that ligand by a linear free energy relationship.¹⁸ Therefore, in order to computationally design ligands that are more selective towards UO_2^{2+} than the standard amidoxime based ligands, the coordination modes of amidoxime- UO_2^{2+} and amidoxime-transition metal cation complexes needed to be elucidated as well. In **Chapters 3 and 4**, we computationally investigate the binding motif of formamidoximate- VO_2^+ and $-VO^{2+}$ complexes, major competing ions in seawater.^{6, 14-15} Density functional theory and wave-function methods were utilized in conjunction with continuum solvation calculations to investigate potential binding motifs of formamidoximate- VO_2^+ and formamidoximate- VO^{2+} complexes. Our investigations of these formamidoximate complexes universally identified the most stable binding motif to be a tautomeric rearranged imino hydroxylamine chelate formed via coordination of the imino nitrogen and hydroxylamine oxygen. The alternative binding motifs for amidoxime chelation to VO_2^{2+} and VO^{2+} via a non-rearranged tautomer and η^2 coordination were found to be ~ 5 kcal/mol and ~ 11 kcal/mol less stable, respectively. Thus, while η^2 -coordination of the oxime functional group is the most stable coordination mode of amidoxime- UO_2^{2+} complexes,^{17, 19-20} it is far less than the tautomeric rearranged imino hydroxylamine chelate in amidoxime- VO_2^+ and amidoxime- VO^{2+} complexes. Thus, we determined that the complexation between poly(acrylamidoxime) fibers and vanadium cations can be restricted by either inhibiting the tautomeric rearrangement from the amidoxime

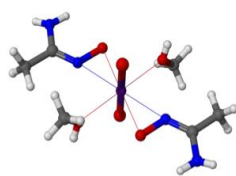
to imino hydroxylamine via substitution of both amine hydrogen atoms with aliphatic or aromatic groups or eliminating the amine group all together.

In **Chapter 5**, we build on the design principles acquired in **Chapters 2-4** to design a ligand, salicylaldoxime that is more selective toward the UO_2^{2+} cation than competing transition metal cations. We found that the binding strength of salicylaldoxime- UO_2^{2+} complexes are $\sim 2\text{-}4$ log β_2 units greater in magnitude than their corresponding acetamidoxime- UO_2^{2+} and benzamidoxime- UO_2^{2+} complexes; moreover, the selectivity of salicylaldoxime towards the UO_2^{2+} cation over competing Cu^{2+} and Fe^{3+} cations is far greater than the selectivities reported for glutarimidedioxime in the literature. The higher UO_2^{2+} selectivity can likely be attributed to the different coordination modes observed for salicylaldoxime- UO_2^{2+} and salicylaldoxime-transition metal complexes. Density functional theory calculations show that salicylaldoxime coordinates to UO_2^{2+} as a dianion species formed by η^2 -coordination of the aldoximate and monodentate binding of the phenolate group. In contrast, salicylaldoxime coordinates to transition metal cations as a monoanion species via a chelate formed between phenolate and the oxime N; the complexes are stabilized via hydrogen bonding interactions between the oxime OH group and phenolate. Thus, by coupling the experimentally determined thermodynamic constants and the results of theoretical computations, we are able to derive a number of ligand design principles to further improve the UO_2^{2+} cation affinity, and thus further increase the selectivity, of salicylaldoxime derivatives.

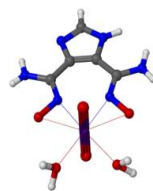
Acyclic Amidoxime- UO_2^{2+} Complexes



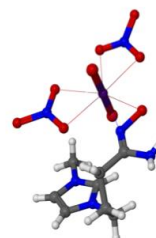
BARYOK (UO_2^{2+})



BARYUQ (UO_2^{2+})

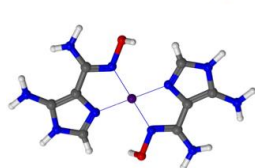


HORWOC (UO_2^{2+})

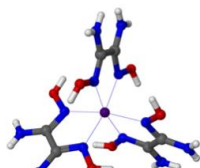


QEBPOE (UO_2^{2+})

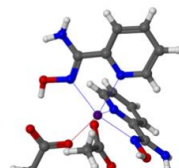
Acyclic Amidoxime-Transition Metal Cation Complexes



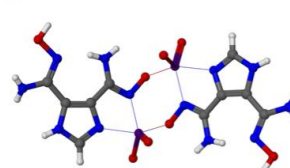
AICOCU10 (Cu^{2+})



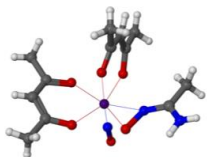
CIMMIW (Ni^{2+})



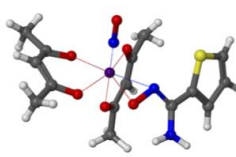
YOHFEI (Cd^{2+})



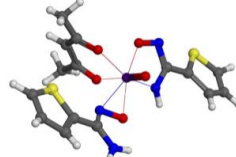
HORWIW (VO_2^+)



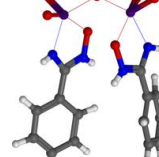
FOWJAC (Mo^{5+})



RASBOC (MoO^{4+})



RASBIW (MoO^{4+})



SAFSUN (MoO_2^{4+})

Figure 1.2. Representative acyclic amidoxime- UO_2^{2+} and -transition metal cation complexes adapted from the CSD.

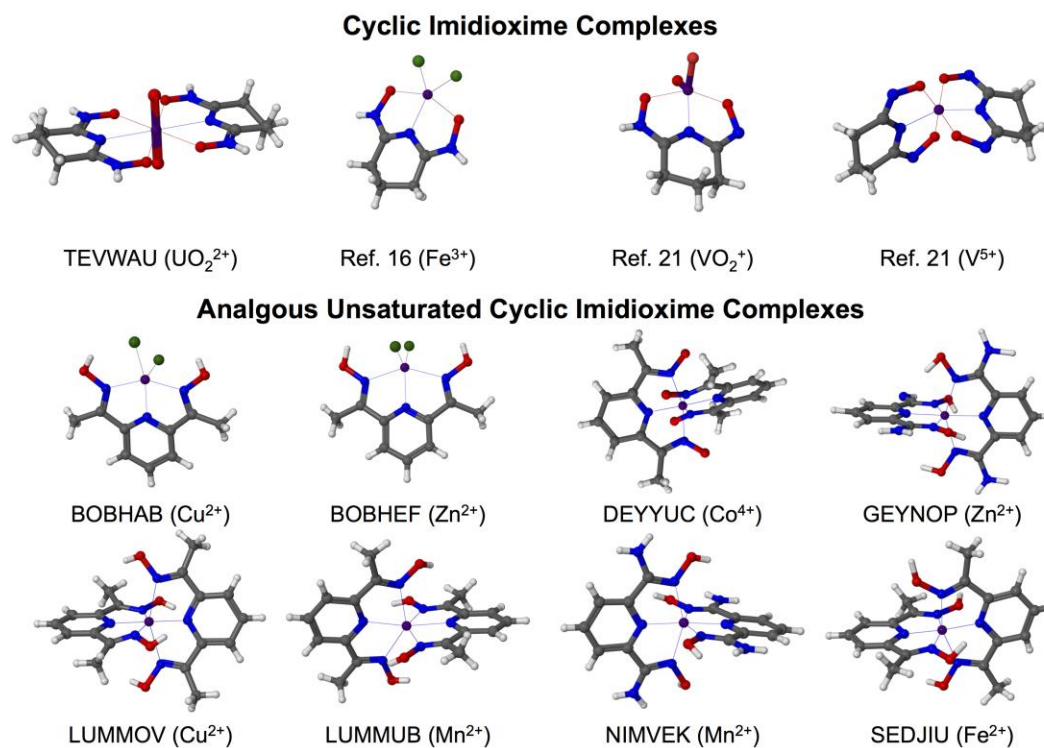


Figure 1.3. Representative cyclic amidoxime- UO_2^{2+} and –transition metal cation complexes and analogous unsaturated-transition metal cation complexes adapted from the CSD.

Finally, in **Chapter 6** we potentiometrically determine the proton affinity distribution of the classical poly(acrylamidoxime) fiber between pH 2 and pH 10 via the Stable Numerical Solution of the Adsorption Integral Equation Using Splines (SAIUS) algorithm.⁴¹⁻⁴³ These values are of great importance because the comparison of the acidity constants of poly(acrylamidoxime) monomer units to the acidity of their representative small ligands, is incomplete.⁴¹⁻⁴³ The pK_a values of pure chemical compounds, like small ligands, are a sum of delta functions; in contrast, the acidity of polymers is more accurately described as a continuous distribution of proton affinities.⁴¹⁻⁴³ This work lays the foundation for resolving the metal cation affinity distribution of the poly(acrylamidoxime) fibers, which can aid in improving the uranium selectivity of subsequent generations of chelating polymers.⁴¹⁻⁴³

References

1. Davies, R. V.; Kennedy, J.; McIlroy, R. W.; Spence, R.; Hill, K. M., Extraction of Uranium from Sea Water. *Nature* **1964**, *203*, 1110–1115.
2. Uranium 2014: Resources, Production and Demand. OECD Nuclear Energy Agency, International Atomic Energy Agency: 2014; Vol. NEA No. 7209.
3. Saito, K.; Miyauchi, T., Chemical Forms of Uranium in Artificial Seawater. *J. Nucl. Sci. Technol.* **1982**, *19*, 145–150.
4. Choppin, G. R., Soluble Rare Earth and Actinide Species in Seawater. *Mar. Chem.* **1989**, *28*, 19-26.
5. Endrizzi, F.; Rao, L., Chemical Speciation of Uranium(VI) in Marine Environments: Complexation of Calcium and Magnesium Ions with $[(\text{UO}_2)(\text{CO}_3)_3]^{4-}$ and the Effect on the Extraction of Uranium from Seawater. *Chem. Eur. J.* **2014**, *20*, 14499-14506.
6. Kim, J.; Tsouris, C.; Mayes, R. T.; Oyola, Y.; Saito, T.; Janke, C. J.; Dai, S.; Schneider, E.; Sachde, D., Recovery of Uranium from Seawater: A Review of Current Status and Future Research Needs. *Sep. Sci. Technol.* **2012**, *48*, 367–387.
7. Tamada, M.; Seko, N.; Yoshii, F., Application of Radiation-Graft Material for Metal Adsorbent and Crosslinked Natural Polymer for Healthcare Product. . *Radiat. Phys. Chem.* **2004**, *71* 221–225.
8. Seko, N.; Katakai, A.; Hasegawa, S.; Tamada, M.; Kasai, N.; Takeda, H.; Sugo, T.; Saito, K., Aquaculture of Uranium in Seawater by a Fabric-Adsorbent Submerged System *Nucl. Technol.* **2003**, *144*, 274–278.
9. Schenk, H. J.; Astheimer, L.; Witte, E. G.; Schwochau, K., Development of Sorbers for the Recovery of Uranium from Seawater. 1. Assessment of Key Parameters and Screening Studies of Sorber Materials. *Sep. Sci. Technol.* **1982**, *17*, 1293-1308.

10. Astheimer, L.; Schenk, H. J.; Witte, E. G.; Schwochau, K., Development of Sorbers for the Recovery of Uranium from Seawater. Part 2. The Accumulation of Uranium from Seawater by Resins Containing Amidoxime and Imidoxime Functional Groups. *Sep. Sci. Technol.* **1983**, *18*, 307–339.
11. Kawai, T.; Saito, K.; Sugita, K.; Katakai, A.; Seko, N.; Sugo, T.; Kawakami, T.; Kanno, J., Comparison of Amidoxime Adsorbents Prepared by Cografting Methacrylic Acid and 2-Hydroxyethyl Methacrylate with Acrylonitrile onto Polyethylene. . *Ind. Eng. Res. Chem.* **2000**, *39*, 2910-2915.
12. Kawai, T.; Saito, K.; Sugita, K.; Kawakami, T.; Kanno, J.; Katakai, A.; Seko, N.; Sugo, T., Preparation of Hydrophilic Amidoxime Fibers by Cografting Acrylonitrile and Methacrylic Acid from an Optimized Monomer Composition. *Radiat. Phys. Chem.* **2000**, *59*, 405-411.
13. Turekian, K. K., *Oceans*. Prentice Hall: Englewood Cliffs, NJ 1968.
14. Wang, D. L.; Sañudo Wilhelmy, S. A., Vanadium Speciation and Cycling in Costal Waters. . *Mar. Chem.* **2009**, *117*, 52–58.
15. Suzuki, T.; Saito, K.; Sugo, T.; Ogura, H.; Oguma, K., Fractional Elution and Determination of Uranium and Vanadium Adsorbed on Amidoxime Fiber from Seawater. *Anal. Sci.* **2000**, *16*, 429-432.
16. Sun, X.; Xu, C.; Tian, G.; Rao, L., Complexation of Glutarimidedioxime with Fe(III), Cu(II), Pb(II), and Ni(II), the Competing Ions for the Sequestration of U(VI) from Seawater. *Dalton Trans.* **2013**, *42*, 14621-14627.
17. Vukovic, S.; Watson, L. A.; Kang, S. O.; Custelcean, R.; Hay, B. P., How Amidoximate Binds the Uranyl Cation. *Inorg. Chem.* **2012**, *51*, 3855–3859.

18. Tian, G.; Teat, S. J.; Zhang, Z.; Rao, L., Sequestering Uranium from Seawater: Binding Strength and Modes of Uranyl Complexes with Glutarimidedioxime. *Dalton Trans.* **2012**, *41*, 11521–11908.
19. Barber, P. S.; Kelley, S. P.; Rogers, R. D., Highly Selective Extraction of the Uranyl Ion with Hydrophobic Amidoxime-Functionalized Ionic Liquids via η^2 Coordination. *RSC Adv.* **2012**, *2*, 8526-8530.
20. Kelley, S. P.; Barber, P. S.; Mullins, P. H.; Rogers, R. D., Structural Clues to $\text{UO}_2^{2+}/\text{VO}_2^+$ Competition in Seawater Extraction Using Amidoxime-Based Extractants. *Chem. Commun.* **2014**, *50*, 12504-12507.
21. Leggett, C. J.; Parker, B. F.; Teat, S. J.; Zhang, Z.; Dau, P. D.; Lukens, W. W.; Peterson, S. M.; Cardenas, A. J. P.; Warner, M. G.; Gibson, J. K.; Arnold, J.; Rao, L., Structural and Spectroscopic Studies of a Rare Nonoxido V(V) Complex Crystallized from Aqueous Solution. *Chem. Sci.* **2016**, Accepted (DOI: 10.1039/c5sc03958d).
22. Nicholson, G. A.; Petersen, J. L.; McCormick, B. J., Comparison of the Molecular Structures of Five-Coordinate Copper(II) and Zinc(II) Complexes of 2,6-Diacetylpyridine Dioxime. *Inorg. Chem.* **1982**, *21*, 3274-3280.
23. Namli, H.; Azaz, A. D.; Karabulut, S.; Çelen, B.; Kurtaran, R.; Kazak, C., Synthesis, Characterization, Crystal Structure and Biological Activity of the Cobalt(IV) Complex of 2,6-Diacetylpyridine Dioxime: $[\text{Co}(\text{dapdo})_2]$. *Transition Met. Chem.* **2007**, *32*, 266-270.
24. Konidaris, K. F.; Giouli, M.; Raptopoulou, C. P.; Psycharis, V.; Verginadis, I. I.; Vasiliadis, A.; Afendra, A. S.; Karkabounas, S.; Manessi-Zoupa, E.; Stamatatos, T. C., Employment of Pyridyl Oximes and Dioximes in Zinc(II) Chemistry: Synthesis, Structural and Spectroscopic Characterization, and Biological Evaluation. *Inorg. Chim. Acta* **2013**, *396*, 49–59.

25. Glynn, C. W.; Turnbull, M. M., Complexes of 2,6-Diacetylpyridine Dioxime (dapdoH₂). Crystal Structures of [M(dapdoH₂)₂](ClO₄)₂ (M = Cu and Mn). *Transition Met. Chem.* **2002**, 27, 822-831.
26. Bovenzi, B. A.; Pearse, G. A.; Pearse Jr., G. A., The Synthesis and Crystal Structures of Pyridine-2,6-dicarboxamideoxime, C₇H₉N₅O₂, and its Nickel(II) and Copper(II) Co-ordination Compounds. *J. Chem. Soc., Dalton Trans.* **1997**, 2793-2798.
27. Vasilevsky, I.; Stenkamp, R. E.; Lingafelter, E. C.; Rose, N. J., Syntheses and Structures of μ -Oxo-Bis[dichloroiron(III)]-Bis-[2,6-Diacetylpyridinedioximate(-1)]Iron(II) and Related Compounds. *J. Coord. Chem.* **1988**, 19, 171-187.
28. Stout, C. D.; Sundaralingam, M.; Lin, G. H.-Y., Stereochemistry of Nucleic Acids and Their Constituents. XXI. The Crystal and Molecular Structure of Bis-(4-aminoimidazole-5-carboxamidoxime)copper(II) Perchlorate, a Degradation Product of Adenine N¹-oxide. *Acta Crystallogr., Sect. B: Struct. Sci.* **1972**, 28, 2136-2142.
29. Nenwa, J.; Djonwouo, P. L.; Bélombé, M. M.; Nfor, E. N.; Emmerling, F., Transition Metal Complexes of Oxamide Dioxime: Synthesis, Characterization and X-ray Structure of Isomorphous [Ni(H₂oxado)₃](BF₄)₂ and [Ni(H₂oxado)₃](ClO₄)₂. *ScienceJet* **2013**, 2 43.
30. Liu, J., Crystal Structure of Bis-(Acetato-[kappa]O)Bis-(Pyridine-2-carboxamide Oxime [kappa]2N,N')Cadmium Ethanol Disolvate. *Acta Crystallogr., Sect. E: Struct. Rep. Online* **2014**, 70, 142-144
31. Chilou, V.; Gouzerh, P.; Jeannin, Y.; Robert, F., Reaction of Oxomolybdenum Complexes with Amidoximes. Synthesis and Structure of a Nitrosylacetamidoximate(1-) Complex with a N,O-side-on Bonded Acetamidoximate(1-) Ligand: [Mo(acac)₂(CH₃C(NH₂)NO) (no)]. *Inorg. Chim. Acta* **1987**, 133, 205-206.

32. Roh, S.-G.; Proust, A.; Robert, F.; Gouzerh, P., Coordination Chemistry of Polyoxomolybdates: The Versatile Behavior of Amidoximes. *J. Cluster Sci.* **1996**, *7*, 593-627.
33. Chilou, V.; Gouzerh, P.; Jeannin, Y.; Robert, F., Synthesis and X-ray Structures of Molybdenum(VI) Complexes with Benzamide Oximes. A Rare Linear Tetramolybdenum Compound $[\text{Mo}_4\text{O}_{11}\{p\text{-TolC}(\text{NH}_2)\text{NHO}\}_2\{p\text{-TolC}(\text{NH})\text{NHO}\}\{p\text{-TolC}(\text{NH})\text{NO}\}]^-$. *J. Chem. Soc., Chem. Commun.* **1989**, 76-78.
34. Dürüst, N.; Akay, M. A.; Dürüst, Y.; Kiliç, E., Protonation Constants of Some N-Substituted Amidoximes in a 50% Ethanol-Water Mixture (v/v). *Anal. Sci.* **2001**, *16*, 825-827.
35. Hirotsu, T.; Katoh, S.; Sugasaka, K.; Seno, M.; Itagaki, T., Binding Ability of Acetamide Oxime with Proton, Copper(II), and Dioxouranium(VI) in Aqueous Solutions *J. Chem. Soc., Dalton Trans.* **1986**, *8*, 1609-1611.
36. Bunton, C. A.; Nelson, S. E.; Quan, C., Micellar Effects Upon Dephosphorylation by Amidoximes. *J. Org. Chem.* **1982**, *47*, 1157-1160.
37. Aubort, J. D.; Hudson, R. F., Enhanced Reactivity of Nucleophiles: Orbital Symmetry and the So-Called " α -Effect" *J. Chem. Soc. D: Chem. Commun.* **1970**, *15*, 937-938.
38. Simanenko, Y. S.; Prokop'eva, T. M.; Belousova, I. A.; Popov, A. F.; Karpichev, E. A., Amidoximes as Effective Acceptors of Acyl Group. *Theor. Exp. Chem.* **2001**, *37*, 288-295.
39. Martell, A. E.; Hancock, R. D., *Metal Complexes in Aqueous Solutions*. Plenum Press: New York, 1996.
40. Hay, B. P.; Chagnes, A.; Cote, A. G., On the Metal Ion Selectivity of Oxoacid Extractants. *Solvent Extr. Ion Exch.* **2013**, *31*, 95-105.
41. Jagiełło, J., Stable Numerical Solution of the Adsorption Integral Equation Using Splines. *Langmuir* **1994**, *10*, 2778-2785.

42. Jagiełło, J.; Bandosz, T. J.; Putyera, K.; Schwarz, J. A., Determination of Proton Affinity Distributons for Chemical Systems in Aqueous Environments Using a Stable Numerical Solution of the Adsorption Integral Equation. . *J. Colloid Interface Sci.* **1995**, *172*, 341-346.
43. Ballif, J. B.; Lerf, C.; Schläpfer, C. W., The Proton Affinity Spectrum of Polyethylenimine. *Chimia* **1994**, *48*, 336-340.

Chapter 2 : Acidity of the Amidoxime Functional Group in Aqueous Solution: A Combined Experimental and Computational Study

A version of this chapter was originally published by Nada Mehio, Mark A. Lashley, Joseph W. Nugent, Lyndsay Tucker, Bruna Correia, Chi-Linh Do-Thanh, Sheng Dai, Robert D. Hancock, and Vyacheslav S. Bryantsev in the *Journal of Physical Chemistry B*:

Mehio, N.; Lashley, M. A.; Nugent, J. W.; Tucker, L.; Correia, B.; Do-Thanh, C-L.; Dai, S.; Hancock, R. D.; Bryantsev, V.S. “Acidity of the Amidoxime Functional Group in Aqueous Solution: A Combined Experimental and Computational Study.” *J. Phys. Chem. B* **2015**, 119, 3567–3576.

Abstract

Poly(acrylamidoxime) adsorbents are often invoked in discussions of mining uranium from seawater. While the amidoxime-uranyl chelation mode has been established, a number of essential binding constants remain unclear. This is largely due to the wide range of conflicting pK_a values that have been reported for the amidoxime functional group. To resolve this existing controversy we investigated the pK_a values of the amidoxime functional group using a combination of experimental and computational methods. Experimentally, we used spectroscopic titrations to measure the pK_a values of representative amidoximes, acetamidoxime and benzamidoxime. Computationally, we report on the performance of several protocols for predicting the pK_a values of aqueous oxoacids. Calculations carried out at the MP2 or M06-2X levels of theory combined with solvent effects calculated using the SMD model provide the best overall performance with a root mean square deviation of 0.46 pK_a units and 0.45 pK_a units, respectively. Finally, we employ our two best methods to predict the pK_a values of promising, uncharacterized amidoxime ligands, which provides a convenient means for screening suitable amidoxime monomers for future generations of poly(acrylamidoxime) adsorbents.

2.1. Introduction

Global energy demands are currently being met by high-carbon emission fossil fuels anticipated to diminish over time. Consequentially, an increased emphasis has been placed on further developing alternative sources of energy.¹ Nuclear energy is a promising alternative as there is an estimated 4.5 billion tons of uranium dissolved in seawater¹, largely in the form of uranyl tricarbonat, $^{1-3} \text{UO}_2(\text{CO}_3)_3^{4-}$, while only 5,000 tons of uranium are needed annually to meet today's energy needs.⁴ Thus, there has been a great interest in developing an adsorbent material capable of sequestering uranium since the idea was first put forth five decades ago.¹ However, there are a number of challenges associated with developing an adsorbent material capable of selectively extracting uranium from seawater. The primary challenge is that uranium is present at very low concentrations in seawater, about 3 ppb,¹ with competing metal cations that are present in much higher concentrations.³ However, despite the complications associated with extracting uranium from seawater, the following developments in adsorbent material development have made industrial scale mining a possibility: (1) a systematic screening of 200 organic polymers that identified poly(acrylamidoxime) as the only material capable of extracting uranium at pH 8.3, the approximate pH of seawater^{5, 6} and (2) the development of grafting techniques enabled manufacturing of poly(acrylamidoxime) fibers on a large scale.⁷

Poly(acrylamidoxime) fibers are polymers bearing random mixtures of the carboxyl and the amidoxime functional group linked by propyl chains^{8, 9}. The ratio of carboxyl monomers to amidoxime monomers is roughly a 35:65 ratio, respectively.⁹ The selectivity and capacity of poly(acrylamidoximes) can be improved by examining the stability of amidoxime- UO_2^{2+} complexes relative to amidoxime complexes formed with other metals found in seawater.¹⁰ The stability of metal-ligand complexes, such as amidoxime- UO_2^{2+} complexes, is conveyed in the form of binding constants, or $\log K_1$ values. As depicted in **Figure 2.1**, the $\log K_1$ values are fit

relative to the acid dissociation constants of the ligand, or pK_a values. Moreover, the basicity of amidoximate species gives insight into the metal cation affinity of amidoximate species as the two properties are correlated by linear free energy relationships.¹¹ Thus, knowledge of the amidoxime functional group's dissociation constants is of critical importance. Herein, we report the pK_a values of acetamidoxime and benzamidoxime, prototypical amidoxime ligands.

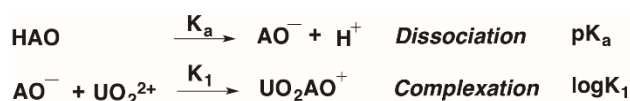


Figure 2.1. The strength of a metal-ligand interaction is conveyed in the form of a complexation constant, $\log K_1$. The amidoxime functional group (HAO) releases a proton to bind to UO_2^{2+} ; therefore, one needs to know the pK_a of HAO to determine the $\log K_1$ value.

Acetamidoxime is a prototypical sp^3 hybridized amidoxime that is representative of the amidoxime monomer on poly(acrylamidoxime) structures. While acetamidoxime has been characterized a number of times in recent years, there has been a discrepancy in the acid dissociation constant, pK_a , values that have been reported. Moreover, while the acetamidoximate pK_a value can be found in the literature, a wide range of pK_a values have been reported, such as 10.6,¹² 11.6,¹³ 12.6,¹⁴ 12.9,¹⁵ and 13.3.¹⁶ This discrepancy makes it difficult to accurately measure and report the formation constants, $\log K$, of essential acetamidoxime complexes. Benzamidoxime is a prototypical sp^2 hybridized amidoxime. Neither protonation constants, nor formation constants have been reported for benzamidoxime in the literature. These values are essential because they can be used to incorporate sp^2 -hybridized structures into future generations of amidoxime chelating polymers. Thus, the direct measurement of the pK_a values of acetamidoxime and benzamidoxime by an accurate spectroscopic method is of great relevance.

Herein, we report the pK_a values of acetamidoxime measured via 1H -NMR titrations and the pK_a values of benzamidoxime measured via UV/Vis titrations.

In addition, we employed computational methods to investigate the acidity of the amidoxime functional group (basicity of the corresponding amidoximate ligand). Specifically, we report on the performance of several computational protocols for predicting the pK_a values of aqueous amidoximes, oximes, alcohols, carboxylic acids, hydroxamic acids, and inorganic acids. A total of 25 methods combining density functional theory (DFT),^{17, 18} second-order Möller-Plesset perturbation theory (MP2),^{19, 20} and coupled-cluster theory with singles, doubles, and perturbative triples excitations (CCSD(T))²¹⁻²³ with continuum solvation calculations are evaluated. We found that linear least-square fitting of pK_a values predicted by combining calculations at the MP2 or M06-2X²⁴ level of theory with the SMD²⁵ solvation model yielded the most accurate predicted pK_a values. These computed pK_a values provide a convenient method for screening suitable amidoxime monomers for future generations of poly(acrylamidoxime) adsorbents. Using the most accurate computational protocol among those we have tested, we investigate the acidity of promising, uncharacterized amidoxime ligands.

2.2. Experimental Methods

2.2.1. Materials and Methods

Acetamidoxime was prepared by treating acetonitrile (99.9%, Fisher-Scientific) with NH_2OH (50 wt% solution in water, Aldrich) according to known procedures.²⁶ Benzamidoxime was prepared by treating benzonitrile (Eastman) with NH_2OH (50 wt% solution in water, Aldrich) according to known procedures.²⁷ All solutions were made up in deionized water (Milli-Q, Waters Corp.) of $>18\text{ M}\Omega\text{ cm}^{-1}$ resistivity.

2.2.2. pH Measurements

The pH was monitored using a VWR Symphony SB70P pH meter or VWR Symphony B10P with a Beckman Coulter glass pH Ag/AgCl electrode. The meters were standardized using a strong acid/strong base titration method with 0.0100N HCl and 0.0100N NaOH standardized solutions (Alfa Aesar) and a calibration curve fitted to determine the Nernst slope and E° correction factors. The results of these standardizations can be found in **Appendix A, Figure A.1**. Prior to each titration, the pH meter was calibrated using a NIST pH buffer set (1.68, 4, 7, 10, 12.45). Humidified nitrogen was employed to purge as much CO₂ and O₂ from the solution and to provide mild agitation sufficient to mix all additions.

The uncertainty associated with our pH measurements was determined statistically by measuring and fitting the pK_a values of five known acids. A standard deviation of 0.03 pH units was obtained. However, due to the uncertainty in accurately measuring pH values greater than 12, a more conservative error estimate of 0.10 pH units should be associated with pK_a values of 12 or greater.

2.2.3. ¹H-NMR Titrations

All acetamidoxime spectra were collected using Bruker Avance 600 MHz spectrometer (Bruker Biospin, Boston, MA, USA). A 50 mL solution of analyte was prepared by dissolving acetamidoxime (2×10^{-3} M) and DSS (0.25%) in 10% D₂O/H₂O. All spectra were acquired by using solvent suppressant techniques with the following Bruker pulse programs: COSY, cosydfesgpphm; HSQC, hsqcedetgp; TOCSY, mlevesgpph; and ROESY, rsoesygesgpph. TOCSY and ROESY spectra were acquired by using spin lock and a mixing time of 70 ms and 300 ms, respectively. The data was fit in Excel by using Solver to minimize the MAE between

theoretical and observed $^1\text{H-NMR}$ shifts.²⁸ The theoretical $^1\text{H-NMR}$ shifts are obtained by summing the product of each individual species' α -fraction and its characteristic $^1\text{H-NMR}$ shift, or the shift that coincides with the respective species half-equivalence point.²⁸ Solver minimizes the MAE by varying pK_a values and the corresponding $^1\text{H-NMR}$ shifts.²⁸

2.2.4. UV/Vis Titrations

UV-Vis spectroscopy was performed using an Agilent Technologies Cary-100 UV-Vis Spectrophotometer, Cary WinUV Scan program version 4.20 with 1 cm matched quartz cells. The scan method used a double beam mode with zero/baseline correction. Reference solutions were comprised of the same volume of MilliQ water at the same initial pH of the analyzed solution with comparable additions of base or acid to account for any possible change in refractive index. We used a jacketed titration cell connected to a constant temperature water bath set to 25.0 ± 0.1 °C to titrate 50 mL samples of 10^{-4} M benzamidoxime. The data was fit in Excel by using solver to minimize the MAE between theoretical and observed absorbance data at six different wavelengths.²⁸ Theoretical absorbance data is generated by summing the product of each individual species' α -fraction and its characteristic absorbance, or the absorbance value that coincides with the respective species half-equivalence point.²⁸ Solver minimizes the MAE by varying pK_a values and corresponding absorbance values.²⁸

2.3. Computational Methods

2.3.1. pK_a Calculations

By definition, the acid dissociation constants, or pK_a values, are given by the following relationship:

$$\text{pK}_a = -\log(K_a) = \Delta G_{\text{solv,deprot}}^*(\text{HA})/(\ln(10) RT) \quad [1]$$

We calculated the pK_a of each acid in the training set by calculating $\Delta G_{solv,deprot}^*(HA)$ using the thermodynamic cycle constructed in **Figure 2.2**.²⁹⁻³¹

$$\Delta G_{solv,deprot}^*(HA) = \Delta G_{g,deprot}^0(HA) + \Delta G^{0 \rightarrow *}_{\rightarrow *} + [\Delta G_{solv}^*(A^-) + \Delta G_{solv}^*(H^+) - \Delta G_{solv}^*(HA)] \quad [2]$$

In this cycle, $\Delta G_{g,deprot}^0(HA)$ and $\Delta G_{solv,deprot}^*(HA)$ are the gas phase and the solution phase standard free energies of deprotonation, respectively, and $\Delta G_{solv}^*(X)$ is the standard solvation free energy of species X . In order for the thermodynamic cycle to be properly implemented, each reactant and product in the gas phase and the reactants and products in solution must be in the same standard state. The conversion from an ideal gas standard state of 1 atm (24.46 L mol⁻¹) to an ideal solution standard state of 1 M (1 mol L⁻¹) at 298 K is given by the following relationship:

$$\Delta G^{0 \rightarrow *} = RT \ln(24.46) = 1.89 \text{ kcal/mol} \quad [3]$$

Thus, the correction term in the upper leg of the thermodynamic cycle is given by applying this conversion correction to each gas phase reactant and product.

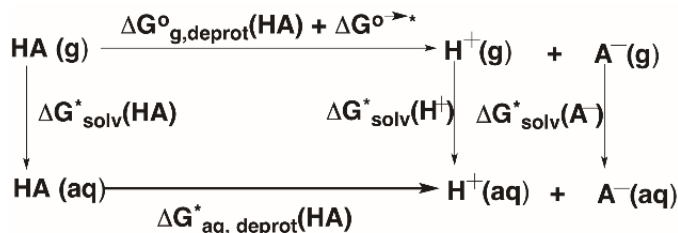


Figure 2.2. Thermodynamic cycle used to predict pK_a values.

2.3.2. Gas Phase Calculations

Electronic structure calculations were carried out using the Gaussian 09 Revision D.01³² and NWChem 6.3³³ software packages. We compared three density functionals' ability to

reproduce experimental gas phase experimental deprotonation energies of 16 molecules. Specifically, the B3LYP,^{34, 35} M06,²⁴ and M06-2X functionals were employed. The geometries and vibrational frequencies of each molecule were computed using the B3LYP functional with a 6-311++G** basis set. The standard Gibbs free energy of each reactant in the gas phase were computed using the rigid rotor-harmonic oscillator approximation and the recommended scaling of zero-point energies (0.9877).³⁶

Likewise, the deprotonation energies were obtained at the MP2/aug-cc-pVTZ and CCSD(T) /aug-cc-pVDZ levels of theory. MP2/aug-cc-pVDZ was the highest level of theory employed in all geometry optimization calculations. An aug-cc-pVTZ basis set was employed in all MP2 calculations because it yielded deprotonation energies close to the complete basis set (CBS) limit. Indeed, test calculations for water, methanol, and phenol demonstrated that extending a basis set from aug-cc-pVTZ to aug-cc-pV6Z changes the deprotonation energies by less than 0.15 kcal/mol. Assuming that the difference between the CCSD(T) and MP2 energies is only marginally contingent upon the basis set,³⁷ the CCSD(T) reaction energies at the aug-cc-pVTZ level can be estimated with the following formulas:

$$\Delta E(CCSD(T)) = \Delta E(CCSD(T)/aug-cc-pVDZ) + \delta MP2 \quad [4]$$

$$\delta MP2 = \Delta E(MP2/aug-cc-pVTZ) - \Delta E(MP2/aug-cc-pVDZ) \quad [5]$$

2.3.3. Implicit Solvation Calculations

Five continuum solvent models were evaluated in this study: the IEFPCM model³⁸⁻⁴⁰ implemented in Gaussian 09 Revision D.01, the CPCM model^{41, 42} implemented in Gaussian 09 Revision D.01, the SMD model implemented in Gaussian 09 Revision D.01, the COSMO model⁴³ implemented in NWChem 6.3, and the SVPE model⁴⁴⁻⁴⁶ as implemented in GAMESS.⁴⁷

The electronic energies in the solvent reaction field were computed at the B3LYP/6-31+G* level of theory for the IEPCM, CPCM, and SMD solvation model. The electronic energies in the solvent reaction field were computed at the B3LYP/6-31++G** level of theory for the COSMO model and the SVPE2 model. The SVPE solvation model defines the cavity surfaces in terms of the electronic isodensity contours of a molecule. We computed the SVPE solvation energies using the adjusted (0.0016 e/a₀³, SVPE2) values of the isodensity contour of each molecule because this adjustment gave better agreement between the computed and experimental pK_a values in our previous study of a series of aliphatic C-H acids in DMSO.²⁹ The solvation free energy of the proton in water, $\Delta G_{solv}^*(H^+)$, was treated as an adjustable parameter whose value was altered to minimize the difference between the computational and experimental pK_a values.

2.4. Results and Discussion

As noted in **Section 2.1**, a wide range of conflicting pK_a values that have been reported for the amidoxime functional group in the literature. To resolve this controversy we investigated the pK_a values of the amidoxime functional group using a combination of experimental and computational methods. Experimentally, we used spectroscopic titrations to measure the pK_a values of representative amidoximes, acetamidoxime and benzamidoxime. Specifically, we used ¹H-NMR titrations to measure the pK_a values of acetamidoxime and UV/Vis titrations to measure the pK_a values of benzamidoxime. Computationally, we report on the performance of 25 protocols for predicting the pK_a values of aqueous oxoacids. The most accurate computational protocols that achieve an accuracy of < 0.5 pK_a units are used to predict the pK_a values of several uncharacterized amidoxime ligands.

2.4.1. pK_a Measurements

The pK_a values of acetamidoxime were evaluated by recording its aqueous spectra as a function of pH. A plot of the ¹H-NMR shifts versus pH can be found in **Figure 2.3**. The spectra corresponding to the ¹H-NMR shifts in Figure 3 are located in **Appendix A, Figure A.2**. The acetamidoxime pK_a values are summarized in **Table 2.1**. The ¹H-NMR shifts in **Figure 2.3** and **Figure A.2** represent the ¹H-NMR shifts of the protons on the methyl functional group. The first pK_a corresponds to the deprotonation of the cationic acetamidoxime species; it entails the deprotonation of the protonated nitrogen oxime, as illustrated in **Figure 2.3**. The second pK_a corresponds to the deprotonation of the neutral acetamidoxime species; it entails the deprotonation of the hydroxyl group, as illustrated in **Figure 2.3**. The acetamidoxime pK_{a2} value we measured spectroscopically was within < 0.1 pK_a units of the kinetically measured acetamidoxime pK_{a2} reported by Karpichev and colleagues.¹⁶

The pK_a value reported by Karpichev and colleagues¹⁶ was more accurate than the pK_a values reported by others who measured these values via potentiometry.¹²⁻¹⁵ Potentiometric titration data is unreliable below pH 2 and above pH 12 because water has a buffering reaction in those regions.⁴⁸⁻⁵⁰ Therefore, the pK_a values of very acidic and very basic ligands cannot be measured accurately by potentiometric titration, because it is difficult to accurately discriminate between water's reactions with the base or acid and the ligand's reaction with the base or acid using mass balance equations.⁴⁸⁻⁵⁰ However, spectroscopic methods, such as ¹H-NMR and UV/VIS titrations, provide reliable data in these regions because the water signal can be suppressed or set as the background, respectively.⁴⁸⁻⁵⁰ Thus, when the pK_a of a ligand is computed in terms of the ¹H-NMR shifts, or the absorbance, water's reaction with the base or acid is not a component of the pK_a calculation.⁴⁸⁻⁵⁰

The pK_a values of benzamidoxime were evaluated by recording its aqueous absorption spectra as a function of pH. Representative spectra are shown in **Figure 2.4**. The benzamidoxime pK_a values are summarized in **Table 2.2**. The first pK_a corresponds to the deprotonation of the cationic benzamidoxime species; it entails the deprotonation of the protonated nitrogen oxime. The second pK_a corresponds to the deprotonation of the neutral benzamidoxime species; it entails the deprotonation of the hydroxyl group. The pK_{a2} value was consistent with the pK_{a2} value reported by Karpichev and colleagues¹⁶ for a similar structure, meta-amidoxime azine. The meta-amidoxime azine had a pK_{a2} value of 11.98 and the pK_a value of benzamidoxime is 12.36. This is expected because the azine ring on meta-amidoxime is more electron withdrawing than the benzene ring on benzamidoxime; thus, providing greater stability to the anionic species.

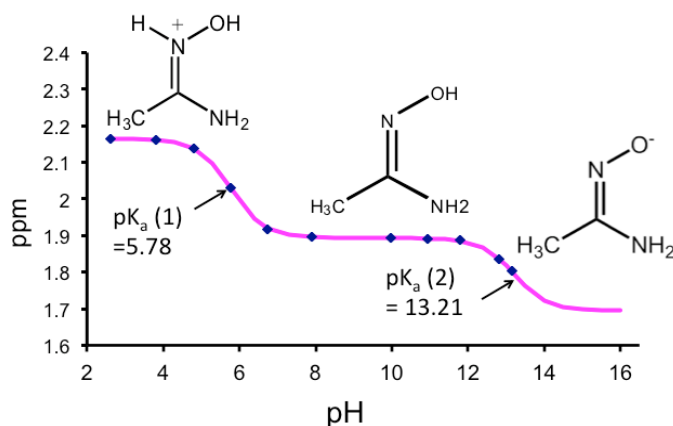


Figure 2.3. ^1H -NMR shifts of aqueous acetamidoxime (2×10^{-3} M) versus pH at 25 °C and 0.0 M ionic strength.

The corresponding spectra can be found in **Appendix A**, (**Figure A.2**).

2.4.2. Predicting Gas Phase Acidities

First, we will compare the accuracy of the gas phase acidities predicted using three density functionals, such as B3LYP, M06, and M06-2X, and post-Hartree-Fock methods, such as MP2 and CCSD(T). The B3LYP functional was selected due to its popularity and reasonable accuracy,^{29, 30} while as the M06 family was selected for its accurate description of main-group thermochemical properties.^{24, 52} The CCSD(T) gas phase acidities were used as a benchmark against which the accuracy of the DFT and MP2 gas phase acidities were evaluated. The mean absolute error (MEA) and the root mean square deviation (RMSD) convey each method's ability to replicate the experimental gas phase acidity values.⁵³ The MEA and RMSD of each value can be found in the last two rows of **Table 2.3**.

As anticipated, the gas phase acidities obtained by CCSD(T) calculations were in best agreement with the experimental gas phase acidities,⁵³ with a MEA of 1.0 kcal/mol and a RMSD of 1.2 kcal/mol. In most cases, the CCSD(T) gas phase acidities fall within the experimental uncertainty of 1-2 kcal/mol.⁵³ Among the DFT methods, the M06-2X functional yielded gas phase acidities in best agreement with experimental values,⁵³ with a MEA of 2.6 kcal/mol and a RMSD of 2.8 kcal/mol. The M06 functional, B3LYP functional, and MP2 levels of theory yielded similar results, with MEAs of 3.7 kcal/mol, 3.4 kcal/mol, and 3.3 kcal/mol and RMSDs of 3.9 kcal/mol, 3.5 kcal/mol, and 3.4 kcal/mol, respectively. The magnitude of the MP2 error is consistent with that reported for neutralization reactions between H^+ and OH^- species.⁵⁴

2.4.3. The Accuracy of pK_a Calculations in Water

Next, we will evaluate the accuracy of the 25 methods used to predict the pK_a values in water. The training set consists of 16 oxoacids with pK_a values ranging between -3 and 15.7.^{16, 55}

The training set was selected because the acids have a small number of conformations that can be systematically investigated, cover a wide range of representative oxoacids, and have accurate experimental pK_a values in the literature. **Table 2.4** summarizes the performance of the 25 protocols for computing the pK_a in the form of MEAs and RMSDs. The three density functionals and the two post-Hartree-Fock methods used to evaluate the gas phase acidities were combined with five continuum solvation models to predict the pK_a of each acid in the training set. All combinations were considered. In order to correct for deficiencies introduced by the solvation model, pK_a values computed using Eq. (3) were correlated^{56, 57} with the experimental values using linear regression analysis,^{44, 45} where a and b are fitting parameters:

$$pK_a[Pred.] = a + b \times pK_a[Comp.] \quad [6]$$

The value of fitting parameter a can be incorporated into the solvation free energy of the proton in water, $\Delta G_{solv}^*(H^+)$, which was treated as an adjustable parameter (**Section 2.3.1**). The MEAs and RMSDs obtained from the regression analysis of each pK_a calculation protocol are listed in **Table 2.4**. The pK_a values predicted by all 25 methods for each acid in the training set can be found in **Appendix A, Tables A.1-A.5**.

Table 2.1. Acetamidoxime pK_a values at 25 °C. The pK_{a1} values was obtained at 0.0 M ionic strength and the pK_{a2} value was obtained at 0.3 M ionic strength.

Dissociation	Dissociation	
Reaction	Constant	
$H_2A^+ \rightarrow HA + H^+$	5.78	pK_{a1}
$HA \rightarrow A^- + H^+$	13.21	pK_{a2}

Table 2.2. Benamidoxime pK_a values at 25 °C. The pK_{a1} value was obtained at 0.0 M ionic strength and the pK_{a2} was obtained at 0.3 M ionic strength.

Dissociation	Dissociation	
Reaction	Constant	
$\text{H}_2\text{A}^+ \rightarrow \text{HA} + \text{H}^+$	4.85	pK _{a1}
$\text{HA} \rightarrow \text{A}^- + \text{H}^+$	12.36	pK _{a2}

While the CCSD(T) method attained the highest accuracy in predicting gas phase acidities and pK_a values with all solvation models except SMD, the combination of MP2 or M06-2X and SMD yielded the highest accuracy in predicting pK_a values overall (**Figure 2.5**). The computed and predicted pK_a values from our two best methods are tabulated in **Table 2.6**. The M06 and B3LYP functionals yielded pK_a values of similar accuracy. The choice of the continuum solvent model has a significant bearing on the predictive power of the pK_a models tested. The SMD solvation model is the most accurate solvation model for predicting the pK_a values of oxoacids in water. However, it should be noted that the slope obtained by all 25 pK_a protocols is significantly less than one. While the discrepancy between the fitted slope and the ideal value can be partially attributed to the accuracy level of DFT for the protocols in which DFT methods were applied,⁵⁶ the primary reason for the discrepancy is the gross underestimation of the solvation energies of the conjugate base species by all implicit solvation models using the default recommended parameters, as listed in **Table 2.5**. More accurate solvation energies of conjugate base species within the dielectric continuum approximation can be obtained by decreasing the atomic radii of the conjugate base species.^{31, 58, 59} For example, using the default Gaussian 98 atomic radii⁶⁰⁻⁶³ gave better estimates of the solvation energies of anionic phenolate and carboxylate species, but resulted in the overestimated solvation energies of the

corresponding acid species. Alternatively, others were able to obtain more accurate conjugate base solvation energies by explicitly adding water molecules to their structures.^{64, 65} While this approach improves the accuracy of the computed conjugate base solvation energies, there are a number of challenges associated with the implementation of this method, such as determining the optimal number of explicit water molecules and elucidating the optimal conformation of the water-solute cluster.^{30, 65, 66} In this work, we chose to use the default solvation parameters of the implicit solvation model and to account for the deficiencies of the theoretical models by correlating the computed pK_a values with their corresponding experimentally obtained pK_a values. The results demonstrate that when the SMD solvation model is employed, Eq. 6 provides a reliable description of aqueous oxoacid energies across 19 pK_a units, comparable to the best accuracy of the gas phase calculations discussed earlier.

2.4.4. Predicting the pK_a Values of Potential Amidoxime Monomers

Having developed pK_a calculation protocols that predict the pK_a values of oxoacids within the accuracy of < 0.5 pK_a units and the pK_a values of acetamidoxime and benzamidoxime within < 0.2 pK_a units, we can now examine the acidity of a variety of promising amidoxime monomers for future generations of poly(acrylamidoxime) adsorbents. The pK_a calculations in water are carried out at the MP2/aug-cc-pVTZ and M06-2X/6-311++G** levels of theory with solvent corrections obtained using the SMD solvation model. These two protocols were selected because they are the most reliable protocols for predicting the pK_a values of aqueous oxoacids. In the absence of experimental data, these calculations provide a theoretical scale of ligand basicity that can be used to assess the complexation ability of promising amidoximate ligands. The results of these calculations are summarized in **Figure 2.6**.

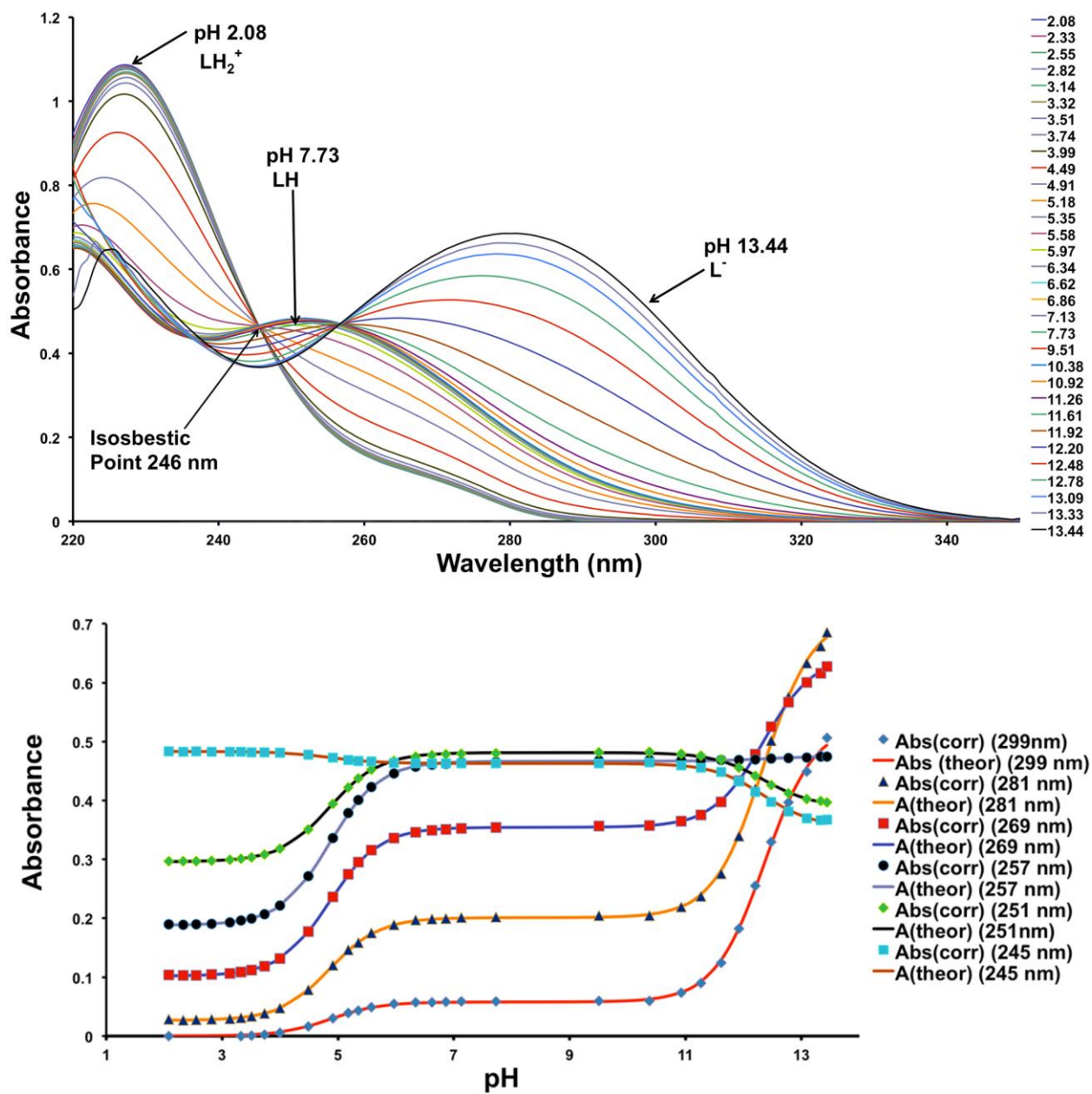


Figure 2.4. (Top) Spectra of benamidoxime (10^{-4} M) in aqueous solution at 25 °C and 0.0 M ionic strength. (Bottom) Variation of absorbance at six different wavelengths of 10^{-4} M benamidoxime in aqueous solution as a function of pH. The points are experimental values, whereas the solid lines are theoretical curves fitted to the experimental data using Solver.⁵¹

Table 2.3. The computed and experimental gas phase acidities (deprotonation energies) of 16 oxoacids (kcal/mol).^a

Acid	B3LYP	M06	M06-2X	MP2	CCSD(T)	Experimental ^c
1. Water	382.7	384.7	385.9	379.9	383.7	383.7
2. Methanol	372.4	371.3	375.4	372.7	375.3	376.0
3. Phenol	339.5	338.3	340.2	339.2	342.0	342.3
4. Formic Acid	334.0	333.7	335.6	334.4	337.2	339.2
5. Benzoic Acid	331.5	331.0	331.4	330.2	333.0	333.0
6. Acetaldoxime	355.9	355.5	357.6	355.2	358.9	358.6
7. Benzaldoxime	341.9	341.1	343.7	342.4	346.6	345.9
8. Acetohydroxamic Acid	344.3	344.3	345.2	345.7	347.2	
9. Benzohydroxamic Acid	339.7	340.0	342.2	341.6	344.5	
10. Nitric Acid	314.2	314.2	313.0	317.0	318.9	317.8
11. Sulfuric Acid	301.0	301.5	300.8	302.3	304.9	302.3
12. Phosphoric Acid	318.3	319.0	319.0	319.1	321.8	323.0
13. Carbonic Acid	327.5	327.9	328.6	328.0	330.7	
14. Acetamidoxime	359.7	359.5	361.6	357.8	361.1	
15. Benzamidoxime	345.8	345.5	345.9	344.4	349.5	
16. Azine-Amidoxime ^b	341.6	341.5	342.3	339.8	345.4	
Mean Absolute Error	3.4	3.7	2.6	3.3	1.0	
Root Mean Square Deviation	3.5	3.9	2.8	3.4	1.3	

^aThe 6-311++G** basis set was employed for all B3LYP, M06, and M06-2X calculations. The aug-cc-pVTZ basis set was employed for all MP2 calculations. The CCSD(T) energies were obtained by combining CCSD(T)/aug-cc-pVDZ with the difference in energy between MP2/aug-cc-pVDZ and MP2/aug-cc-pVTZ of each acid. The ZPE and thermal corrections were calculated at the B3LYP/6-311++G** level of theory.

^bThe full name of this structure is (Z)-N-hydroxynicotinimidamide.

^cReference 53

Table 2.4. Comparison of the accuracy of the pK_a calculations in water for the training set of 16 oxoacids using a combination of five gas phase and four implicit solvation methods. The mean absolute error and the root mean square deviation (in parentheses) of the pK_a values obtained by the least square fitting of each method are listed below.^a

Method	IEFPCM	CPCM	SMD	COSMO	SVPE2
B3LYP/6-311++G**	0.61(0.73)	0.60(0.73)	0.42(0.51)	0.99(1.12)	0.63(0.84)
M06/6-311++G**	0.68(0.87)	0.68(0.87)	0.48(0.56)	1.08(1.26)	0.76(1.05)
M06-2X/6-311++G**	0.63(0.76)	0.62(0.76)	0.35(0.45)	0.93(1.09)	0.67(0.89)
MP2/aug-cc-pVTZ	0.67(0.74)	0.67(0.74)	0.33(0.46)	0.90(1.12)	0.63(0.79)
CCSD(T)/aug-cc-pVDZ + δ MP2	0.53(0.59)	0.53(0.59)	0.45(0.49)	0.88(1.00)	0.48(0.66)

^aZPE and thermal corrections are calculated in the gas phase at the B3LYP/6-311++G** level of theory. B3LYP and the 6-31+G* basis set was used for all solvation calculations except the COSMO and SVPE2 calculations where B3LYP and a 6-311++G** basis set were used instead.

Table 2.5. Comparison of the free energies of solvation of five conjugate base species to literature values derived applying the cluster pair approximation.

Species	SMD	CPCM	IEFPCM	COSMO	Ref. 31
OH ⁻	-95.6	-83.3	-83.3	-90.9	-104.7
CH ₃ O ⁻	-78.8	-71.2	-71.2	-81.0	-95.0
C ₆ H ₅ O ⁻	-60.8	-57.1	-57.0	-66.7	-71.9
C ₆ H ₅ O ₂ ⁻	-64.6	-60.3	-60.2	-68.4	-72.8
HCO ₂ ⁻	-69.4	-65.4	-65.4	-72.1	-76.2

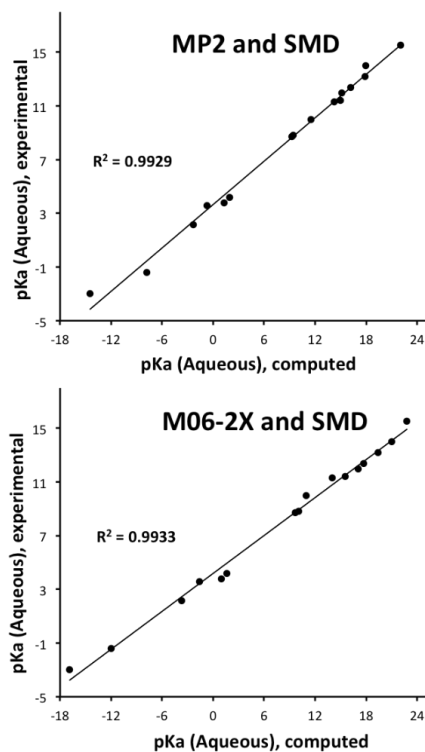


Figure 2.5. A comparison of the computed and experimental pK_a values of 16 oxoacids in water. The computed pK_a values were obtained at the MP2/aug-cc-pVTZ (*top*) and M06-2X/6-311++G** (*bottom*) levels of theory with solvent corrections obtained using the SMD solvation models. ZPE and thermal corrections were calculated in the gas phase at the B3LYP/6-311++G** level of theory.

Table 2.6. The computed, predicted, and experimental aqueous pK_a values of 16 oxoacids.^a

Acid	MP-2 and SMD ^b		M06-2X and SMD ^c		Expt.
	Comp.	Pred.	Comp.	Pred.	
1. Water	19.64	15.01	22.73	15.80	15.70
2. Methanol	22.10	15.55	22.78	14.91	15.54
3. Phenol	11.55	9.87	10.96	9.35	9.99
4. Formic Acid	1.32	4.36	0.97	4.64	3.77
5. Benzoic Acid	1.95	4.70	1.61	4.94	4.20
6. Acetaldoxime	15.00	11.73	15.52	11.50	11.42
7. Benzaldoxime	14.26	11.33	13.98	10.77	11.30
8. Acetohydroxamic Acid	9.24	8.63	9.67	8.74	8.70
9. Benzohydroxamic Acid	9.41	8.72	10.06	8.93	8.81
10. Nitric Acid	-7.82	-0.56	-12.01	-1.47	-1.40
11. Sulfuric Acid	-14.46	-4.13	-16.86	-3.75	-3.00
12. Phosphoric Acid	-2.31	2.41	-3.66	2.46	2.15
13. Carbonic Acid	-0.73	3.26	-1.58	3.44	3.60
14. Acetamidoxime	17.86	13.27	19.38	13.31	13.21
15. Benzamidoxime	15.13	12.37	17.73	12.54	12.36
16. Azine-Amidoxime ^{e,f}	21.59	11.80	17.04	12.21	11.98

^aThe computed and predicted pK_a values were obtained at the MP2/aug-cc-pVTZ and M06-2X/6-311++G** levels of theory with solvent corrections obtained using the SMD solvation models. ZPE and thermal corrections were calculated in the gas phase at the B3LYP/6-311++G** level of theory.

$$^b pK_a[Pred.] = 0.538 \times pK_a[Comp.]; \Delta G_{solv}^*(H^+) = -266.08 \text{ kcal/mol}$$

$$^c pK_a[Pred.] = 0.471 \times pK_a[Comp.]; \Delta G_{solv}^*(H^+) = -267.09 \text{ kcal/mol}$$

^dReference 48

^fReference 16

^fThe full name of this structure is (Z)-N-hydroxynicotinimidamide.

A recently published study demonstrated that the metal cation affinity of the amidoxime group can be enhanced by increasing electron donation to the oxime group.⁶⁶ In light of this result, the authors proposed that imidazolidine-oxime and imidazole-oxime, acids **17** and **18** in **Figure 2.6** respectively, would be promising monomer units for future generations of poly(acrylamidoxime) chelating adsorbents.⁶⁶ We found that the electron donating imidazolidine and imidazole groups did indeed substantially increase the basicity of the oximate, with computed MP2 and SMD predicted pK_a values of 14.37 and 15.27, respectively, and M06-2X and SMD predicted pK_a values of 14.30 and 14.98, respectively.

On the other hand, increasing the electron donating property of the amine functional group by substituting one proton with a methyl group had a minor effect on the acidity of the oxime functional group in amidoxime structures. For example, acid **20**, yielded a MP2 and SMD predicted pK_a value of 13.28 and a M06-2X and SMD predicted pK_a value of 13.48, which is approximately 0.01 pK_a units and 0.1 pK_a units greater in value than the predicted pK_a of acetamidoxime, respectively. Likewise, increasing the electron properties of the amine group in acetamidoximes by substituting both protons with methyl groups, acid **19**, had a minor effect on the predicted pK_a values. The MP2 and SMD protocol predicted a pK_a value of 13.32, 0.05 pK_a units greater in value than the predicted pK_a value of acetamidoxime while as the M06-2X and SMD protocol predicted a pK_a value of 12.95, 0.3 pK_a units less than the predicted pK_a of acetamidoxime, which is smaller in magnitude than the MEA of this method. On the other hand, we found that substituting an amine proton with a phenyl group, acid **21**, yielded an MP2 and SMD predicted pK_a value of 12.73 and an M06-2X and SMD predicted pK_a value of 12.69. These pK_a values are roughly 0.6 pK_a units lesser in value than the predicted pK_a value of acetamidoxime and roughly 0.3 pK_a units and 0.2 pK_a units greater in value than the predicted

pK_a value of benzamidoxime, respectively. This is likely due to the stabilizing effect the phenyl group has on the conjugate base species. The results demonstrate that substituting amine protons with simple aliphatic functional groups does not significantly change the acidity of the amidoxime functional group, while substituting amine protons with aromatic structures increases the acidity of the amidoxime functional group due to the stabilizing effect of resonance on the conjugate base species.

2.5. Conclusion

Currently, poly(acrylamidoxime) fibers are the optimum materials of mining uranium from seawater. The success of poly(acrylamidoximes) has been widely attributed to the amidoxime functional group.^{4-6, 10, 66} While the amidoxime-uranyl chelation mode has been established, a number of essential binding constants remain unclear. This is largely due to the wide range of conflicting pK_{a2} values that have been reported for the amidoxime functional group in the literature. Herein, we reported spectroscopically measured pK_{a2} values of representative amidoximes, acetamidoxime (13.21) and benzamidoxime (12.36). We then reported on the performance of 25 computational protocols for predicting the pK_a values of aqueous oxoacids and amidoximes. This investigation revealed that the choice of solvation model had great bearing on the success of the protocol. The best results were universally obtained with the SMD solvation model. Overall, the most successful computational protocol is the protocol that combines either MP2 (MEA of 0.33 pK_a units and RMSD of 0.46 pK_a units) or M06-2X optimized structures (MEA 0.35 pK_a units and RMSD of 0.45 pK_a units) with solvent effects calculated using the SMD model. Both methods are capable of predicting the pK_a values of acetamidoxime and benzamidoxime with an accuracy of better than 0.2 pK_a units. Mutual consistency of experimental and theoretical results resolves the existing controversy in assigning

the pK_a value of acetamidoxime and lends credit to the computational protocol to predict the pK_a values of promising, uncharacterized amidoxime ligands. We found that substituting amine protons with simple aliphatic functional groups has a minor effect on the acidity of the amidoxime functional group, while substituting amine protons with aromatic structures increases the acidity of the amidoxime functional group due to the stabilizing effect of resonance on the conjugate base species. However, we found that substituting the amine functional group with an electron-donating cyclic imide, such as imidazolidine and imidazole, did indeed substantially decrease the acidity of the oxime functional group. Hence, our study provides a convenient means for designing and screening suitable amidoxime monomers for future generations of poly(acrylamidoxime) adsorbents.

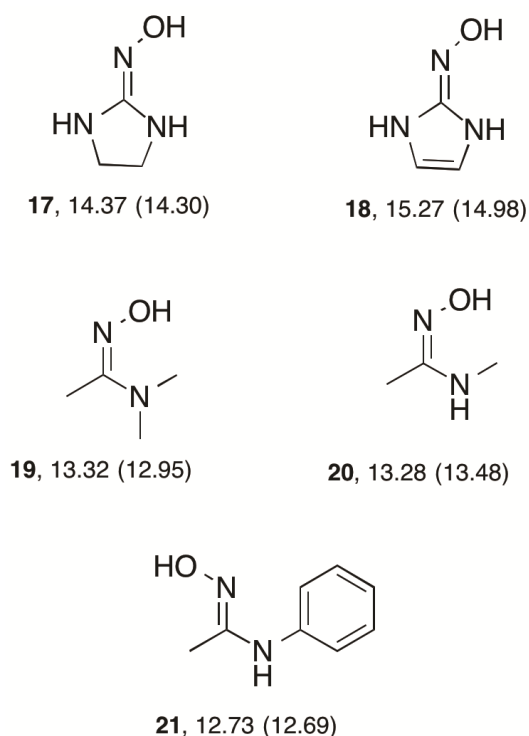


Figure 2.6. The pK_a values in water computed at the MP2/aug-cc-pVTZ and the M06-2X/6-311++G** (in parentheses) level of theory with solvent corrections obtained using the SMD solvation model. ZPE and thermal corrections were obtained at the B3LYP/6-311++G** level of theory.

References

1. Davies, R. V.; Kennedy, J.; McIlroy, R. W.; Spence, R.; Hill, K. M., Extraction of Uranium from Sea Water. *Nature* **1964**, *203*, 1110-1115.
2. Saito, K.; Miyauchi, T., Chemical Forms of Uranium in Artificial Seawater. *J. Nucl. Sci. Technol.* **1982**, *19*, 145-150.
3. Choppin, G. R., Soluble Rare Earth and Actinide Species in Seawater. *Mar. Chem.* **1989**, *28*, 19-26.
4. Kim, J.; Tsouris, C.; Mayes, R. T.; Oyola, Y.; Saito, T.; Janke, C. J.; Dai, S.; Schneider, E.; Sachde, D., Recovery of Uranium from Seawater: A Review of Current Status and Future Research Needs. *Sep. Sci. Technol.* **2012**, *48* (3), 367-387.
5. Schenk, H. J.; Astheimer, L.; Witte, E. G.; Schwochau, K., Development of Sorbers for the Recovery of Uranium from Seawater. 1. Assessment of Key Parameters and Screening Studies of Sorber Materials. *Sep. Sci. Technol.* **1982**, *17* (11), 1293-1308.
6. Astheimer, L.; Schenk, H. J.; Witte, E. G.; Schwochau, K., Development of Sorbers for the Recovery of Uranium from Seawater. Part 2. The Accumulation of Uranium from Seawater by Resins Containing Amidoxime and Imidoxime Functional Groups. *Sep. Sci. Technol.* **1983**, *18*, 307-339.
7. Sodaye, H.; Nisan, S.; Poletiko, C.; Prabhakar, S.; Tewari, P. K., Extraction of Uranium from the Concentrated Brine Rejected by Integrated Nuclear Desalination Plants. *Desalination* **2009**, *235* (1-3), 9-32.
8. Kawai, T.; Saito, K.; Sugita, K.; Katakai, A.; Seko, N.; Sugo, T.; Kawakami, T.; Kanno, J., Comparison of Amidoxime Adsorbents Prepared by Cograftering Methacrylic Acid and 2-Hydroxyethyl Methacrylate with Acrylonitrile onto Polyethylene. *Ind. Eng. Res. Chem.* **2000**, *39*, 2910-2915.

9. Kawai, T.; Saito, K.; Sugita, K.; Kawakami, T.; Kanno, J.; Katakai, A.; Seko, N.; Sugo, T., Preparation of Hydrophilic Amidoxime Fibers by Cograftering Acrylonitrile and Methacrylic Acid from an Optimized Monomer Composition. *Radiat. Phys. Chem.* **2000**, *59*, 405-411.
10. Vukovic, S.; Watson, L. A.; Kang, S. O.; Custelcean, R.; Hay, B. P., How Amidoximate Binds the Uranyl Cation. *Inorg. Chem.* **2012**, *51* (6), 3855-3859.
11. Hay, B. P.; Chagnes, A.; Cote, A. G., On the Metal Ion Selectivity of Oxoacid Extractants. *Solvent Extr. Ion Exch.* **2013**, *31*, 95-105.
12. Dürüst, N.; Akay, M. A.; Dürüst, Y.; Kiliç, E., Protonation Constants of Some N-Substituted Amidoximes in a 50% Ethanol-Water Mixture (v/v). *Anal. Sci.* **2001**, *16*, 825-827.
13. Hirotsu, T.; Katoh, S.; Sugasaka, K.; Seno, M.; Itagaki, T., Binding Ability of Acetamide Oxime with Proton, Copper(II), and Dioxouranium(VI) in Aqueous Solutions. *J. Chem. Soc., Dalton Trans.* **1986**, (8), 1609-1611.
14. Bunton, C. A.; Nelson, S. E.; Quan, C., Micellar Effects Upon Dephosphorylation by Amidoximes. *J. Org. Chem.* **1982**, *47*, 1157-1160.
15. Aubort, J. D.; Hudson, R. F., Enhanced reactivity of nucleophiles: orbital symmetry and the so-called "[small alpha]-effect". *J. Chem. Soc. D: Chem. Comm.* **1970**, (15), 937-938.
16. Simanenko, Y. S.; Prokop'eva, T. M.; Belousova, I. A.; Popov, A. F.; Karpichev, E. A., Amidoximes as Effective Acceptors of Acyl Group. *Theor. Exp. Chem.* **2001**, *37*, 288-295.
17. Hohenberg, P.; Kohn, W., Inhomogeneous Electron Gas. *Phys. Rev.* **1964**, *136*, B864-B871.
18. Kohn, W.; Sham, L. J., Self-Consistent Equations Including Exchange and Correlation Effects. *Phys. Rev.* **1965**, *140*, A1133-A1138.

19. Møller, C.; Plesset, M. S., Note on an Approximation Treatment for Many-Electron Systems. *Phys. Rev.* **1934**, *46*, 618-22.
20. Head-Gordon, M.; Pople, J. A.; Frisch, M. J., MP2 Energy Evaluation by Direct Methods *Chem. Phys. Lett.* **1988**, *153*, 503-506.
21. Purvis, G. D.; Bartlett, R. J., A Full Coupled- Cluster Singles and Doubles Model: The Inclusion of Disconnected Triples. *J. Chem. Phys.* **1982**, *76*, 1910-1918.
22. Raghavachari, K.; Trucks, G. W.; Pople, J. A.; Head-Gordon, M., A Fifth-Order Perturbation Comparison of Electron Correlation Theories. *Chem. Phys. Lett.* **1989**, *157*, 479-483.
23. Watts, J. D.; Gauss, J.; Bartlett, R. J., Coupled- Cluster Methods with Noniterative Triple Excitations for Restricted Open- Shell Hartree–Fock and Other General Single Determinant Reference Functions. Energies and Analytical Gradients. *J. Chem. Phys.* **1993**, *98*, 8718-8733.
24. Zhao, Y.; Truhlar, D. G., The M06 Suite of Density Functionals for Main Group Thermochemistry, Thermochemical Kinetics, Noncovalent Interactions, Excited States, and Transition Elements: Two New Functionals and Systematic Testing of Four M06-Class Functionals and 12 Other Functionals. *Theor. Chem. Acc.* **2008**, *120*, 215-241.
25. Marenich, A. V.; Cramer, C. J.; Truhlar, D. G., Universal Solvation Model Based on Solute Electron Density and a Continuum Model of the Solvent Defined by the Bulk Dielectric Constant and Atomic Surface Tensions. *J. Phys. Chem. B* **2009**, *113*, 6378-6396.
26. Kovács, D.; Wölfling, J.; Szabó, N.; Szécsi, M.; Kovács, I.; Zupkó, I.; Frank, É., An Efficient Approach to Novel 17-5'-(1',2',4')-Oxadiazolyl Androstenes via the Cyclodehydration of Cytotoxic O-Steroidacylamidoximes, and an Evaluation of Their Inhibitory Action on 17 α -Hydroxylase/C17,20-Lyase. *Eur. J. Med. Chem.* **2013**, *70*, 649-660.

27. García-Álvarez, R.; Díaz-Álvarez, A. E.; Borge, J.; Crochet, P.; Cadierno, V., Ruthenium-Catalyzed Rearrangement of Aldoximes to Primary Amides in Water. *Organometallics* **2012**, *31*, 6482-6490.
28. Billo, E. J., *EXCEL for Chemists*. 2 ed.; Wiley-CH: New York, 2001.
29. Bryantsev, V. S., Predicting the Stability of Aprotic Solvents in Li-Air Batteries: pK_a Calculations of Aliphatic C-H Acids in Dimethyl Sulfoxide. *Chem. Phys. Let.* **2013**, *558*, 42-47.
30. Bryantsev, V. S.; Diallo, M. S.; Goddard III, W. A., pK_a Calculations of Aliphatic Amines, Diamines, and Aminoamides via Density Functional Theory with a Poisson-Boltzmann Continuum Solvent Model. *J. Phys. Chem. A* **2007**, *111*, 4422-4430.
31. Kelly, C. P.; Cramer, C. J.; Truhlar, D. G., Aqueous Solvation Free Energies of Ions and Ion–Water Clusters Based on an Accurate Value for the Absolute Aqueous Solvation Free Energy of the Proton. *J. Phys. Chem. B* **2006**, *110*, 16066–16081.
32. Frisch, M. J.; Trucks, G. W.; Schlegel, H. B.; Scuseria, G. E.; Robb, M. A.; Cheeseman, J. R.; Scalmani, G.; Barone, V.; Mennucci, B.; Petersson, G. A.; Nakatsuji, H.; Caricato, M.; Li, X.; Hratchian, H. P.; Izmaylov, A. F.; Bloino, J.; Zheng, G.; Sonnenberg, J. L.; Hada, M.; Ehara, M.; Toyota, K.; Fukuda, R.; Hasegawa, J.; Ishida, M.; Nakajima, T.; Honda, Y.; Kitao, O.; Nakai, H.; Vreven, T.; Montgomery, J. A., Jr. ; Peralta, J. E.; Ogliaro, F.; Bearpark, M.; Heyd, J. J.; Brothers, E.; Kudin, K. N.; Staroverov, V. N.; Kobayashi, R.; Normand, J.; Raghavachari, K.; Rendell, A.; Burant, J. C.; Iyengar, S. S.; Tomasi, J.; Cossi, M.; Rega, N.; Millam, M. J.; Klene, M.; Knox, J. E.; Cross, J. B.; Bakken, V.; Adamo, C.; Jaramillo, J.; Gomperts, R.; Stratmann, R. E.; Yazyev, O.; Austin, A. J.; Cammi, R.; Pomelli, C.; Ochterski, J. W.; Martin, R. L.; Morokuma, K.; Zakrzewski, V. G.; Voth, G. A.; Salvador, P.; Dannenberg, J. J.; Dapprich, S.;

Daniels, A. D.; Farkas, Ö.; Foresman, J. B.; Ortiz, J. V.; Cioslowski, J.; Fox, D. J. *Gaussian 09 Revision D.01*, Gaussian, Inc.: Wallingford, CT, 2009.

33. Valiev, M.; Bylaska, E. J.; Govind, N.; Kowalski, K.; Straatsma, T. P.; van Dam, H. J. J.; Wang, D.; Nieplocha, J.; Apra, E.; Windus, T. L.; de Jong, W. A., NWChem: A Comprehensive and Scalable Open-Source Solution for Large Scale Molecular Simulations. *Comput. Phys. Commun.* **2010**, *181*, 1477-1489.

34. Becke, A. D., Density-Functional Thermochemistry. III. The Role of Exact Exchange. *J. Chem. Phys.* **1993**, *98*, 5648–5652.

35. Lee, C.; Yang, W.; Parr, R. G., Development of the Colle-Salvetti Correlation-Energy Formula Into a Functional of the Electron Density. *Phys. Rev. B* **1988**, *37*, 785–789.

36. Andersson, M. P.; Uvdal, P., New Scale Factors for Harmonic Vibrational Frequencies Using the B3LYP Density Functional Method with the Triple- ζ Basis Set 6-311+G(d,p). *J. Phys. Chem. A* **2005**, *109*, 2937-2941.

37. Koch, H.; Fernández, B.; Christiansen, O., The Benzene–Argon Complex: A Ground and Excited State Ab Initio Study. *J. Chem. Phys.* **1998**, *108*, 2784-2790.

38. Cancès, E.; Mennucci, B.; Tomasi, J., A New Integral Equation Formalism for the Polarizable Continuum Model: Theoretical Background and Applications to Isotropic and Anisotropic Dielectrics. *J. Chem. Phys.* **1997**, *107*, 3032-3041.

39. Mennucci, B.; Cancès, E.; Tomasi, J., Evaluation of Solvent Effects in Isotropic and Anisotropic Dielectrics and in Ionic Solutions with a Unified Integral Equation Method: Theoretical Bases, Computational Implementation, and Numerical Applications. *J. Phys. Chem. B* **1997**, *101* (49), 10506-10517.

40. Cancès, E.; Mennucci, B., New Applications of Integral Equations Methods for Solvation Continuum Models: Ionic Solutions and Liquid Crystals. *J. Mat. Chem.* **1998**, *23*, 309-326.
41. Barone, V.; Cossi, M., Quantum Calculation of Molecular Energies and Energy Gradients in Solution by a Conductor Solvent Model. *J. Phys. Chem. A* **1998**, *102*, 1995-2001.
42. Cossi, M.; Rega, N.; Scalmani, G.; Barone, V., Energies, Structures, and Electronic Properties of Molecules in Solution with the C-PCM Solvation Model. *J. Comp. Chem.* **2003**, *24*, 669-681.
43. Klamt, A.; Schuurmann, G., COSMO: A New Approach to Dielectric Screening in Solvents with Explicit Expressions for the Screening Energy and Its Gradient. *J. Chem. Soc. Perkin Trans. 2* **1993**, (5), 799-805.
44. Chipman, D. M., Charge Penetration in Dielectric Models of Solvation. *J. Chem. Phys.* **1997**, *106*, 10194-10206.
45. Zhan, C.-G.; Bentley, J.; Chipman, D. M., Volume Polarization in Reaction Field Theory. *J. Chem. Phys.* **1998**, *108*, 177-192.
46. Chipman, D. M., New Formulation and Implementation for Volume Polarization in Dielectric Continuum Theory. *J. Chem. Phys.* **2006**, *124*, 224111.
47. Schmidt, M. W.; Baldridge, K. K.; Boatz, J. A.; Elbert, S. T.; Gordon, M. S.; Jensen, J. H.; Koseki, S.; Matsunaga, N.; Nguyen, K. A.; Su, S.; Windus, T. L.; Dupuis, M.; Montgomery Jr, J. A., General Atomic and Molecular Electronic Structure System. *J. Comput. Chem.* **1993**, *14*, 1347-1363.
48. Martell, A. E.; Hancock, R. D., *Metal Complexes in Aqueous Solutions*. Plenum Press: New York, 1996.

49. Tsukube, H. F., Hiroyuki; Odani, Akira; Takeda, Yasuyuki; Kudo, Yoshihiro; Inoue; Yoshihisa; Liu, Yu; Sakamoto, Hidefumi; Kimura, Keichi, Determination of Stability Constants. In *Comprehensive Supramolecular Chemistry*, Lehn, J. M. A., J.L.; Davis, J. E. D.; MacNicol, D. D.; Vogtle, F.; , Ed. Pergamon: New York, 1996; Vol. 8.
50. Contescu, C.; Popa, V. T.; Miller, J. B.; Ko, E. I.; Schwarz, J. A., Proton Affinity Distributions of $\text{TiO}_2\text{-SiO}_2$ and $\text{ZrO}_2\text{-SiO}_2$ Mixed Oxides and Their Relationship to Catalyst Activities for 1-Butene Isomerization. *J. Catal.* **1995**, *157*, 244-258.
51. Hancock, R. D., Molecular Mechanics Calculations and Metal Ion Recognition. *Acc. Chem. Res.* **1990**, *23*, 253-257.
52. Zhao, Y.; Truhlar, D. G., A new local density functional for main-group thermochemistry, transition metal bonding, thermochemical kinetics, and noncovalent interactions. *J. Chem. Phys.* **2006**, *125*, 194101.
53. NIST Chemistry Webbook. NIST: Gaithersburg, MD, 2005. <http://webbook.nist.gov/chemistry/>.
54. Bryantsev, V. S.; Diallo, M. S.; van Duin, A. C. T.; Goddard, W. A., Evaluation of B3LYP, X3LYP, and M06-Class Density Functionals for Predicting the Binding Energies of Neutral, Protonated, and Deprotonated Water Clusters. *J. Chem. Theory Comput.* **2009**, *5*, 1016-1026.
55. Smith, R. M.; Martell, A. E., *Critical Stability Constants*. Plenum Press: New York, 1981.
56. Klamt, A.; Eckert, F.; Diedenhofen, M.; Beck, M. E., First Principles Calculations of Aqueous pK_a Values for Organic and Inorganic Acids Using COSMO-RS Reveal an Inconsistency in the Slope of the pK_a Scale. *J. Phys. Chem. A* **2003**, *107*, 9380-9386.

57. Eckert, F.; Leito, I.; Kaljurand, I.; Kütt, A.; Klamt, A.; Diedenhofen, M., Prediction of acidity in acetonitrile solution with COSMO-RS. *J. Comput. Chem.* **2009**, *30*, 799-810.
58. Liptak, M. D.; Shields, G. C., Accurate pK_a Calculations for Carboxylic Acids Using Complete Basis Set and Gaussian-n Models Combined with CPCM Continuum Solvation Methods. *J. Am. Chem. Soc.* **2001**, *123*, 7314-7319.
59. Liptak, M. D.; Gross, K. C.; Seybold, P. G.; Feldgus, S.; Shields, G. C., Absolute pK_a Determinations for Substituted Phenols. *J. Am. Chem. Soc.* **2002**, *124*, 6421-6427.
60. Shields, G. C.; Seybold, P. G., *Computational Approaches for the Prediction of pK_a Values*. CRC Press: Boca Raton, FL, 2013; p 175.
61. Amado, A. M.; Fiuza, S. M.; Batista de Carvalho, L. A. E.; Ribeiro-Claro, P. J. A., On the Effects of Changing Gaussian Program Version and SCRF Defining Parameter: Isopropylamine as a Case Study. *Bull. Chem. Soc. Jpn.* **2012**, *85*, 962-975.
62. Cramer, C. J., *Essentials of Computational Chemistry: Theories and Models*. 2 ed.; John Wiley & Sons Ltd: Chichester, West Sussex, England, 2004.
63. Barone, V.; Cossi, M.; Tomasi, J., A New Definition of Cavities for the Computation of Solvation Free Energies by the Polarizable Continuum Model. *J. Chem. Phys.* **1997**, *107*, 3210.
64. Marenich, A. V.; Ding, W.-D.; Cramer, C. J.; Truhlar, D. G., Resolution of a Challenge for Solvation Modeling: Calculation of Dicarboxylic Acid Dissociation Constants Using Mixed Discrete-Continuum Solvation Models. *J. Phys. Chem. Lett.* **2012**, *3*, 1437-1442.
65. Pliego, J. R., Jr.; Riveros, J. M., The Cluster-Continuum Model for the Calculation of the Solvation Free Energy of Ionic Species. *J. Phys. Chem. A* **2001**, *105*, 7241-7247.
66. Abney, C. W.; Liu, S.; Lin, W.-B., Tuning Amidoximate to Enhance Uranyl Binding: A Density Functional Theory Study. *J. Phys. Chem. A* **2013**, *117*, 11558-11565.

Chapter 3 : Theoretical Study of the Coordination Behavior of Formate and Formamidoximate with Dioxovanadium (V) Cation: Implications for Selectivity towards Uranyl

A version of this chapter was originally published by Nada Mehio, J. Casey Johnson, Sheng Dai, and Vyacheslav S. Bryantsev in *Physical Chemistry Chemical Physics*:

Mehio, N.; Johnson, J. C.; Dai, S.; Bryantsev, V. S. "Theoretical Study of the Coordination Behavior of Formate and Formamidoximate with Dioxovanadium (V) Cation: Implications for Selectivity towards Uranyl." *Phys. Chem. Phys. Chem.* **2015**, 17, 31715-31726.

Abstract

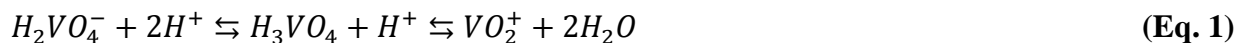
Poly(acrylamidoxime)-based fibers bearing random mixtures of carboxylate and amidoxime groups are the most widely utilized materials for extracting uranium from seawater. However, the competition between uranyl (UO_2^{2+}) and vanadium ions poses a significant challenge to the industrial mining of uranium from seawater using the current generation of adsorbents. To design more selective adsorbents, a detailed understanding of how major competing ions interact with carboxylate and amidoxime ligands is required. In this work, we employ density functional theory (DFT) and wave-function methods to investigate potential binding motifs of the dioxovanadium ion, VO_2^+ , with water, formate, and formamidoximate ligands. Employing higher level of theory calculations (CCSD(T)) resolve the existing controversy between the experimental results and previous DFT calculations for the structure of the hydrated VO_2^+ ion. Consistent with the EXAFS data, CCSD(T) calculations predict higher stability of the distorted octahedral geometry of $\text{VO}_2^+(\text{H}_2\text{O})_4$ compared to the five-coordinate complex with a single water molecule in the second hydration shell, while all seven tested DFT methods yield the reverse stability of the two conformations. Analysis of the relative stabilities of formate- VO_2^+ complexes indicates that both monodentate and bidentate forms may coexist in thermodynamic equilibrium in solution. Investigations of VO_2^+ coordination with the formamidoximate anion has revealed the existence of seven possible binding motifs, four of which are within ~ 4.0

kcal/mol of each other. Calculations establish that the most stable binding motif entails the coordination of oxime oxygen and amide nitrogen atoms via a tautomeric rearrangement of amidoxime to imino hydroxylamine. The difference in the most stable VO_2^+ and UO_2^{2+} binding conformation has important implications for the design of more selective UO_2^{2+} ligands.

3.1 Introduction

Due to the high carbon emissions associated with the diminishing global supply of fossil fuels, there has been great interest in developing alternative sources of energy. In light of this interest, extensive research efforts spanning multiple decades have focused on developing a commercial method for mining uranium from seawater.¹ While there is an estimated 4.5 billion tons of uranium dissolved in seawater, largely in the form of uranyl tricarbonate,²⁻⁴ $\text{UO}_2(\text{CO}_3)_3^{4-}$, there are a number of challenges associated with developing an adsorbent material capable of extracting uranium from seawater. These challenges primarily stem from the fact that UO_2^{2+} is present in very low concentrations, roughly 3 ppb,² while numerous competing metal cations are at much higher concentrations.⁴ Currently, poly(acrylamidoxime) fibers are the most widely utilized adsorbents for mining uranium from seawater. Poly(acrylamidoximes) were first identified in a screening of 200 organic polymers as the only adsorbent capable of extracting UO_2^{2+} from pH 8.3 aqueous solutions, the approximate pH of seawater.^{5, 6} However, poly(acrylamidoxime) fibers are not perfectly selective towards UO_2^{2+} in seawater. In particular, one of the greatest challenges associated with the commercial use of poly(acrylamidoxime) fibers is the competition between UO_2^{2+} and vanadium ions.⁷ In addition to reducing the UO_2^{2+} capacity of poly(acrylamidoxime) fibers, vanadium cations bind so strongly that stripping the cations irreversibly damages the adsorbent.^{1, 8} Due to the near order of magnitude difference in concentrations in seawater, this paper we will focus on vanadium(V) species rather than

vanadium(IV).^{7, 9} More specifically, the orthovanadate ion, H_2VO_4^- , is in equilibrium with the pervanadyl ion, VO_2^+ , in aqueous solutions:



However, in slightly basic conditions, such as seawater, the orthovanadate is the dominant species. Nevertheless, the equilibrium can be shifted to the right in the presence of organic ligands capable of interacting with the VO_2^+ cation.⁷⁻⁹ For example, Rogers et al.¹⁰ demonstrated that an amidoximate- VO_2^+ complex can be crystallized from neutral solutions. Thus, understanding how poly(acrylamidoxime) fibers interact with the VO_2^+ cation is essential for the rational design of subsequent generations of chelating polymer adsorbents.

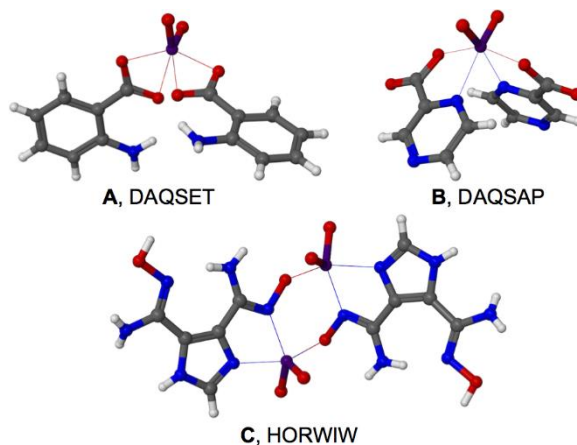


Figure 3.1. Crystal structures of amidoximate- VO_2^+ and carboxylate- VO_2^+ complexes. The DAQSET complex and the DAQSAP complex are representative of the two carboxylate- VO_2^+ binding modes observed in the CSD. The HORWIW complex is the only reported amidoximate- VO_2^+ crystal structure.

Current state-of-the-art adsorbents based on poly(acrylamidoxime) fibers are based on a random copolymer of carboxylate and amidoxime monomers at a 40:60 monomer ratio, respectively.^{11, 12} Therefore, in order for the interactions between poly(acrylamidoximes) and

VO₂⁺ cations to be understood, the binding motif of simple, representative carboxylate and amidoxime ligands with VO₂⁺ needs to be established. While a wide variety of carboxylate-VO₂⁺ crystal structures can be found in the Cambridge Structural Database (CSD),¹³ only two crystal structures with pure carboxylate binding motifs can be found. One of these crystal structures, DAQSET,¹⁴ is illustrated in **Figure 3.1.A**. The majority of the carboxylate-VO₂⁺ crystal structures exhibit a mixed binding motif consisting of a monodentate-carboxylate and an amine nitrogen, a pyridine nitrogen, or an ether oxygen chelate. An example of one of these mixed chelate structures, DAQSAP,¹⁴ is illustrated in **Figure 3.1.B**. Moreover, the coordination number of the carboxylate-monoVO₂⁺ crystal structures reported on the CSD varied between five and six. A coordination number five was observed if the carboxylate ligand was rigid, sterically strained, or contained electron withdrawing groups. Furthermore, although Rogers et al.¹⁰ demonstrated the formation of a dimeric complex of a 4,5-di(amidoxime)-functionalized imidazole ligand with the VO₂⁺ ion (HORWIW, **Figure 3.1.C**), the binding motifs with pure amidoxime ligands to VO₂⁺ have yet to be established.

In addition to the various ligand-VO₂⁺ binding motifs, there is also a disagreement between the experimental and density functional theory (DFT) calculations for the structure of the hydrated VO₂⁺ ion. Extended X-ray absorption fine structure (EXAFS) and large-angle X-ray scattering (LAXS) data show that the hydrated VO₂⁺ ion adopts a very distorted octahedral configuration.¹⁵ In contrast, static B3LYP calculations suggested that the first shell hydration structure for VO₂⁺ consisted of only three water molecules.¹⁶ Furthermore, Car-Parinello molecular dynamics (MD) simulations performed using the BP86 density functional predicted the hydrated VO₂⁺ structure to be approximately an equal mixture of the five- and six-coordinate

structures.¹⁷ The application of higher levels of theory is crucial to resolve the inconsistency of experimental and theoretical results.

Herein, we report the results of a computational investigation of the interactions of the dioxovanadium (V) ion, VO_2^+ with formate and formamidoximate anions. The chosen ligands are small enough that high-level *ab initio* calculations are readily performed. To resolve the discrepancy between the experimental¹⁵ and computed^{16, 17} structures of hydrated VO_2^+ complexes, we used as benchmarks calculated relative energies obtained at the coupled-cluster theory with single, double, and perturbative triple excitations (CCSD(T)) in the aug-cc-pVDZ basis set. Calculations at various levels of theory, such as CCSD(T)/aug-cc-pVDZ, MP2/aug-cc-pVQZ, and several DFT/aug-cc-pVDZ methods including Grimme's DFT-D3 dispersion correction were applied to identify how carboxylate and amidoximate ligands interact with the VO_2^+ ion. This understanding provides an important step for developing a computational protocol for predicting the log K values for the formation of VO_2^+ complexes and lays the foundation for the rational design of ligands that are more selective for the UO_2^{2+} ion.

3.2. Methods

Electronic structure calculations were carried out using the Gaussian 09 Revision D.01¹⁸ and NWChem 6.5 software packages.¹⁹ CCSD(T) calculations²⁰⁻²² were employed with the aug-cc-pVDZ basis set^{23, 24} to determine the benchmark relative energies of VO_2^+ complexes, in which Moller-Plesset perturbation theory (MP2) method^{25, 26} and density functionals^{27, 28} are evaluated against. Geometry optimizations were performed at the MP2 and DFT levels using the aug-cc-pVDZ basis set, except for the bare VO_2^+ cation, where the highest level of theory used

was CCSD(T)/aug-cc-pVTZ. Only the valence electrons on C, N, and O and the subvalence electrons (3s, 3p) on V were correlated in the MP2 and CCSD(T) calculations.

We used a family of augmented correlation-consistent basis sets^{23, 24} (aug-cc-pVnZ, $n =$ D, T, Q) for the basis set expansion in the MP2 calculations. The CCSD(T) binding energies at the aug-cc-pVQZ level of theory were estimated with the following equations:

$$\text{CCSD(T)} + \delta\text{MP2} = \Delta\text{E}(\text{CCSD(T)}/\text{aug-cc-pVDZ} // \text{MP2}/\text{aug-cc-pVDZ}) + \delta\text{MP2} \quad (\text{Eq. 2})$$

$$\delta\text{MP2} = \Delta\text{E}(\text{MP2}/\text{aug-cc-pVQZ} // \text{MP2}/\text{aug-cc-pVDZ}) - \Delta\text{E}(\text{MP2}/\text{aug-cc-pVDZ}) \quad (\text{Eq. 3})$$

Zero-point energies (ZPE) and thermal corrections were obtained at the MP2 level without scaling using the effective core potential (ECP)²⁹⁻³² LANL2TZ basis set for vanadium and the 6-311++G(d,p) basis set for the other atoms.

While there is a general consensus that DFT is better suited than MP2 for the study of open-shelled systems involving metal ion center,³³ the performance of MP2 for closed-shell systems involving a metal ion center remains unclear. In order to determine the optimal level of theory for studying these systems, we examined the ability of seven density functionals to reproduce the benchmark electronic binding energies (CCSD(T) + δMP2) of VO_2^+ complexes. The density functionals tested include one Generalized Gradient Approximation (GGA) functional (PBE^{34, 35}), three hybrid GGA functionals (B3LYP,^{36, 37} ωB97xD ,^{38, 39} and B97D3^{40, 41}), two local meta-GGA functional (M06-L⁴² and TPSS⁴³), and one hybrid meta-GGA functional (M06⁴²). The aug-cc-pVDZ basis set was employed in all DFT calculations. We found that DFT and MP2 methods could give different geometries of VO_2^+ complexes, where in some cases the six-coordinate complexes were stationary point only at the MP2 level and four-coordinate complexes were stationary points only at the DFT level. In light of this discrepancy, Grimme's D3 dispersion corrections⁴⁴ were applied to B3LYP, PBE, TPSS, and M06-L density functionals

to provide a better account of noncovalent interactions. Single-point CCSD(T)/aug-cc-pVDZ calculations using MP2/aug-cc-pVDZ and B3LYP/aug-cc-pVDZ geometries were performed to determine the sensitivity of the CCSD(T) relative energies to changes in geometries of VO_2^+ complexes obtained at different levels of theory.

A transition state search with the B3LYP/aug-cc-pVDZ method was performed using a standard Berny algorithm implemented in Gaussian,¹⁸ starting from the partially optimized geometry at the same level of theory along the chosen reaction coordinate and the precalculated Hessian. Intrinsic reaction coordinate calculations (IRC) were performed to ensure that transition-state structures connect their respective reactants and products.

Using the gas phase geometries obtained at the MP2/aug-cc-pVDZ level, implicit solvent corrections were obtained with the IEF-PCM model⁴⁵⁻⁴⁷ in Gaussian 09, using the default atomic radii of the universal force field (UFF). Electronic energies in the solvent reaction field were computed using the ECP LANL2TZ basis set for vanadium and the 6-31+G(d) basis set for the other atoms. Relative energies in aqueous solutions were reported by combining electronic energies at the CCSD(T)/aug-cc-pVDZ + δMP2 level of theory, with ZPE and thermal corrections obtained at the MP2/LANL2TZ(V)/6-311++G(d,p) level and the solvation energies calculated using the IEF-PCM solvation model.

3.3. Results and Discussion

As noted in the Introduction, there is an incompleteness of data describing the binding modes and coordination numbers of amidoximate- VO_2^+ and pure carboxylate- VO_2^+ complexes. In order to supplement this lack of data, we computationally elucidated binding modes and coordination numbers of formamidoximate- VO_2^+ and formate- VO_2^+ complexes. First, we analyzed the bonding nature in the VO_2^+ cation, which provides the foundations for

understanding the coordination properties of this oxoion, in addition to highlighting the potential limitations of the MP2 and DFT methods in predicting the structure of VO_2^+ complexes. Second, we resolved the discrepancy between the experimental results and previous DFT calculations for the structure of the hydrated VO_2^+ cation. Next, we determined the optimal coordination numbers and binding modes of formate- VO_2^+ and formamidoxime- VO_2^+ complexes. Finally, corroborated by crystal structure analysis, the theoretical results suggest a strategy for the design of amidoxime ligands that are more selective toward the uranyl ion.

3.3.1. VO_2^+ Cation in the Gas Phase

To lay the groundwork for a clear understanding of the potential ligand binding motifs, it is necessary to first understand the structure and electronic properties of the bare VO_2^+ cation. Due to the absence of an experimental VO_2^+ gas phase geometry, the structural properties, i.e. bond distances and angles, are obtained from the CCSD(T) optimized structure and used as benchmarks against the DFT and MP2 predicted structure. As seen in **Table 3.1**, the MP2 optimized structures overestimate the $\text{V}=\text{O}$ bond distance while underestimating the $\text{O}=\text{V}=\text{O}$ bond angle, whereas the DFT optimized structures underestimate the $\text{V}=\text{O}$ bond distance and overestimate the $\text{O}=\text{V}=\text{O}$ bond angle. Consequentially, MP2 leads to an overestimation of the coordination number for VO_2^+ , while DFT leads to an underestimation of the coordination number for VO_2^+ .

Figure 3.2 shows the five highest occupied molecular orbitals (HOMOs) obtained at the B3LYP/aug-cc-pVDZ level of theory, illustrating the vanadium and oxygen bonding nature. HOMO-5 represents a σ bond between oxygen p_y and vanadium $d_{x^2-y^2}$ atomic orbitals (AOs). An additional σ bond is seen in HOMO-4, formed from the oxygen p_x and the vanadium d_{xy} AOs. HOMO-3 and HOMO-2 represent π bonds between oxygen p_z and vanadium d_{xz} and d_{yz}

AOs, respectively. HOMO-1 represents a weakly bonding interaction between oxygen p_x vanadium d_{z^2} AOs and, finally, the HOMO represents non-bonding oxygen p_y AOs.

Table 3.1. Geometrical parameters of VO_2^+ in the gas phase.^a

Theory	V=O (Å)	O=V=O (Degrees)
MP2	1.609	101.68
MP2/aug-cc-pVTZ	1.620	101.20
CCSD(T)	1.572	105.19
CCSD(T)/aug-cc-pVTZ	1.570	105.43
B3LYP	1.550	105.91
M06	1.540	105.91
M06-L	1.559	106.22
ω B97XD	1.535	106.03
B97D3	1.560	105.61
PBE-D3	1.565	105.51
TPSS-D3	1.567	105.56
M06-L-D3	1.559	106.22
B3LYP-D3	1.559	106.22

^aThe aug-cc-pVDZ basis set was employed in all calculations unless otherwise specified.

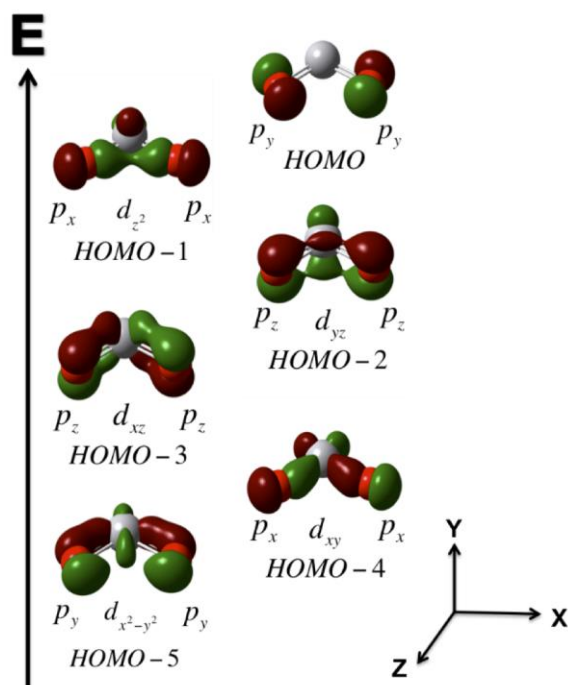


Figure 3.2. Several occupied molecular orbitals (MOs) illustrating the bonding in the VO_2^+ cation. Dominant atomic contributions to each MO are shown. The MOs were obtained at the B3LYP/aug-cc-pVDZ level of theory with an MO isovalue surface of $0.04 \text{ (e/\text{\AA}^3)}^{1/2}$.

We note that the weakly bonding HOMO-1 orbital becomes a non-bonding orbital in the octahedral complex with four water molecules. In contrast to linear UO_2^{2+} that forms two σ -bonds with $5f_z^3$ and $6d_z^2$ AOs at the angle of 180° ,⁴⁸ the availability of only d-orbitals in transition metals results in the geometry of dioxometal ions that is always bent. Moreover, comparison of the $\text{U}\equiv\text{O}$ bond in UO_2^{2+} and the $\text{V}=\text{O}$ bond in VO_2^+ reveals that the oxygen atoms in VO_2^+ are more capable of engaging in hydrogen bonded interaction than those in UO_2^{2+} ; the latter only very weakly interacts with hydrogen bond donors.⁴⁸ The extent to which the d-orbitals on vanadium are available for interaction with ligand orbitals depends on the strength of interaction with the vanadyl oxygen atoms. For example, d-orbitals involved in the formation of σ -bonds between vanadium and oxygen will be the least available for bonding with ligands. Consequentially, for VO_2^+ in a distorted octahedral geometry, ligands occupying equatorial

positions on opposite sides of the V=O bond are always more weakly bound (having longer bonds) than ligands occupying axial positions perpendicular to the VO_2^+ plane.

3.3.2. Hydrolyzed VO_2^+ Complexes

As stated in **Section 3.1**, the pervanadyl ion is not the dominant dioxovanadium (V) species in alkaline aqueous solutions, but rather in equilibrium (**Eq. 1**) with vanadic acid H_3VO_4 and the dominant orthovanadate H_2VO_4^- species.⁷⁻⁹ However, it has been demonstrated that this equilibrium can be shifted towards the VO_2^+ species in the presence of coordinating ligands.¹⁰ In order to gain a better understanding of the aqueous chemistry of dioxovanadium (V), the relative energies of hydrated and hydrolyzed $\text{VO}_2(\text{H}_2\text{O})_3^+$ complexes in the presence and absence of the formamidoximate ligand are compared. The MP2 optimized $\text{VO}_2(\text{H}_2\text{O})_3^+$ complexes and their relative CCSD(T) + δMP2 Gibbs free energies in the gas phase and in aqueous solution can be found in **Figure 3.3**. The CCSD(T) + δMP2 results are consistent with experimental data, indicating that the hydrolyzed species, $\text{H}_2\text{VO}_3(\text{H}_2\text{O})_2^+$ and $\text{H}_2\text{VO}_4(\text{H}_2\text{O})^+$, are more stable than the hydrated cation, $\text{VO}_2(\text{H}_2\text{O})_3^+$, in neutral aqueous solutions.

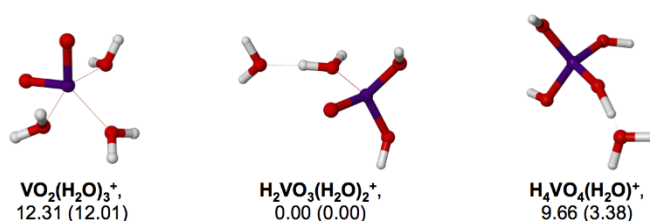


Figure 3.3. Structures of hydrated and hydrolyzed $\text{VO}_2(\text{H}_2\text{O})_3^+$ complexes and relative energies in the gas phase and in aqueous solution (in parentheses) in units of kcal/mol.

While the hydrolyzed dioxovanadium(V) species are more stable than the hydrated VO_2^+ cation in neutral aqueous solution, in the presences of a binding ligand the equilibrium can be

can be shifted towards VO_2^+ .¹⁰ To explore this potential equilibrium change, the interaction between formamidoximate and dioxovanadium(V) in aqueous solution were computationally investigated with hydrated and hydrolyzed formamidoximate-dioxovanadium(V) complexes. While the results are sensitive to the number of water molecules in the complex, below we will only discuss the results for the largest complex studied, which contains three water molecules. Accordingly, the MP2 optimized $\text{VO}_2(\text{AO})(\text{H}_2\text{O})_3$ complexes and their relative CCSD(T) + δMP2 Gibbs free energies in the gas phase and aqueous solution can be found in **Figure 3.4**. As anticipated, the results obtained from CCSD(T) + δMP2 calculations indicate that the hydrated $\text{VO}_2(\text{AO})(\text{H}_2\text{O})_3^+$ complex is more stable than the hydrolyzed $\text{H}_2\text{VO}_3(\text{AO})(\text{H}_2\text{O})_2^+$ complex. Thus, due to the consistency between experimental and computational data indicating that hydrated formamidoximate-dioxovanadium(V) complexes are more stable than their corresponding hydrolyzed complexes, in what follows we will only investigate the interactions of formate and formamidoximate ligands with the hydrated VO_2^+ cation. However, since the relative population of the two forms can strongly depend on solution pH, ligand binding strength, and the presence of other ions, further investigation of the hydrolyzed species warrants a separate study.

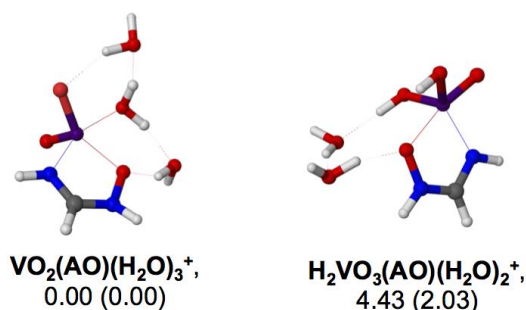


Figure 3.4. Structures of hydrated and hydrolyzed $\text{VO}_2(\text{AO})(\text{H}_2\text{O})_3$ complexes and relative energies in the gas phase and in aqueous solution (in parentheses) in units of kcal/mol.

3.3.3. Hydrated VO_2^+ Complexes

To gain insight into the discrepancy between experimental and previously computed coordination number of hydrated $\text{VO}_2(\text{H}_2\text{O})_4^+$ complexes, relative energies of five- and six-coordinate species are computed. Prior reported DFT calculations (B3LYP/6-311+G(d,p) coupled with the SMD solvation model) predicted the $\text{VO}_2(\text{H}_2\text{O})_4^+$ complex to be a five-coordinate structure,¹⁶ while Car–Parrinello molecular dynamics (MD) simulations found the hydrated VO_2^+ complex to be an equilibrium mixture of five- and six-coordinate structures.¹⁷ However, our results obtained at the CCSD(T) + δMP2 and MP2 levels are found to be in agreement with experimental EXAFS data, indicating that the six-coordinate $\text{VO}_2(\text{H}_2\text{O})_4^+$ complex is more stable than the five-coordinate $\text{VO}_2(\text{H}_2\text{O})_4^+$ conformer. The MP2 optimized $\text{VO}_2(\text{H}_2\text{O})_4^+$ complexes and their relative CCSD(T) + δMP2 Gibbs free energies in the gas phase and in aqueous solution are shown in **Figure 3.5**, while the relative electronic energies are tabulated by level of theory in **Table 3.2**.

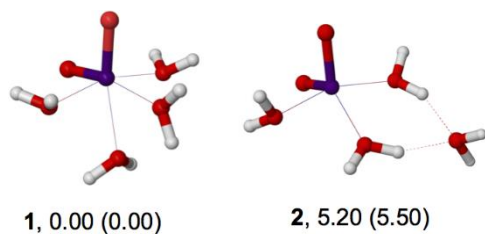


Figure 3.5. Structures of $\text{VO}_2(\text{H}_2\text{O})_4^+$ complexes and relative energies in the gas phase and in aqueous solution (in parentheses) in units of kcal/mol.

Inspecting the results further, the five-coordinate $\text{VO}_2(\text{H}_2\text{O})_4^+$ complex was favored by all density functionals except M06-L. Applying the D3 dispersion correction to B3LYP and M06-L did not significantly alter this result (<0.3 kcal/mol). However, these results are consistent with those obtained from the DFT optimization of the gas-phase VO_2^+ cation. This is

due to the underestimation of the V=O bond length by DFT, which causes an increased stability in the anti-bonding character of the vanadium *d*-orbitals, consequently decreasing the coordination number of the VO₂⁺ complexes. The M06-L density functional, which was parameterized for main-group and transition element thermochemistry, kinetics and noncovalent interactions⁴² was an exception, likely due to the closer V=O bond lengths to the CCSD(T)/aug-cc-pVTZ results. We should note that clusters with only four water molecules might be too small to accurately predict the coordination number in bulk water. Nevertheless, the use of higher levels of theory provides greater consistency between the EXAFS and computational coordination number of the hydrated VO₂⁺ ion.

3.3.4. Formate-VO₂⁺ Complexes

Next, the relative energies of pure monodentate and bidentate carboxylate-VO₂⁺ complexes are compared, in addition to investigating the preferred coordination number of simple VO₂(HCOO)(H₂O)_x complexes (*x* = 1, 2). Based on CCSD(T)/aug-cc-pVDZ + δ MP2 energies, the bidentate, five-coordinate VO₂(HCOO)(H₂O) complex is slightly preferred over the monodentate, four-coordinate VO₂(HCOO)(H₂O) complex (**Figure 3.6**). This result is consistent with the mixed carboxylate-amine, pyridine, and ether chelates observed for the majority of the carboxylate-VO₂⁺ crystals in the CSD. However, this is in direct contrast to the formation of carboxylate-UO₂²⁺ complexes; UO₂²⁺ strongly prefers bidentate coordination of carboxylate ligands about its equatorial plane.⁴⁹

Table 3.2. Relative gas phase electronic energies of five- and six-coordinate $\text{VO}_2(\text{H}_2\text{O})_4^+$ clusters in kcal/mol.^a

Theory	1 (c.n.= 6)	2 (c.n. = 5)
MP2	0.00	2.60
MP2/aug-cc-pVQZ//MP2	0.00	3.79
CCSD(T)//MP2	0.00	2.58
CCSD(T) + δ MP2	0.00	3.77
B3LYP	3.88	0.00
CCSD(T)//B3LYP	0.00	0.90
M06	0.83	0.00
M06-L	0.00	0.89
ω B97XD	2.45	0.00
B97D3	2.86	0.00
PBE-D3	2.64	0.00
TPSS-D3	1.49	0.00
M06-L-D3	0.00	0.90
B3LYP-D3	2.21	0.00

^aThe aug-cc-pVDZ basis set was employed in all calculations unless otherwise specified. c.n. denotes coordination number.

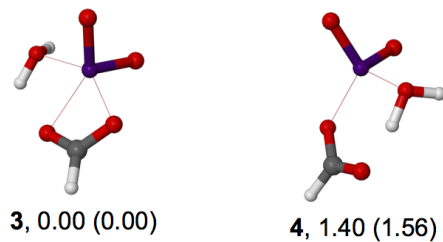


Figure 3.6. Structures of $\text{VO}_2(\text{HCOO})(\text{H}_2\text{O})$ complexes and relative energies in the gas phase and in aqueous solution (in parentheses) in units of kcal/mol.

The relative electronic energies of five- and four-coordinate $\text{VO}_2(\text{HCOO})(\text{H}_2\text{O})$ complexes are tabulated by level of theory in **Table 3.3**. With the exception of the B97D3 functional and the PBE functional with D3 corrections, the five-coordinate $\text{VO}_2(\text{HCOO})(\text{H}_2\text{O})$ complex was more stable than the four-coordinate one. Excluding the M06-L functional, all the DFT functionals underpredicted the stability of the five-coordinate $\text{VO}_2(\text{HCOO})(\text{H}_2\text{O})$ complex, which is again consistent with the underpredicted V=O bond lengths obtained from DFT. Conversely, MP2 overpredicted the stability of the five-coordinate $\text{VO}_2(\text{HCOO})(\text{H}_2\text{O})$ complex, which is consistent with the overpredicted V=O bond lengths obtained with MP2. Applying the D3 correction to the B3LYP and M06-L density functionals did not significantly alter these results (≤ 0.1 kcal/mol).

Examining the effects of adding an additional water to form $\text{VO}_2(\text{HCOO})(\text{H}_2\text{O})_2$, it is observed that the five-coordinate complex, **5**, is far more stable than the six-coordinate complex, **8** (**Figure 3.7**). Furthermore, the monodentate five-coordinate $\text{VO}_2(\text{HCOO})(\text{H}_2\text{O})_2$ complex, **7**, is less stable than the bidentate five-coordinate carboxylate complex, **5**, by ~ 4 kcal/mol. This is likely due to hydrogen bond formed between the water and the unbound oxygen on the formate anion instead of the VO_2^+ oxygen. As a result, monodentate carboxylate- VO_2^+ complexes should become more stable with additional water molecules, as they will provide additional stabilizing hydrogen bonds to both the carboxylate and the VO_2^+ cations. This hypothesis was confirmed with $\text{VO}_2(\text{HCOO})(\text{H}_2\text{O})_3$ complexes. The relative Gibbs free energies of these complexes in the gas phase and in aqueous solution can be found in **Figure A.3** of **Appendix B**. Applying the same reasoning, complex **6** is less stable than complex **5**, owing to the lack of hydrogen bonding with the VO_2^+ cation, while in complex **5**, the second water molecule is interacting with both the carboxylate oxygen and an oxygen atom on the VO_2^+ cation. Strong hydrogen-bonding ability of

oxygen atoms in VO_2^+ is consistent with the non-bonding character of one of their lone pairs (**Figure 3.2**).

Looking closer at the relative electronic energies of the five- and six-coordinate $\text{VO}_2(\text{HCOO})(\text{H}_2\text{O})_2$ complexes (**Table 3.4**), the seven density functionals employed in this study can be separated into two groups, functionals that behave like the B3LYP (ω B97XD, B97D3, PBE-D3, TPSS-D3, and B3LYP-D3) and functionals that behave like the M06 functional (M06L, M06-L-D3). Based on this grouping, DFT calculations of $\text{VO}_2(\text{HCOO})(\text{H}_2\text{O})_2$ were only carried out at the B3LYP and M06 levels of theory. Consistent with previous results, MP2 calculations overpredict the stability of the six-coordinate $\text{VO}_2(\text{HCOO})(\text{H}_2\text{O})_2$ complex, **8**, relative to the CCSD(T) prediction. Optimization of complex **8** at the CCSD/aug-cc-pVDZ level of theory resulted in a five-coordinated geometry, indicating that the six-coordinate structure is not a stationary point at this level. This result confirms that MP2 indeed significantly overestimated the stability of complex **8**. Likewise, the six-coordinate $\text{VO}_2(\text{HCOO})(\text{H}_2\text{O})_2$ complex is not stable at the B3LYP or M06 level of theory. The four-coordinate $\text{VO}_2(\text{HCOO})(\text{H}_2\text{O})_2$ complex was only located at the DFT level of theory. Single-point CCSD(T) calculations of the four-coordinate complex indicate that the stability of the complex is over-predicted at the DFT level of theory. Along these lines, DFT calculations slightly under-predicted the stability of all three five-coordinate $\text{VO}_2(\text{HCOO})(\text{H}_2\text{O})_2$ complexes. In contrast, MP2 calculations incorrectly predicted complex **5** to be less stable than complexes **6** and **7**. It appears that MP2 calculations overpredict the stability of hydrogen bonds between the oxygen atoms on carboxylate anions and water molecules.

Table 3.3. Relative gas phase electronic energies of five- and six-coordinate $\text{VO}_2(\text{HCOO})(\text{H}_2\text{O})$ in kcal/mol.^a

Theory	3 (c.n. = 5)	4 (c.n. = 4)
MP2	0.00	9.27
MP2/aug-cc-pVQZ//MP2	0.00	7.85
CCSD(T)//MP2	0.00	4.02
CCSD(T) + δ MP2	0.00	2.60
B3LYP	0.00	0.05
CCSD(T)//B3LYP	0.00	5.61
M06	0.00	2.93
M06-L	0.00	4.49
ω B97XD	0.00	1.36
B97D3	1.33	0.00
PBE-D3	0.36	0.00
TPSS-D3	0.00	1.20
M06-L-D3	0.00	4.48
B3LYP-D3	0.00	0.05

^aThe aug-cc-pVDZ basis set was employed in all calculations unless otherwise specified. c.n. denotes coordination number.

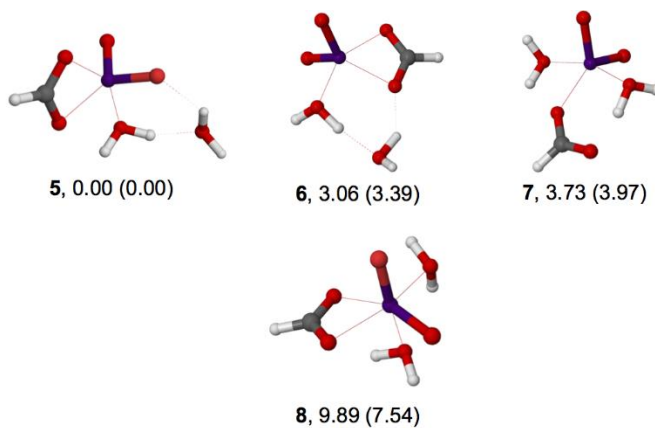
**Figure 3.7.** Structures of $\text{VO}_2(\text{HCOO})(\text{H}_2\text{O})_2$ complexes and relative energies in the gas phase and in aqueous solution (in parentheses) in units of kcal/mol.

Table 3.4. Relative gas phase electronic energies of $\text{VO}_2(\text{HCOO})(\text{H}_2\text{O})_2$ complexes in kcal/mol.^a All energies are given relative to the five-coordinate complex **5** in Figure 7.

Theory	6 (c.n. = 5)	7 (c.n. = 5)	8 (c.n. = 6)	(c.n. = 4) ^b
MP2	-1.66	-1.84	0.69	
MP2/aug-cc-pVQZ//MP2	-1.73	-1.22	0.83	
CCSD(T)//MP2	1.55	0.76	7.71	
CCSD(T) + δ MP2	1.48	1.38	7.85	
B3LYP	1.24	0.65		1.23
CCSD(T)//B3LYP	1.07	-0.51		6.70
M06	1.59	0.67		3.64

^aThe aug-cc-pVDZ basis was employed in all calculations unless otherwise specified. c.n. denotes coordination number.

^bThis structure is not illustrated in Figure 7, because it is not a stable minimum at the MP2 level of theory.

As eluded to in the discussion of $\text{VO}_2(\text{HCOO})(\text{H}_2\text{O})_2$, hydration effects will become greater with added waters. Accordingly, computations on $\text{VO}_2(\text{HCOO})(\text{H}_2\text{O})_3$ complexes were carried out at the same levels of theory as the $\text{VO}_2(\text{HCOO})(\text{H}_2\text{O})_2$ complexes (**Figure A.3** and **Table A.6** of **Appendix B**). These calculations further confirmed the higher instability of the six-coordinate complex at all levels of theory. Moreover, it was found that the five-coordinate monodentate $\text{VO}_2(\text{HCOO})(\text{H}_2\text{O})_3$ complex was energetically very similar to the five-coordinate bidentate $\text{VO}_2(\text{HCOO})(\text{H}_2\text{O})_3$ complex in aqueous solution, revealing that the average coordination mode is likely an equilibrium mixture of the two forms.

3.3.5. Formamidoximate- VO_2^+ Complexes

Moving now to the amidoxime ligand systems, the relative electronic energies of $\text{VO}_2(\text{AO})(\text{H}_2\text{O})$, $\text{VO}_2(\text{AO})(\text{H}_2\text{O})_2$, and $\text{VO}_2(\text{AO})(\text{H}_2\text{O})_3$ complexes are examined. CCSD(T) + δ MP2 energies of four- and five-coordinate $\text{VO}_2(\text{AO})(\text{H}_2\text{O})_n$ complexes are used as benchmarks

against the DFT and MP2 optimized structures. Starting with $\text{VO}_2(\text{AO})(\text{H}_2\text{O})$, surprisingly, the lowest energy complex obtained at the CCSD(T) + δMP2 level of theory was a five-coordinate amine nitrogen and oxime oxygen chelate complex **9** (**Figure 3.8**). This geometry entails a tautomeric rearrangement of the formamidoximate ligand, which leads to a structure that is ~5 kcal/mol more stable than the non-tautomeric form, **13** in aqueous solution. This indicates that the proton transfer between the amine nitrogen and the oxime nitrogen is essential to the formation of monoamidoxime- VO_2^+ complexes. Interestingly, the η^2 coordinating complexes **11** and **12** are found to be higher in energy (less stable) than the tautomeric species. This is an important result due to the fact that amidoxime- UO_2^{2+} η^2 complexes are generally more stable.⁵⁰ This has significant implications for the design of UO_2^{2+} selective ligands, a topic discussed in greater detail in the next section.

Monodentate formamidoximate- VO_2^+ complexes were investigated as well. A stable monodentate nitrogen complex, **10**, was obtained at the MP2 level. However, the monodentate oxygen complex converges into to an η^2 complex **12**. Complex **10** is less stable than complex **9** by ~1.5 kcal/mol in aqueous solution. Moreover, it should be noted that the formation of **10** entails proton transfer from the water ligand to the formamidoximate ligand. The neutralization of the formamidoximate ligand appears to have a stabilizing effect on complex **10**. Additionally, the formation of four-membered chelate rings via bidentate amine nitrogen and oxime nitrogen atoms, **15** and **14**, is far less stable than the formation of coordination modes depicted in **9-13**. Therefore, these coordination modes are not included in subsequent analysis of formamidoximate- VO_2^+ complexes.

The relative electronic energies of the four- and five-coordinate $\text{VO}_2(\text{AO})(\text{H}_2\text{O})$ complexes are tabulated by level of theory in **Table 3.5**. With the exception of complex **10**, all

calculations for $\text{VO}_2(\text{AO})(\text{H}_2\text{O})$ complexes consistent relative energies. Complex **10** is slightly more stable than **9** at the B3LYP, B97D3, and B3LYP-D3 levels (by 0.4–1.3 kcal/mol), while it is significantly less stable than **9** at the MP2 level (by 9.2–9.3 kcal/mol). Again, some overestimation of the instability of low-coordinate VO_2^+ complexes by MP2 calculations is consistent with the shorter bond lengths obtained from MP2 optimizations of bare, gas-phase VO_2^+ cations. On the other hand, DFT, MP2, and CCSD(T) predicted relative electronic energies of complexes of **9**, **12**, **13**, and **14** within 3 kcal/mol of the CCSD(T) + δMP2 value.

Next, looking at systems containing two waters, $\text{VO}_2(\text{AO})(\text{H}_2\text{O})_2$ (**Figure 3.9**), results are consistent with those found in the monohydrate complexes. Specifically, the five-coordinate amine nitrogen and oxime oxygen tautomeric chelate, **16**, is the minimum energy structure. Likewise, without the tautomeric rearrangement, structure **19** is predicted to be less stable. Again, similar to the monohydrate case, complex **18**, involving η^2 coordination, is only the third most stable complex. In addition, the complex formed from monodentate nitrogen coordination, complex **17**, is significantly more stable than the complex formed from monodentate oxygen coordination, **20**.

As mentioned in **Section 3.3.4**, the behavior of the DFT functionals employed in this study can be split into two groups, B3LYP-like and M06-like. Therefore, the B3LYP and M06 functionals were the only functionals tested for $\text{VO}_2(\text{AO})(\text{H}_2\text{O})_2$ and $\text{VO}_2(\text{AO})(\text{H}_2\text{O})_3$ complexes. MP2, CCSD(T), and DFT calculations consistently identified **16** as the most stable complex (**Table 3.6**). The relative stabilities obtained for complexes **16-20** at all levels of theory were within < 4 kcal/mol of the best method, except for **19**, where, as before B3LYP calculations overestimated the stability of the four-coordinate complex.

Finally, analyzing three water systems, the tautomerically rearranged formamidoximate ligand complex is again found to be the most stable in the structures searched (**Figure 3.10**, complex **21**). Consistent with the results of the mono- and dihydrate complexes, structure **21** is ~4 kcal/mol more stable than the alternative tautomeric form **24**. The monodentate nitrogen **22** and the five-coordinate η^2 **23** are the second and third most stable complexes, respectively. We were also able to locate the six-coordinate η^2 complex, **25**, as a local minimum, but it was highly unstable.

Compiling the relative electronic energies of the four- and five-coordinate trihydrate complexes (**Table 3.7**), it is again observed that CCSD(T), MP2 with large basis sets, and DFT calculations consistently identified **21** as the most stable complex. In regards to the six-coordinate complex, **25**, a stationary point on the MP2 potential energy surface was found, however not on the DFT potential energy surface. Given the significant instability of the complex, this structure was likely identified as a local minimum by MP2 calculations due to the tendency of MP2 to under-predict the stability of high coordination VO_2^+ complexes.

3.3.6. Implications for Ligand Design

As mentioned in **Section 3.3.5**, the most stable binding motif obtained for $\text{VO}_2(\text{AO})(\text{H}_2\text{O})_n$, complexes (**9**, **16**, **21**) was a five-coordinate amine nitrogen and oxime oxygen chelate involving a tautomeric shift of hydrogen from the amide to oxime nitrogen atom. In modeling complexation behavior of amidoximate ligands, an important question arises as to whether such tautomeric transformation is feasible in aqueous solution. The amidoxime-imino hydroxylamine tautomerization in the absence of complexing ions was investigated by Arshadi et al.⁵¹ They reported that the energy barrier for tautomerization was prohibitively high in the gas phase (33-71 kcal/mol), but could be reduced substantially in the presence of explicit solvent

molecules. Following this approach, we constructed a structural model for tautomerization of formamidoxime assisted by three water molecules, as seen in **Figure 3.11**. Consistent with the previous study,⁵¹ the amidoxime form is ~9 kcal/mol more stable than the imino hydroxylamine form. The computed free energy barrier is ~25 kcal/mol for the forward and ~16 kcal/mol for the backward reaction. Since the relative stability of the two forms when bound to VO_2^+ is the opposite of that in the case of a free ligand, the reaction barrier involving the VO_2^+ -amidoximate complex is expected to be ≤ 16 kcal/mol. **Figure 3.12** provides an illustrative example of such complex, where, in addition to VO_2^+ , five water molecules were placed into the system to adequately coordinate VO_2^+ and provide a pathway for proton transfer through a network of hydrogen bonds. We find that the transition state for the rate-limiting step lies only 9.5 kcal/mol above the initial complex, supporting very fast tautomeric proton exchange and equilibration to the most stable chelate structure.

While η^2 coordination of the oxime functional group is the most stable coordination mode of amidoximate- UO_2^{2+} complexes,⁵⁰ it is consistently found to be the third most stable coordination mode for those structures investigated. Based on these aforementioned results, it is suggested that the complexation between poly(acrylamidoxime) fibers and VO_2^+ cations can be restricted by either inhibiting the tautomeric rearrangement from the amidoxime to imino hydroxylamine via substitution of both amine hydrogens with alkyl groups or eliminating the amine group all together. Incorporating these concepts into ligands design will be an essential aspect to improving the UO_2^{2+} selectivity of future generations of chelating polymers.

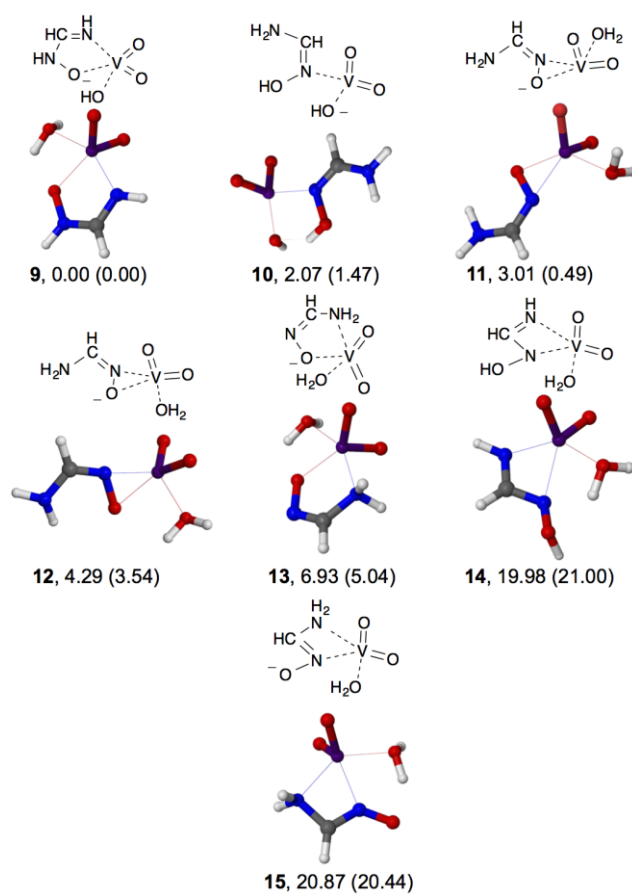


Figure 3.8. Structures of $\text{VO}_2(\text{AO})(\text{H}_2\text{O})$ complexes (AO=formamidoximate) and relative energies in the gas phase and in aqueous solution (in parentheses) in units of kcal/mol.

Table 3.5. Relative gas phase electronic energies of four- and five-coordinate VO₂(HAO)(H₂O) complexes in kcal/mol.^a All energies are given relative to five-coordinate complex 9 in Figure 8.

Theory	10 (c.n.= 4)	11 (c.n.= 5)	12 (c.n.= 5)	13 (c.n.= 5)	14 (c.n.= 5)	15 (c.n.= 5)
MP2	9.19	9.91	6.49	6.64	18.14	16.91
MP2/aug-cc-pVDZ//MP2	9.31	9.74	6.52	8.98	19.50	18.67
CCSD(T)//MP2	3.47	5.30	5.96	5.01	19.86	19.39
CCSD(T) + δ MP2	3.59	5.12	5.99	7.35	21.23	21.15
B3LYP	-0.52	4.89	4.60	9.34	22.71	19.65
M06	2.84	6.64	6.10	10.29	21.33	20.64
M06-L	3.69	4.76	4.81	9.19	21.73	18.88
ω B97XD	0.66	6.45	5.90	9.25	22.09	20.15
B97D3	-1.28	3.24	3.41	7.48	20.92	14.42
PBE-D3	0.53	3.93	4.10	8.71	21.42	14.49
TPSS-D3	1.05	4.07	4.42	7.85	21.10	15.27
M06-L-D3	3.67	4.76	4.81	9.20	21.74	18.88
B3LYP-D3	-0.38	5.56	5.18	8.73	22.04	18.98

^aThe aug-cc-pVDZ basis set was employed in all calculations unless otherwise specified. c.n. denotes coordination number.

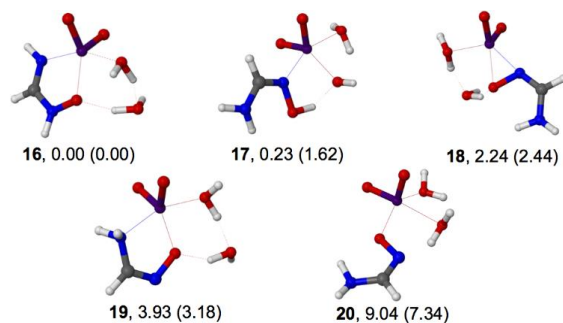


Figure 3.9. Structures of $\text{VO}_2(\text{AO})(\text{H}_2\text{O})_2$ complexes (AO=formamidoximate) and relative energies in the gas phase and in aqueous solution (in parentheses) in units of kcal/mol.

Table 3.6. Relative gas phase electronic energies of five-coordinate $\text{VO}_2(\text{HAO})(\text{H}_2\text{O})_2$ complexes in kcal/mol.^a All energies are given relative to five-coordinate complex 16 in Figure 3.9.

Theory	17 (c.n. = 5)	18 (c.n. = 5)	19 (c.n. = 4)	20 (c.n. = 5)
MP2	3.68	4.37	11.71	5.22
MP2/aug-cc-pVQZ//MP2	4.04	4.17	11.95	6.60
CCSD(T)//MP2	1.72	4.22	9.91	3.62
CCSD(T) + δ MP2	2.07	4.03	10.15	5.00
B3LYP	1.46	2.79	3.59	3.73
M06	1.51	1.57	7.10	7.49

^aThe aug-cc-pVDZ basis set was employed in all calculations unless otherwise specified. c.n. denotes coordination number.

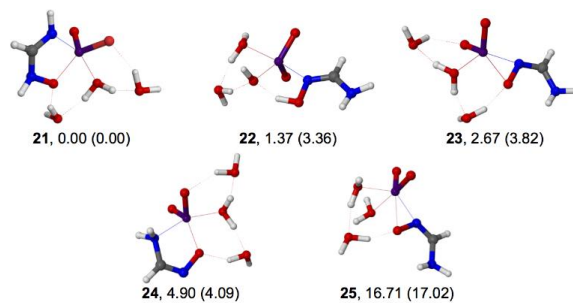


Figure 3.10. Structures of $\text{VO}_2(\text{AO})(\text{H}_2\text{O})_3$ complexes (AO=formamidoximate) and relative energies in the gas phase and in aqueous solution (in parentheses) in units of kcal/mol.

Table 3.7. Relative gas phase electronic energies of five- and six-coordinate $\text{VO}_2(\text{HAO})(\text{H}_2\text{O})_3$ complexes in kcal/mol.^a All energies are given relative to five-coordinate complex 21 in Figure 10.

Theory	22 (c.n. = 5)	23 (c.n. = 5)	24 (c.n. = 5)	25 (c.n. = 6)
MP2	-0.38	3.76	5.69	9.00
MP2/aug-qz//MP2	0.64	3.81	7.34	10.04
CCSD(T)//MP2	0.25	4.12	4.48	15.22
CCSD(T) + δ MP2	1.27	4.16	6.14	16.26
B3LYP	1.39	2.57	7.19	
M06	0.98	3.56	8.13	

^aThe aug-cc-pVDZ basis set was employed in all calculations unless otherwise specified. c.n. denotes coordination number.

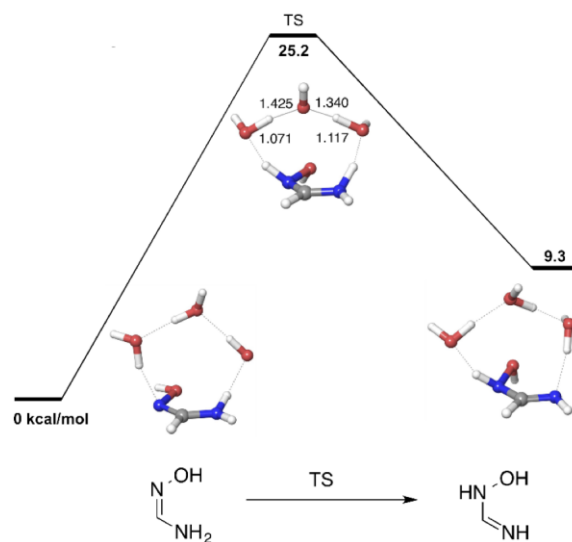


Figure 3.11. Reaction free-energy profile for tautomerization of formamidoxime calculated in the presence of three solvent (water) molecules (kcal/mol). Implicit solvation corrections are obtained using the IEF-PCM solvation model. DFT-optimized O-H bond lengths in the transition state are shown (Å).

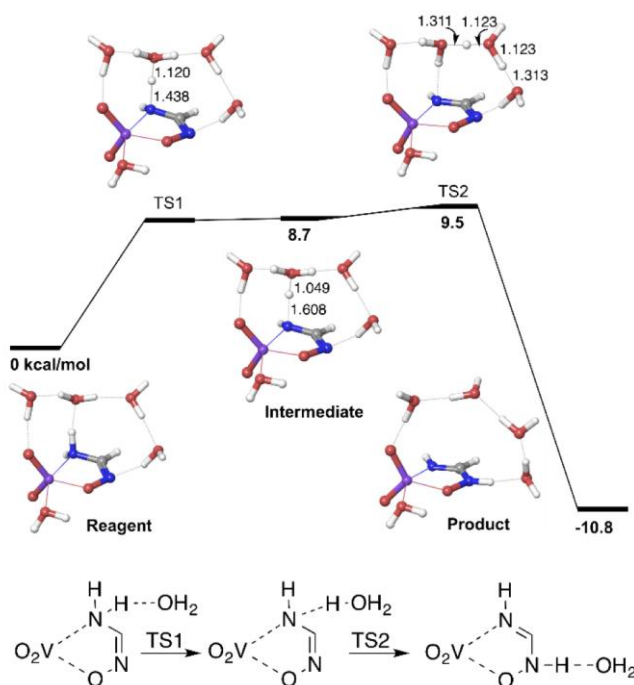


Figure 3.12. Reaction free-energy profile for tautomerization of formamidoximate coordinated to VO_2^+ in the presence of five solvent (water) molecules (kcal/mol). Implicit solvation corrections are obtained using the IEF-PCM solvation model. DFT-optimized O–H bond lengths in the transition and intermediate states are shown (Å).

Finally, searching the Cambridge Structural Database (CSD, 2014 release, version 5.36) for an unspecified transition metal and an amidoximate ligand with “any” bond specification for all carbon-nitrogen bonds and amine proton with no error and no disorder yielded 216 hits. These were further scrutinized to remove duplicate structures, structures containing amidoximate and imino hydroxylamine ligands that are not directly bonded to the metal center, structures that did not contain amidoximate or imino hydroxylamine ligands, and polynuclear complexes. As illustrated in **Figure 3.13**, the remaining 78 complexes can be classified into four categories: imino hydroxylamine-transition metal chelate complexes (**Type 1**) that are representative of the tautomeric rearranged formamidoximate- VO_2^+ binding motif observed in **9**, **16**, and **21**, monodentate oxime nitrogen complexes (**Type 2**) that are representative of the binding motif observed in **10**, **17**, and **22**, η^2 complexes (**Type 3**) that are representative of the binding motif

observed in **11**, **18**, and **23**, and amidoximate-transition metal chelate complexes (**Type 4**) that are representative of the binding motif observed in **12**, **19**, and **24**. Approximately 78% of the complexes obtained were **Type 2** complexes, such as CIMMIW,⁵² IMAXNI,⁵³ and YOHFEI.⁵⁴ Although the **Type 2** complexes were the most prevalent complexes, they were only observed for bisamidoximate ligands and amidoximatee ligands linked to amines and pyridines. **Type 1** complexes, such as CUHJUK,⁵⁵ NEKLEW,⁵⁶ and POLFED,⁵⁷ are the most prevalent amidoximate complexes observed in the absence of additional amidoximates, amines, and pyridines (~ 18%). The remaining 4% of complexes observed were **Type 3**, such as RASBOC⁵⁸ and BASBIW.⁵⁸ However, RASBIW is listed as a **Type 4** complex in **Figure 3.13** because it was the only complex that exhibited the **Type 4** binding motif. These results lend merit to our observation, that in the absence of pyridines, amines, and additional amidoximate species, the most stable binding motif is the **Type 1** binding motif.

3.4. Conclusion

In this work, we computationally elucidated the binding motif and coordination numbers of formamidoximate-VO₂⁺ and formate-VO₂⁺ complexes by investigating the relative energies of 25 formate-VO₂⁺, formamidoximate-VO₂⁺, and hydrated VO₂⁺ complexes. We employed CCSD(T) calculations in the aug-cc-pVDZ basis set to determine benchmark relative energies of VO₂⁺ complexes to evaluate MP2 and various DFT methods. Compared to the highest level of theory employed, DFT methods tend to underestimate, while MP2 tend to overestimate the coordination number of hydrated VO₂⁺ complexes. In particular, CCSD(T) and MP2 calculations predict higher stability of the six-coordinate VO₂(H₂O)₄⁺ complexes, compared to the five-coordinated complex where one of the water molecules is outside of the first shell, while all

tested DFT methods yield the reversed stability of the two configurations. Thus, employing higher level of theory calculations has resolved the discrepancy between the experimental and computational coordination number of the hydrated VO_2^+ ion.

Moreover, our investigation of formate- VO_2^+ complexes revealed that the average coordination mode of pure carboxylate- VO_2^+ complexes in aqueous solution is an equilibrium mixture of monodentate and bidentate species. Our investigation of formamidoximate- VO_2^+ complexes universally identified the most stable binding motif formed by chelating a tautomericallly rearranged imino hydroxylamine ligand via the amine nitrogen and the oxime oxygen. Transition state calculations identified the low-energy pathway for interconversion between the two forms, supporting fast rearrangement to the thermodynamically more stable tautomer. In contrast, previous studies showed the most stable amidoxime- UO_2^{2+} complexes are formed via η^2 coordination of the oxime functional group.⁵⁰ The difference in the binding motifs for complexation with UO_2^{2+} and VO_2^+ has important implications for ligand design. The UO_2^{2+} selectivity of poly(acrylamidoxime) fibers could be improved by designing ligands that either contain only η^2 coordination sites of the oxime functional group or do not permit a tautomeric rearrangement from amidoxime to imino hydroxylamine by substituting both amine hydrogen atoms with alkyl group. The results provide an important step for developing a computational protocol for predicting the stability constants for VO_2^+ complexes. Combined with the demonstrated ability to predict the stability constants for UO_2^{2+} complexes,⁵⁹ this will provide the essential foundation for the rational design of ligands with enhanced uranyl affinity and selectivity.

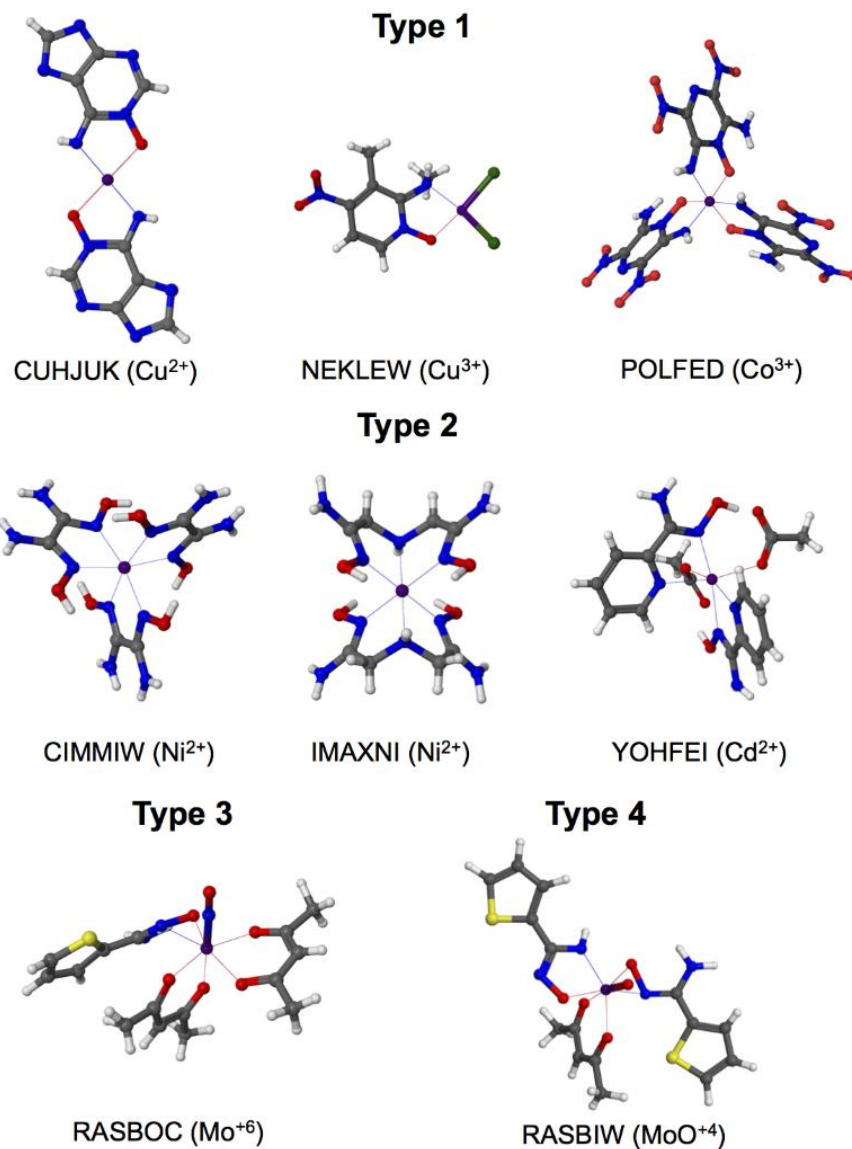


Figure 3.13. Crystal structures of amidoximate-transition metal complexes from the CSD. The Type 1 complexes are representative of the tautomericly rearranged binding mode observed in complexes 9, 16, and 21. The Type 2 complexes are representative of the monodentate oxime nitrogen binding mode observed in complexes 10, 17, and 22. The Type 3 complex is representative of the η^2 binding mode observed in complexes 11, 18, and 23. The Type 4 complex is representative of the unrearranged binding motif observed in complexes 12, 19, and 24.

References

1. Kim, J. S.; Tsouris, C.; Mayes, R. T.; Oyola, Y.; Saito, T.; Janke, C. J.; Dai, S.; Schneider, E.; Sachde, D., Recovery of Uranium from Seawater: A Review of Current Status and Future Research Needs. *Sep. Sci. Technol.* **2013**, *48*, 367-387.
2. Davies, R. V.; Kennedy, J.; McIlroy, R. W.; Spence, R.; Hill, K. M., Extraction of Uranium from Sea Water. *Nature* **1964**, *203*, 1110–1115.
3. Saito, K.; Miyauchi, T., Chemical Forms of Uranium in Artificial Seawater. *J. Nucl. Sci. Technol.* **1982**, *19*, 145–150.
4. Choppin, G. R., Soluble Rare Earth and Actinide Species in Seawater. *Mar. Chem.* **1989**, *28*, 19-26.
5. Schenk, H. J.; Astheimer, L.; Witte, E. G.; Schwochau, K., Development of Sorbers for the Recovery of Uranium from Seawater. 1. Assessment of Key Parameters and Screening Studies of Sorber Materials. *Sep. Sci. Technol.* **1982**, *17*, 1293-1308.
6. Astheimer, L.; Schenk, H. J.; Witte, E. G.; Schwochau, K., Development of Sorbers for the Recovery of Uranium from Seawater. Part 2. The Accumulation of Uranium from Seawater by Resins Containing Amidoxime and Imidoxime Functional Groups. *Sep. Sci. Technol.* **1983**, *18*, 307–339.
7. Wang, D. L.; Sañudo Wilhelmy, S. A., Vanadium Speciation and Cycling in Coastal Waters. *Mar. Chem.* **2009**, *117*, 52–58.
8. Suzuki, T.; Saito, K.; Sugo, T.; Ogura, H.; Oguma, K., Fractional Elution and Determination of Uranium and Vanadium Adsorbed on Amidoxime Fiber from Seawater. *Anal. Sci.* **2000**, *16*, 429-432.

9. Abbasse, G.; Ouddane, B.; Fischer, J. C., Determination of Trace Levels of Dissolved Vanadium in Seawater by Use of Synthetic Complexing Agents and Inductively Coupled Plasma-Atomic Emission Spectroscopy (ICP-AES). *Anal. Bioanal. Chem.* **2002**, *374*, 873-878.
10. Kelley, S. P.; Barber, P. S.; Mullins, P. H. K.; Rogers, R. D., Structural Clues to $\text{UO}_2^{2+}/\text{VO}_2^+$ Competition in Seawater Extraction Using Amidoxime-Based Extractants. *Chem. Commun.* **2014**, *50*, 12504-12507.
11. Kawai, T.; Saito, K.; Sugita, K.; Katakai, A.; Seko, N.; Sugo, T.; Kawakami, T.; Kanno, J., Comparison of Amidoxime Adsorbents Prepared by Cograftering Methacrylic Acid and 2-Hydroxyethyl Methacrylate with Acrylonitrile onto Polyethylene. *Ind. Eng. Res. Chem.* **2000**, *39*, 2910-2915.
12. Kawai, T.; Saito, K.; Sugita, K.; Kawakami, T.; Kanno, J.; Katakai, A.; Seko, N.; Sugo, T., Preparation of Hydrophilic Amidoxime Fibers by Cograftering Acrylonitrile and Methacrylic Acid from an Optimized Monomer Composition. *Radiat. Phys. Chem.* **2000**, *59*, 405-411.
13. Allen, F. H., The Cambridge Structural Database: A Quarter of a Million Crystal Structures and Rising. *Acta Cryst. B* **2002**, *58*, 380-386.
14. Süss-Fink, G.; Stanislas, S.; Shul'pin, G. B.; Nizova, G. V.; Stoeckli-Evans, H.; Neels, A.; Bobillier, C.; Claude, S., Oxidative Functionalisation of Alkanes: Synthesis, Molecular Structure and Catalytic Implications of Anionic Vanadium(V) Oxo and Peroxo Complexes Containing Bidentate N,O Ligands *J. Chem. Soc., Dalton Trans.* **1999**, 3169-3175.
15. Krakowiak, J.; Lundberg, D.; Persson, I., A Coordination Chemistry Study of Hydrated and Solvated Cationic Vanadium Ions in Oxidation States +III, +IV, and +V in Solution and Solid State. *Inorg. Chem.* **2012**, *51*, 9598-9609.

16. Sepehr, F.; Paddison, S. J., The Solvation Structure and Thermodynamics of Aqueous Vanadium Cations. *Chem. Phys. Lett.* **2013**, 585, 53-58.
17. Bühl, M.; Parrinello, M., Medium Effects on ^{51}V NMR Chemical Shifts: A Density Functional Study. *Chem. Eur. J.* **2001**, 7, 4487-4494.
18. Frisch, M. J.; Trucks, G. W.; Schlegel, H. B.; Scuseria, G. E.; Robb, M. A.; Cheeseman, J. R.; Scalmani, G.; Barone, V.; Mennucci, B.; Petersson, G. A.; Nakatsuji, H.; Caricato, M.; Li, X.; Hratchian, H. P.; Izmaylov, A. F.; Bloino, J.; Zheng, G.; Sonnenberg, J. L.; Hada, M.; Ehara, M.; Toyota, K.; Fukuda, R.; Hasegawa, J.; Ishida, M.; Nakajima, T.; Honda, Y.; Kitao, O.; Nakai, H.; Vreven, T.; Montgomery, J. A., Jr. ; Peralta, J. E.; Ogliaro, F.; Bearpark, M.; Heyd, J. J.; Brothers, E.; Kudin, K. N.; Staroverov, V. N.; Kobayashi, R.; Normand, J.; Raghavachari, K.; Rendell, A.; Burant, J. C.; Iyengar, S. S.; Tomasi, J.; Cossi, M.; Rega, N.; Millam, M. J.; Klene, M.; Knox, J. E.; Cross, J. B.; Bakken, V.; Adamo, C.; Jaramillo, J.; Gomperts, R.; Stratmann, R. E.; Yazyev, O.; Austin, A. J.; Cammi, R.; Pomelli, C.; Ochterski, J. W.; Martin, R. L.; Morokuma, K.; Zakrzewski, V. G.; Voth, G. A.; Salvador, P.; Dannenberg, J. J.; Dapprich, S.; Daniels, A. D.; Farkas, Ö.; Foresman, J. B.; Ortiz, J. V.; Cioslowski, J.; Fox, D. J. *Gaussian 09 Revision D.01*, Gaussian, Inc.: Wallingford, CT, 2009.
19. Valiev, M.; Bylaska, E. J.; Govind, N.; Kowalski, K.; Straatsma, T. P.; van Dam, H. J. J.; Wang, D.; Nieplocha, J.; Apra, E.; Windus, T. L.; de Jong, W. A., NWChem: A Comprehensive and Scalable Open-Source Solution for Large Scale Molecular Simulations. *Comput. Phys. Commun.* **2010**, 181, 1477-1489.
20. Purvis, G. D.; Bartlett, R. J., A Full Coupled-Cluster Singles and Doubles Model: The Inclusion of Disconnected Triples. *J. Chem. Phys.* **1982**, 76, 1910-1918.

21. Raghavachari, K.; Trucks, G. W.; Pople, J. A.; Head-Gordon, M., A Fifth-Order Perturbation Comparison of Electron Correlation Theories. *Chem. Phys. Lett.* **1989**, *157*, 479-483.
22. Watts, J. D.; Gauss, J.; Bartlett, R. J., Coupled-Cluster Methods with Noniterative Triple Excitations for Restricted Open-Shell Hartree–Fock and Other General Single Determinant Reference Functions. Energies and Analytical Gradients. *J. Chem. Phys.* **1993**, *98*, 8718–8733.
23. Dunning, T. H. J., Gaussian Basis Sets for Use in Correlated Molecular Calculations. I. The Atoms Boron through Neon and Hydrogen. *J. Chem. Phys.* **1989**, *90*, 1007-1023.
24. Kendall, R. A.; Dunning, T. H. J.; Harrison, R. J., Electron Affinities of the First- Row Atoms Revisited. Systematic Basis Sets and Wave Functions. *J. Chem. Phys.* **1992**, *96*, 6796-6806.
25. Head-Gordon, M.; Pople, J. A.; Frisch, M. J., MP2 Energy Evaluation by Direct Methods. *Chem. Phys. Lett.* **1988**, *153*, 503-506.
26. Møller, C.; Plesset, M. S., Note on an Approximation Treatment for Many-Electron Systems. *Phys. Rev.* **1934**, *46*, 618-622.
27. Hohenberg, P.; Kohn, W., Inhomogeneous Electron Gas. *Phys. Rev.* **1964**, *136*, B864–B871.
28. Kohn, W.; Sham, L. J., Self-Consistent Equations Including Exchange and Correlation Effects. *Phys. Rev.* **1965**, *140*, A1133–A1138.
29. Hay, P. J.; Wadt, W. R., Ab Initio Effective Core Potentials for Molecular Calculations. Potentials for K to Au Including the Outermost Core Orbitals. *J. Chem. Phys.* **1985**, *82*, 299-310.
30. Hay, P. J.; Wadt, W. R., Ab Initio Effective Core Potentials for Molecular Calculations. Potentials for the Transition Metal Atoms Sc to Hg. *J. Chem. Phys.* **1985**, *82*, 270-283.

31. Hay, P. J.; Wadt, W. R., Ab Initio Effective Core Potentials for Molecular Calculations. Potentials for Main Group Elements Na to Bi. *J. Chem. Phys.* **1985**, *82*, 284-298.
32. Roy, L. E.; Hay, P. J.; Martin, R. L., Revised Basis Sets for the LANL Effective Core Potentials. *J. Chem. Theory Comput.* **2008**, *4*, 1029-1031.
33. Ricca, A.; Bauschlicher Jr., C. W., A Comparison of Density Functional Theory with Ab Initio Approaches for Systems Involving First Transition Row Metals. *Theor. Chim. Acta* **1995**, *92*, 123-131.
34. Perdew, J. P.; Burke, K.; Ernzerhof, M., Generalized Gradient Approximation Made Simple. *Phys. Rev. Lett.* **1996**, *77*, 3865-3868.
35. Perdew, J. P.; Burke, K.; Ernzerhof, M., Errata: Generalized Gradient Approximation Made Simple. *Phys. Rev. Lett.* **1997**, *78*, 1396.
36. Becke, A. D., Density-Functional Thermochemistry. III. The Role of Exact Exchange. . *J. Chem. Phys.* **1993**, *98*, 5648–5652.
37. Lee, C.; Yang, W.; Parr, R. G., Development of the Colle-Salvetti Correlation-Energy Formula Into a Functional of the Electron Density. *Phys. Rev. B* **1988**, *37*, 785–789.
38. Chai, J.-D.; Head-Gordon, M., Systematic Optimization of Long-Range Corrected Hybrid Density Functionals. *J. Chem. Phys.* **2008**, *128*, 084106.
39. Chai, J.-D.; Head-Gordon, M., Long-Range Corrected Hybrid Density Functionals with Damped Atom-Atom Dispersion Corrections. *Phys. Chem. Chem. Phys.* **2008**, *10*, 6615-6620.
40. Grimme, S., Semiempirical GGA-Type Density Functional Constructed with a Long-Range Dispersion Correction. *J. Comp. Chem.* **2006**, *27*, 1787-1799.
41. Grimme, S.; Ehrlich, S.; Goerigk, L., Effect of the Damping Function in Dispersion Corrected Density Functional Theory. *J. Comp. Chem.* **2011**, *32*, 1456-1465.

42. Zhao, Y.; Truhlar, D. G., The M06 Suite of Density Functionals for Main Group Thermochemistry, Thermochemical Kinetics, Noncovalent Interactions, Excited States, and Transition Elements: Two New Functionals and Systematic Testing of Four M06-Class Functionals and 12 Other Functionals. *Theor. Chem. Acc.* **2008**, *120*, 215-241.
43. Tao, J. M.; Perdew, J. P.; Staroverov, V. N.; Scuseria, G. E., Climbing the Density Functional Ladder: Nonempirical Meta-Generalized Gradient Approximation Designed for Molecules and Solids. *Phys. Rev. Lett.* **2003**, *91*, 146401.
44. Grimme, S.; Antony, J.; Ehrlich, S.; Krieg, H., A Consistent and Accurate Ab Initio Parameterization of Density Functional Dispersion Correction (DFT-D) for the 94 Elements H-Pu. *J. Chem. Phys.* **2010**, *132*, 154104.
45. Miertuš, S.; Scrocco, E.; Tomasi, J., Electrostatic Interaction of a Solute with a Continuum. A Direct Utilization of ab initio Molecular Potentials for the Prevision of Solvent Effects. *Chem. Phys.* **1981**, *55*, 117-129.
46. Cancès, E.; Mennucci, B.; Tomasi, J., A New Integral Equation Formalism for the Polarizable Continuum Model: Theoretical Background and Applications to Isotropic and Anisotropic Dielectrics. *J. Chem. Phys.* **1997**, *107*, 3032–3041.
47. Mennucci, B.; Cancès, E.; Tomasi, J., Evaluation of Solvent Effects in Isotropic and Anisotropic Dielectrics and in Ionic Solutions with a Unified Integral Equation Method: Theoretical Bases, Computational Implementation, and Numerical Applications. *J. Phys. Chem. B* **1997**, *101*, 10506–10517.
48. Cotton, S., *Lanthanide and Actinide Chemistry*. Wiley: Hoboken, New Jersey, USA, 2006.

49. Su, J.; Zhang, K.; Schwarz, W. H. E.; Li, J., Uranyl-Glycine-Water Complexes in Solution: Comprehensive Computational Modeling of Coordination Geometries, Stabilization Energies, and Luminescence Properties. *Inorg. Chem.* **2011**, *50*, 2082-2093.
50. Vukovic, S.; Watson, L. A.; Kang, S. O.; Custelcean, R.; Hay, B. P., How Amidoximate Binds the Uranyl Cation. *Inorg. Chem.* **2012**, *51*, 3855–3859.
51. Tavakol, H.; Arshadi, S., Theoretical Investigation of Tautomerism in N-Hydroxy Amidines. *J. Mol. Model* **2009**, *15*, 807–816.
52. Nenwa, J.; Djonwouo, P. L.; Bélombé, M. M.; Nfor, E. N.; Emmerling, F., Transition Metal Complexes of Oxamide Dioxime: Synthesis, Characterization and X-ray Structure of Isomorphous $[\text{Ni}(\text{H}_2\text{oxado})_3](\text{BF}_4)_2$ and $[\text{Ni}(\text{H}_2\text{oxado})_3](\text{ClO}_4)_2$. *ScienceJet* **2013**, *2*, 43.
53. Cullen, D. L.; Lingafelter, E. C., Crystal structures of Bis[2,2'-Iminobis(acetamidoxime)]Nickel(II) Chloride Dihydrate and Bis[2,2'-Iminobis(acetamidoxime)]Copper(II) Chloride. *Inorg. Chem.* **1970**, *9*, 1865–1877.
54. Liu, J., Crystal Structure of Bis-(Acetato-[kappa]O)Bis-(Pyridine-2-carboxamide Oxime-[kappa]2N,N')Cadmium Ethanol Disolvate. *Acta Crystallogr., Sect. E: Struct. Rep. Online* **2014**, *70*, 142-144
55. Sletten, E.; Marthinsen, T.; Sletten, J., Metal Complexes of Purine-N-oxides. I. The Crystal Structure of a Copper(II) Complex of Doubly Deprotonated Adenine-N1-oxide. *Inorg. Chim. Acta* **1984**, *93*, 37-41.
56. Puszko, A.; Kochel, A.; Wietrzyk, J.; Filip-Psurska, B.; Jezierska, J.; Puszyńska-Tuszkano, M.; Staszak, Z.; Adach, A.; Lorenc, J.; Cieslak-Golonka, M., Structure–Activity Relationship Disturbed by a Solvolytic Process: Study on the $[\text{Cu}(\text{II})\text{-4-Nitropyridine N-Oxide Derivative}]$ System. *Polyhedron* **2013**, *50*, 146-153.

57. Liu, J.-J.; Liu, Z.-L.; Cheng, J., Synthesis, Crystal Structure, and Catalytic Properties of Two Energetic Complexes Containing 2,6-Diamino-3,5-dinitropyrazine-1-oxide. *Chinese J. Inorg. Chem.* **2014**, *30*, 696-704.
58. Roh, S.-G.; Proust, A.; Robert, F.; Gouzerh, P., Coordination Chemistry of Polyoxomolybdates: The Versatile Behavior of Amidoximes. *J. Cluster Sci.* **1996**, *7*, 593-627.
59. Vukovic, S.; Hay, B. P.; Bryantsev, V. S., Predicting Stability Constants for Uranyl Complexes Using Density Functional Theory. *Inorg. Chem.* **2015**, *54*, 3995-4001.

Chapter 4 : Theoretical Study of Oxovanadium(IV) Complexation with Formamidoximate: Implications for the Design of Uranyl-Selective Adsorbents

A version of this chapter was originally published by Nada Mehio, Alexander S. Ivanov, Austin P. Ladshaw, Sheng Dai, and Vyacheslav S. Bryantsev in *Industrial & Engineering Chemistry Research*:

Mehio, N.; Ivanov, A. S.; Ladshaw, A. P.; Dai, S.; Bryantsev, V. S. "Theoretical Study of Oxovanadium (IV) Complexation with Formamidoximate: Implications for the Design of Uranyl-Selective Adsorbents." *Ind. Eng. Chem. Res.* **2015**, in press (DOI: 10.1021/acs.iecr.5b03398)

Abstract

Poly(acrylamidoxime) fibers are the current state of the art adsorbent for mining uranium from seawater. However, the competition between uranyl (UO_2^{2+}) and vanadium ions poses a challenge to mining on the industrial scale. In this work, we employ density functional theory (DFT) and coupled-cluster methods (CCSD(T)) in the restricted formalism to investigate potential binding motifs of the oxovanadium(IV) ion (VO^{2+}) with the formamidoximate ligand. Consistent with experimental EXAFS data, the hydrated six-coordinate complex is predicted to be preferred over the hydrated five-coordinate complex. Our investigation of formamidoximate- VO^{2+} complexes universally identified the most stable binding motif formed by chelating a tautomericallly rearranged imino hydroxylamine via the imino nitrogen and hydroxylamine oxygen. The alternative binding motifs for amidoxime chelation via a non-rearranged tautomer and η^2 coordination are found to be ~ 11 kcal/mol less stable. Natural bond orbital analysis was performed to understand the nature of the interactions in the VO^{2+} complexes. The difference in the most stable VO^{2+} and UO_2^{2+} binding conformation has important implications for the design of more selective UO_2^{2+} ligands.

4.1. Introduction

With the development of advanced nuclear energy systems, the demand for uranium is expected to increase. There is an estimated 4.5 billion tons of uranium dissolved in seawater, largely in the form of uranyl tricarbonat, $\text{UO}_2(\text{CO}_3)_3^{4-}$.¹⁻³ Consequentially, extensive research efforts spanning five decades have focused on developing adsorbents for extracting uranium from seawater.⁴ This research is complicated by the fact that uranium is present in very low concentrations, roughly 3 ppb,¹ while numerous competing metal cations are present at much higher concentrations.³ Currently, the most widely utilized adsorbents are poly(acrylamidoxime) fibers, which were first identified in a screening of 200 organic polymers as the only adsorbent capable of extracting uranium from pH 8.3 aqueous solution, the approximate pH of seawater.^{5, 6} However, poly(acrylamidoxime) fibers are not perfectly selective towards uranium in seawater. In particular, there is great interest in understanding the interaction between poly(acrylamidoxime) fibers and vanadium ions, because the competition between UO_2^{2+} and vanadium ions remains a great challenge.⁷ In addition to reducing the UO_2^{2+} capacity of poly(acrylamidoxime) fibers, vanadyl cations bind so strongly that stripping the cations irreversibly damages the adsorbant.^{4, 8} The vanadium(V) species is present in higher concentrations than vanadium(IV) species in seawater, but the ratio is significantly dependent upon the season, the water depth, and the marine life present.^{7, 9} Moreover, the kinetics of vanadium(IV) complexation is much faster than vanadium(V) complexation, which justifies the detailed investigation of both species. Recently, we have studied the interaction between the formamidoximate ligand and the dioxovanadium(V) cation, VO_2^+ .¹⁰ In the current work, we will study the oxovanadium(IV), VO^{2+} , complexation with the formamidoximate anion. Understanding how amidoxime functional groups interact with vanadium ions is essential for the rational design of subsequent generations of chelating polymer adsorbents.

Poly(acrylamidoxime) fibers are polymers bearing random mixtures of propyl linked carboxylate and amidoxime monomers at a 40 to 60 monomer ratio, respectively.^{11, 12} Therefore, in order for the interaction between poly(acrylamidoximes) and VO²⁺ cations to be understood, the binding motif of simple, representative carboxylate and amidoxime ligands to VO²⁺ needs to be established. About 250 carboxylate-VO²⁺ crystal structures can be found in the Cambridge Structural Database (CSD, 2014 release, version 5.36) after applying no errors, no disorder, and non-polymeric filters¹³ and excluding polynuclear complexes. A single example of a crystal structure with a pure carboxylate binding motif, XUTLON,¹⁴ is illustrated in **Figure 4.1.A**. The remainder of the carboxylate-VO²⁺ crystal structures exhibits a mixed binding motif consisting of a monodentate-carboxylate and an amine nitrogen, a pyridine nitrogen, or an ether oxygen chelate. An example of one of these mixed chelate structures, LOPHIJ,¹⁵ is illustrated in **Figure 4.1.B**. Of the carboxylate-VO²⁺ complexes, 74% were six-coordinate, 18% were seven-coordinate, and 8% were five-coordinate. Five-coordinate complexes were observed if the carboxylate ligand was rigid, sterically strained, or contained electron withdrawing groups. Seven-coordinate complexes were observed for half of all VO²⁺ complexes that contained η^2 coordinated peroxide, nitrosyl, hydroxylamine, and N-hydroxylamine ligands. However, despite this abundance of carboxylate-VO²⁺ crystal data in the CSD, no amidoxime-VO²⁺ crystal structures have been reported.

Herein, we report the results of a computational investigation of the interactions of the oxovanadium (IV) ion, VO²⁺, with the formamidoximate anion. The chosen ligand is small enough that high-level *ab initio* calculations could readily be performed. Calculations at various levels of theory, such as B3LYP/aug-cc-pVDZ, M06/aug-cc-pVDZ, and CCSD(T)/aug-cc-pVDZ//B3LYP/aug-cc-pVDZ were applied to identify how the amidoximate ligand interacts

with the VO^{2+} ion. The natural bond orbital (NBO) analysis was performed to elucidate the nature of these interactions. Theoretical results lay the foundation for the rational design of ligands that are more selective for the UO_2^{2+} ion.

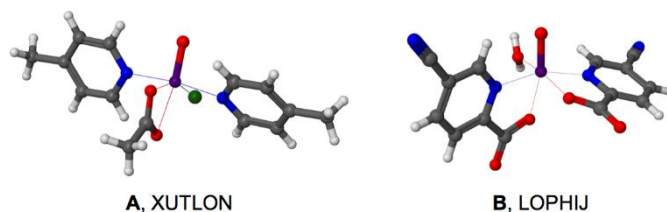


Figure 4.1. Crystal structures of carboxylate- VO^{2+} complexes. The XUTLON complex, (acetato- O,O')-chloro-bis(4-methylpyridine- N)-oxo-vanadium(IV), and the LOPHIJ complex, aqua-bis(5-cyanopyridine-2-carboxylato- N,O)-oxido-vanadium(IV) dihydrate, are representative of the two carboxylate- VO_2^+ binding modes observed in the CSD.

4.2. Methods

4.2.1. Electronic Structure Calculations

Electronic structure calculations were carried out using the Gaussian 09 Revisions C.01 and D.01.¹⁶ Geometry optimization was performed with density functionals,^{17, 18} specifically, B3LYP,^{19, 20} M06,²¹ using the aug-cc-pVDZ basis set.^{22, 23} Additionally, we employed single-point coupled-cluster CCSD(T)/aug-cc-pVDZ calculations²⁴⁻²⁶ in the restricted formalism as implemented in Gaussian 09 using the geometries of VO^{2+} complexes obtained with B3LYP/aug-cc-pVDZ (denoted R/R-CCSD(T)//B3LYP hereafter). Only the valence C, H, N, and O electrons and the valence and sub-valence 3s and 3p V electrons were correlated in the R/R-CCSD(T) calculations. Single-point R/R-CCSD(T)/aug-cc-pVDZ calculations in which only the valence electrons were correlated were also carried out and the results can be found in **Appendix C**. Additionally, the competitive complexation with the UO_2^{2+} and VO_2^+ ions was

investigated at comparable levels of theory. The standard Stuttgart small-core (SSC) 1997 relativistic effective core potential (RECP) was used for uranium, replacing 60 core electrons to account for scalar relativistic effects.²⁷ The valence electrons in this basis set at the R/R-CCSD(T) level are represented by a contracted [8s/7p/6d/4f] basis. The most diffuse f function (having an exponent of 0.005) on U was removed in the DFT calculations to improve SCF convergence. Zero-point energies (ZPE) and thermal corrections were obtained at the B3LYP level without scaling using the 6-311++G** basis set. Using the gas phase geometries obtained at the B3LYP/aug-cc-pVDZ level, implicit solvent corrections were obtained at 298 K with the IEF-PCM model²⁸⁻³⁰ in Gaussian 09, using the default atomic radii of the united force field (UFF) (denoted R/R-CCSD(T)//B3LYP//IEF-PCM(UFF) hereafter). Electronic energies in the solvent reaction field were computed at the B3LYP/6-31+G* level. For comparison, relative energies in the aqueous phase obtained using the SMD solvation model³¹ are given in **Appendix C**. In general, the two solvation models yield similar trends in complex stability, with the SMD method giving higher weight to complexes with lower coordination numbers.

A transition state search with the B3LYP/aug-cc-pVDZ method was performed using a standard Berny algorithm implemented in Gaussian 09,¹⁶ starting from the partially optimized geometry at the same level of theory along the chosen reaction coordinate and the precalculated Hessian. Intrinsic reaction coordinate calculations (IRC) were performed to ensure that transition-state structures connect their respective reactants and products.

4.2.2. Natural Bond Orbital (NBO) Analysis

Chemical bonding analysis was performed with the NBO method^{32, 33} at the B3LYP/6-31G* level using NBO 6.0 program.³⁴ NBO analysis provides a good quantitative description of

interatomic and intermolecular interactions in accordance with the basic Pauling-Slater-Coulson representations of bond polarization and hybridization.^{32, 33} Since all studied VO²⁺ complexes are open-shell systems, the analyses of the individual electron densities were carried out separately for α (spin-up) and β (spin-down) orientations. The latter reflect the two different ways by which a single electron can occupy an orbital in terms of the spin direction. The donor-acceptor interaction energy in the NBOs was estimated via second-order perturbation theory analysis of the Fock matrix.^{32, 33} For each donor orbital (i) and acceptor orbital (j), the stabilization energy $E^{(2)}$ associated with $i \rightarrow j$ delocalization is given by:

$$E_{i,j}^{(2)} = -o_i \frac{\langle i | \hat{F}_{(i,j)} | j \rangle^2}{\epsilon_j - \epsilon_i}$$

where o_i is the donor orbital occupancy, $\hat{F}_{(i,j)}$ is the Fock operator, and ϵ_i and ϵ_j are the orbital energies.

4.2.3. Calculation of the Complexation Free Energies

Complexation free energies in aqueous solution, ΔG_{aq} , were calculated using the methodology described in ref 35. According to the thermodynamic cycle shown in **Figure 4.2**, ΔG_{aq} is given by:

$$\Delta G_{\text{aq}} = \Delta G_{\text{g}}^{\circ} + \Delta \Delta G_{\text{solv}}^* + (n-1)\Delta G^{\circ \rightarrow *} + nRT \ln([\text{H}_2\text{O}])$$

where $\Delta G_{\text{g}}^{\circ}$ is the free energy of complexation in the gas phase and $\Delta \Delta G_{\text{solv}}^*$ is the difference in the solvation free energies for a complexation reaction

$$\Delta \Delta G_{\text{solv}}^* = \Delta G_{\text{solv}}^*([\text{M}(\text{AO})(\text{H}_2\text{O})_{m-n}]^{\text{x}-1}) + n\Delta G_{\text{solv}}^*(\text{H}_2\text{O}) - \Delta G_{\text{solv}}^*([\text{M}(\text{H}_2\text{O})_m]^{\text{x}}) - \Delta G_{\text{solv}}^*(\text{AO}^-)$$

Here, AO denotes the formamidoxime ligand and M can be VO^{2+} , VO_2^+ , or UO_2^{2+} . The standard state correction terms must be introduced to connect $\Delta G^\circ_{\text{g}}$, $\Delta\Delta G^*_{\text{solv}}$, and $\Delta\Delta G_{\text{aq}}$ defined using different standard state conventions. $\Delta G^{\circ \rightarrow *}$ = 1.89 kcal/mol ($T = 298.15$ K) is the free energy change for the conversion of 1 mol of solute from the gas phase at a standard state of 1 atm (24.46 L/mol) to the aqueous phase at a standard state of 1 mol/L. Likewise, $RT \ln([\text{H}_2\text{O}]) = 2.38$ kcal/mol ($T = 298.15$ K) is the free energy change for the conversion of 1 mol of solvent from the aqueous phase at 1 mol/L to pure water at a standard state of 55.34 mol/L.

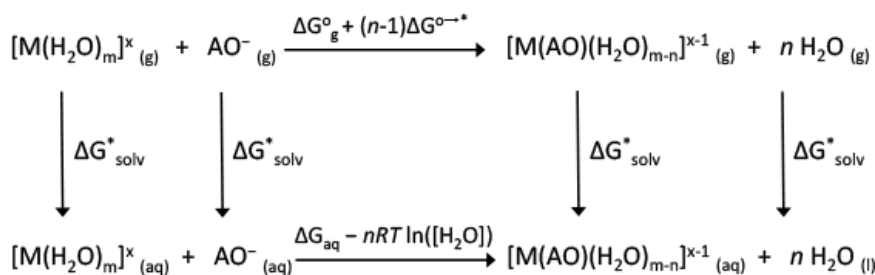


Figure 4.2. Thermodynamic cycle used to calculate ΔG_{aq}

4.3. Results and Discussion

As noted in the Introduction, there is an absence of data describing the binding modes and coordination numbers of amidoximate- VO^{2+} complexes. In order to supplement this lack of data, we computationally elucidated the binding mode, coordination number, and the nature of interaction in formamidoximate- VO^{2+} complexes. First, we examined the electronic structure of the bare VO^{2+} cation and a set of hydrated and hydrolyzed VO^{2+} complexes to better understand the aqueous chemistry of the VO^{2+} . Second, we determined the optimal coordination numbers and binding modes of formamidoximate- VO^{2+} complexes. Next, we investigated the competitive binding of formamidoximate toward UO_2^{2+} , VO_2^+ , and VO^{2+} cations. Finally, from our

theoretical results we derived a strategy for the design of amidoxime ligands that are expected to be more selective toward the uranyl ion.

4.3.1. VO^{2+} Cation in the Gas Phase

To better understand the nature of interactions between VO^{2+} ion and ligands, it is important to first elucidate chemical bonding picture of the bare VO^{2+} cation. The results of natural bond orbital (NBO) analysis for VO^{2+} are shown in **Figure 4.3**. NBO revealed one singly occupied d -type lone pair on the vanadium atom and one s -type lone pair on the oxygen atom with an occupation number (ON) of 1.99 $|e|$, as well as one two-center two-electron (2c-2e) σ bond (ON = 2.00 $|e|$) and two 2c-2e π bonds (ON = 2.00 $|e|$) originating from the interactions between oxygen $2p$ and vanadium $3d$ atomic orbitals and thus making a total of three vanadium to oxygen bonds in VO^{2+} . The revealed covalent bonds, which are more polarized toward the oxygen atom, have an ideal occupancy of 2.00 $|e|$, indicating that single Lewis structure $[\text{V}\equiv\text{O}]^{2+}$ should be a good representation of the complete electron density of the VO^{2+} cation.

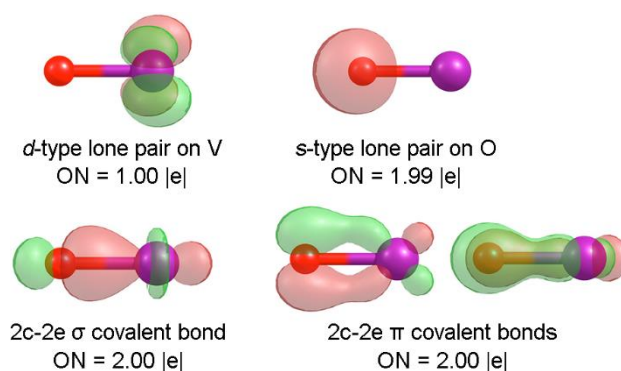


Figure 4.3. NBO chemical bonding pattern for the VO^{2+} cation (the isodensity value is 0.15 au). ON stands for occupation numbers.

4.3.2. Hydrated VO^{2+} Complexes

The electronic structure and geometry of the VO^{2+} cation in the octahedral ligand field has been the subject of research since the 1950s.³⁵⁻³⁸ **Figure 4.4** shows the singly occupied molecular orbitals (SOMOs) of representative hydrate and formamidoximate VO^{2+} complexes obtained at the B3LYP/aug-cc-pVDZ level of theory. Consistent with previous studies³⁵⁻³⁸ and the results for the VO^{2+} in the gas phase, the VO^{2+} SOMOs of all studied complexes are vanadium d_{xy} atomic orbitals (AOs) oriented to minimize the repulsion with the lone pairs of ligand donor atoms.

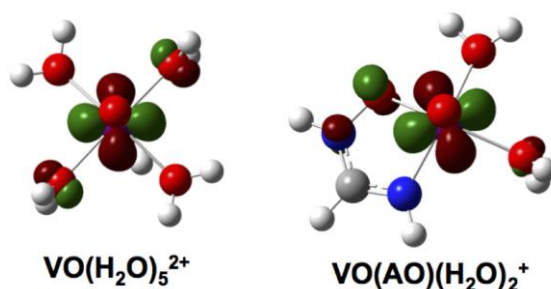


Figure 4.4. Singly-occupied molecular orbitals (SOMOs) of the representative water and formamidoximate VO^{2+} complexes. Dominant atomic contributions to each SOMO are shown with the VO^{2+} oxygen perpendicular to the plane. The SOMOs were obtained at the B3LYP/aug-cc-pVDZ level of theory.

To gain insight into the geometry and the coordination number of aqueous VO^{2+} complexes, first, we will compare the relative energies of five- and six-coordinate, hydrated and hydrolyzed $\text{VO}(\text{H}_2\text{O})_5^{2+}$ complexes. The B3LYP optimized $\text{VO}(\text{H}_2\text{O})_5^{2+}$ complexes and their relative R/R-CCSD(T)//B3LYP Gibbs free energies in the gas phase and in aqueous solution can be found in **Figure 4.5**. The results obtained from the R/R-CCSD(T)//B3LYP//IEF-PCM(UFF) calculations are consistent with experimental data,³⁵⁻³⁸ indicating that hydrated complexes, **1** and **2**, are more stable than the hydrolyzed complex, **3**, in neutral aqueous solution. Moreover, of the

hydrated complexes, the C_{2v} , six-coordinate complex **1** is preferred over the C_1 , five-coordinate complex **2** by ~ 3 kcal/mol. Once again, this is consistent with the EXAFS data indicating that the VO^{2+} cation is most stable as a hydrated, six-coordinate complex of C_{2v} symmetry in aqueous solution.³⁶

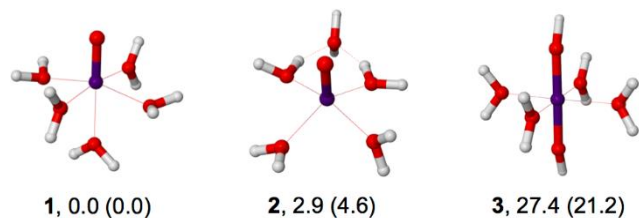


Figure 4.5. Structures and relative Gibbs free energies (kcal/mol) of $VO(H_2O)_5^{2+}$ complexes in aqueous solution and in the gas phase (in parentheses). The electronic energies were obtained at the R/R-CCSD(T)//B3LYP level of theory.

The relative electronic energies of the five- and six-coordinate $VO(H_2O)_5^{2+}$ complexes are tabulated by level of theory in **Table 4.1**. B3LYP marginally preferred complex **2** over complex **1** in the gas phase, while M06 and R/R-CCSD(T)//B3LYP marginally preferred complex **1** over complex **2** in the gas phase. The hydrated complexes are far more stable than the hydrolyzed complexes at all levels of theory. This behavior is typical for oxometal ions with a triple $M\equiv O$ bond. It appears that DFT overpredicts the stability of the hydrolyzed complexes relative to R/R-CCSD(T), i.e., underestimates the energy of the $V\equiv O$ bond compared to the $V-OH$ bond.

Table 4.1. Relative electronic energies (gas phase) of five- and six-coordinate $\text{VO}(\text{H}_2\text{O})_5^{2+}$ clusters in kcal/mol.^{a,b}

Theory	1 (c.n.=6)	2 (c.n.=5)	3 (c.n.=6)
B3LYP	2.0	0.0	13.8
M06	0.0	1.6	10.7
R/R-CCSD(T)//B3LYP	0.0	4.3	24.3

^aThe aug-cc-pVDZ basis set was employed in all calculations.

^bc.n. denotes coordination number.

Table 4.2 shows a comparison of the calculated and experimental bond distances and $\text{V}\equiv\text{O}$ stretching frequencies of the hydrated VO^{2+} cation. We find that both B3LYP and M06 $\text{V}\equiv\text{O}$ and $\text{V}-\text{O}_{\text{aq}}$ bond lengths in the six-coordinate $\text{VO}(\text{H}_2\text{O})_5^{2+}$ complex are in reasonable agreement with the EXAFS data,³⁶ with an average error of 0.07 Å. The $\text{V}\equiv\text{O}$ stretching frequencies obtained with B3LYP and M06 are somewhat larger than the experimental one,³⁹ likely because the calculated $\text{V}\equiv\text{O}$ bond lengths are 0.08–0.09 Å shorter than the experimental value and the cluster model we considered did not include a second coordination sphere.

Table 4.2. Comparison of experimental and calculated geometrical parameters and $\text{V}\equiv\text{O}$ stretching frequencies of the hydrated VO^{2+} cation^a

Method	$\text{V}\equiv\text{O}$ (Å)	$\text{V}-\text{O}_{\text{eq}}$ (Å)	$\text{V}-\text{O}_{\text{ax}}$ (Å)	$\text{V}\equiv\text{O}$ Frequency (cm^{-1})
Experiment	1.628 ± 0.005	2.024 ± 0.007	2.20 ± 0.05	985 ± 50
B3LYP/aug-cc-pVDZ	1.55	2.09	2.27	1135
M06/aug-cc-pVDZ	1.54	2.08	2.25	1139

^aBond distances are obtained using EXAFS in the presence of a sulfate anion.³⁷ The $\text{V}\equiv\text{O}$ stretching frequency is obtained using IR in the presence of a sulfate anion.⁴⁰ DFT calculations are carried out for a six-coordinate $\text{VO}(\text{H}_2\text{O})_5^{2+}$ complex **1**.

We performed NBO analyses to investigate the type and the strength of interactions of the VO^{2+} cation with water and formamidoximate ligands. **Table 4.3** shows the significant stabilization interaction energies $E^{(2)}$ for different types of donor-acceptor interactions in the studied VO^{2+} systems. First, let us focus the discussion on the hydrated VO^{2+} complexes. According to the results of NBO analysis for $\text{VO}(\text{H}_2\text{O})_5^{2+}$ the strongest donor-acceptor interactions ($\text{LP}_\text{O} \rightarrow \text{LP}^*_\text{V}$) occur between the water oxygen *sp* (*s* 50.02%; *p* 49.98%) hybridized lone pair (LP_O) and the vanadium 4s and 3d orbitals (LP^*_V). This indicates that the occupied electron lone pairs of the water oxygen enter into the vacant valence orbitals of VO^{2+} to form 2c-2e $\text{V} \leftarrow \text{:O}$ dative bonding. Through such donor-acceptor coordinate bonds, stable hydrated $\text{VO}(\text{H}_2\text{O})_5^{2+}$ complexes are generated. As can be seen in **Figure 4.5**, complex **1** is the most stable and highly coordinate system since VO^{2+} has five dative bonds with all five water molecules surrounding the cation. Though complex **2** is only five-coordinate, lacking the sixth ligand - the axial water oxygen, it is still energetically competitive conformer because of the formation of hydrogen bonding ($E^{(2)} = 33.2$ kcal/mol) between the water molecules in the first and the second coordination spheres. As expected from a chemical bonding point of view, complex **3** is the least stable since the protonation of VO^{2+} , resulting in $\text{V}(\text{OH})_2^{2+}$, is a highly unfavorable process that would lead to the breaking of the strong π bonds (**Figure 4.3**) in VO^{2+} cation. **Table 4.3** also displays weaker interactions of $\text{CR}_\text{V} \rightarrow \text{BD}^*_{\text{Ligand}}$, $\text{LP}_\text{V} \rightarrow \text{BD}^*_{\text{Ligand}}$, and $\text{LP}_\text{V} \rightarrow \text{RY}^*_{\text{Ligand}}$, associated with the partial donation of electron density from the vanadium orbitals (CR_V , LP_V) into acceptor orbitals of the adjacent ligands ($\text{BD}^*_{\text{Ligand}}$, $\text{RY}^*_{\text{Ligand}}$). The appearance of this weak $\text{V} \rightarrow \text{Ligand}^*$ back-donation interaction helps to further stabilize the VO^{2+} complexes by diminishing the accumulation and repulsion of negative charge around the VO^{2+} ion because of the formation of dative bonds between V and ligands.

4.3.3. Formamidoximate-VO²⁺ Complexes

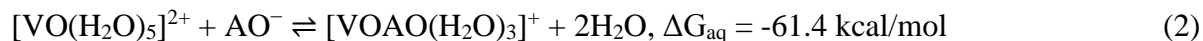
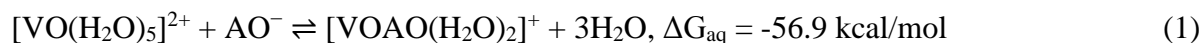
Moving now to amidoxime ligands (AO), complexes with two, VO(AO)(H₂O)₂⁺, and three, VO(AO)(H₂O)₃⁺, explicit water molecules have been examined. Although the amidoxime functional group is weakly acidic (acetamidoxime has an experimental pK_a of 13.21 and a calculated pK_a of 13.3),⁴⁰ we examine the coordination of amidoximate species to VO²⁺ because it has been demonstrated experimentally and computationally in the literature that the amidoximate species coordinates to metal cations.⁴¹⁻⁴⁵ Starting with the VO(AO)(H₂O)₂⁺ complexes, the lowest energy complex obtained at the R/R-CCSD(T)//B3LYP//IEF-PCM(UFF) level of theory was a five-coordinate amine nitrogen and oxime oxygen chelate **4** in **Figure 4.6**. This geometry entails a tautomeric rearrangement of the formamidoximate ligand, which leads to a structure that is ~11 kcal/mol more stable than the non-tautomeric form, **5**. This indicates that the proton transfer between the amine nitrogen and the oxime nitrogen is essential to the formation of the most stable amidoximate-VO²⁺ complexes. Interestingly, the η² coordinating complex **6** is also found to be significantly higher in energy (by ~12 kcal/mol) than **4**. This is an important result due to the fact that amidoximate-UO₂²⁺ η² complexes are generally more stable than the chelate complexes.^{44, 45} These results have significant implications for the design of UO₂²⁺ selective ligands, a topic discussed in the next section. Additionally, we find that a chelate complex **7** formed via amine and oxime nitrogen atoms are significantly less stable than all the binding motifs discussed thus far. Therefore, this binding motif will not be further considered.

The relative electronic energies of the five-coordinate VO(AO)(H₂O)₂⁺ complexes are tabulated by level of theory in **Table 4.4**. DFT optimizations of all four complexes yielded similar relative electronic energies. Moreover, all DFT and R/R-CCSD(T)//B3LYP calculations consistently identified complex **4** as the most stable complex and predicted the relative electronic energies of complexes **5**, **6**, and **7** to be within 1–4 kcal/mol of the R/R-CCSD(T)//B3LYP value.

The relative energies of monodentate complexes could not be examined with two explicit water molecules because the coordination number would be too low. In order to compare the relative stability of monodentate and bidentate binding motifs, $\text{VO}(\text{AO})(\text{H}_2\text{O})_3^+$ complexes with an additional water molecule were considered. Similar to a case with one less water molecule, the lowest energy complex obtained at all levels of theory was the five-coordinate tautomeric, or the amine nitrogen and oxime oxygen chelate, **8** in **Figure 4.7**. The alternative binding motifs are found to be significantly less stable. In particular, the two five-coordinate monodentate complexes obtained, **10** and **15**, are, respectively, ~ 8 kcal/mol and ~ 17 kcal/mol less stable than **8**. Interestingly, both **10** and **15** bear a hydroxyl ligand formed via the transfer of a proton from a water molecule to the oxime oxygen and the amine nitrogen, respectively. Likewise, the non-tautomeric forms, **11** and **13**, and η^2 -coordinated forms, **12** and **14**, are ~ 10 - 12 kcal/mol less stable than their analogous tautomeric chelates, **8** and **9**, respectively. In general, the five-coordinate conformers of different binding motifs (**8**, **11**, and **12**) are slightly more stable (by 0.7 – 3.1 kcal/mol) than the analogous six-coordinate conformer (**9**, **13**, and **14**). The most favorable position of the water molecule in the second coordination sphere (**8**, **11**, and **12**) adopts a hydrogen-bonded arrangement with two water molecules in the inner coordination sphere. Other placements to interact with the amidoximate ligand and the vanadium oxo group were tested, but the resulting complexes appeared to be slightly less stable.

The relative electronic energies of the five- and six-coordinate $\text{VO}(\text{AO})(\text{H}_2\text{O})_3^+$ complexes are tabulated by level of theory in **Table 4.5**. All DFT and R/R-CCSD(T) calculations consistently identified complex **8** as the most stable complex and with the exception of complex **13** predicted the relative electronic energies of complexes **9** -**15** to be within 5 kcal/mol of the R/R-CCSD(T)//B3LYP value.

In order to justify the formation of formamidoximate-VO²⁺ complexes **4** [VOAO(H₂O)₂]⁺ and **8** [VOAO(H₂O)₃]⁺ representing the lowest energy configurations found by our computational search, we calculated the corresponding free energies of complexation (eq 1 and eq 2, respectively) at the R/R-CCSD(T)//B3LYP//IEF-PCM(UFF) level of theory.



Large negative values of ΔG_{aq} for reactions (1) and (2) suggest that AO⁻ displaces water molecules from six-coordinate complex **1** [VO(H₂O)₅]⁺ in aqueous solution.

Finally, in order to find out the reason of the high stability of the chelate binding motif in the studied formamidoximate-VO²⁺ complexes, we performed NBO analysis that enables to assess the strength of interatomic and intermolecular interactions. The results of NBO analyses for complexes **4-8** and **10-12**, which represent different formamidoximate-VO²⁺ binding modes, are shown in **Table 4.3**. According to these results, the addition of the negatively charged formamidoximate ligands to the hydrated vanadyl ion complexes results in the decreased charge on the VO²⁺ due to the formation of dative bonds (complete natural charge analysis for complexes **1-3**, **4-7**, and **8**, **10-12** is shown in **Figures A.4, A.5, and A.6** of **Appendix C**). Though the total amount of electron density shifted from the formamidoximate oxygen and nitrogen donor lone pairs (LP_O→LP*_V, LP_N→LP*_V) to the vanadyl ion LP*_V is almost identical for all studied formamidoximate complexes (as one can judge from the relative VO²⁺ charges in different complexes), the strength of LP_N→LP*_V interactions is ~15 kcal/mol higher for the most stable complexes **4** and **8** than for complexes **5**, **6**, **11**, and **12**. In addition, for complexes **4** and **8** with the chelate binding motif NBO revealed one more distinctive feature – very strong ($E^{(2)} = 90.2 \text{ kcal/mol}$) π -type donation LP_N→BD*_{CN} within the ligand leading to the equalization of the

N-C bond lengths and the formation of the delocalized three-center four-electron (3c-4e) hyperbonding, which can be represented by the resonance structures shown in **Figure 4.8**. It is now evident that by giving increased weight to II-type structure (**Figure 4.8**), the system readjusts to give higher anionic character at the amine nitrogen, thereby increasing the Lewis basicity of the ligand and strengthening VO^{2+} coordination in complexes **4** and **8**. While complex **7** also possesses 3c-4e C-N-C bonding, it was found to be 24.4 kcal/mol less stable (**Figure 4.6**) due to the unfavorable electrostatic interactions and the large strain energy that formamidoximate ligand pays when binding to VO^{2+} ion via the amine and oxime nitrogen atoms. In spite of the fact that NBO identified strong donor-acceptor interactions (**Table 4.3**) in complex **10**, the amount of charge transferred from the ligands to VO^{2+} is less compared to other $\text{VO}(\text{AO})(\text{H}_2\text{O})_3^+$ complexes. This can be attributed to the partial charge delocalization from the hydroxyl ligand to the adjacent protonated oxime group because of the hydrogen bond formation ($\text{LP}_{\text{O}} \rightarrow \text{BD}^*_{\text{NH}}$) with $E^{(2)} = 20.1$ kcal/mol. Complexes **5**, **6**, **11**, and **12** lack the pronounced resonance behavior and are completely described by having only localized one-center two-electron and two-center two-electron bonds. Thus, the stability of the chelate binding motif in complexes **4** and **8** is enhanced by the ligand resonance promoting stronger coordination to VO^{2+} cation.

Table 4.3. Significant donor-acceptor natural bond orbital interactions and their second-order stabilization energies $E^{(2)}$ (kcal/mol). The starred and unstarred labels correspond to Lewis (donor) and non-Lewis (acceptor) NBOs, respectively. Ligands contributing to the particular interaction are shown in parentheses. LP denotes an occupied lone pair; RY* denotes a Rydberg orbital; CR denotes a one-center core pair.

Complex	Donor NBO \rightarrow Acceptor NBO in selected VO ²⁺ complexes					Charge on VO ²⁺ unit
	LP _O \rightarrow LP [*] _V	LP _O \rightarrow LP [*] _V	LP _N \rightarrow LP [*] _V	CR _V \rightarrow BD [*] _{Ligand}	Total	
	(H ₂ O)	(AO)	(AO)	LP _V \rightarrow BD [*] _{Ligand}		
				LP _V \rightarrow RY [*] _{Ligand}		
1	188.7	-	-	8.0	196.7	+1.07
2	184.2	-	-	8.1	192.3	+1.13
3	158.3	-	-	6.5	164.8	-
4	84.8	83.0	61.5	10.2	239.5	+0.86
5	84.1	95.6	46.2	9.1	235.0	+0.86
6	77.0	82.6	44.8	13.6	218.0	+0.84
7	82.9	-	111.9	13.4	208.2	+0.88
8	89.3	83.2	62.3	11.0	245.8	+0.83
10	183.6 ^{\$}	69.6	-	7.6	260.8	+0.86
11	86.3	95.4	45.6	9.2	236.5	+0.85
12	79.6	85.8	48.4	13.8	227.6	+0.83

^{\$} $E^{(2)}$ second-order stabilization energies in complex **10** are tabulated for LP_O \rightarrow LP^{*}_V (H₂O and OH⁻ ligands) interactions.

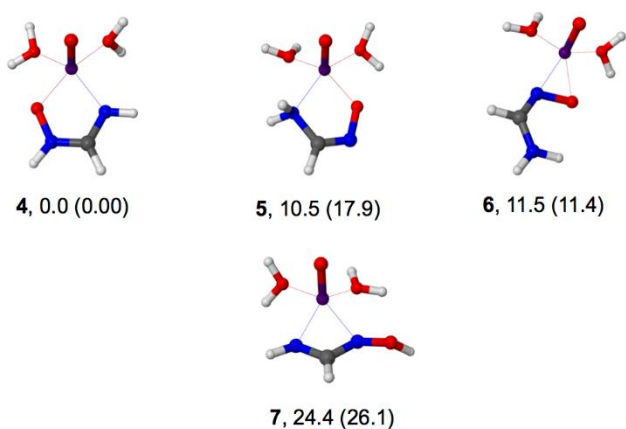


Figure 4.6. Structures and relative Gibbs free energies (kcal/mol) of $\text{VO}(\text{AO})(\text{H}_2\text{O})_2^+$ complexes in aqueous solution and in the gas phase (in parentheses). The electronic energies were obtained at the R/R-CCSD(T)//B3LYP level of theory.

Table 4.4. Relative electronic energies (gas phase) of five-coordinate $\text{VO}(\text{AO})(\text{H}_2\text{O})_2^+$ complexes in kcal/mol.^{a,b}

Theory	4 (c.n.=5)	5 (c.n.=5)	6 (c.n.=5)	7 (c.n.=5)
B3LYP	0.0	21.3	9.5	28.6
M06	0.0	22.2	10.7	26.7
R/R-CCSD(T)//B3LYP	0.0	18.1	13.2	27.9

^aThe aug-cc-pVDZ basis set was employed in all calculations.

^bc.n. denotes coordination number.

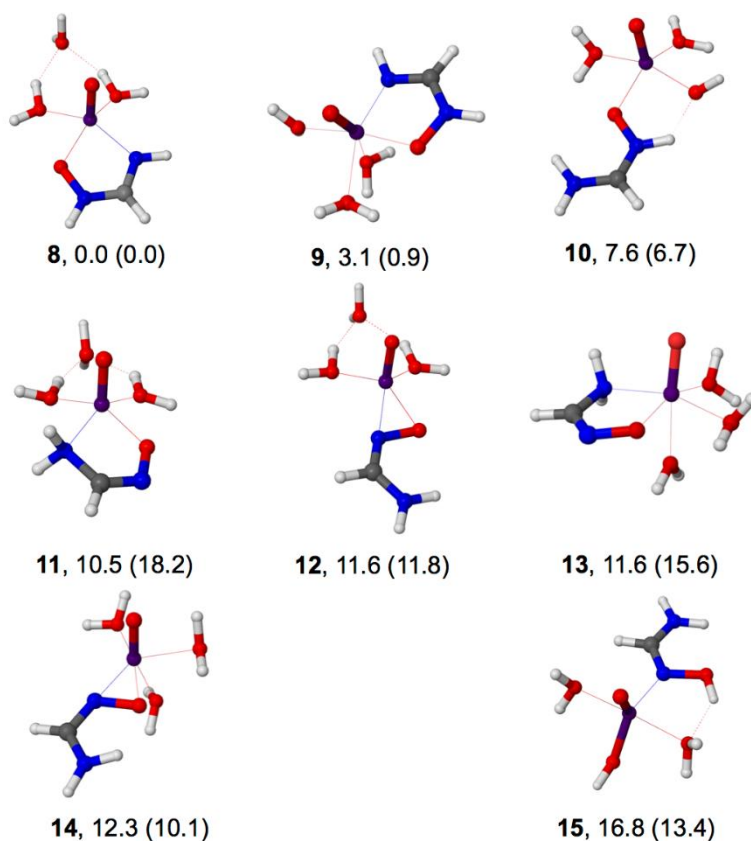


Figure 4.7. Structures and relative Gibbs free energies (kcal/mol) of $\text{VO}(\text{AO})(\text{H}_2\text{O})_3^+$ complexes in aqueous solution and in the gas phase (in parentheses). The electronic energies were obtained at the R/R-CCSD(T)//B3LYP level of theory.

Table 4.5. Relative electronic energies (gas phase) of five- and six-coordinate $\text{VO}(\text{AO})(\text{H}_2\text{O})_3^+$ complexes in kcal/mol.^{a,b}

Theory	8	9	10	11	12	13	14	15
	(c.n.=5)	(c.n.=6)	(c.n.=5)	(c.n.=5)	(c.n.=5)	(c.n.=6)	(c.n.=6)	(c.n.=5)
B3LYP	0.0	5.8	4.4	21.5	9.7	24.9	15.0	9.0
M06	0.0	3.5	7.8	23.3	11.4	23.0	14.0	12.3
R/R- CCSD(T)//B3LYP	0.0	1.0	7.6	18.7	13.6	16.5	12.0	13.9

^aThe aug-cc-pVDZ basis set was employed in all calculations.

^bc.n. denotes coordination number.

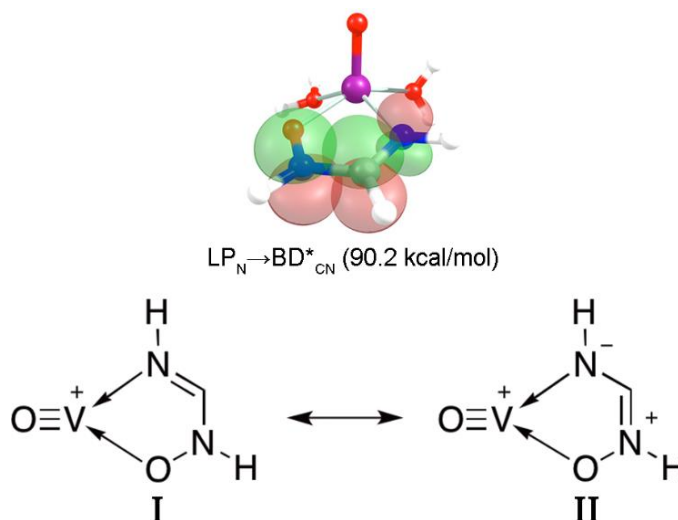


Figure 4.8. Strong π -type $\text{LP}_\text{N} \rightarrow \text{BD}^*_{\text{CN}}$ interaction with associated second-order stabilization energy shown in parentheses. I and II – resonance structures for the most stable $\text{VO}(\text{AO})(\text{H}_2\text{O})_2^+$ complex.

4.3.4. Implications for Ligand Design

As mentioned in **Section 4.3.3**, the most stable binding motif obtained for $\text{VO}(\text{AO})(\text{H}_2\text{O})_n^+$ ($n = 2, 3$), complexes (**4**, **8**, and **9**) was an amine nitrogen and oxime oxygen chelate involving a tautomeric shift of hydrogen from the amide to oxime nitrogen atom. In light of this result, an important question arises as to whether such tautomeric transformation is feasible in aqueous solution. Arshadi et al.⁴⁶ computationally investigated the amidoxime-imino hydroxylamine tautomerization in the absence of complexing ions at the B3LYP level of theory and they reported that the amidoxime form is ~ 10 kcal/mol more stable than the imino hydroxylamine form. Moreover, they found a prohibitively high energy barrier for tautomerization in the gas phase (>30 kcal/mol) that could be reduced substantially in the presence of explicit solvent molecules (≤ 20 kcal/mol).⁴⁶ Since the relative stability of the two tautomers is reversed when bound to VO^{2+} (as follows from the comparison of relative stabilities of **4**, **8**, **9** with **5**, **11**, and **13**, respectively), the reaction barrier of amidoximate- VO^{2+} complexes

is expected to be much smaller than for a free amidoxime ligand. **Figure 4.9** provides an example of a pathway for proton transfer from a formamidoximate-VO²⁺ complex to a formimino hydroxylamine-VO²⁺ complex assisted by four water molecules. We find a very flat reaction energy profile with two transition states lying only 2.6 (TS1) and 0.9 (TS2) kcal/mol above the initial complex. This supports very fast tautomeric proton exchange and equilibration to the most stable chelate structure.

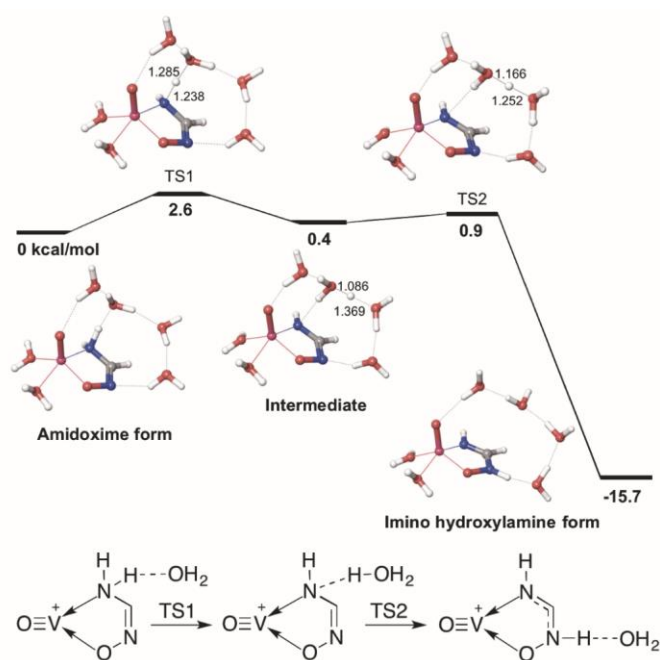
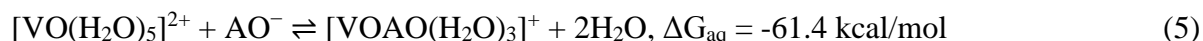
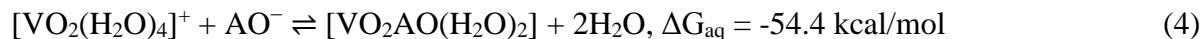
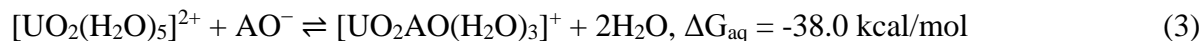


Figure 4.9. Reaction energy (electronic energy with solution correction) profile for tautomerization of formamidoximate coordinated to VO²⁺ in the presence of four additional solvent (water) molecules (kcal/mol). Implicit solvation corrections are obtained using the IEF-PCM solvation model. DFT-optimized O-H bond lengths in the transition and intermediate states are shown (Å).

To provide a deeper understanding of formamidoxime selectivity toward UO²⁺, VO₂⁺, and VO²⁺ ions, it would also be useful to examine their competitive binding. Given that the geometries of the predominant solvated UO²⁺ and VO₂⁺ ions and their complexes with

formamidoximate ligand are known,^{10, 44, 45} we can compute the R/R-CCSD(T)//B3LYP//IEF-PCM(UFF) free energies (ΔG_{aq}) for complexation reactions (3), (4), and (5) (calculations at different levels of theory and the free energies for additional displacement reactions are shown in **Tables A.10-A.12 of Appendix C**).



The results of these calculations indicate that formamidoxime has better selectivity to VO_2^+ and VO^{2+} rather than UO_2^{2+} , which is in accord with recent experimental data⁴⁷ confirming higher vanadium adsorption capacity of amidoxime-based fibers in natural seawater. It is also worth noting that ΔG_{aq} values for VO_2^+ (eq 4) do not provide a true measurement of the binding strength with vanadium(V) species in seawater, because the orthovanadate ion, H_2VO_4^- being in equilibrium with the VO_2^+ cation in aqueous solution, is the most stable solvated form of the dioxovanadium (V) at pH of seawater.^{7, 9, 10} Overall, it is obvious that designing ligands with higher selectivity and binding affinity toward uranium versus vanadium is of immense importance.

While η^2 coordination of the oxime functional group is the most stable coordination mode of amidoximate- UO_2^{2+} complexes,^{44, 45} it is consistently found to be ~11 kcal/mol less stable than the tautomeric rearranged imino hydroxylamine- VO^{2+} chelate. Thus, we suggest that the complexation between poly(acrylamidoxime) fibers and VO^{2+} cations can be restricted by either inhibiting the tautomeric rearrangement from the amidoxime to imino hydroxylamine via substitution of both amine hydrogen atoms with aliphatic or aromatic groups or eliminating the

amine group all together. Incorporating these concepts into ligand design will be an essential aspect to improving the UO_2^{2+} selectivity of future generations of chelating polymers.

The CSD search of VO^{2+} complexes containing coordinated oxime ligands with the no errors, no disorder, and non-polymeric filters¹³ yielded 10 mononuclear complexes. As illustrated in **Figure 4.10**, these complexes can be classified into two categories: η^2 (**Type 1**) that is representative of the binding motif observed in **6**, **12**, and **14**; and monodentate oxygen (**Type 2**) that is representative of the binding motif observed in **10**. While 60% of the complexes were **Type 2** complexes, such as BEGDOI, NEYVIY, and PAVHIE, they were only observed for oximate ligands in the presence of a coordinating RO^- group. This is consistent with the hydroxyl species formed via proton transfer observed in complex **10**. **Type 1** complexes, such as DEYMIE, DEYMOK, and WIDRIL, were universally observed in the absence of additional coordinating groups.

4.4 Conclusion

Poly(acrylamidoxime) fibers are the current state of the art adsorbent for mining uranium from seawater. However, the competition between uranium and vanadium ions poses a significant challenge to the industrial scale mining of uranium,⁷ because in addition to reducing the uranium loading capacity of the fibers, the vanadium stripping process irreversibly damages the fibers.^{4, 8} Thus, there is great interest in understanding how poly(acrylamidoxime) fibers interact with various vanadium species present in seawater. In our previous study¹⁰ we investigated how amidoximate binds to the VO_2^+ cation. The focus of the present work is to understand how the amidoximate ligand binds to the VO^{2+} cation. While a wide variety of

carboxylate-VO²⁺ crystal structures have been reported,¹³ no amidoxime-VO²⁺ complexes have been reported thus far.

Our investigation of formamidoximate-VO²⁺ complexes universally identified the most stable binding motif formed by chelating a tautomerically rearranged imino hydroxylamine ligand via the amine nitrogen and the oxime oxygen. Transition state calculations identified the low-energy pathway for interconversion between the two forms, supporting fast rearrangement to the thermodynamically more stable tautomer. Such unusual stability of the chelate binding mode can be attributed to the resonance enhancement of donor-acceptor coordinate bonding between the formamidoximate ligand and the oxovanadium(IV) ion, as shown by the NBO analysis.

Though comparison of the calculated complexation free energies shows higher formamidoxime selectivity toward vanadium versus uranium species, the uranium uptake can be increased through structural modifications of the ligand. Indeed, previous studies of uranyl coordination showed that the most stable amidoxime-UO₂²⁺ complexes are formed via η^2 coordination of the oxime functional group.^{44, 45} Thus, the difference in the binding motifs for complexation with UO₂²⁺ and VO²⁺ has important implications for ligand design. Specifically, these results indicate that the UO₂²⁺ selectivity of poly(acrylamidoxime) fibers could be improved by designing ligands that either contain only η^2 coordination sites of the oxime functional group or do not permit a tautomeric rearrangement from amidoxime to imino hydroxylamine. The latter can be achieved by substituting both amine hydrogen atoms with aliphatic or aromatic groups. These results provide a first step for developing a computational protocol for predicting the stability constants for VO²⁺ complexes. Furthermore, in conjunction with the recently developed protocol for predicting the stability constants for uranyl⁴⁸ complexes,

this work will provide the essential foundation for the rational design of ligands with enhanced uranyl affinity and selectivity.

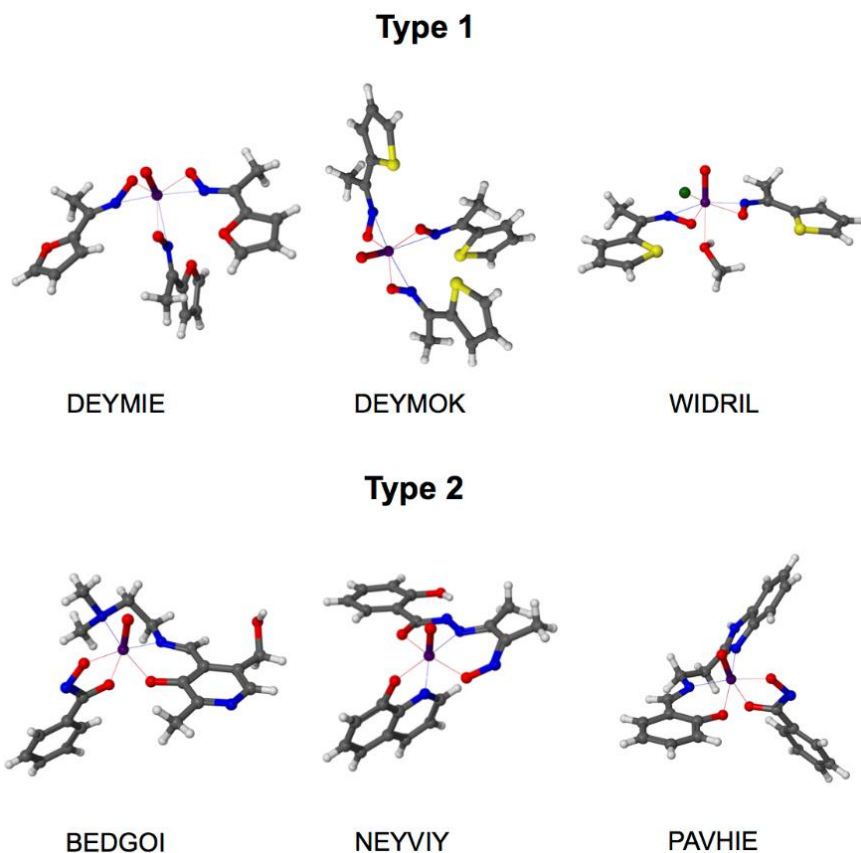


Figure 4.10. CSD crystal structures of oximate-VO²⁺ complexes. The DEYMIE (oxo-tris(2-acetylfulranoximato)-vanadium(IV)), DEYMOK (oxo-tris(2-acetylthiopheneoximato)-vanadium(IV) benzene solvate), and WIDRIL (chloro-methanol-oxo-bis(1-(2-thienyl)ethanone oximato)-vanadium(IV)) complexes are representative of the η^2 binding mode observed in complexes 6, 12, and 14. The BEDGOI ((4-(((2-(Dimethylamino)ethyl)imino)methyl)-5-(hydroxymethyl)-2-methylpyridin-3-olato)-(N-(hydroxy)benzenecarboximidato)-oxo-vanadium), NEYVIY((2-Hydroxy-N-(3-((hydroxy)imino)butan-2-ylidene)benzenecarbohydrazonato)(oxo)(quinolin-8-olato)vanadium), and PAVHIE ((Benzhydroxamato)-(N-salicylidene-2-(benzimidazole-2-yl)ethylamine)-oxo-vanadium(IV)) complexes are representative of the monodentate oxygen binding mode observed in complex 10.

References

1. Davies, R. V.; Kennedy, J.; McIlroy, R. W.; Spence, R.; Hill, K. M., Extraction of Uranium from Sea Water. *Nature* **1964**, *203*, 1110–1115.
2. Saito, K.; Miyauchi, T., Chemical Forms of Uranium in Artificial Seawater. *J. Nucl. Sci. Technol.* **1982**, *19*, 145–150.
3. Choppin, G. R., Soluble Rare Earth and Actinide Species in Seawater. *Mar. Chem.* **1989**, *28*, 19-26.
4. Kim, J. S.; Tsouris, C.; Mayes, R. T.; Oyola, Y.; Saito, T.; Janke, C. J.; Dai, S.; Schneider, E.; Sachde, D., Recovery of Uranium from Seawater: A Review of Current Status and Future Research Needs. *Sep. Sci. Technol.* **2013**, *48*, 367-387.
5. Schenk, H. J.; Astheimer, L.; Witte, E. G.; Schwochau, K., Development of Sorbers for the Recovery of Uranium from Seawater. 1. Assessment of Key Parameters and Screening Studies of Sorber Materials. *Sep. Sci. Technol.* **1982**, *17*, 1293-1308.
6. Astheimer, L.; Schenk, H. J.; Witte, E. G.; Schwochau, K., Development of Sorbers for the Recovery of Uranium from Seawater. Part 2. The Accumulation of Uranium from Seawater by Resins Containing Amidoxime and Imidoxime Functional Groups. *Sep. Sci. Technol.* **1983**, *18*, 307–339.
7. Wang, D. L.; Sañudo Wilhelmy, S. A., Vanadium Speciation and Cycling in Coastal Waters. *Mar. Chem.* **2009**, *117*, 52–58.

8. Suzuki, T.; Saito, K.; Sugo, T.; Ogura, H.; Oguma, K., Fractional Elution and Determination of Uranium and Vanadium Adsorbed on Amidoxime Fiber from Seawater. *Anal. Sci.* **2000**, *16*, 429-432.
9. Abbasse, G.; Ouddane, B.; Fischer, J. C., Determination of Trace Levels of Dissolved Vanadium in Seawater by Use of Synthetic Complexing Agents and Inductively Coupled Plasma-Atomic Emission Spectroscopy (ICP-AES). *Anal. Bioanal. Chem.* **2002**, *374*, 873-878.
10. Mehio, N.; Johnson, J. C.; Dai, S.; Bryantsev, V. S., Theoretical Study of the Coordination Behavior of Formate and Formamidoximate with Dioxovanadium (V) Cation: Implications for Selectivity towards Uranyl. *Phys. Chem. Chem. Phys.*, DOI: 10.1039/C5CP06165B.
11. Kawai, T.; Saito, K.; Sugita, K.; Katakai, A.; Seko, N.; Sugo, T.; Kawakami, T.; Kanno, J., Comparison of Amidoxime Adsorbents Prepared by Cografting Methacrylic Acid and 2-Hydroxyethyl Methacrylate with Acrylonitrile onto Polyethylene. *Ind. Eng. Res. Chem.* **2000**, *39*, 2910-2915.
12. Kawai, T.; Saito, K.; Sugita, K.; Kawakami, T.; Kanno, J.; Katakai, A.; Seko, N.; Sugo, T., Preparation of Hydrophilic Amidoxime Fibers by Cografting Acrylonitrile and Methacrylic Acid from an Optimized Monomer Composition. *Radiat. Phys. Chem.* **2000**, *59*, 405-411.
13. Allen, F. H., The Cambridge Structural Database: A Quarter of a Million Crystal Structures and Rising. *Acta Cryst. B* **2002**, *58*, 380-386.

14. Schupp, J. D.; Duraj, S. A.; Richman, R. M.; Hepp, A. F.; Fanwick, P. E., The Crystal and Molecular Structure of Acetatochlorobis(4-methylpyridine) oxovanadium (IV). *J. Coord. Chem.* **2010**, *55*, 1045-1051.
15. Koleča-Dobravc, T.; Lodyga-Chruscinska, E.; Symonowicz, M.; Sanna, D.; Meden, A.; Perdih, F.; Garribba, E., Synthesis and Characterization of VIVO Complexes of Picolinate and Pyrazine Derivatives. Behavior in the Solid State and Aqueous Solution and Biotransformation in the Presence of Blood Plasma Proteins. *Inorg. Chem.* **2014**, *53*, 7960-7976.
16. Frisch, M. J.; Trucks, G. W.; Schlegel, H. B.; Scuseria, G. E.; Robb, M. A.; Cheeseman, J. R.; Scalmani, G.; Barone, V.; Mennucci, B.; Petersson, G. A.; Nakatsuji, H.; Caricato, M.; Li, X.; Hratchian, H. P.; Izmaylov, A. F.; Bloino, J.; Zheng, G.; Sonnenberg, J. L.; Hada, M.; Ehara, M.; Toyota, K.; Fukuda, R.; Hasegawa, J.; Ishida, M.; Nakajima, T.; Honda, Y.; Kitao, O.; Nakai, H.; Vreven, T.; Montgomery, J. A., Jr. ; Peralta, J. E.; Ogliaro, F.; Bearpark, M.; Heyd, J. J.; Brothers, E.; Kudin, K. N.; Staroverov, V. N.; Kobayashi, R.; Normand, J.; Raghavachari, K.; Rendell, A.; Burant, J. C.; Iyengar, S. S.; Tomasi, J.; Cossi, M.; Rega, N.; Millam, M. J.; Klene, M.; Knox, J. E.; Cross, J. B.; Bakken, V.; Adamo, C.; Jaramillo, J.; Gomperts, R.; Stratmann, R. E.; Yazyev, O.; Austin, A. J.; Cammi, R.; Pomelli, C.; Ochterski, J. W.; Martin, R. L.; Morokuma, K.; Zakrzewski, V. G.; Voth, G. A.; Salvador, P.; Dannenberg, J. J.; Dapprich, S.; Daniels, A. D.; Farkas, Ö.; Foresman, J. B.; Ortiz, J. V.; Cioslowski, J.; Fox, D. J. *Gaussian 09 Revision D.01*, Gaussian, Inc.: Wallingford, CT, 2009.
17. Hohenberg, P.; Kohn, W., Inhomogeneous Electron Gas. *Phys. Rev.* **1964**, *136*, B864–B871.

18. Kohn, W.; Sham, L. J., Self-Consistent Equations Including Exchange and Correlation Effects. *Phys. Rev.* **1965**, *140*, A1133–A1138.
19. Becke, A. D., Density-Functional Thermochemistry. III. The Role of Exact Exchange. . *J. Chem. Phys.* **1993**, *98*, 5648–5652.
20. Lee, C.; Yang, W.; Parr, R. G., Development of the Colle-Salvetti Correlation-Energy Formula Into a Functional of the Electron Density. *Phys. Rev. B* **1988**, *37*, 785–789.
21. Zhao, Y.; Truhlar, D. G., The M06 Suite of Density Functionals for Main Group Thermochemistry, Thermochemical Kinetics, Noncovalent Interactions, Excited States, and Transition Elements: Two New Functionals and Systematic Testing of Four M06-Class Functionals and 12 Other Functionals. *Theor. Chem. Acc.* **2008**, *120*, 215-241.
22. Dunning, T. H. J., Gaussian Basis Sets for Use in Correlated Molecular Calculations. I. The Atoms Boron through Neon and Hydrogen. *J. Chem. Phys.* **1989**, *90*, 1007-1023.
23. Kendall, R. A.; Dunning, T. H. J.; Harrison, R. J., Electron Affinities of the First- Row Atoms Revisited. Systematic Basis Sets and Wave Functions. *J. Chem. Phys.* **1992**, *96*, 6796-6806.
24. Purvis, G. D.; Bartlett, R. J., A Full Coupled-Cluster Singles and Doubles Model: The Inclusion of Disconnected Triples. *J. Chem. Phys.* **1982**, *76*, 1910-1918.
25. Raghavachari, K.; Trucks, G. W.; Pople, J. A.; Head-Gordon, M., A Fifth-Order Perturbation Comparison of Electron Correlation Theories. *Chem. Phys. Lett.* **1989**, *157*, 479-483.

26. Watts, J. D.; Gauss, J.; Bartlett, R. J., Coupled-Cluster Methods with Noniterative Triple Excitations for Restricted Open-Shell Hartree–Fock and Other General Single Determinant Reference Functions. Energies and Analytical Gradients. *J. Chem. Phys.* **1993**, *98*, 8718–8733.
27. Dolog, M.; Stoll, H.; Preuss, H.; Pitzer, R. M., Relativistic and Correlation Effects for Element 105 (Hahnium, Ha): A Comparative Study of M and MO (M = Nb, Ta, Ha) Using Energy-Adjusted Ab Initio Pseudopotentials. *J. Phys. Chem.* **1993**, *97*, 5852–5859.
28. Miertuš, S.; Scrocco, E.; Tomasi, J., Electrostatic Interaction of a Solute with a Continuum. A Direct Utilization of ab initio Molecular Potentials for the Prevision of Solvent Effects. *Chem. Phys.* **1981**, *55*, 117–129.
29. Cancès, E.; Mennucci, B.; Tomasi, J., A New Integral Equation Formalism for the Polarizable Continuum Model: Theoretical Background and Applications to Isotropic and Anisotropic Dielectrics. *J. Chem. Phys.* **1997**, *107*, 3032–3041.
30. Mennucci, B.; Cancès, E.; Tomasi, J., Evaluation of Solvent Effects in Isotropic and Anisotropic Dielectrics and in Ionic Solutions with a Unified Integral Equation Method: Theoretical Bases, Computational Implementation, and Numerical Applications. *J. Phys. Chem. B* **1997**, *101*, 10506–10517.
31. Marenich, A. V.; Cramer, C. J.; Truhlar, D. G., Universal Solvation Model Based on Solute Electron Density and a Continuum Model of the Solvent Defined by the Bulk Dielectric Constant and Atomic Surface Tensions. *J. Phys. Chem. B* **2009**, *113*, 6378–6396.

32. Foster, J. P.; Weinhold, F., Natural Hybrid Orbitals. *J. Am. Chem. Soc.* **1980**, *102*, 7211-7218.
33. Reed, A. E.; Curtiss, L. A.; Weinhold, F., Intermolecular Interactions from a Natural Bond Orbital, Donor-Acceptor Viewpoint *Chem. Rev.* **1988**, *88* 899–926.
34. Glendening, E. D.; Badenhoop, J. K.; Reed, A. E.; Carpenter, J. E.; Bohmann, J. A.; Morales, C. M.; Landis, C. R.; Weinhold, F. *NBO, version 6.0.*, Theoretical Chemistry Institute, University of Wisconsin, Madison: Madison, Wisconsin, 2013.
35. Winkler, J. R.; Gray, H. B., Electronic Structure of Oxo-Metal Ions. In *Molecular Electronic Structures of Transition Metal Complexes I*, Mingos, D. M. P.; Day, P.; Dahl, J. P., Eds. Springer-Verlag Berlin Heidelberg: New York, 2012; Vol. 142, pp 17-28.
36. Krakowiak, J.; Lundberg, D.; Persson, I., A Coordination Chemistry Study of Hydrated and Solvated Cationic Vanadium Ions in Oxidation States +III, +IV, and +V in Solution and Solid State. *Inorg. Chem.* **2012**, *51*, 9598-9609.
37. Jørgensen, C. K., Comparative Ligand Field Studies. IV. Vanadium(IV), Titanium(III), Molybdenum(V), and other Systems with one d-Electron. *Acta Chem. Scand.* **1957**, *11*, 73-85.
38. Taube, H., *Mechanistic Aspects of Inorganic Reactions*. American Chemical Society: Washington DC, 1982; Vol. 198.
39. Selbin, J.; Holmes Jr., L. H.; McGlynn, S. P., Electronic Structures, Spectra and Magnetic Properties of Oxycations-IV: Ligation Effects on the Infra-red Spectrum of the Vanadyl Ion. *J. Inorg. Nucl. Chem.* **1963**, *25*, 1359-1369.

40. Mehio, N.; Lashley, M. A.; Nugent, J. W.; Tucker, L.; Correia, B.; Do-Thanh, C.-L.; Dai, S.; Hancock, R. D.; Bryantsev, V. S., Acidity of the Amidoxime Functional Group in Aqueous Solution: A Combined Experimental and Computational Study. *J. Phys. Chem. B* **2015**, *119*, 3567–3576.
41. Tian, G.; Teat, S. J.; Zhang, Z.; Rao, L., Sequestering Uranium from Seawater: Binding Strength and Modes of Uranyl Complexes with Glutarimidedioxime. *Dalton Trans.* **2012**, *41*, 11579-11586.
42. Tian, G.; Teat, S. J.; Rao, L., Thermodynamic Studies of U(VI) Complexation with Glutardiamidoxime for Sequestration of Uranium from Seawater. *Dalton Trans.* **2013**, *42*, 5690-5696.
43. Sun, X.; Xu, C.; Tian, G.; Rao, L., Complexation of Glutarimidedioxime with Fe(III), Cu(II), Pb(II), and Ni(II), the Competing Ions for the Sequestration of U(VI) from Seawater. *Dalton Trans.* **2013**, *42*, 14621-14627.
44. Vukovic, S.; Watson, L. A.; Kang, S. O.; Custelcean, R.; Hay, B. P., How Amidoximate Binds the Uranyl Cation. *Inorg. Chem.* **2012**, *51*, 3855–3859.
45. Kelley, S. P.; Barber, P. S.; Mullins, P. H. K.; Rogers, R. D., Structural Clues to $\text{UO}_2^{2+}/\text{VO}_2^+$ Competition in Seawater Extraction Using Amidoxime-Based Extractants. *Chem. Commun.* **2014**, *50*, 12504-12507.
46. Tavakol, H.; Arshadi, S., Theoretical Investigation of Tautomerism in N-Hydroxy Amidines. *J. Mol. Model* **2009**, *15*, 807–816.

47. Das, S.; Liao, W.-P.; Flicker Byers, M.; Tsouris, C.; Janke, C. J.; Mayes, R. T.; Schneider, E. A.; Kuo, L.-J.; Wood, J.; Gill, G. A.; Dai, S., Alternative Alkaline Conditioning of Amidoxime Based Adsorbent for Uranium Extraction from Seawater. *Ind. Eng. Chem. Res* **2015**, DOI: 10.1021/acs.iecr.5b03210.
48. Vukovic, S.; Hay, B. P.; Bryantsev, V. S., Predicting Stability Constants for Uranyl Complexes Using Density Functional Theory. *Inorg. Chem.* **2015**, *54*, 3995-4001.

Chapter 5 : Quantifying the Binding Strength of Salicylaldoxime-Uranyl Complexes Relative to Competing Salicylaldoxime-Transition Metal Ion Complexes in Aqueous Solution: A Combined Experimental and Computational Study

A version of this chapter was originally published in *Dalton Transactions* by Nada Mehio, Alexander S. Ivanov, Neil J. Williams, Richard T. Mayes, Vyacheslav S. Bryantsev, Robert D. Hancock, and Sheng Dai:

Mehio, N.; Ivanov, A. S.; Williams, N. J.; Bryantsev, V. S.; Hancock, R. D.; Dai, S. “Quantifying the Binding Strength of Salicylaldoxime-Uranyl Complexes Relative to Competing Salicylaldoxime-Transition Metal Ion Complexes in Aqueous Solution: A Combined Experimental and Computational Study.” *Dalton Trans.*, accepted.

Abstract

The design of new ligands and investigation of UO_2^{2+} complexations are an essential aspect of reducing the cost of extracting uranium from seawater, improving the sorption efficiency for uranium and the selectivity for uranium over competing ions (such as the transition metal cations). The binding strengths of salicylaldoxime- UO_2^{2+} complexes were quantified for the first time and compared with the binding strengths of salicylic acid- UO_2^{2+} and representative amidoxime- UO_2^{2+} complexes. We found that the binding strengths of salicylaldoxime- UO_2^{2+} complexes are $\sim 2\text{-}4 \log \beta_2$ units greater in magnitude than their corresponding salicylic acid- UO_2^{2+} and representative amidoxime- UO_2^{2+} complexes; moreover, the selectivity of salicylaldoxime towards the UO_2^{2+} cation over competing Cu^{2+} and Fe^{3+} cations is far greater than those reported for salicylic acid and glutarimidedioxime in the literature. The higher UO_2^{2+} selectivity can likely be attributed to the different coordination modes observed for salicylaldoxime- UO_2^{2+} and salicylaldoxime-transition metal complexes. Density functional theory calculations indicate that salicylaldoxime can coordinate to UO_2^{2+} as a dianion species formed by η^2 coordination of the aldoximate and monodentate binding of the phenolate group. In contrast, salicylaldoxime coordinates to transition metal cations as a monoanion species via a

chelate formed between phenolate and the oxime N; the complexes are stabilized via hydrogen bonding interactions between the oxime OH group and phenolate. By coupling the experimentally determined thermodynamic constants and the results of theoretical computations, we are able to derive a number of ligand design principles to further improve the UO_2^{2+} cation affinity, and thus further increase the selectivity of salicylaldoxime derivatives.

5.1 Introduction

In recent years, there has been great interest in developing low-carbon emission energy sources as an alternative to the widely utilized, high-carbon emission fossil fuels. Nuclear energy is a promising alternative as there is an abundance of fuel, including an estimated 4.5 billion tons of uranium dissolved in seawater,¹ largely in the form of a uranyl tricarbonat calcium salt, $\text{Ca}_2\text{UO}_2(\text{CO}_3)_3$,¹⁻⁴ while only 5000 tons of uranium are needed annually to meet today's energy needs.⁵ However, there are a number of challenges associated with developing an adsorbent capable of extracting uranium from seawater that primarily stem from the fact that UO_2^{2+} is present in very low concentrations, 3.3 ppb,⁶ in the presence of competing metal cations.² Therefore, the development of extremely efficient and selective adsorbents is instrumental to making this process viable. Currently, the leading approach for extraction of uranium from seawater is selective sorption of UO_2^{2+} via a poly(acrylamidoxime)-based sorbent.⁷⁻¹⁰ Poly(acrylamidoxime)-based sorbents are polymers bearing amidoxime, typically generated from acrylonitrile. The addition of acidic co-monomers has been reported to influence the hydrophilicity of the polymer thereby enhancing the sorption capacity.¹¹⁻¹² Amidoximes were first identified in a screening of 200 organic polymers as the only adsorbent capable of extracting UO_2^{2+} from pH 8.3 aqueous solution, the approximate pH of seawater.⁷⁻⁸ However, the amidoxime functional group is not uniquely selective towards the UO_2^{2+} cation in seawater, in

particular, competition with transition metal cations, such as Fe^{3+} (3.4 ppb)⁶, Cu^{2+} (0.9 ppb)⁶, VO^{2+} , and VO_2^+ (1.9 ppb)⁶, remain a major challenge.^{5, 13-15} Therefore, the design of new ligands involving investigations of UO_2^{2+} complexation will play an essential role in reducing the cost of extracting uranium from seawater, improving the sorption efficiency for uranium, and improving the selectivity for uranium over competing ions (such as the transition metal ions).

In order to design a new generation of ligands that are more selective towards the UO_2^{2+} cation we decided to gain more insight into how the amidoxime functional group interacts with transition metal cations by searching the Cambridge Structural Database (CSD).¹⁶ A CSD search (2014 release, version 5.36) of an unspecified transition metal and an amidoximate ligand with “any” bond specification for all carbon-nitrogen bonds and amine proton with the no error, no disorder, and ‘not polymeric’ filters applied yielded 635 hits which were scrutinized to remove duplicate structures, structures containing amidoximate ligands that are not directly coordinated to the metal center, structures that did not contain amidoximate ligands, and polynuclear complexes. As illustrated in **Figure 5.1**, the remaining 84 complexes can be classified into two categories: complexes in which aliphatic or aromatic amine directly plays a role in binding the transition metal center (**Type 1**), and complexes in which an amine does not directly play a role in binding the transition metal center (**Type 2**). Approximately 62% of the complexes obtained were **Type 2** complexes, such as CIMMIW ($\text{C}_6\text{H}_{18}\text{N}_{12}\text{NiO}_6^{2+} \cdot 2(\text{BF}_4^-)$),¹⁷ WOBHUS ($\text{C}_4\text{H}_8\text{CuN}_4\text{O}_7$),¹⁸ TEKYUD ($\text{C}_{20}\text{H}_{24}\text{N}_6\text{NiO}_4$),¹⁹ RASBIW ($\text{C}_{15}\text{H}_{16}\text{MoN}_4\text{O}_5\text{S}_2$),²⁰ and FOWJAC ($\text{C}_{12}\text{H}_{19}\text{MoN}_3\text{O}_6$).²¹ With the exception of three Mo^{6+} and MoO^{4+} η^2 complexes, two of which are illustrated in **Figure 1** (RASBIW and FOWJAC), oximate nitrogen coordination without an amine was only observed for bisamidoximate complexes in the absence of additional amines. In the absence of an additional amidoximate, **Type 1** complexes were observed, whether this

entailed coordination of the amine group in the amidoxime functional group, such as CUHJUK ($\text{C}_{10}\text{H}_6\text{CuN}_{10}\text{O}_2^{2-} \cdot 2(\text{Na}^+) \cdot 8(\text{H}_2\text{O})$)²² and ORUTIF ($\text{C}_{16}\text{H}_{17}\text{N}_4\text{O}_3\text{Tc}$),²³ or coordination of a linked aliphatic or aromatic amine, such as ACOXNI10 ($\text{C}_8\text{H}_{22}\text{CuN}_{10}\text{O}_4^{2+} \cdot 2(\text{Cl}^-)$),²⁴ AICOCU10 ($\text{C}_8\text{H}_{14}\text{CuN}_{10}\text{O}_2^{2+} \cdot 2(\text{ClO}_4^-)$),²⁵ and YOHFEI ($\text{C}_{16}\text{H}_{20}\text{CdN}_6\text{O}_6 \cdot 2(\text{C}_2\text{H}_6\text{O})$).²⁶ These results indicate that monodentate oximate nitrogen coordination to a transition metal is relatively unstable. Moreover, these results indicate that the elimination of the amine functional group can destabilize the interaction between the oximate nitrogen and transition metal cations.

Likewise, salicylic acid is a well-known UO_2^{2+} complexant with a history of use as a ligand for the spectrophotometric analytical determination of uranium.²⁷ Salicylic acid has a UO_2^{2+} stability constant ($\log \beta_1$) value of 13.1²⁸ that is comparable in value to the UO_2^{2+} $\log \beta_1$ value of acetamidoxime ($\log \beta_1 = 13.6$)²⁹ and greater in value than the UO_2^{2+} $\log \beta_1$ value of benzamidoxime, ($\log \beta_1 = 12.4$).²⁹ This is interesting when compared to the $\log \beta_1$ values of ligands bearing each functional group individually, such as phenol ($\log \beta_1 = 5.9$)²⁸ and benzoic acid ($\log \beta_1 = 2.68$)²⁸, suggesting the hydroxyl and carboxylic acid functional groups are interacting synergistically when placed in close proximity in salicylic acid. However, this synergistic effect is not confined to the UO_2^{2+} cation, since salicylic acid forms strong complexes with transition metal cations as well.²⁸

Thus, one such approach to improving the stability and selectivity of salicyl ligands would involve using an oxime group in place of a carboxylic group. We decided to test salicylaldoxime (**Figure 5.2**, structure $\text{H}_2\text{L}^{(\text{I})}$) because it is an aldoxime analog of salicylic acid. An aldoxime is an analog of an amidoxime with a proton in place of the amine, i.e., benzaldoxime relative to benzamidoxime in **Figure 5.2**, structures $\text{HL}^{(\text{III})}$ and $\text{HL}^{(\text{VI})}$, respectively. An advantage to using an aldoxime is that it simultaneously preserves the oximate

group that is capable of η^2 coordination to the UO_2^{2+} cation³⁰⁻³¹ and eliminates the stabilizing effect of amine coordination observed in amidoxime-transition metal cations. Moreover, Rao and co-workers utilized salicylaldoxime in an ion imprinted polymer to extract UO_2^{2+} via an ion-exchange method and demonstrated that it selectively extracted more UO_2^{2+} than competing lanthanide, alkaline, and alkaline earth metal cations and a number of competing transition metal cations, such as Pd^{2+} , Ni^{2+} , Cd^{2+} , Pb^{2+} , Mn^{2+} , Co^{2+} , and Zr^{4+} .³² Herein, we report the results of an investigation into methods for improving the selectivity of salicyl-based ligands by substituting an aldoxime for a carboxylic acid.

5.2 Experimental Methods

5.2.1 Materials and Methods

Salicylaldoxime (Sigma-Aldrich; $\geq 98\%$ purity), uranyl nitrate hexahydrate ($\text{UO}_2(\text{NO}_3)_2 \cdot 6\text{H}_2\text{O}$; B&A Quality) and sodium hydroxide (NaOH ; Ricca Chemical Company; NIST certified) were used as received. Since the UO_2^{2+} cation is prone to hydrolysis, pH 2 stock solutions were prepared by dissolving $\text{UO}_2(\text{NO}_3)_2 \cdot 6\text{H}_2\text{O}$ salt in standardized 0.01 M perchloric acid (10.21 M HClO_4 ; Alfa Aesar; ACS grade). All solutions were made up in deionized water (Milli-Q, Waters Corp.) of $18.2 \text{ M}\Omega \text{ cm}^{-1}$ resistivity.

5.2.2 pH Measurements

The solution pH was monitored using an Oakton 510 Series pH meter with an Oakton WD-35801-00 epoxy body combination pH electrode. The pH meter was standardized by obtaining the Nernstian slope and E° correction factors from the titration curve of a strong acid/strong base titration, specifically, standardized 0.0100 M HClO_4 and 0.0100 M NaOH (Ricca Chemical Company). Prior to each titration, the pH meter was calibrated using pH 4.01, pH 7.00, and pH 10.01 buffers (Thermo Scientific). Nitrogen (N_2) gas was used to purge carbon

dioxide (CO₂) and oxygen (O₂) and to mix the solution via mild agitation. The uncertainty associated with the pH measurements was determined statistically by measuring and fitting the pK_a and log β values of five titration iterations involving the oxime and oximate-UO₂²⁺ complex. A standard deviation of 0.03 log units was obtained.

5.2.3 UV/Vis Titrations

UV/Vis spectroscopy was carried out using a Thermo Scientific Evolution 600 UV-Vis Spectrophotometer, the Thermo Scientific VISION *pro* software, and 1 cm matched quartz cells. The scan method entailed a double beam mode with a zero/baseline correction. Deionized water (Milli-Q, Waters Corp.) of 18.2 MΩ cm⁻¹ resistivity was employed as the reference solution for all pK_a, log β₁, and log β₂ measurements. The reference solution was of the same volume and initial pH as the analyzed solution and comparable additions of acid or base added to the analyzed solution were added to the reference solution to account for any possible change in the refractive index. A jacketed titration cell connected to a constant temperature water bath set to 25.0 ± 0.1 ° C was employed for all pK_a, log β₁, and log β₂ measurements. The titrations involved 100 mL solutions of 5 x 10⁻⁵ M salicylaldoxime for pK_a determination, 100 mL solutions of 4.8 x 10⁻⁵ M salicylaldoxime and 4.8 x 10⁻⁵ uranyl perchlorate for log β₁ determination, and 100 mL solutions of 4.8 x 10⁻⁵ M salicylaldoxime and 4.8 x 10⁻⁶ uranyl perchlorate for log β₂ determination.

The data was analyzed in Excel using Solver to minimize the mean absolute error (MAE) between theoretical and observed absorbance data at six different wavelengths. Summing the product of each individual species' α-fraction and molar absorptivity, or the absorbance value that coincides with the respective species' half-equivalence point, generates theoretical

absorbance data. Solver minimizes the MAE by varying the pK_a and/or $\log \beta$ values of the observed species and their corresponding molar absorptivities.

5.3 Computational Methods

5.3.1 Electronic Structure Calculations

Electronic structure calculations were performed with the Gaussian 09 D.01 software.³³ We adopted the density functional theory (DFT) approach for our calculations using the B3LYP³⁴⁻³⁵ and M06³⁶ density functionals with the standard Stuttgart small-core (SSC) 1997 relativistic effective core potential (RECP)³⁷, the associated contracted [8s/7p/6d/4f] basis set for uranium, [6s/5p/3d] basis set for copper, and the 6-311++G** basis set for the light atoms. Frequency calculations were performed at the B3LYP/SSC/6-31+G* level to ensure that geometries were minima and to compute zero-point energies and thermal corrections using a methodology introduced by Truhlar et al.,³⁸ which is based on the so-called quasiharmonic approximation – the usual harmonic oscillator approximation, except that vibrational frequencies lower than 30 cm^{-1} were raised to 30 cm^{-1} as a way to correct for the well-known breakdown of the harmonic oscillator model for the free energies of low-frequency vibrational modes. Using the gas-phase geometries, implicit solvent corrections were obtained at 298 K with the SMD³⁹ solvation model in Gaussian at the B3LYP/SSC/6-31+G* level of theory. The preference for using a combination of the B3LYP and the M06 functionals with the SMD solvation model was based on the results of our previous studies,^{29, 40-41} which show that the chosen level of theory provides the best overall performance in predicting the $\log \beta$ values of uranyl complexes with negative oxygen and amidoxime donor ligands.

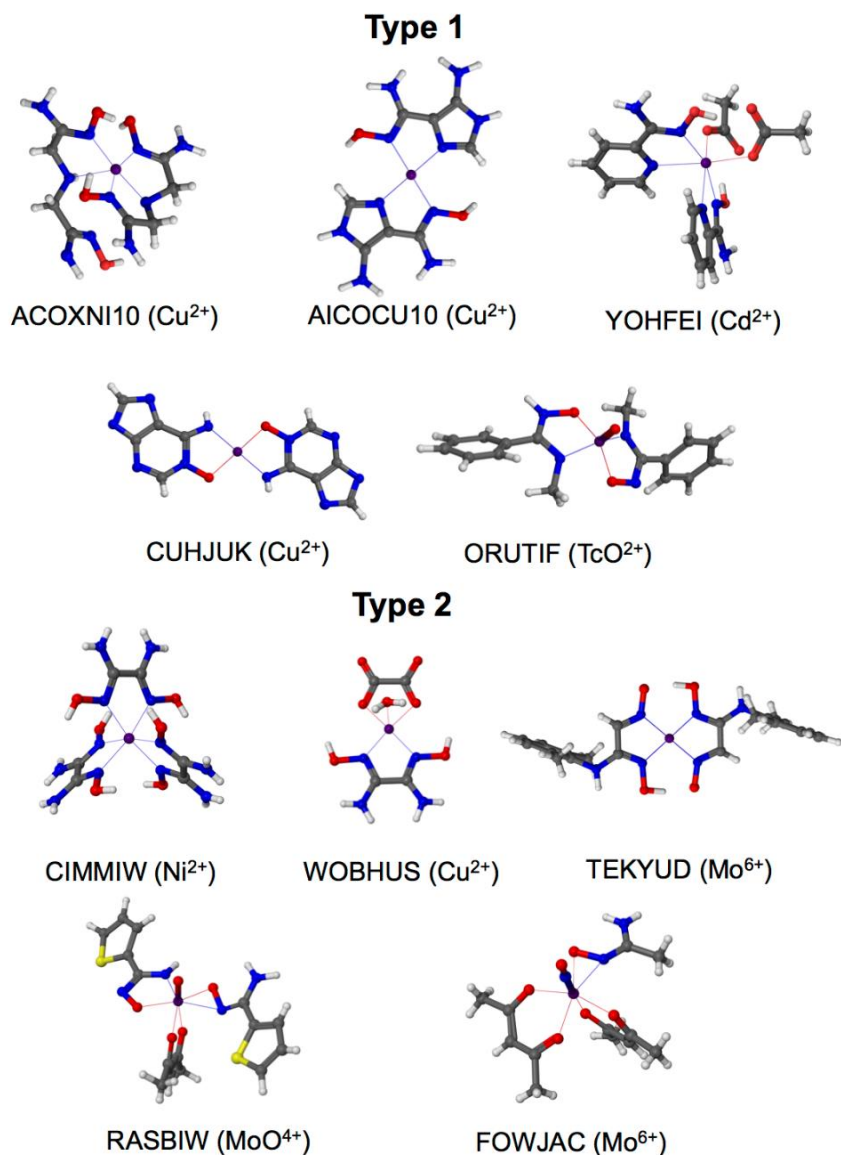


Figure 5.1. Crystal structures of amidoximate-transition metal complexes from the CSD. The **Type1** complexes are representative of complexes in which an amine is directly involved in coordination. The **Type 2** complexes are representative of complexes in which an amine is not directly involved in coordination. The full chemical formulas of the crystal structures are provided in **Table A.13** of **Appendix D** by CSD reference code. Color legend: O, red; N, blue; C, grey; H, white; S, yellow; metal ion, purple.

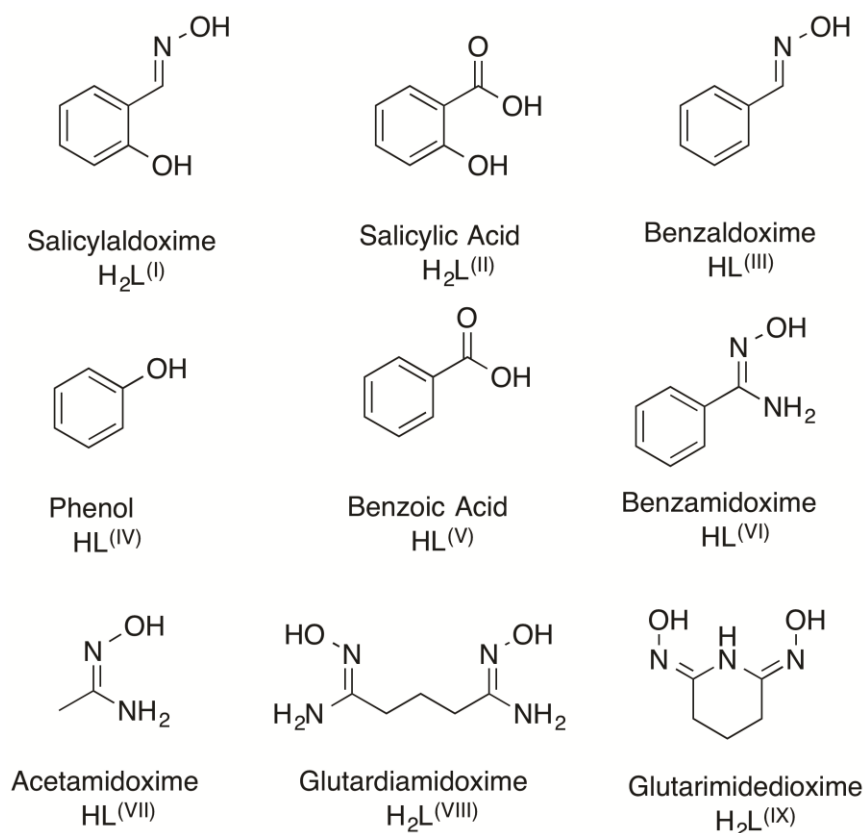


Figure 5.2. Ligands discussed in this paper.

5.3.2. Calculation of the Complexation Free Energies and Stability Constants

Complexation free energies in aqueous solution, ΔG_{aq} , and stability constants ($\log \beta$) were calculated using the methodology described in ref 41.⁴¹ The thermodynamic cycle used in the calculations is shown in **Figure A.7** of **Appendix D**. According to this cycle, ΔG_{aq} is given by:

$$\Delta G_{\text{aq}} = \Delta G_{\text{g}}^{\circ} + \Delta \Delta G_{\text{solv}}^* + (n-1)\Delta G^{\circ \rightarrow *} + nRT \ln([H_2O])$$

where $\Delta G_{\text{g}}^{\circ}$ is the free energy of complexation in the gas phase and $\Delta \Delta G_{\text{solv}}^*$ is the difference in the solvation free energies for a reaction:

$$\Delta \Delta G_{\text{solv}}^* = \Delta G_{\text{solv}}^*([ML(H_2O)_{m-n}]^{x+y}) + n\Delta G_{\text{solv}}^*(H_2O)$$

$$- \Delta G_{\text{solv}}^*([M(\text{H}_2\text{O})_m]^x) - \Delta G_{\text{solv}}^*(\text{L}^y)$$

where L^y denotes the ligand with a charge of y and M can be UO_2^{2+} or Cu^{2+} . The standard state correction terms must be introduced to connect ΔG_{g}^0 , $\Delta \Delta G_{\text{solv}}^*$, and $\Delta \Delta G_{\text{aq}}$ that are defined using different standard state conventions. The free energy change for the conversion of 1 mol of solute from the gas phase at a standard state of 1 atm (24.46 L/mol) to the aqueous phase at a standard state of 1 mol/L at 298.15 K is given by $\Delta G^{0 \rightarrow *}_{\text{g} \rightarrow \text{aq}} = 1.89$ kcal/mol. Likewise, $RT \ln([\text{H}_2\text{O}]) = 2.38$ kcal/mol ($T = 298.15$ K) is the free energy change for the conversion of 1 mol of solvent from the aqueous phase at 1 mol/L to pure water at a standard state of 55.34 mol/L. Finally, the stability constant ($\log \beta$) value is related to free energy change for the complexation reaction by the following equation: $\log \beta = \frac{-\Delta G_{\text{aq}}}{2.303 \cdot RT}$

5.3.3 Natural Bond Orbital (NBO) Analysis

Chemical bonding analysis of $[\text{UO}_2(\text{L}^{\text{I}})(\text{H}_2\text{O})_2]$, $[\text{UO}_2(\text{L}^{\text{III}})(\text{H}_2\text{O})_3]^+$, and $[\text{UO}_2(\text{L}^{\text{IV}})(\text{H}_2\text{O})_4]^+$ complexes was performed with the NBO method⁴²⁻⁴³ at the B3LYP/SSC/6-31G* level using NBO 6.0 program. NBO analysis provides a good quantitative description of interatomic and intermolecular interactions in accordance with the basic Pauling-Slater-Coulson representations of bond polarization and hybridization.⁴²⁻⁴³ The donor-acceptor interaction energy in the NBOs was estimated via second-order perturbation theory analysis of the Fock matrix.⁴²⁻⁴³ For each donor orbital (i) and acceptor orbital (j), the stabilization energy $E^{(2)}$ associated with $i \rightarrow j$ delocalization is given by:

$$E_{i,j}^{(2)} = -o_i \frac{\langle i | \hat{F}_{(i,j)} | j \rangle^2}{e_j - e_i}$$

where o_i is the donor orbital occupancy, $\hat{F}_{(i,j)}^0$ is the Fock operator, and ε_i and ε_j are the orbital energies.

5.4 Results and Discussion

5.4.1 Acidity of Salicylaldoxime

UV/Vis titrations were used to measure the acid dissociation constants, or pK_a values, of salicylaldoxime in aqueous solution. **Figure 5.3 (top)** displays the absorption spectra of salicylaldoxime titrated with NaOH at 25 °C. As illustrated in **Figure 5.3 (bottom)** the spectra were fitted with two deprotonation steps, a neutral to mono-anion dissociation, $H_2L^{(I)}$ to $HL^{(I)-}$, and a mono-anion to di-anion dissociation, $HL^{(I)-}$ to $L^{(I)2-}$. The dissociation steps were observed as a shift in the spectra of protonated and deprotonated species. Specifically, the first dissociation step, $H_2L^{(I)}$ to $HL^{(I)-}$, is reflected in the region between 250 nm and 280 nm; as the pH increased, the absorbance around 250 nm slightly decreased while the absorbance at longer wavelengths (270 nm – 285 nm) slightly increased. In the second dissociation step, $HL^{(I)-}$ to $L^{(I)2-}$, reflected between 290 nm and 340 nm, as the pH increased, the absorbance around 290 nm decreased while absorbance at longer wavelengths (300 nm – 340 nm) increased. The protonation steps corresponding to the spectral changes are tabulated in **Table 5.1**.

DFT calculations at the M06/6-311++G** level of theory and the SMD continuum solvation model were used to elucidate the optimal geometry of the salicylaldoxime species observed during the titration (**Figure A.8 of Appendix D**). According to our results, the first and second deprotonation steps can undoubtedly be assigned to the hydroxyl group and the oxygen of the oxime group, respectively. The first acid dissociation constant ($pK_{a1} = 8.07$) is lower in value than the acid dissociation constant of a phenol ($pK_a = 10.00$).²⁸ The salicylaldoxime phenolate group is less basic than phenolate because the aldoxime group is stabilizing the phenolate via

hydrogen bonding. This behavior has been observed in bisoximate structures as well, where the interaction between two protonated oxime groups decreases the basicity of one oximate group relative to the other due to hydrogen bonding.⁴⁴ The second acid dissociation constant ($pK_{a2} = 11.28$); however, is typical of aromatic oximes, such as benzaldoxime ($pK_a = 11.30$).²⁸ The absence of a pK_{a2} shift with a neighboring phenolate group can be explained in terms of the DFT optimized geometry of the dianion salicylaldoximate species (**Figure A.8 of Appendix D**). The basicity of the aldoximate group is not increased by the presence of the phenolate group because it can reorient itself in a way that minimizes interactions with the phenolate, thus, limiting the destabilizing effect introduced by a neighboring negative charge.

Finally, as listed in **Table 5.1**, acid dissociation constants have been previously reported for salicylaldoxime in the literature. The previously reported acid dissociation constants have been measured via UV/Vis,⁴⁵ Raman,⁴⁶ and potentiometric titrations.⁴⁶ The acid dissociation constants we report are in excellent agreement with the previously reported UV/Vis titration values;⁴⁵ the slight discrepancy can be attributed to differences in ionic strength. However, the Raman and potentiometric titration data were collected in a 50% (wt/wt) ethanol-water mixture at 30 °C⁴⁶ and, therefore, that data will not be discussed in this section.

5.4.2 Comparison of the Acid Dissociation Constants of Salicylaldoxime to Salicylic Acid and Representative Amidoxime Ligands

The second acid dissociation constant, or the dissociation of the aldoxime group ($pK_{a2} = 11.28$) is typical of aromatic oximes, such as benzaldoxime ($pK_a = 11.30$)²⁸. The dissociation of the oxime group on benzamidoxime ($pK_a = 12.36$)⁴⁸ is ~1 order of magnitude greater than the dissociation constants of aromatic oximes because the electron donating nature of the benzamidoxime amine group increases the electron density of the oximate group, thus increasing

the overall basicity of the ligand. As stated in the previous section, while it might be anticipated that the presence of the phenolate would increase the pK_{a2} value of salicylaldoxime it does not increase the pK_{a2} value of phenolate because the aldoximate can reorient itself in a way that minimizes interaction with the neighboring phenolate. In contrast, the second acid dissociation constant of salicylic acid ($pK_{a2} = 13.7$)²⁸ is ~ 3 orders of magnitude greater than the dissociation of phenol ($pK_a = 10.00$)²⁸ because the resonance of the carboxylate group inhibits minimization of charge interactions by the reorientation of carboxylate. Thus, the neighboring charge interactions result in the salicylic acid phenolate group ($pK_{a2} = 13.7$)²⁸ being nearly as basic as the oximate group in acetamidoxime ($pK_a = 13.21$),³⁷ despite the stability provided by the resonance of the benzene ring. This increase in pK_a due to neighboring charge interactions is further supported by the pK_a values reported for glutardiamidoxime ($pK_{a1} = 12.06$, $pK_{a2} = 12.13$)⁴⁹ and glutarimidedioxime ($pK_{a1} = 10.70$, $pK_{a2} = 12.06$)⁵⁰, the pK_{a2} value of the oxime in glutarimidedioxime is greater than its pK_{a1} value because the rigidity of the piperidine ring compels the two oximate groups to interact with one another, while as the pK_{a1} and pK_{a2} values of glutardiamidoxime are nearly equal in value because the flexibility of the propyl chain allows the two oximate groups to reorient themselves in a way that minimizes interaction between the neighboring charges.

5.4.3 Formation of UO_2^{2+} -Salicylaldoxime Complexes

UV/Vis titrations were used to measure the stability constants, or $\log \beta_1$ (1:1 ligand/uranyl complex) and $\log \beta_2$ (2:1 ligand/uranyl complex) values of salicylaldoxime-uranyl complexes in aqueous solution. **Figure 5.4** (*top*) shows the absorption spectra of a 1:1 salicylaldoxime to uranyl solution in a titration with NaOH at 25 °C. As illustrated in **Figure 5.4** (*bottom*) the spectra were best fitted with a model that includes the formation of a uranyl-

salicylaldoximate complex, $[\text{UO}_2\text{L}^{(1)}]$. The dissociation constants and molar absorptivities of the salicyldoxime ligand were used to compute the stability constant and molar absorptivity of the $[\text{UO}_2\text{L}^{(1)}]$ complex. **Figure 5.5** (*top*) shows the absorption spectra of a 10:1 salicylaldoxime to uranyl solution in a titration with NaOH at 25 °C. As conveyed in **Figure 5.5** (*bottom*) the spectra were best fitted with a model that includes the formation of two uranyl-salicylaldoximate complexes, $[\text{UO}_2\text{L}^{(1)}]$ and $[\text{UO}_2(\text{L}^{(1)})_2]^{2-}$. Once again, the dissociation constants and molar absorptivities of the salicylaldoxime ligand were used to compute the stability constant and molar absorptivity of the $[\text{UO}_2\text{L}^{(1)}]$ and $[\text{UO}_2(\text{L}^{(1)})_2]^{2-}$ complexes. The same $\log \beta_1$ value for $[\text{UO}_2\text{L}^{(1)}]$ was obtained from the 1:1 titrations and the 10:1 titrations. **Table 5.1** contains the calculated equilibrium constants. Moreover, it should be noted that we were unable to obtain reasonable agreement between theoretical and experimental absorbance values for the 1:1 and 10:1 titrations when we attempted to fit the data in terms of $[\text{UO}_2(\text{HL}^{(1)})]^+$ and $[\text{UO}_2(\text{HL}^{(1)})_2]$ species. This is significant because the $\text{HL}^{(1)-}$ species is responsible for the formation of salicylaldoxime – transition metal complexes.

In addition, since UO_2^{2+} hydrolyzes in neutral and alkaline aqueous solutions, it is important to determine the effects of pH change on the distribution of species in order to properly account for the formation of hydrolyzed species. Speciation diagrams of the salicylaldoxime- UO_2^{2+} complexes and hydrolyzed UO_2^{2+} species⁵¹ formed in the 1:1 and the 10:1 salicylaldoxime to uranyl solutions were simulated with the HYSS⁵² software. The 1:1 species diagram indicates that the $[\text{UO}_2\text{L}^{(1)}]$ species is dominant between pH 7 and 10, while as the 10:1 species diagram shows that the $[\text{UO}_2\text{L}^{(1)}]$ species is dominant between pH 5 and 8 and that the $[\text{UO}_2\text{L}^{(1)}]^{2-}$ species is dominant between pH 8 and pH 12 (**Figure A.9** of **Appendix D**). In addition, speciation diagrams of the salicylaldoxime- UO_2^{2+} and carbonate- UO_2^{2+} species⁵³

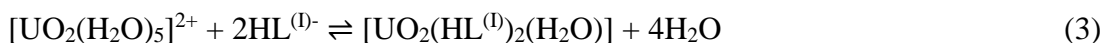
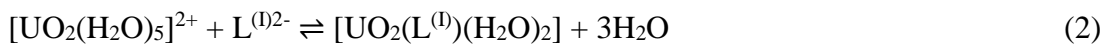
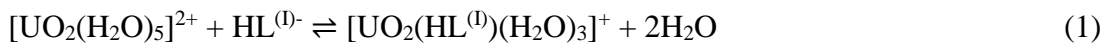
formed at seawater concentrations were also simulated. The obtained speciation diagram (**Figure A.10 of Appendix D**) indicates that the $[\text{UO}_2\text{L}^{(\text{I})}_2]^{2-}$ species displaces carbonate around pH 5 and that it binds ~100% of the UO_2^{2+} in solution between pH 6 and pH 10. Thus, these distributions indicate that salicylaldoxime-uranyl complexes are the dominant uranyl complexes formed at pH 8.3, the approximate pH of seawater; thus, making salicylaldoxime a promising ligand for subsequent generations of chelating polymers.

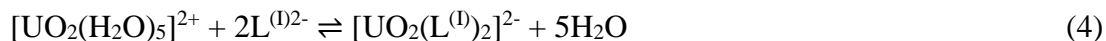
5.4.4 Structures and Stabilities of UO_2^{2+} -Salicylaldoxime Complexes from Theoretical Calculations

In order to elucidate the optimal coordination modes and geometries of uranyl-salicylaldoximate complexes and to justify our conclusions regarding a protonation state of the ligand upon UO_2^{2+} binding, we performed density functional theory (DFT) calculations at the M06/SSC/6-311++G** level of theory. Using the gas phase geometries, implicit solvent corrections were obtained at the B3LYP/SSC/6-31+G* level using the SMD solvation model, whereas the first coordination shell of clusters was treated explicitly. The results of a systematic computational search for low-energy conformations of $[\text{UO}_2(\text{HL}^{(\text{I})})(\text{H}_2\text{O})_3]^+$ complex, representing a singly deprotonated salicylaldoxime ligand bound to the uranyl ion are shown in **Figure 5.6**. Structure **1** of $[\text{UO}_2(\text{HL}^{(\text{I})})(\text{H}_2\text{O})_3]^+$ with a chelate binding motif formed via coordination of the phenolate group and the nitrogen atom of the oxime group was found to be the most energetically stable, however, structures **2**, **3**, and **4** with other binding motifs, including η^2 coordination of the oxime functional group, are only 1.4 – 2.6 kcal/mol higher in energy. When salicylaldoxime ligand binds to UO_2^{2+} ion in a fully deprotonated state, the resulting complex represents a neutral five-coordinate uranyl species $[\text{UO}_2(\text{L}^{(\text{I})})(\text{H}_2\text{O})_2]$ (**Figure 5.7**, structure **5**). The examination of alternative binding modes led to the discovery of structure **6**

formed by bidentate chelation of the aldoximate oxygen and the phenolate group. As can be seen in **Figure 5.7**, structure **6** is 4.7 kcal/mol less stable due to the unfavorable electrostatic interactions and the ring strain placed on the salicylaldoximate during coordination. The addition of a second salicylaldoxime ligand results in the formation of 2:1 uranyl complexes $[\text{UO}_2(\text{HL}^{(I)})_2(\text{H}_2\text{O})]$ and $[\text{UO}_2(\text{L}^{(I)})_2]^{2-}$ (structures **7** and **8**, respectively) depicted in **Figure 5.8**. According to our results, fully deprotonated salicylaldoximes give 2:1 six-coordinate uranyl complex, in which phenolate and oximate functional groups of $\text{L}^{(I)2-}$ form strong dative bonds with UO_2^{2+} , while singly deprotonated salicylaldoximes ($\text{HL}^{(I)-}$) give 12-membered *pseudomacrocyclic* complex, in which the oxygen atoms of the oxime groups are not directly bound to uranyl, but the oxime OH group forms one H-bond to a deprotonated phenolic oxygen atom (**Figure 5.8**). Interestingly, the coordination geometry around the uranyl ion in $[\text{UO}_2(\text{L}^{(I)})_2]^{2-}$ comprises six donor atoms in the equatorial plane, as is typical for small bite bidentate oxygen donor ligands.⁵⁴⁻⁵⁶

Having established the most stable forms of salicylaldoxime ligand ($\text{L}^{(I)2-}$) and the corresponding $[\text{UO}_2(\text{HL}^{(I)})(\text{H}_2\text{O})_3]^+$, $[\text{UO}_2(\text{L}^{(I)})(\text{H}_2\text{O})_2]$, $[\text{UO}_2(\text{HL}^{(I)})_2(\text{H}_2\text{O})]$, and $[\text{UO}_2(\text{L}^{(I)})_2]^{2-}$ complexes, we can now computationally assess their individual stability constant ($\log \beta$) values using our methodology⁴¹ for predicting stability constants of uranyl complexes. Following the approach involving the application of the thermodynamic cycle (**Figure A.7** of **Appendix D**), the complexation free energies in aqueous solution, ΔG_{aq} , were calculated for the equilibrium reactions shown in eqs 1 – 4:





As expected, our DFT-based method permitted reasonably good estimates of relative binding strengths of uranyl complexes, while the absolute complexation energies were significantly overestimated, subsequently leading to inaccurately high $\log \beta$ values. This artifact can be attributed to the fact that the solvation free energy of a multivalent ion is not fully accounted for by treating only the first hydration shell around metal ion explicitly.⁵⁷ However, accurate predictions of the absolute $\log \beta$ values (with root-mean square deviation from experiment <1.0) can be obtained by fitting the experimental data for mono- and divalent negative oxygen, imide dioxime, and amidoxime donor ligands. Indeed, as follows from **Figure 5.9**, the theoretically calculated $\log \beta$ values show a very strong correlation ($R^2 = 0.96$) with the experimental data, suggesting that the derived equation [$\exp \log \beta = 0.5692 \times \text{calc} \log \beta$] possesses a significant predictive power. It is worth noting that **Figure 5.9** presents a refined and augmented plot of experimental $\log \beta$ versus calculated $\log \beta$ which includes a broader range of ligands than the plot and the corresponding prediction equation provided in our previous study, which was confined mostly to a consideration of the negative oxygen donor ligands.⁴¹ A full comparison of experimental, calculated, and predicted $\log \beta$ values is shown in **Table A.14** of **Appendix D**.

The results given in **Table 5.2** verify that our computational protocol provides a reasonably good estimate of the $\log \beta_1$ ($\log \beta_2$) values for 1:1 $[\text{UO}_2(\text{L}^{(1)})(\text{H}_2\text{O})_2]$ and 2:1 $[\text{UO}_2(\text{L}^{(1)})_2]^{2-}$ complexes. The predicted $\log \beta_1$ ($\log \beta_2$) values for 1:1 $[\text{UO}_2(\text{HL}^{(1)})(\text{H}_2\text{O})_3]^+$ and 2:1 $[\text{UO}_2(\text{HL}^{(1)})_2(\text{H}_2\text{O})]$ complexes are significantly lower than those of the uranyl complexes with fully deprotonated salicylaldoxime ligands. Therefore, our calculations indicate that salicylaldoxime can undergo full deprotonation to allow a tridentate uranyl coordination. These findings further confirm the validity of the equilibrium model used to fit our titration data.

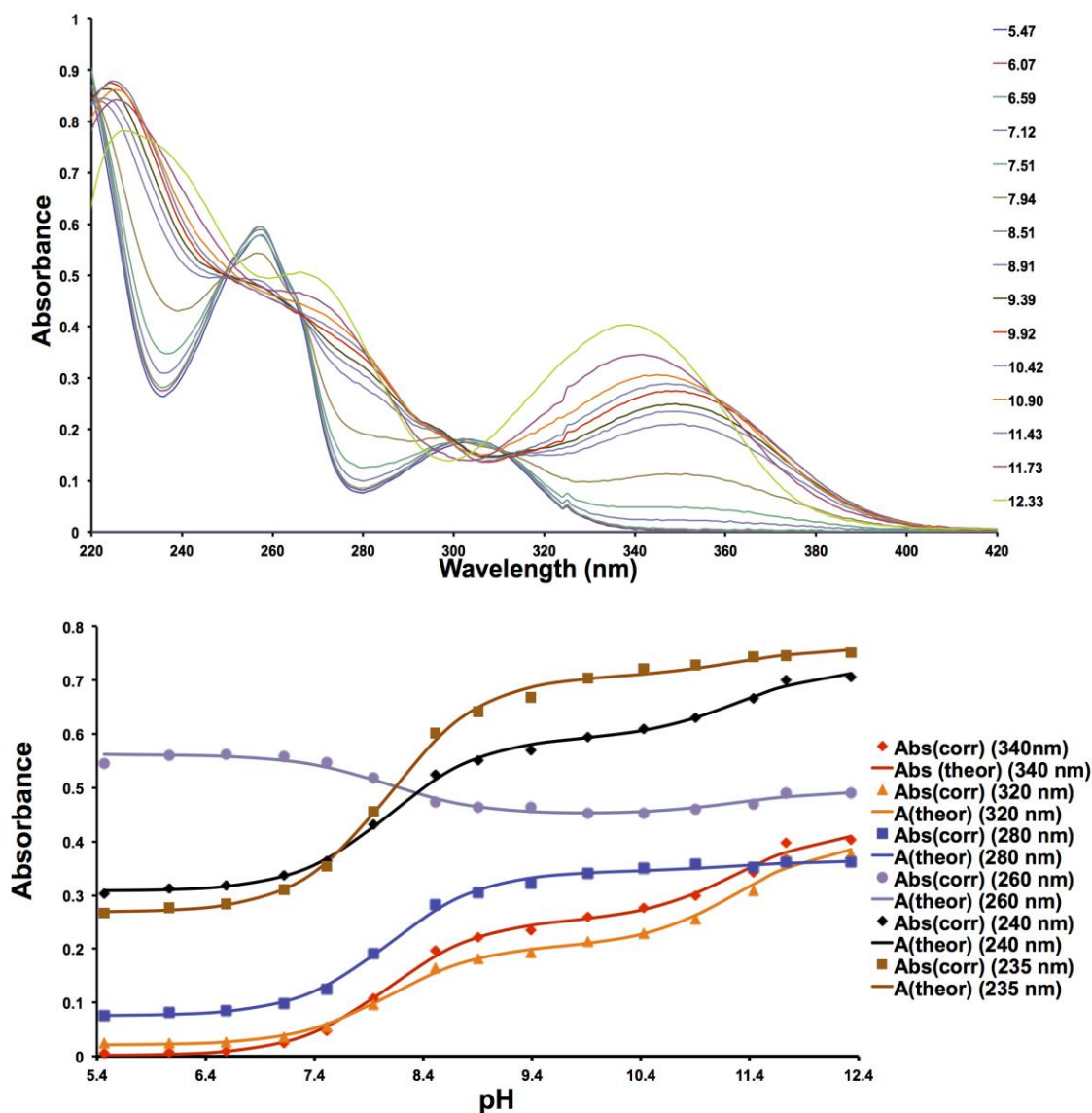


Figure 5.3. (Top) Spectra of salicylaldehyde (5×10^{-5} M) in aqueous solution at 25 °C. The pK_{a1} and pK_{a2} values were obtained at 0.0 M ionic strength. (Bottom) Variation of absorbance at six different wavelengths of 5×10^{-5} M salicylaldehyde in aqueous solution as a function of pH. The points are experimental values, whereas the solid lines are theoretical curves fitted to the experimental data using Solver.

Table 5.1. Salicylaldoxime dissociation and UO_2^{2+} formation constants at 25 °C by ionic strength.

	I = 0.0 M	Ref. 35, I = 0.50 M NaCl	Ref. 35, I = 0.0 M^a	
$\text{H}_2\text{L}^{(1)} \rightleftharpoons \text{HL}^{(1)-} + \text{H}^+$	8.07 ± 0.03	8.551 ± 0.024	8.08	$\text{pK}_{\text{a}1}$
$\text{HL}^{(1)-} \rightleftharpoons \text{L}^{(1)2-} + \text{H}^+$	11.28 ± 0.03	11.728 ± 0.016	11.26	$\text{pK}_{\text{a}2}$
$\text{UO}_2^{2+} + \text{L}^{(1)2-} \rightleftharpoons \text{UO}_2 \text{L}^{(1)}$	16.1 ± 0.03	N/A	N/A	
$\text{UO}_2^{2+} + 2 \text{L}^{(1)2-} \rightleftharpoons \text{UO}_2 \text{L}_2^{(1)2-}$	25.5 ± 0.03	N/A	N/A	

^aCorrected with the Davies equation.⁴⁷

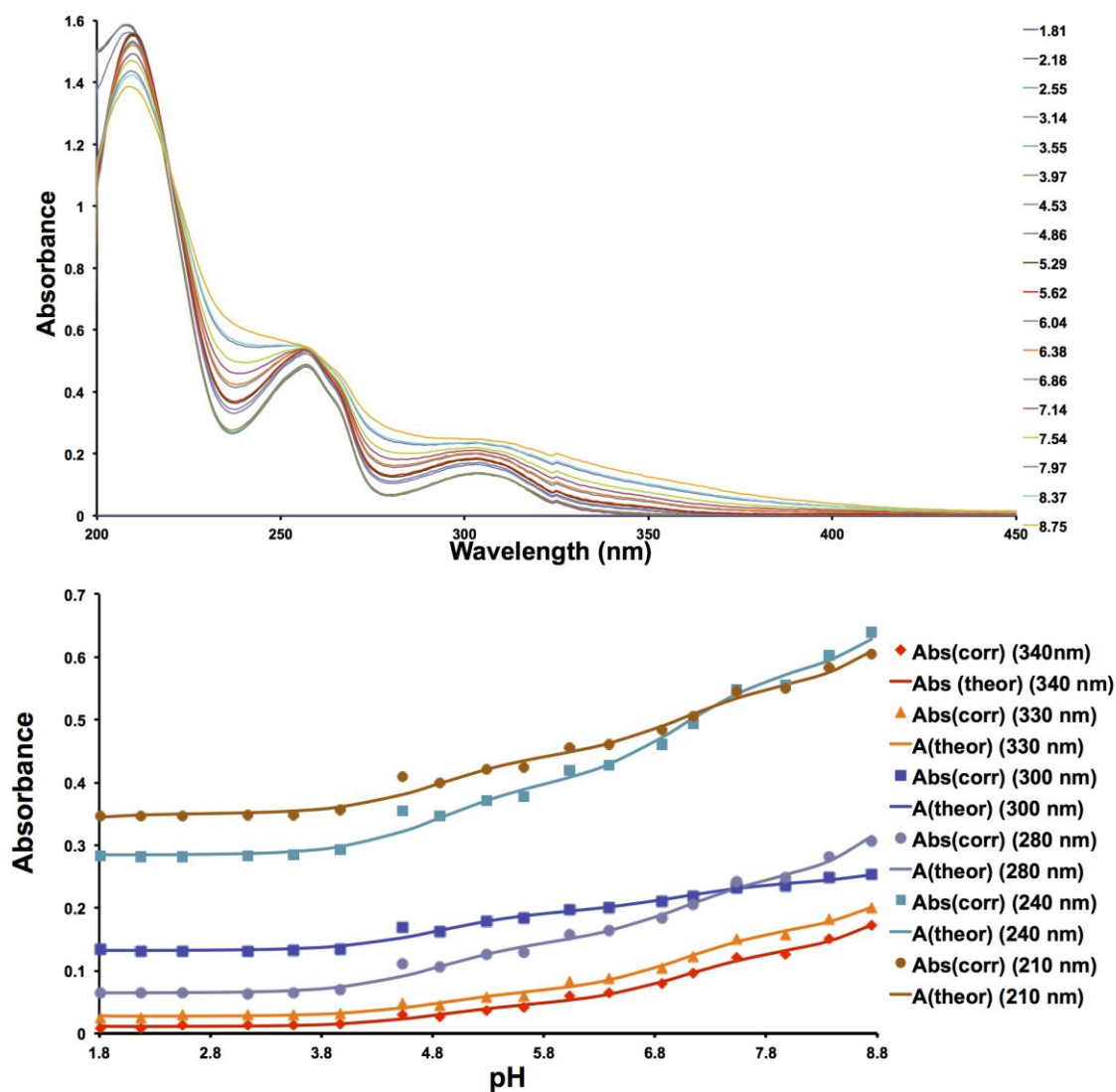


Figure 5.4. (Top) Spectra of salicylaldoxime (4.8×10^{-5} M) and uranyl (4.8×10^{-5} M) in aqueous solution at 25 °C. The $\log \beta_1$ value was obtained at 0.0 M ionic strength. (Bottom) Variation of absorbance at six different wavelengths 4.8×10^{-5} M salicylaldoxime and uranyl in aqueous solution as a function of pH. The points are experimental values, whereas the solid lines are theoretical curves fitted to the experimental data using Solver.

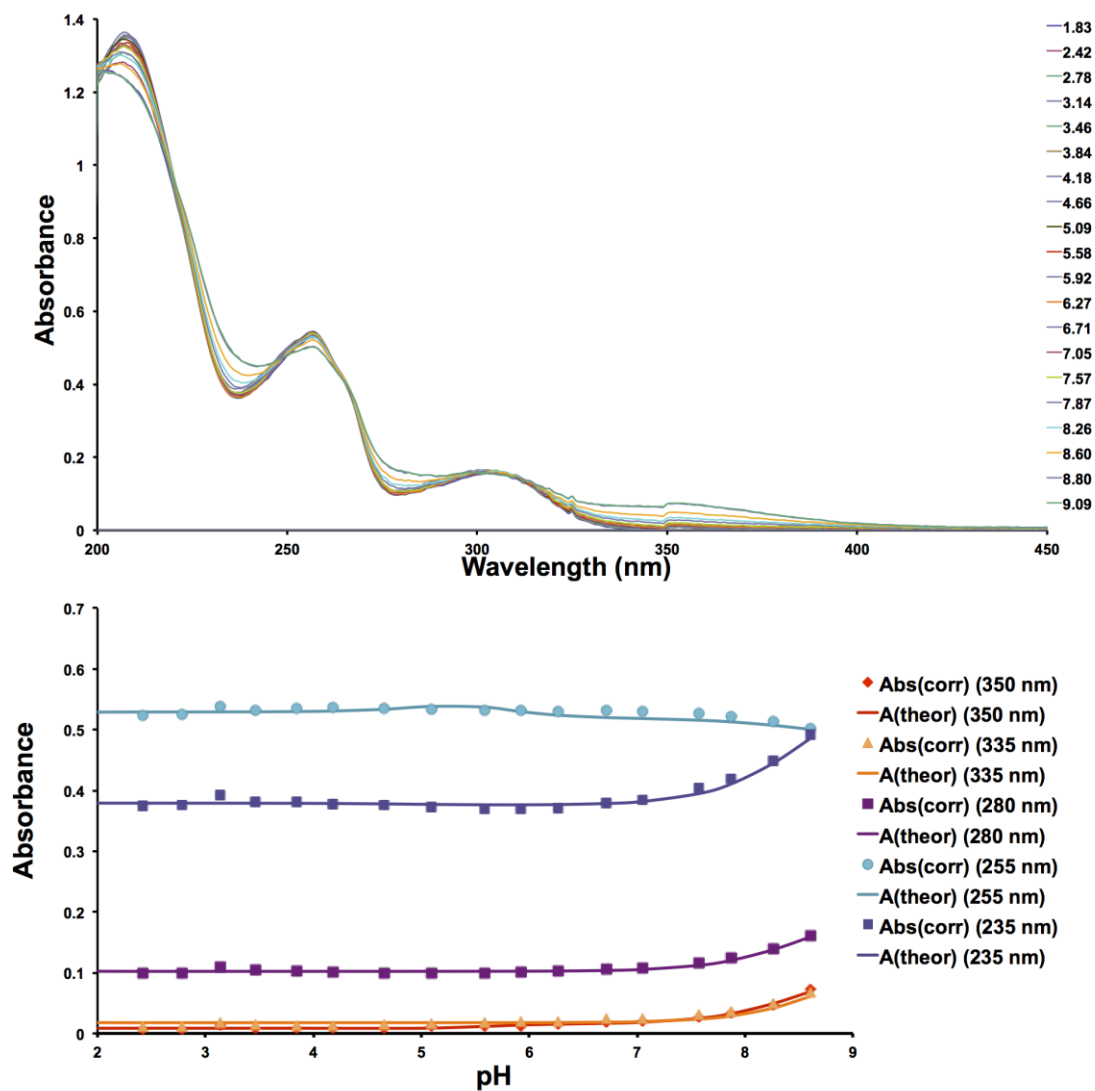


Figure 5.5. (Top) Spectra of salicylaldoxime (4.8×10^{-5} M) and uranyl (4.8×10^{-6} M) in aqueous solution at 25 °C. The $\log \beta_1$ and $\log \beta_2$ values were obtained at 0.0 M ionic strength. (Bottom) Variation of absorbance at five different wavelengths 4.8×10^{-5} M salicylaldoxime and uranyl in aqueous solution as a function of pH. The points are experimental values, whereas the solid lines are theoretical curves fitted to the experimental data using Solver.

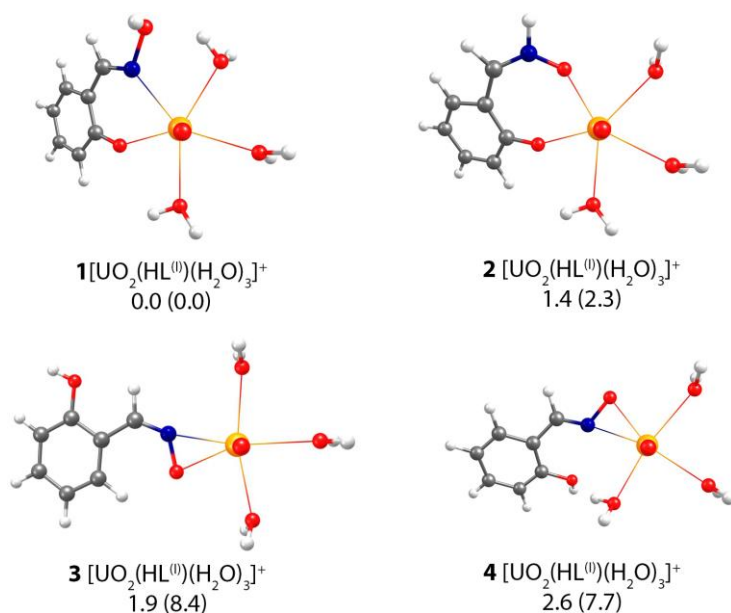


Figure 5.6. Optimized structures (M06/SSC/6-311++G**) of $[\text{UO}_2(\text{HL}^{(0)})(\text{H}_2\text{O})_3]^+$ complex and their relative Gibbs free energies (kcal/mol) in aqueous solution and in the gas phase (in parentheses). Color legend: O, red; N, blue; C, grey; H, white; U, yellow.

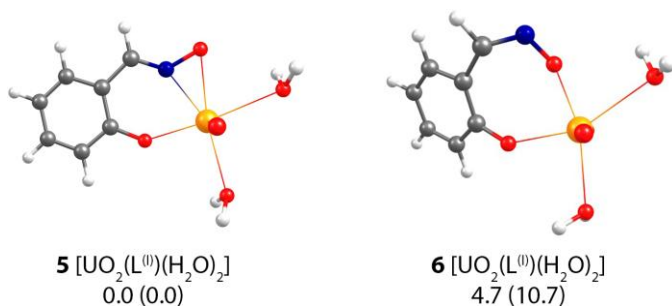
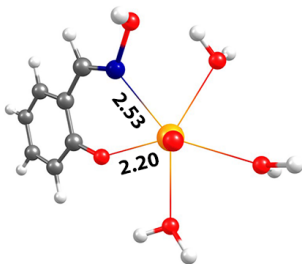
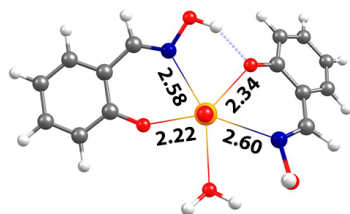


Figure 5.7. Optimized structures (M06/SSC/6-311++G**) of $[\text{UO}_2(\text{L}^{(0)})(\text{H}_2\text{O})_2]$ complex and their relative Gibbs free energies (kcal/mol) in aqueous solution and in the gas phase (in parentheses). Color legend: O, red; N, blue; C, grey; H, white; U, yellow.

**1:1 and 2:1 complexes
with HL^{(I)-}**

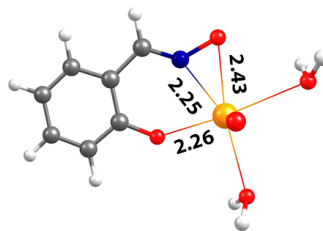


1 [UO₂(HL^(I))(H₂O)₃]⁺

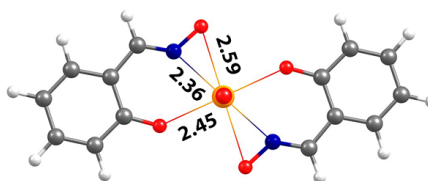


7 [UO₂(HL^(I))₂(H₂O)]

**1:1 and 2:1 complexes
with L^{(II)2-}**



5 [UO₂(L^(II))(H₂O)₂]



8 [UO₂(L^(II))₂]²⁻

Figure 5.8. The most stable structures of 1:1 and 2:1 uranyl complexes with salicylaldoxime (HL^{(I)-} and L^{(II)2-}) and obtained at the M06/SSC/6-311++G** level of theory. Uranyl-ligand bond lengths are shown in Å. Color legend: red represents oxygen, blue represents nitrogen, grey represents carbon, white represents hydrogen, and yellow represents uranium.

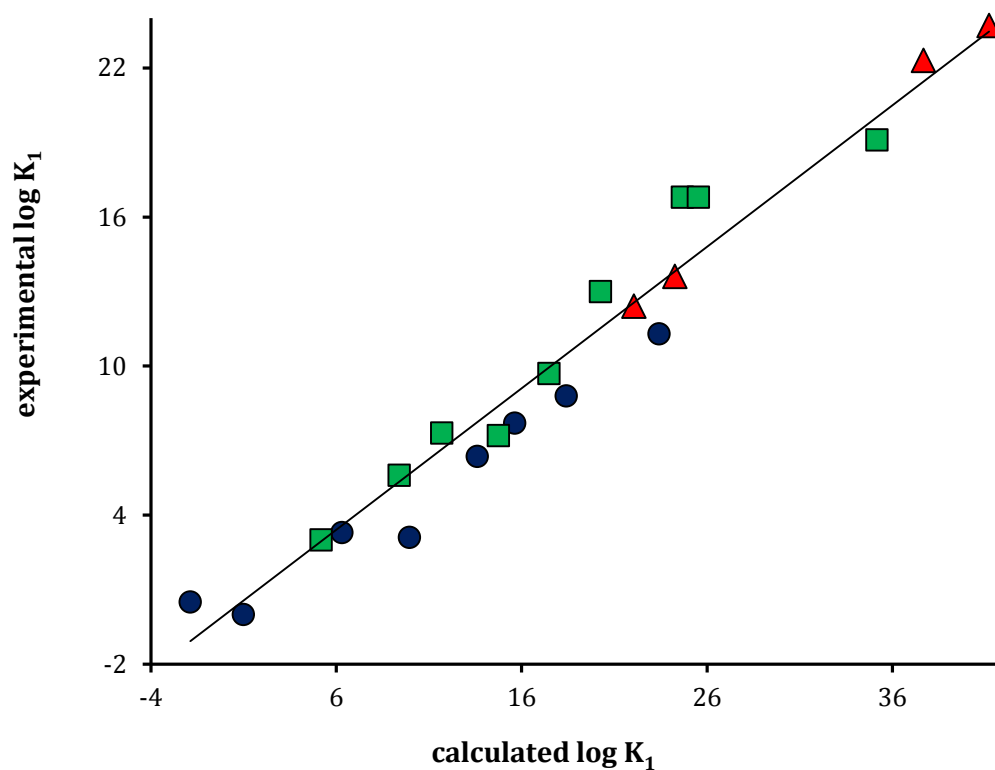


Figure 5.9. Plot of experimental versus calculated stability constants ($\log \beta$) for uranyl complexes with mono- and divalent negative oxygen, imide dioxime, and amidoxime donor ligands. The computed values were obtained at the M06/6-311++G** level of theory with the SMD solvent corrections. The $\log \beta_1$ data for monovalent (blue circles) and divalent (green squares) negative oxygen and imide dioxime donor ligands were taken from ref 41 and 40. The $\log \beta_1$ ($\log \beta_2$) data for 1:1 and 2:1 acet- and benzamidoxime/uranyl complexes (red triangles) were obtained from ref 31. Comparison of experimental, calculated, and predicted $\log \beta$ values is shown in **Table A.14** of **Appendix D**.

Table 5.2. Calculated free energy changes, ΔG_{aq} (kcal/mol), for reactions (1 – 4) and $\log \beta_1$ ($\log \beta_2$) values for 1:1 (2:1) uranyl complexes with salicylaldoxime ligands.

Complex	$\Delta G_{\text{aq}}^{\text{b}}$	$\log \beta_1$ ($\log \beta_2$)	
		predicted ^c	Experimental
$[\text{UO}_2(\text{HL}^{(\text{I})})(\text{H}_2\text{O})_3]^+$	-15.0	6.3	-
$[\text{UO}_2(\text{L}^{(\text{I})})(\text{H}_2\text{O})_2]$	-41.1	17.2	16.1
$[\text{UO}_2(\text{HL}^{(\text{II})})_2(\text{H}_2\text{O})]$	-33.5	14.0	-
$[\text{UO}_2(\text{L}^{(\text{II})})_2]^{2-}$	-69.9	29.2	25.5

^aThe computed ΔG_{aq} values were obtained at the M06/SSC/6-311++G(d,p) level with SMD solvent corrections.

^bCalculated as free energy changes for reactions (1 – 4) using the methodology described in ref 39. ^cPredicted from the derived equation [$\exp \log \beta = 0.5691 \times \text{calc} \log \beta$].

5.4.5 Chemical Bonding Analysis of the UO_2^{2+} -Salicylaldoxime Complex

In order to gain additional insight into the structure and chemical bonding in the salicylaldoxime- UO_2^{2+} complex, we performed natural bond orbital (NBO) analysis that enables us to assess the strength of interatomic and intermolecular interactions. The uranium atom has a closed radon core and six valence electrons, adopting an $[\text{Rn}]5f^36d^17s^2$ electron configuration. In the UO_2^{2+} ion two valence electrons of U have been lost and the remaining four are involved in forming the covalent bonds with the oxygen atoms. NBO analysis of UO_2^{2+} revealed one U-O σ bond, composed of U [hybridization: s 2.9%, d 47.1%, f 50.0%] and O [hybridization: s 12.2%, p 87.8%] natural atomic hybrids, as well as two U-O π bonds, originating from the interactions between oxygen 2p orbitals and uranium df hybrids [hybridization: s 0%, d 50.0%, f 50.0%]. The revealed covalent bonds, which are more polarized toward the oxygen atoms, suggest that single Lewis structure $[\text{O}\equiv\text{U}\equiv\text{O}]^{2+}$ can be used to represent UO_2^{2+} cation. Hence, O- and N-donor ligands can coordinate to the vacant s, d, and f orbitals of the uranyl. Though coordination is possible with the unfilled uranium s orbitals, we found that interactions of the phenolate and

oximate groups with s-type U orbitals are significantly weaker than corresponding interactions with d- and f-orbitals or df hybrids. This can be explained by isotropic nature of uranium s orbitals, which are not directed toward any particular donor ligands, whereas df hybrids have strong directionality along a particular coordination axis. According to the results of NBO analysis, the chemical bonding between UO_2^{2+} and salicylaldoxime has an essentially dative character, i.e., the occupied electron lone pairs of the phenolate O as well as the lone pairs of the oximate O and N enter into the vacant valence orbitals of UO_2^{2+} to form two-center two-electron (2c-2e) $\text{U} \leftarrow \text{:O}$ and $\text{U} \leftarrow \text{:N}$ coordinative bonds. Thus, the salicylaldoxime- UO_2^{2+} complex ($[\text{UO}_2(\text{L}^{(I)})(\text{H}_2\text{O})_2]$) can be described as a Lewis acid (UO_2^{2+}) bonded to a Lewis base (salicylaldoxime). This description means that the strength of donor–acceptor interactions in $[\text{UO}_2(\text{L}^{(I)})(\text{H}_2\text{O})_2]$ would be defined by the Lewis basicity/acidity of the components. The leading $\text{LP}_\text{O} \rightarrow \text{n}^*_\text{U}$ (phenolate), $\text{LP}_\text{O} \rightarrow \text{n}^*_\text{U}$ (oximate), and $\text{LP}_\text{N} \rightarrow \text{n}^*_\text{U}$ (oximate) donor-acceptor NBO interactions associated with the donation of electron density from phenolate and oximate functional groups of salicylaldoxime ligand to UO_2^{2+} are shown in **Figure 5.10, a)**. As indicated in **Table 5.3**, second-order perturbation theory suggests that these interactions stabilize the $[\text{UO}_2(\text{L}^{(I)})(\text{H}_2\text{O})_2]$ complex by 166.0, 73.3, and 123.0 kcal/mol, respectively. NBO charges in **Table 5.3** also show that the addition of the negatively charged salicylaldoxime ligand ($\text{L}^{(I)2-}$) to the UO_2^{2+} ion results in decreased charge on the uranyl ion due to the formation of dative bonds. Since the salicylaldoxime ligand contains phenolate and oximate donor groups, it would be interesting to examine the strength of donor-acceptor interactions in benzaldoxime- UO_2^{2+} and phenol- UO_2^{2+} complexes bearing each functional group individually. The results of NBO analysis for $[\text{UO}_2(\text{L}^{(\text{III})})(\text{H}_2\text{O})_3]^+$ and $[\text{UO}_2(\text{L}^{(\text{IV})})(\text{H}_2\text{O})_4]^+$ complexes are summarized in **Figure 5.10 b), c)** and **Table 5.3**. As one may see, the benzaldoximate ligand ($\text{L}^{(\text{III})-}$) provides stronger

donor-acceptor interactions with UO_2^{2+} than the phenolate ($\text{L}^{(\text{IV})-}$) ligand. These results are in accord with the predicted stability constant ($\log \beta_1$) values for the benzaldoxime- UO_2^{2+} and phenol- UO_2^{2+} complexes, which suggest higher $\log \beta_1$ of $[\text{UO}_2(\text{L}^{(\text{III})})(\text{H}_2\text{O})_3]^+$ ($\log \beta_1 = 12.2$) compared to $\log \beta_1$ of $[\text{UO}_2(\text{L}^{(\text{IV})})(\text{H}_2\text{O})_4]^+$ ($\log \beta_1 = 7.7$). As follows from the results of our NBO analysis (**Table 5.3**), the strength of $\text{LP}_\text{O} \rightarrow \text{n}^*_\text{U}$ interactions is ~ 57 kcal/mol higher for the UO_2^{2+} -phenol complex than for the salicylaldoxime- UO_2^{2+} complex. Interestingly, while the strength of the overall ($\text{LP}_\text{O} \rightarrow \text{n}^*_\text{U}$ and $\text{LP}_\text{N} \rightarrow \text{n}^*_\text{U}$) interactions of the oximate group is ~ 35 kcal/mol higher for the benzaldoxime- UO_2^{2+} than for the salicylaldoxime- UO_2^{2+} complex, the individual $\text{LP}_\text{O} \rightarrow \text{n}^*_\text{U}$ and $\text{LP}_\text{N} \rightarrow \text{n}^*_\text{U}$ contributions to the $E^{(2)}$ second-order stabilization energy are different. The NBO results (**Table 5.3**) indicate that the salicylaldoxime- UO_2^{2+} complex is more stabilized by $\text{LP}_\text{N} \rightarrow \text{n}^*_\text{U}$ than $\text{LP}_\text{O} \rightarrow \text{n}^*_\text{U}$ donor-acceptor interactions, whereas $\text{LP}_\text{O} \rightarrow \text{n}^*_\text{U}$ are the leading interactions in the benzaldoxime- UO_2^{2+} complex.

5.4.6 Comparison of the Formation Constants of Salicylaldoxime- UO_2^{2+} , Salicylic Acid- UO_2^{2+} , and Representative Amidoxime- UO_2^{2+} Complexes

The data in **Table 1** indicates that salicylaldoxime- UO_2^{2+} complexes ($\log \beta_1 = 16.1$, $\log \beta_2 = 25.5$) are 2-4 orders of magnitude stronger than salicylic acid- UO_2^{2+} ($\log \beta_1 = 13.1$, $\log \beta_2 = 21.8$)²⁸, benzamidoxime- UO_2^{2+} ($\log \beta_1 = 12.4$, $\log \beta_2 = 22.3$)²⁹, and acetamidoxime- UO_2^{2+} ($\log \beta_1 = 13.6$, $\log \beta_2 = 23.7$)²⁹. As stated in **Section 4.5**, the stronger complexes formed between salicylaldoxime and UO_2^{2+} can be attributed to the fact that the overall $E^{(2)}$ of salicylaldoxime- UO_2^{2+} complexes is ~ 130 - 140 kcal/mol greater in magnitude than the $E^{(2)}$ of individual phenolate- UO_2^{2+} and benzaldoximate- UO_2^{2+} complexes, the primary donor-acceptor NBO interactions contributing to the formation of salicylic acid- UO_2^{2+} and amidoxime- UO_2^{2+} complexes, respectively. In contrast, the salicylaldoxime $\log \beta_2$ value is ~ 1 - 2 orders of

magnitude weaker than the $\log \beta_2$ values of glutardiamidoxime ($\log \beta_1 = 17.3$, $\log \beta_2 = 26.1$)⁴⁹ and glutarimidedioxime ($\log \beta_1 = 17.8$, $\log \beta_2 = 27.5$)⁵⁰ because, as stated in Section 4.5, oximate forms stronger donor-acceptor NBO interactions with UO_2^{2+} than phenolate. Thus, it is expected that the stability provided by two oximates in a UO_2^{2+} is greater than the stability provided by an oximate and a phenolate.

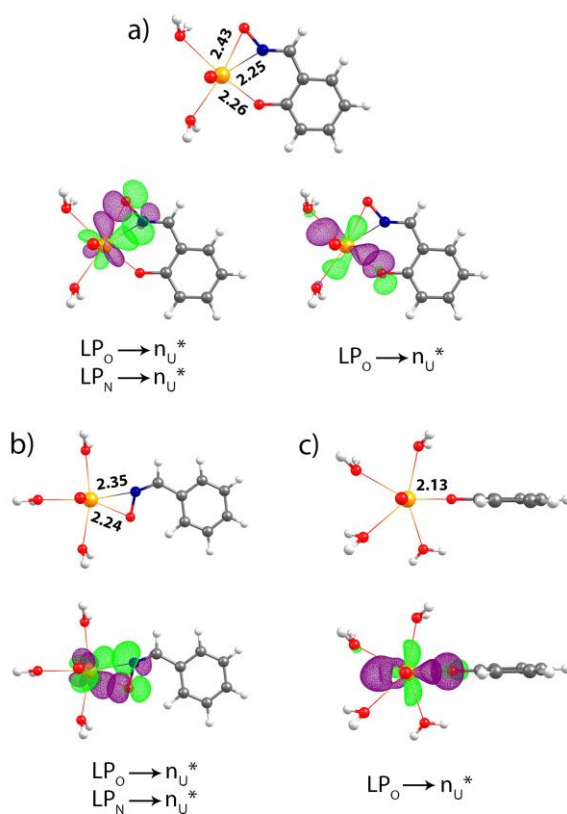


Figure 5.10. Donor-acceptor interactions with leading contributions to second-order stabilization energies of a) uranyl phenolate $[\text{UO}_2(\text{L}^{\text{IV}})(\text{H}_2\text{O})_4]^+$, b) uranyl benzaldoximate $[\text{UO}_2(\text{L}^{\text{III}})(\text{H}_2\text{O})_3]^+$, and c) uranyl salicylaldoximate $[\text{UO}_2(\text{L}^{\text{I}})(\text{H}_2\text{O})_2]$ complexes. Uranyl-ligand bond lengths are shown in Å.

Table 5.3. Significant donor-acceptor natural bond orbital interactions and their second-order stabilization energies $E^{(2)}$ (kcal/mol). The starred and unstarred labels correspond to Lewis (donor) and non-Lewis (acceptor) NBOs, respectively. Functional groups of ligands contributing to the particular interaction are shown in parentheses. LP denotes an occupied lone pair; CR denotes a one-center core pair; n* denotes vacant UO_2^{2+} orbitals; RY^* denotes a Rydberg orbital.

Complex	Donor NBO \rightarrow Acceptor NBO in selected UO_2^{2+} complexes					Charge on UO_2^{2+} unit
	LPo \rightarrow n* _U	LPo \rightarrow n* _U	LP _N \rightarrow n* _U	CR _U \rightarrow BD* _{Ligand}	Total	
	(phenolate)	(oximate)	(oximate)			
$[\text{UO}_2\text{L}^{(\text{IV})}]^+$	223.3	-	-	9.2	232.5	+0.83
$[\text{UO}_2\text{L}^{(\text{III})}]^+$	-	152.4	79.2	9.1	240.6	+0.82
$[\text{UO}_2\text{L}^{(\text{I})}]$	166.0	73.3	123.0	10.6	373.0	+0.64

5.4.7 Comparison of the UO_2^{2+} Selectivity of Salicylaldoxime, Salicylic Acid, and Representative Amidoxime Ligands

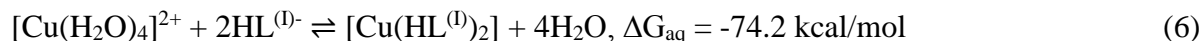
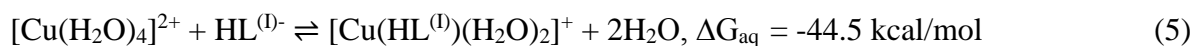
As stated earlier, the selectivity of the amidoxime functional group towards the UO_2^{2+} cation in relation to competing transition metal cations, such as Fe^{3+} , Cu^{2+} , VO^{2+} , and VO_2^+ , remains a major challenge.^{5, 13-15} Therefore, the design of new ligands that are more selective towards the UO_2^{2+} cation will play an essential role in developing commercially viable chelating polymer extractants. The uranyl selectivity of a ligand can be assessed by comparing UO_2^{2+} formation constants to transition metal cation formation constants. In this manuscript, we will examine $\text{UO}_2^{2+}/\text{Cu}^{2+}$ and $\text{UO}_2^{2+}/\text{Fe}^{3+}$ selectivity of salicylaldoxime because the Cu^{2+} and Fe^{3+} formation constants of salicylaldoxime have been previously reported in the literature. We are currently working on measuring the salicylaldoxime- VO_2^+ and salicylaldoxime- VO^{2+} equilibrium constants in our laboratory and the $\text{UO}_2^{2+}/\text{VO}_2^+$ and $\text{UO}_2^{2+}/\text{VO}^{2+}$ selectivity of salicylaldoxime will be explored in greater detail in a subsequent manuscript. The Cu^{2+} and Fe^{3+} formation constants of salicylaldoxime, salicylic acid, and glutarimidedioxime from the literature are provided in **Table A.13**. In addition to the fact that the formation constants of

salicylaldoxime- UO_2^{2+} complexes ($\log \beta_1 = 16.1$, $\log \beta_2 = 25.5$) are greater in magnitude than the formation constants of salicylic acid- UO_2^{2+} complexes ($\log \beta_1 = 13.1$, $\log \beta_2 = 21.8$)²⁸, salicylaldoxime is also more selective towards uranyl than salicylic acid. Specifically, salicylaldoxime is more selective towards the UO_2^{2+} cation than the competing Cu^{2+} ($\log \beta_1 = 10.12$, $\log \beta_2 = 15.78$)⁵⁸ and Fe^{3+} ($\log \beta_1 = 9.38$, $\log \beta_2 = 16.73$)⁵⁹ cations by 8.8 and 9.7 $\log \beta_2$ units, respectively, while as salicylic acid is more selective towards Fe^{3+} ($\log \beta_1 = 16.35$, $\log \beta_2 = 28.25$)²⁸ by 6.4 $\log \beta_2$ units and less selective towards Cu^{2+} ($\log \beta_1 = 10.60$, $\log \beta_2 = 18.45$)²⁸ by 3.3 $\log \beta_2$ units. Similarly, while salicylaldoxime forms UO_2^{2+} complexes that are 2 $\log \beta_2$ units weaker than the UO_2^{2+} complexes formed with glutarimidedioxime ($\log \beta_1 = 17.8$, $\log \beta_2 = 27.5$)⁵⁰, glutarimidedioxime is ~ 16 $\log \beta_2$ units more selective towards the Fe^{3+} cation ($\log \beta_1 = 25.66$, $\log \beta_2 = 43.94$)¹⁵ and ~ 3 $\log \beta_2$ units less selective towards the Cu^{2+} cation ($\log \beta_1 = 18.94$, $\log \beta_2 = 24.71$).¹⁵ While salicylic acid and glutarimidedioxime coordinate to UO_2^{2+} , Cu^{2+} , and Fe^{3+} with very similar binding motifs (**Figure A.11 of Appendix D**),^{15, 50, 60-62} salicylaldoxime coordinates to UO_2^{2+} in a very different manner, thus making salicylaldoxime more selective towards UO_2^{2+} .

The complexes formed between the transition metals and salicylaldoxime and its derivatives have been extensively investigated via binding constant studies and crystallography.^{28, 63} Salicylaldoxime coordinates to transition metal cations as a monoanion species via a chelate formed between phenolate and the oxime N; the complexes are stabilized via hydrogen bonding interactions between the oxime OH group and phenolate.⁶³⁻⁶⁴ Cu^{2+} characteristically forms *trans* square planar complexes with two salicylaldoxime ligands coordinated around the metal center (**Figure A.12 of Appendix D**).^{63-64, 65} While an abundance of polynuclear Fe^{3+} -salicylaldoxime crystal structures (**Figure A.12 of Appendix D**) have been

reported,⁶⁶ a mononuclear Fe³⁺-salicylaldoxime crystal structure is yet to be reported, however, there is consensus in the literature that mononuclear Fe³⁺-salicylaldoxime complexes are octahedral.⁶³

We selected Cu²⁺ as a representative transition metal for our DFT investigations, because binding motifs and other structural features of Cu²⁺-salicylaldoxime complexes are well known. Moreover, salicylaldoxime reagents are widely used in the extraction of Cu²⁺ and currently account for approximately 25% of worldwide copper production.⁶⁷ Our calculations reveal that the formation of Cu²⁺ complexes with a singly deprotonated salicylaldoxime ligand (HL^{(I)-}) is a thermodynamically favorable process (eqs 5 and 6).



According to our results, the most stable structure of [Cu(HL^(I))(H₂O)₂]⁺ is formed via coordination of the phenolate group and the nitrogen atom of the oxime group as shown in **Figure 5.11** (structure **9**). 2:1 [Cu(HL^(I))₂] complex represents 14-membered *pseudomacrocyclic* system, in which the oxime OH groups form H-bonds to deprotonated phenolic oxygen atoms (**Figure 5.11**, structure **10**). Thus, 1:1 Cu²⁺ complex with a singly deprotonated salicylaldoxime (HL^{(I)-}) is structurally similar to [UO₂(HL^(I))(H₂O)₃]⁺ complex, while 2:1 [Cu(HL^(I))₂] complex has more H-bonds between the oxime and the phenolate groups than 2:1 uranyl complex [UO₂(HL^(I))₂(H₂O)] (**Figure 5.8**, structure **7**). However, while UO₂²⁺ forms stable complexes with L^{(I)2-}, we were not able to achieve any local minima for [Cu(L^(I))(H₂O)₂], because in the process of optimization the oxygen atom of the oximate group, having an excess of negative charge, attracted hydrogen atom of a nearby water molecule resulting in the protonation of the oximate group. Hence, Cu²⁺ complexes with a fully deprotonated salicylaldoxime do not exist in

aqueous solution. This phenomenon is likely due to the significantly smaller ionic radius of Cu^{2+} (compared to uranium), which cannot accommodate simultaneous binding of the phenolate and the oximate functional groups. Now it is clear that higher salicylaldoxime selectivity towards the UO_2^{2+} ($\log \beta_1 = 16.1$, $\log \beta_2 = 25.5$) versus the Cu^{2+} ($\log \beta_1 = 10.1$, $\log \beta_2 = 15.8$)⁵⁸ and other transition metals can be attributed to the difference in the binding motifs. Uranyl-salicylaldoxime complexes are stabilized by strong dative interactions with phenolate and oximate groups, promoting stronger coordination to UO_2^{2+} cation, whereas the corresponding stabilization is diminished in the Cu^{2+} -salicylaldoxime complexes. The difference in the binding motifs for complexation with UO_2^{2+} and transition metal cations may have important implications for the design of new salicylaldoxime based ligands. For instance, Tasker and co-workers^{64, 68} showed that 3-substitution of salicylaldoximes influences their copper (II) binding strength by buttressing of interligand hydrogen bonding. Since uranyl complexes with salicylaldoxime lack the corresponding hydrogen bonds, analogous 3-substitution will likely lead to the completely opposite effect, which can further alter salicylaldoxime selectivity.

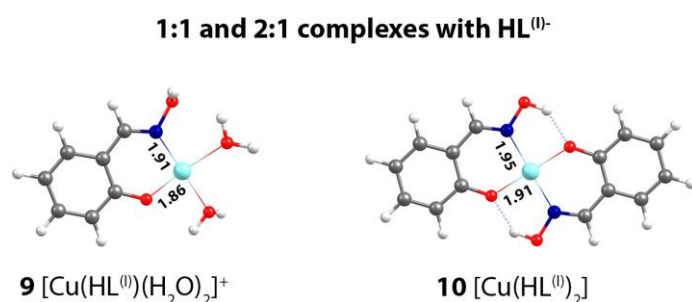


Figure 5.11. The most stable structures of 1:1 and 2:1 Cu^{2+} complexes with salicylaldoxime ($\text{HL}^{(0)-}$) obtained at the M06/SSC/6-311++G** level of theory. Uranyl-ligand bond lengths are shown in Å. Color legend: red represents oxygen, blue represents nitrogen, grey represents carbon, white represents hydrogen, and turquoise represents copper.

5.5 Conclusion

In this work, the binding strength of the salicylaldoxime- UO_2^{2+} complexes was determined to be $\sim 2\text{--}4 \log \beta_2$ units greater in magnitude than those of salicylic acid- UO_2^{2+} and representative amidoxime- UO_2^{2+} complexes. Furthermore, the selectivity of salicylaldoxime towards the UO_2^{2+} cation was found to be greater than those of salicylic acid and glutarimidedioxime reported in the literature. The higher UO_2^{2+} selectivity of salicylaldoxime can likely be attributed to the fact that salicylic acid and glutarimidedioxime coordinate to UO_2^{2+} and competing metal cations with very similar binding motifs,^{15, 50, 60-62} while as salicylaldoxime coordinates to UO_2^{2+} in a very different manner from competing transition metal cations, thus, making it more selective towards UO_2^{2+} . An abundance of crystallographic data on the CSD indicates that salicylaldoxime coordinates to transition metal cations as a monoanion species via a chelate formed between phenolate and the oxime N and that the complexes are stabilized via hydrogen bonding interactions between the oxime OH group and phenolate.^{63-64, 68} In contrast, our experimental and theoretical results show that salicylaldoxime coordinates to UO_2^{2+} as a dianion species formed by η^2 -coordination of the aldoximate and monodentate binding of the phenolate group. Thus, uranyl-salicylaldoxime complexes are stabilized by strong dative interactions with phenolate and oximate groups, promoting stronger coordination to UO_2^{2+} cation, as suggested by the NBO analysis; whereas the corresponding stabilization is diminished in the transition metal cation-salicylaldoxime complexes. Building on these experimental and theoretical results, we are able to propose a number of ligand design principles to further improve the UO_2^{2+} cation affinity and thus increase the selectivity of salicylaldoxime derivatives; namely, destabilizing the interligand hydrogen bonding that greatly influences the binding strength of salicylaldoxime-transition metal cation complexes.^{64, 68} Experimental efforts toward

the synthesis of salicylaldoxime-based ligands with high UO_2^{2+} binding affinity and selectivity are currently underway in our laboratory.

References

1. Davies, R. V.; Kennedy, J.; McIlroy, R. W.; Spence, R.; Hill, K. M., Extraction of Uranium from Sea Water. *Nature* **1964**, *203*, 1110-1115.
2. Choppin, G. R., Soluble Rare Earth and Actinide Species in Seawater. *Mar. Chem.* **1989**, *28*, 19-26.
3. Saito, K.; Miyauchi, T., Chemical Forms of Uranium in Artificial Seawater. *J. Nucl. Sci. Technol.* **1982**, *19*, 145-150.
4. Endrizzi, F.; Rao, L., Chemical Speciation of Uranium(VI) in Marine Environments: Complexation of Calcium and Magnesium Ions with $[(\text{UO}_2)(\text{CO}_3)_3]^{4-}$ and the Effect on the Extraction of Uranium from Seawater. *Chem. Eur. J.* **2014**, *20*, 14499-14506.
5. Kim, J.; Tsouris, C.; Mayes, R. T.; Oyola, Y.; Saito, T.; Janke, C. J.; Dai, S.; Schneider, E.; Sachde, D., Recovery of Uranium from Seawater: A Review of Current Status and Future Research Needs *Sep. Sci. Technol.* **2012**, *48*, 367-387.
6. Turekian, K. K., *Oceans*. Prentice Hall: Englewood Cliffs, NJ, 1968.
7. Schenk, H. J.; Astheimer, L.; Witte, E. G.; Schwochau, K., Development of Sorbers for the Recovery of Uranium from Seawater. 1. Assessment of Key Parameters and Screening Studies of Sorber Materials. *Sep. Sci. Technol.* **1982**, *17*, 1293-1308.
8. Astheimer, L.; Schenk, H. J.; Witte, E. G.; Schwochau, K., Development of Sorbers for the Recovery of Uranium from Seawater. Part 2. The Accumulation of Uranium from Seawater by Resins Containing Amidoxime and Imidoxime Functional Groups. *Sep. Sci. Technol.* **1983**, *18*, 307-339.
9. Kawai, T.; Saito, K.; Sugita, K.; Kawakami, T.; Kanno, J.; Katakai, A.; Seko, N.; Sugo, T., Preparation of Hydrophilic Amidoxime Fibers by Cograftering Acrylonitrile and Methacrylic Acid from an Optimized Monomer Composition. *Radiat. Phys. Chem.* **2000**, *59*, 405-411.
10. Yue, Y.; Mayes, R. T.; Kim, J.; Fulvio, P. F.; Sun, X.-G.; Tsouris, C.; Chen, J.; Brown, S.; Dai, S., Seawater Uranium Sorbents: Preparation from a Mesoporous Copolymer Initiator by Atom-Transfer Radical Polymerization. *Angew. Chem. Int. Ed.* **2013**, *125*, 13700-13704.
11. Kawai, T.; Saito, K.; Sugita, K.; Katakai, A.; Seko, N.; Sugo, T.; Kawakami, T.; Kanno, J., Comparison of Amidoxime Adsorbents Prepared by Cograftering Methacrylic Acid and 2-Hydroxyethyl Methacrylate with Acrylonitrile onto Polyethylene. *Ind. Eng. Res. Chem.* **2000**, *39*, 2910-2915.

12. Kawai, T.; Saito, K.; Sugita, K.; Kawakami, T.; Kanno, J.; Katakai, A.; Seko, N.; Sugo, T., Preparation of Hydrophilic Amidoxime Fibers by Cograftering Acrylonitrile and Methacrylic Acid from an Optimized Monomer Composition. . *Radiat. Phys. Chem.* **2000**, *59* (405-411).
13. Wang, D. L.; Sañudo Wilhelmy, S. A., Vanadium Speciation and Cycling in Costal Waters. *Mar. Chem.* **2009**, *117*, 52-58.
14. Suzuki, T.; Saito, K.; Sugo, T.; Ogura, H.; Oguma, K., Fractional Elution and Determination of Uranium and Vanadium Adsorbed on Amidoxime Fiber from Seawater. *Anal. Sci.* **2000**, *16*, 429-432.
15. Sun, X.; Xu, C.; Tian, G.; Rao, L., Complexation of Glutarimidedioxime with Fe(III), Cu(II), Pb(II), and Ni(II), the Competing Ions for the Sequestration of U(VI) from Seawater. *Dalton Trans.* **2013**, *42*, 14621-14627.
16. Allen, F. H., The Cambridge Structural Database: A Quarter of a Million Crystal Structures and Rising. *Acta Cryst. B* **2002**, *58*, 380-386.
17. Nenwa, J.; Djonwouo, P. L.; Bélombé, M. M.; Nfor, E. N.; Emmerling, F., Transition Metal Complexes of Oxamide Dioxime: Synthesis, Characterization and X-ray Structure of Isomorphous [Ni(H₂oxado)₃](BF₄)₂ and [Ni(H₂oxado)₃](ClO₄)₂. *ScienceJet* **2013**, *2*, 43.
18. Nenwa, J.; Djonwouo, P. L.; Nfor, E. N.; Bélombé, M. M.; Jeanneau, E.; Mbarki, M.; Fokwa, B. P. T., A Dimeric Copper(II) Complex of Oxalate and Oxamide Dioxime Ligands: Synthesis, Crystal Structure, Thermal Stability, and Magnetic Properties. *Zeitschrift für Naturforschung B* **2014**, *69*, 321–326.
19. Ülkü, D.; Ercan, F.; Macit, M.; Gülce, A., Bis[N-(2,6-dimethylphenyl)aminoglyoximato-N,N']nickel(II). *Acta Crystallogr., Sect. C: Cryst. Struct. Commun.* **1996**, *52*, 2680-2682.
20. Roh, S.-G.; Proust, A.; Robert, F.; Gouzerh, P., Coordination Chemistry of Polyoxomolybdates: The Versatile Behavior of Amidoximes. *J. Cluster Sci.* **1996**, *7*, 593-627.
21. Chilou, V.; Gouzerh, P.; Jeannin, Y.; Robert, F., Reaction of Oxomolybdenum Complexes with Amidoximes. Synthesis and Structure of a Nitrosylacetamidoximato(1-) Complex with a N,O-Side-on Bonded Acetamidoximate(1-) Ligand: [Mo(acac)₂(CH₃C(NH₂)NO)(no)]. *Inorg. Chim. Acta* **1987**, *133*, 205-206.
22. Sletten, E.; Marthinsen, T.; Sletten, J., Metal Complexes of Purine-N-oxides. I. The Crystal Structure of a Copper(II) Complex of Doubly Deprotonated Adenine-N¹-oxide. . *Inorg. Chim. Acta* **1984**, *93*, 37-41.
23. Thipyapong, K.; Uehara, T.; Tooyama, Y.; Braband, H.; Alberto, R.; Arano, Y., *Inorg. Chem.* **2011**, *50*, 992-998.

24. Cullen, D. L.; Lingafelter, E. C., Crystal Structures of Bis[2,2'-iminobis(acetamidoxime)]nickel(II) Chloride Dihydrate and Bis[2,2'-iminobis(acetamidoxime)]copper(II) Chloride. *Inorg. Chem.* **1970**, *9*, 1865-1877.
25. Stout, C. D.; Sundaralingam, M.; Lin, G. H.-Y., Stereochemistry of Nucleic Acids and their Constituents. XXI. The Crystal and Molecular Structure of Bis-(4-aminoimidazole-5-carboxamidoxime)copper(II) Perchlorate, a Degradation Product of Adenine N¹-Oxide. *Acta Crystallogr., Sect. B: Struct. Crystallogr. Cryst. Chem.* **1972**, *28*, 2136-2142.
26. Liu, J., Crystal Structure of Bis-(Acetato-[kappa]O)Bis-(Pyridine-2-carboxamide Oxime-[kappa]2N,N')Cadmium Ethanol Disolvate. . *Acta Crystallogr., Sect. E: Struct. Rep. Online* **2014**, *70*, 142-144.
27. Thomason, P. F.; Nutting, L. A.; Koskela, U.; Byerly, W. M., ORNL 1641 Chemistry: The Salicylate Method for Determining Microgram Amounts of Uranium. US Department of Energy: Oak Ridge National Lab, 1955.
28. Smith, R. M.; Martell, A. E., *Critical Stability Constants*. New York, 1981.
29. Lashley, M. A.; Mehio, N.; Nugent, J. W.; Holguin, E.; Do-Thanh, C.-L.; Dai, S.; Bryantsev, V. S.; Hancock, R. D., Amidoximes as Ligand Functionalities for Braided Polymeric Materials for the Recovery of Uranium from Seawater. *Polyhedron* **2016**, (DOI: 10.1016/j.poly.2016.01.026).
30. Vukovic, S.; Watson, L. A.; Kang, S. O.; Custelcean, R.; Hay, B. P., How Amidoximate Binds the Uranyl Cation. *Inorg. Chem.* **2012**, *51*, 3855–3859.
31. Beirakhov, A. G.; Orlova, I. M.; Ashurov, Z. R.; Lobanova, G. M.; Mikhailov, Y. N.; Schelokov, R. N., Mixed Dioxocarbonato- α -dioximato-uranate(VI) Complexes. *Russ. J. Inorg. Chem.* **1991**, *36*, 654-658.
32. Preetha, C. R.; Gladis, J. M.; Rao, T. P., Removal of Toxic Uranium from Synthetic Nuclear Power Reactor Effluents Using Uranyl Ion Imprinted Polymer Particles. *Environ. Sci. Technol.* **2006**, *40*, 3070-3074.
33. Frisch, M. J.; Trucks, G. W.; Schlegel, H. B.; Scuseria, G. E.; Robb, M. A.; Cheeseman, J. R.; Scalmani, G.; Barone, V.; Mennucci, B.; Petersson, G. A.; Nakatsuji, H.; Caricato, M.; Li, X.; Hratchian, H. P.; Izmaylov, A. F.; Bloino, J.; Zheng, G.; Sonnenberg, J. L.; Hada, M.; Ehara, M.; Toyota, K.; Fukuda, R.; Hasegawa, J.; Ishida, M.; Nakajima, T.; Honda, Y.; Kitao, O.; Nakai, H.; Vreven, T.; Montgomery, J. A., Jr. ; Peralta, J. E.; Ogliaro, F.; Bearpark, M.; Heyd, J. J.; Brothers, E.; Kudin, K. N.; Staroverov, V. N.; Kobayashi, R.; Normand, J.; Raghavachari, K.; Rendell, A.; Burant, J. C.; Iyengar, S. S.; Tomasi, J.; Cossi, M.; Rega, N.; Millam, M. J.; Klene, M.; Knox, J. E.; Cross, J. B.; Bakken, V.; Adamo, C.; Jaramillo, J.; Gomperts, R.; Stratmann, R. E.; Yazyev, O.; Austin, A. J.; Cammi, R.; Pomelli, C.; Ochterski, J. W.; Martin, R. L.;

Morokuma, K.; Zakrzewski, V. G.; Voth, G. A.; Salvador, P.; Dannenberg, J. J.; Dapprich, S.; Daniels, A. D.; Farkas, Ö.; Foresman, J. B.; Ortiz, J. V.; Cioslowski, J.; Fox, D. J., *Gaussian 09 Revision D.01*. Wallingford, CT: Gaussian, Inc. , 2009.

34. Becke, A. D., Density-Functional Thermochemistry. III. The Role of Exact Exchange. *J. Chem. Phys.* **1993**, *98*, 5648–5652.
35. Lee, C.; Yang, W.; Parr, R. G., Development of the Colle-Salvetti Correlation-Energy Formula Into a Functional of the Electron Density. *Phys. Rev. B* **1988**, *37*, 785–789.
36. Zhao, Y.; Truhlar, D. G., The M06 Suite of Density Functionals for Main Group Thermochemistry, Thermochemical Kinetics, Noncovalent Interactions, Excited States, and Transition Elements: Two New Functionals and Systematic Testing of Four M06-Class Functionals and 12 Other Functionals *Theor. Chem. Acc.* **2008**, *120*, 215–241.
37. Dolg, M.; Stoll, H.; Preuss, H.; Pitzer, R. M., Relativistic and Correlation Effects for Element 105 (Hahnium, Ha): A Comparative Study of M and MO (M = Nb, Ta, Ha) Using Energy-Adjusted Ab Initio pseudopotentials. *J. Phys. Chem.* **1993**, *97*, 5852-5859.
38. Ribeiro, R. F.; Marenich, A. V.; Cramer, C. J.; Truhlar, D. G., Use of Solution-Phase Vibrational Frequencies in Continuum Models for the Free Energy of Solvation. *J. Phys. Chem. B* **2011**, *115*, 14556-14562.
39. Marenich, A. V.; Cramer, C. J.; Truhlar, D. G., Universal Solvation Model Based on Solute Electron Density and a Continuum Model of the Solvent Defined by the Bulk Dielectric Constant and Atomic Surface Tensions. *J. Phys. Chem. B* **2009**, *113*, 6378–6396.
40. Chatterjee, S.; Bryantsev, V. S.; Brown, S.; Johnson, J. C.; Grant, C. D.; Mayes, R. T.; Hay, B. P.; Dai, S.; Saito, T., Synthesis of Naphthalimidedioxime Ligand-Containing Fibers for Uranium Adsorption from Seawater. *Ind. Eng. Res. Chem.* **2015**, (DOI: 10.1021/acs.iecr.5b03212).
41. Vukovic, S.; Hay, B. P.; Bryantsev, V. S., Predicting Stability Constants for Uranyl Complexes Using Density Functional Theory. *Inorg. Chem.* **2015**, *54*, 3995-4001.
42. Foster, J. P.; Weinhold, F., Natural Hybrid Orbitals. *J. Am. Chem. Soc.* **1980**, *102*, 7211-7218.
43. Reed, A. E.; Curtiss, L. A.; Weinhold, F., Intermolecular Interactions from a Natural Bond Orbital, Donor-Acceptor Viewpoint *Chem. Rev.* **1988**, *88* 899–926.
44. Dürüst, N.; Akay, M. A.; Dürüst, Y.; Kiliç, E., Protonation Constants of Some N-Substituted Amidoximes in a 50% Ethanol-Water Mixture (v/v). *Anal. Sci.* **2001**, *16*, 825–827.

45. Tshuma, J.; Alarcón-Ángeles^b, G.; Palacios-Beasa, E.; Vargas-García^{aa}, R.; Ramírez-Silva^b, M. T.; Rojas-Hernández^b, A., Spectrophotometric Determination of Acidity Constants of Salicylaldoxime in Aqueous Solution at 25 °C and Ionic Strength of 0.5M Controlled with NaCl. *Spectrochim. Acta, Part A* **2007**, *66*, 879–883.
46. Elbagerma, M. A.; Edwards, H. G. M.; Azimi, G.; Scowen, I. J., Raman Spectroscopic Determination of the Acidity Constants of Salicylaldoxime in Aqueous Solution. *J. Raman Spectrosc.* **2010**, *42*, 505-511.
47. Davies, C. W., *Ion Association*. Butterworths: Washington, DC, 1962.
48. Mehio, N.; Lashley, M. A.; Nugent, J. W.; Tucker, L.; Correia, B.; Do-Thanh, C.-L.; Dai, S.; Hancock, R. D.; Bryantsev, V. S., Acidity of the Amidoxime Functional Group in Aqueous Solution: A Combined Experimental and Computational Study. *J. Phys. Chem. B* **2015**, *119*, 3567-3576.
49. Tian, G.; Teat, S. J.; Rao, L., Thermodynamic Studies of U(VI) Complexation with Glutardiamidoxime for Sequestration of Uranium from Seawater. *Dalton Trans.* **2013**, *42*, 5690-5696.
50. Tian, G.; Teat, S. J.; Zhang, Z.; Rao, L., Sequestering Uranium from Seawater: Binding Strength and Modes of Uranyl Complexes with Glutarimidedioxime. *Dalton Trans.* **2012**, *41*, 11579-11586.
51. Grenthe, I.; Drozdynski, J.; Fujino, T.; Buck, E. C.; Albrecht-Schmitt, T. E.; Wolf, S. F., *Uranium*. 3 ed.; Springer: Netherlands, 2006; Vol. 1.
52. Alderighi, L.; Gans, P.; Ienco, A.; Peters, D.; Sabatini, A.; Vacca, A., Hyperquad Simulation and Speciation (HySS): A Utility Program for the Investigation of Equilibria Involving Soluble and Partially Soluble Species. *Coord. Chem. Rev.* **1999**, *184*, 311-318.
53. Guillaumont, R.; Fanghanel, T.; Fuger, J.; Grenthe, I.; Neck, V.; Palmer, D. A.; Rand, M. H., *Update on the Chemical Thermodynamics of Uranium, Neptunium, Plutonium, Americium, and Technetium*. Elsevier B. V.: Amsterdam, 2003.
54. Vallet, V.; Wahlgren, U.; Grenthe, I., Probing the Nature of Chemical Bonding in Uranyl(VI) Complexes with Quantum Chemical Methods. *J. Phys. Chem. A* **2012**, *116*, 12373-12380.
55. Yuan, L.-Y.; Sun, M.; Mei, L.; Wang, L.; Zheng, L.-R.; Gao, Z.-Q.; Zhang, J.; Zhao, Y.-L.; Chai, Z.-F.; Shi, W.-Q., New Insight of Coordination and Extraction of Uranium(VI) with N-Donating Ligands in Room Temperature Ionic Liquids: N,N'-Diethyl-N,N'-ditolyldipicolinamide as a Case Study. *Inorg. Chem.* **2015**, *54*, 1992-1999.

56. Denning, R. G., Electronic Structure and Bonding in Actinyl Ions and their Analogs. *J. Phys. Chem. A* **2007**, *111*, 4125-4143.
57. Bryantsev, V. S.; Diallo, M. S.; III, W. A. G., Computational Study of Copper(II) Complexation and Hydrolysis in Aqueous Solutions Using Mixed Cluster/Continuum Models. *J. Phys. Chem. A* **2009**, *113*, 9559-9567.
58. Lucia, M.; Campos, A. M.; van den, C. M. G., Determination of Copper Complexation in Sea Water by Cathodic Stripping Voltammetry and Ligand Competition with Salicylaldoxime. *Anal. Chim. Acta* **1994**, *284*, 481-496.
59. Burger, K.; Egyed, I., Some Theoretical and Practical Problems in the Use of Organic Reagents in Chemical Analysis - V: Effect of Electrophilic and Nucleophilic Substituents on the Stability of Salicylaldoxime Complexes of Transition Metals. *J. Inorg. Nucl. Chem.* **1965**, *27*, 2361-2370.
60. Bharara, M. S.; Strawbridge, K.; Vilsek, J. Z.; Bray, T. H.; Gordon, A. E. V., Novel Dinuclear Uranyl Complexes with Asymmetric Schiff Base Ligands: Synthesis, Structural Characterization, Reactivity, and Extraction Studies. *Inorg. Chem.* **2007**, *46*, 8309-8315.
61. Muhonen, H., *catena*-Poly{[bis(2-amino-2-methyl-1-propanol)copper(II)- μ -salicylato(2-)-O:O',O'']-copper(II)- μ -[salicylato(2-)-O',O'':O]} Tetrakis(2-propanol). *Acta Cryst. B* **1982**, *28*, 2041-2043.
62. Nurchi, V. M.; Crespo-Alonso, M.; Toso, L.; Lachowicz, J. I.; Crisponi, G.; Alberti, G.; Biesuz, R.; Domínguez-Martín, A.; Niclós-Gutiérrez, J.; González-Pérez, J. M.; Zoroddu, M. A., Iron^{III} and Aluminium^{III} Complexes with Substituted Salicyl-Aldehydes and Salicylic Acids. *J. Inorg. Biochem.* **2013**, *128*, 174-182.
63. Smith, A. G.; Tasker, P. A.; White, D. J., The Structures of Phenolic Oximes and Their Complexes. *Coord. Chem. Rev.* **2003**, *241*, 61-85.
64. Forgan, R. S.; Wood, P. A.; Campbell, J.; Henderson, D. K.; McAllister, F. E.; Parsons, S.; Pidcock, E.; Swart, R. M.; Tasker, P. A., Supramolecular Chemistry in Metal Recovery; H-bond Buttressing to Tune Extractant Strength. *Chem. Commun.* **2007**, 4940-4942.
65. Orioli, P. L.; Lingafelter, E. C.; Brown, B. W., The Crystal Structure of Bis(5-chlorosalicylaldoximato)copper(II). *Acta Cryst.* **1964**, *17*, 1113-1118.
66. Thrope, J. M.; Beddoes, R. L.; Collison, D.; Garner, C. D.; Helliwell, M.; Holmes, J. M.; Tasker, P. A., Surface Coordination Chemistry: Corrosion Inhibition by Tetranuclear Cluster Formation of Iron with Salicylaldoxime. *Angew. Chem. Int. Ed.* **1999**, *1999*, 1119-1121.

67. Kordosky, G. A., In *International Solvent Extraction Conference*, CapeTown, South Africa, 2002; pp 853-862.
68. Forgan, R. S.; Roach, B. D.; Wood, P. A.; White, F. J.; Campbell, J.; Henderson, D. K.; Kamenetzky, E.; McAllister, F. E.; Parsons, S.; Pidcock, E.; Richardson, P.; Swart, R. M.; Tasker, P. A., Using the Outer Coordination Sphere to Tune the Strength of Metal Extractants. *Inorg. Chem.* **2011**, *50*, 4515-4522.

Chapter 6 : Acidity of the Poly(acrylamidoxime) Adsorbent in Aqueous Solution: Determination of the Proton Affinity Distribution via Potentiometric Titrations

A version of this chapter was originally published by Nada Mehio, Ben Williamson, Yatsandra Oyola, Richard T. Mayes, Chris Janke, Suree Brown, and Sheng Dai in *Industrial & Engineering Chemistry Research*:

Mehio, N.; Williamson, B.; Oyola, Y.; Mayes, R. T.; Janke, C.; Brown, S.; Dai, S. “Acidity of the Poly(acrylamidoxime) Adsorbent in Aqueous Solution: Determination of the Proton Affinity Distribution via Potentiometric Titrations” *Ind. Eng. Chem. Res.* **2015**, in press (DOI: 10.1021/acs.iecr.5b03211).

Abstract

Poly(acrylamidoxime) fibers are the current state of the art adsorbent for mining uranium from seawater. While the acid dissociation constants, pK_a , of characteristic amidoxime and carboxylate ligands have been reported in the literature, the proton affinity distribution of the poly(acrylamidoxime) fiber is yet to be established. Herein, we report the poly(acrylamidoxime) proton affinity distribution between pH 2 and pH 10 via the Stable Numerical Solution of the Adsorption Integral Equation Using Splines (SAIUS) algorithm. Two peaks in the proton affinity distribution of poly(acrylamidoxime) were observed: the neutral to anionic dissociation of the carboxylate monomer between pH 3.2 and pH 4.4 ($pK_a \sim 4.0$) and the protonated to neutral dissociation of the acyclic amidoxime monomer between pH 5.6 and pH 6.8 ($pK_a \sim 6.1$). The acidity constants obtained for the carboxylate and amidoximate monomers vary from the acidity constants of acetic acid and acetamidoxime, respectively. These variations in acidity can be attributed to charge interactions between the carboxylate ($pK_a \sim 4.76$) and amidoxime ($pK_a \sim 5.78$) monomers. This is a first step to resolving the metal cation affinity distribution of the poly(acrylamidoxime) fibers, which can aid in improving the selectivity of subsequent generations of chelating polymers used to mine uranium from seawater.

6.1. Introduction

With growing concerns over high-carbon emissions, research into alternative sources of energy is becoming increasingly important. Nuclear energy is a promising alternative to high-carbon emission fossil fuels. Moreover, there is an estimated 4.5 billion tons of uranium,¹ the primary fuel source in nuclear fission, dissolved in seawater, while only 61,600 metric tons are needed annually to meet current global energy demands.² The dominant form of the uranyl ion in seawater is the tricarbonato complex, $\text{UO}_2(\text{CO}_3)_3^{4-}$,^{1, 3, 4} which associates with Ca^{2+} , a major cation in seawater, to form a $\text{Ca}_2\text{UO}_2(\text{CO}_3)_3^0$ _(aq) ternary complex, the dominant uranyl species in seawater.⁵ The primary challenge associated with mining uranium from seawater is developing an adsorbent capable of selectively extracting uranium at very low concentrations, approximately 3 ppb,¹ in a complex electrolyte consisting of a myriad of ions that are present at much higher concentrations. Currently, the most widely utilized adsorbents are poly(acrylamidoxime) fibers.⁶ Poly(acrylamidoximes), **Figure 6.1**, were first identified in a functional screening of 200 organic polymers as the only polymer capable of extracting uranium at pH 8.30, the approximate pH of seawater.^{7, 8} Poly(acrylamidoximes) are a random copolymer of carboxylate and amidoxime monomers at a 35:65 ratio, respectively.^{9, 10} While the acid dissociation constants, pK_a , and uranyl formation constants, $\log K$, of characteristic amidoxime^{11, 12} and carboxylate small molecules¹³ have been reported, the protonation and the metal cation affinity of the poly(acrylamidoxime) fiber itself has yet to be reported. These values are of great consequence because the comparison of the acidity and binding affinity of poly(acrylamidoxime) monomer units to the pK_a and $\log K$ values of their representative, yet idealized small ligands, is incomplete. The stability constants of pure chemical compounds, like small ligands, are a sum of delta functions; in contrast, the proton and metal cation affinities of polymers are more accurately described as a continuous distribution of affinities.¹⁴ As such, the pK_a values of

polymers have been reported as distributions in the literature, moreover, it has been demonstrated that the range of the distribution can be shifted by variations in polymer architecture.¹⁵⁻²¹

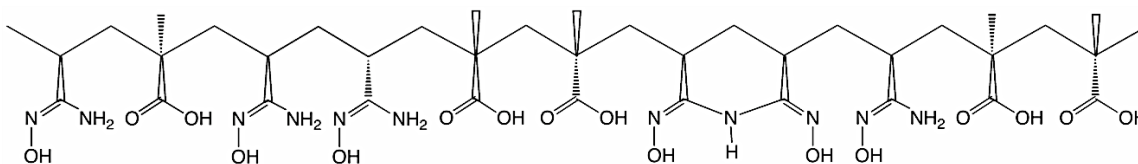


Figure 6.1. Schematic depiction of a small subsection of the poly(acrylamidoxime) fiber.

One approach for quantifying the protonation and metal cation affinities of aqueous polymers is to resolve their continuous distribution by pH.¹⁴ The resolution of affinity distributions of polymers is a special case of binding heterogeneity.^{14, 22} The resolution of protonation and metal cation affinity distributions of a polymer system are identical, with the exception of the influence of coordination number in binding affinity distributions.²² Consequentially, the remainder of our discussion will focus on resolving the protonation distribution of aqueous polymers. The protonation distributions of a polymer system are given by the adsorption isotherm integral equation:

$$Q(\text{pH}) = \int_{-\infty}^{\infty} q(\text{pH}, \text{pK}_a) f(\text{pK}_a) d\text{pK}_a \quad [1]$$

where $Q(\text{pH})$ is the proton binding isotherm, $f(\text{pK}_a)$ is the distribution of acidic sites in terms of their pK_a values in the interval $(\text{pK}_a \cdot d\text{pK}_a, \text{pK}_a + d\text{pK}_a)$, and $q(\text{pH}, \text{pK}_a)$ is the fraction of sites having a certain pK_a value at a particular pH.¹⁴ The main challenge of resolving protonation distributions is the fact that the adsorption isotherm integral equation is a Fredholm integral equation of the first kind, making it an ill-posed inverse problem.^{14, 23} As such, several approximate methods for solving the adsorption isotherm integral equation have been

proposed²³⁻²⁹ and used to calculate the protonation distribution from experimental data.^{14, 22, 30-37} One such solution, the Stable Numerical Solution of the Adsorption Integral Equation Using Splines, or SAIUS, is a method that combines regularization principles with a B-spline representation of the distribution function, $f(pK_a)$.^{14, 23} This solution is convenient and optimal because it requires fewer variables than discrete representations of the adsorption isotherm integral equation and ensures that the chosen solution contains all the information that can be extracted from the data while excluding artifacts.^{14, 23} Herein, we report the poly(acrylamidoxime) proton affinity distribution via the SAIUS algorithm. This is a first step to resolving the metal cation affinity distribution of the poly(acrylamidoxime) adsorbent, which can aid in improving the selectivity of subsequent generations of chelation polymers used in metal extractions.

6.2. Methods

6.2.1. Synthesis

Tetrahydrofuran (THF), dimethylsulfoxide (DMSO), dimethylformamide (DMF), methanol, hydroxylamine hydrochloride, potassium hydroxide (KOH), acrylonitrile, and methacrylic acid were purchased from Sigma-Aldrich and used as received. Hydroxylamine was generated by the neutralization of the hydrochloride with KOH in an aqueous solution containing 50 wt% methanol.

Hollow gear-shaped polyethylene fiber was supplied by Hills, Inc., and used after removal of the poly(lactic acid) sheath via washing with THF at 60°C. The polyethylene was irradiated with a 200 kGy average dose at the NEO Beam Electron Beam Cross-linking Facility (Mercury Plastics, Middlefield, OH). After irradiation, the polyethylene was added to a DMSO solution containing acrylonitrile and methacrylic acid within an inert atmosphere glovebag. The

irradiated polyethylene and monomer solutions were then transferred to a 65°C oven for 18 hours. Following polymerization, the grafted polyethylene was washed with DMF and methanol followed by drying at 40°C for 48 hours. The degree of grafting was gravimetrically determined to be 248 %. The grafted acrylonitrile-co-methacrylic acid copolymer was converted to amidoxime-co-methacrylic acid by contacting the fiber with 5 % hydroxylamine in an aqueous solution containing 50 wt % methanol for 24 hours at 80°C. After amidoximation, the grafted fibers were washed with water and methanol and dried in a 40°C oven for 48 hours.

6.2.2. Materials and Characterization Methods

Elemental analysis (EA) for C, H, N, O, and Cl was performed by Galbraith Laboratories, Inc. (Knoxville TN). Solid-state ^{13}C CP/MAS (cross-polarization/magic-angle spinning) NMR spectra were acquired on a Varian Inova 400 MHz spectrometer and referenced to an external standard, hexamethylbenzene, at 17.17 ppm.

6.2.3. Potentiometric Titrations

Potentiometric titrations were performed with a Mettler-Toledo G20 Compact Titrator and a Mettler-Toledo DG115-SC combination glass electrode. The pH meter was standardized by using the calibration curve of a strong acid/strong base titration method, KHP standardized 0.0100 N HClO_4 (Alfa Aesar; ACS grade concentrated acid) and 0.0100 N NaOH (Ricca Chemical Company; NIST certified), to determine the Nernst slope and E° correction factors. Prior to each titration, the pH meter was calibrated using a pH 4.01, pH 7.00, and pH 10.01 buffer set (Thermo Scientific). The microburette dispenses 0.01 mL of titrant into solution every 30 seconds for the entire duration of the titration. The 100 mL analyte solution was composed of 0.049-0.053 g of poly(acrylamidoxime) fiber, 0.1 N NaClO_4 (6 M NaClO_4 , Teknova), and 0.0100

M HClO₄. A 0.1000 N NaOH (Fisher Scientific, NIST Certified) solution was used as the titrant. The titration was carried out in a jacketed titration cell connected to a constant temperature water bath set to 25.0 ± 0.1 °C under humidified nitrogen gas flow. Humidified nitrogen was employed to purge CO₂ and O₂ from the analyte solution and to provide mild agitation sufficient enough to mix all additions made during the titration. The titration curves obtained, which consisted of 980 data points, were later transformed into proton binding isotherms, Q(pH), using the proton balance equation and a theoretical blank reference.^{32, 33} The pH range over which experimental data can be accurately analyzed via potentiometry is limited by the buffering capacity of water < pH 2 and > pH 12.^{13, 38-40} As such, all pH measurements were confined to pH values between pH 2 and pH 12.

6.2.4. SAIUS Algorithm

The SAIUS algorithm, a method that is widely used to numerically solve the adsorption isotherm integral equation (Eq. 1),^{14, 23} was used to resolve the proton affinity distribution of aqueous poly(acrylamidoxime). The SAIUS algorithm modifies Eq. 1 to accurately account for the fact that the experimental proton binding isotherm is only known within a specific pH range, pH₁ to pH_n.^{14, 23} As such, the adsorption isotherm integral equation is represented by the following equation in the SAIUS algorithm:

$$Q(pH) = \int_{\alpha}^{\beta} q(pH, pK_a) f(pK_a) dpK + Q_0 \quad [2]$$

Where α and β are the integration limits and Q_0 is an arbitrary constant representing the quantity of protons bound to sites with pK_a values outside the integration limits, it does not contribute to the calculated distribution function because it is a differential quantity.^{14, 23} A Langmuir equation is used to compute $q(pH, pK_a)$.^{14, 23}

$$q(pH, pK_a) = [1 + 10^{(pH-pK_a)}]^{-1} \quad [3]$$

Since $f(pK_a)$ is unknown, it is represented by a linear combination of B-spline functions with equally spaced knots in the range of (α, β) .^{14, 23} A combination of 25 B-spline functions were used in this analysis to solve for $f(pK_a)$. Thus, the formulation transforms an integration problem to a system of linear equations in which the spline coefficients and Q_0 are unknown.^{14, 23} However, since system of equation problems are typically ill-posed and cannot be solved with least squares methods alone, the SAIUS algorithm provides a stable solution by combining least squares methods with a regularization method that applies a smoothing term, $\lambda > 0$, and a non-negativity constraint.^{14, 23}

6.3. Results and Discussion

The fibers were characterized by elemental analysis (EA) and solid-state ^{13}C CP/MAS (cross-polarization/magic-angle spinning) NMR. The EA result of the as-grafted P(AN-co-MAA) fiber revealed that the AN/methacrylic acid (MAA) molar ratio was 65.69%:34.31%, which is significantly lower than the AN/MAA molar ratio in the feed, 79.11%:20.89% (or 70%:30% wt/wt). This is consistent with results in a similar system, a gamma-ray induced grafting copolymerization of AN and MAA on PE films, where the AN component in copolymers was reported to be very low in spite of its increase in the feed, indicating a much lower reactivity ratio of AN than that of MAA.⁴¹

The ^{13}C CP/MAS NMR spectrum of the as-grafted fiber confirmed the presence of $-\text{CN}$ and $-\text{COOH}$ groups at 120 and 178 ppm, respectively (**Figure 6.2**, trace (a)). After amidoximation (AO) at 80 °C for 24 h, the $-\text{CN}$ signal was no longer observed and broad signals, covering 143-169 ppm, appeared (**Figure 6.2**, trace (b)). These broad signals were

composed of at least two signals. A more upfield signal centered around 150 ppm was assigned to cyclic imidedioxime.^{42, 43} Another signal which appeared as an obscure shoulder around 157 ppm was assigned to open-chain amidoxime.⁴²⁻⁴⁴ In agreement with literature reports, the cyclic imidedioxime is expected as a major product from the AO reaction in aqueous solutions at elevated temperatures.⁴²⁻⁴⁸ The formation of cyclic imidedioxime also indicates that simultaneous grafting of AN and MAA did not yield completely random copolymers. In the carbonyl region, two signals at 177 and 184 ppm, assigned to -COOH and -COO^- , respectively, were observed.⁴⁹

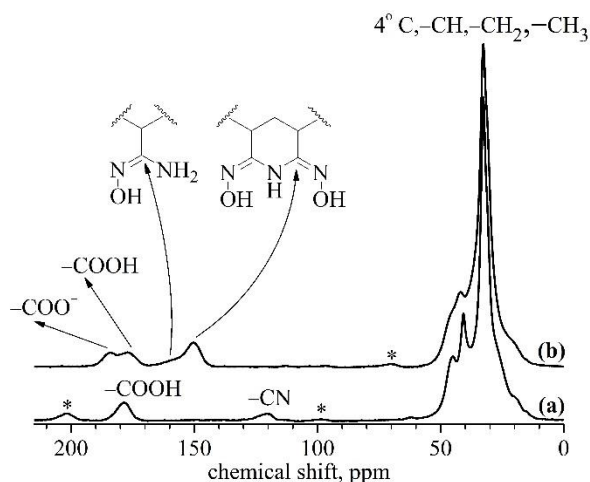


Figure 6.2. 100-MHz ^{13}C CP/MAS NMR spectra of (a) grafted and (b) amidoximated fibers. (* denotes spinning sideband, spinning speed 8.0 kHz).

Table 6.1 and **Figure 6.3** summarize the pK_a values of carboxylate and amidoxime ligands that are representative of the carboxylate and amidoxime monomers. Acetic acid is representative of the carboxylate monomer, acetamidoxime is representative of the acyclic amidoxime monomer, and glutarimidedioxime is representative of the cyclic amidoxime monomer.^{12, 48} Of the aqueous dissociations depicted in **Figure 6.3**, only the following

dissociations are likely to be observed in the potentiometric experimental window: the neutral to anionic dissociation of the carboxylate monomer, the protonated to neutral dissociation of the acyclic amidoxime monomer, and the neutral to mono-anionic dissociation of the cyclic amidoxime monomer. However, before comparing the acidity of the poly(acrylamidoxime) monomer units to the acidity of their representative small ligands, it should be noted that the pK_a values of pure chemical compounds, like small ligands, are a sum of delta functions and, consequentially, the pK_a values cannot be represented as a distribution of continuous peaks.¹⁴ Therefore, when comparing the proton affinity distribution of poly(acrylamidoxime) monomer units to the pK_a values of their analogous small ligands, the peaks of the distribution, not the entire range of the distribution, will be related to the pK_a values.

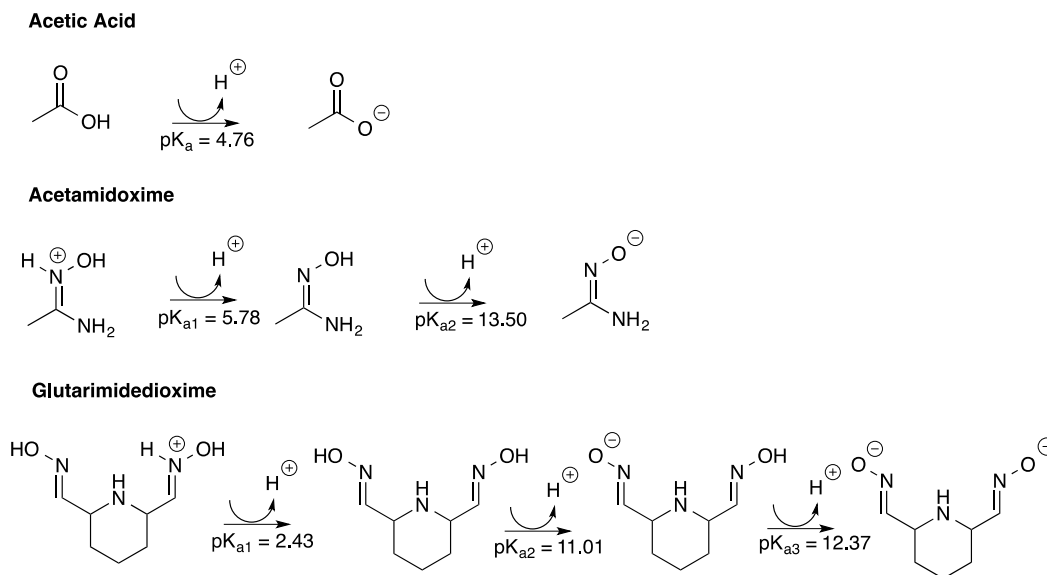


Figure 6.3. Schematic representing the dissociation of acetic acid,¹³ acetamidoxime,¹¹ and glutarimidedioxime¹² in aqueous solution. The following ligands are representative of poly(acrylamidoxime) monomer.

Table 6.1. Dissociation constants of acetic acid,¹³ acetamidoxime,¹¹ and glutarimidoxime¹¹ at 25 °C in aqueous solution. Ionic strength corrections were applied with the Davies equation

Acid	pK _a	Ionic Strength Corrected pK _a
Acetic Acid	4.76	N/A ^a
Acetamidoxime	5.78	N/A
	13.21	13.50 ^b
Glutarimidedioxime	2.12	2.43 ^c
	10.70	11.01 ^c
	12.06	12.37 ^c

^aReported at 0.0 M ionic strength.

^bReported at 0.3 M NaClO₄ ionic strength.

^cReported at 0.5 M NaCl ionic strength.

Figure 6.4 displays a representative titration curve obtained from titrating a 100 mL solution containing 0.049g of poly(acrylamidoxime) fiber, 0.1 M NaClO₄, and 0.1 M HClO₄ with 0.1 M NaOH at 25 °C. The proton affinity distribution and adsorption isotherm of a classical poly(acrylamidoxime) fiber can be observed in **Figure 6.5**. Two peaks in the proton affinity distribution can be observed in the following pH regions: pH 3.2-4.4 and pH 5.6-6.8. Of those peaks in proton affinity distributions, with the maxima observed at pH 4.0 and pH 6.1, respectively (**Table 6.2**). The peaks in proton affinity can be attributed to the following dissociations: the neutral to anionic dissociation of the carboxylate monomer (pH 3.2-4.4, pK_a ~ 4.0) and the protonated to neutral dissociation of the acyclic amidoxime monomer (pH 5.6-6.8, pK_a ~ 6.1). The acidity constants of the carboxylate and amidoximate monomers vary from the acidity of acetic acid and acetamidoxime, respectively. While the neutral to anionic dissociation of the carboxylate monomer is ~0.7 pK_a units lower than the analogous dissociation of acetic

acid, the protonated to neutral dissociation of the acyclic amidoxime monomer is ~ 0.5 pK_a units more basic than the analogous dissociation of acetamidoxime. These variations in acidity can be attributed to charge interactions between the carboxylate and amidoxime. Specifically, the close proximity of positively charged amidoxime and neutral carboxylic acid monomers stabilized the dissociation of the carboxylic acid into carboxylate at a lower pK_a value via hydrogen bonding interactions. In contrast, the hydrogen bonding interactions between the positively charged amidoxime and the negatively charged carboxylate monomers destabilized the protonated to neutral dissociation of amidoxime at the anticipated pK_a value; thus, increasing the pK_a value of the acyclic amidoxime monomer unit.

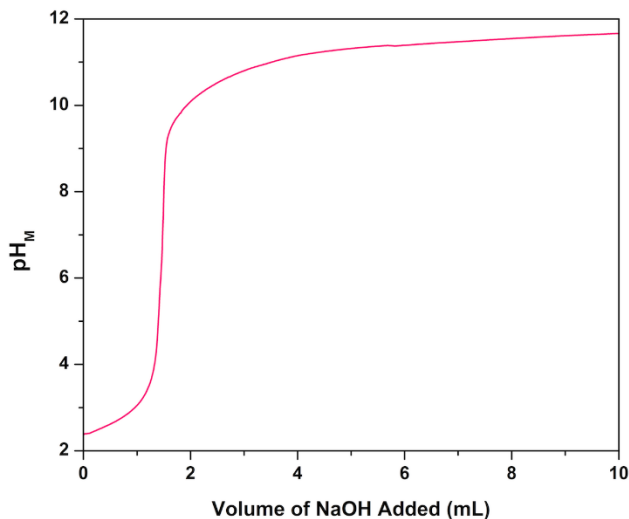


Figure 6.4. Titration of 0.049 g of poly(acrylamidoxime) in 100 mL of 0.1 M NaClO₄ and 0.0100 M HClO₄ with 0.100 M NaOH at 25 °C.

Moreover, it should be noted that the protonated to neutral and neutral to mono-anion dissociations of the cyclic amidoxime that were anticipated to occur around pH 2.43 and pH 11.01, respectively, were not observed at those pH values. Rather, two peaks were observed at pH 2.0 and pH 12.1 and these peaks can likely be ascribed to the protonated to neutral and

neutral to mono-anion dissociations of the cyclic amidoxime; however, due to the close proximity of the water buffering reaction, the peaks were not included in the poly(acrylamidoxime) distribution plot shown in **Figure 6.5**. The large shift in the neutral to mono-anion dissociation of the cyclic amidoxime is likely due to the destabilizing effect of the large concentration of negatively charged carboxylate monomers. Furthermore, while the size of the peaks in the proton affinity distribution is related to the relative abundance of the two groups, the proton affinity distribution provided in **Figure 6.5** cannot quantitatively convey the relative abundance of carboxylate to amidoxime on the fiber because the amidoxime peak only accounts for the acyclic amidoxime monomers.

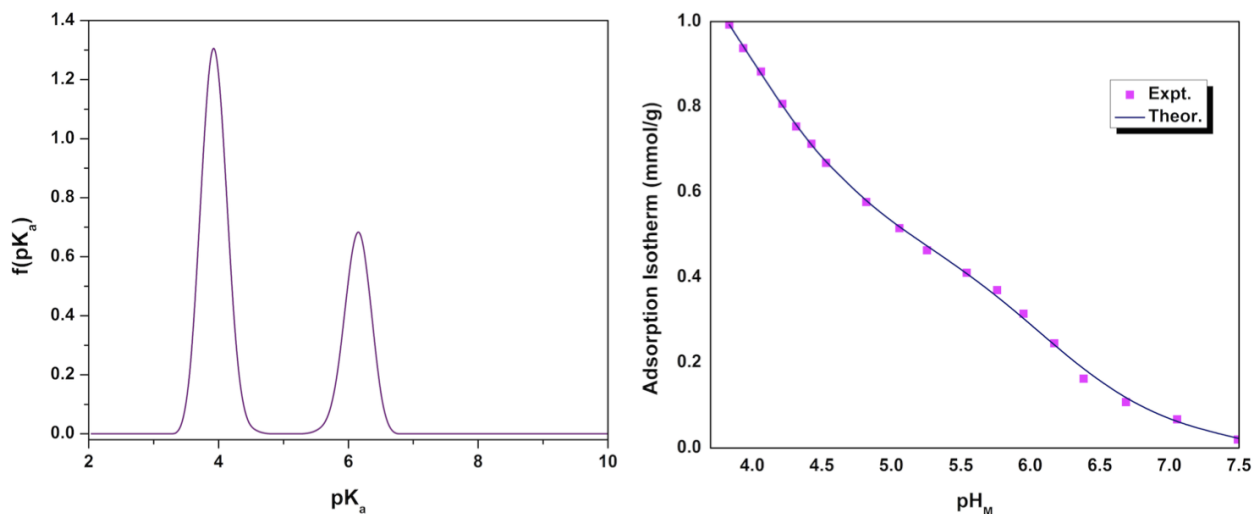


Figure 6.5. (Left) The normalized proton affinity distribution of poly(acrylamidoxime). (Top Right) Theoretical and experimental adsorption isotherm of poly(acrylamidoxime).

Table 6.2. Proton affinities of the carboxylate and amidoxime monomers and their corresponding small molecule pK_a values.

Acid	pK _a	Monomer	pK _a
Acetic Acid	4.76	Carboxylate	4.0
Acetamidoxime	5.78	Acyclic Amidoxime	6.1
	13.21		N/A ^a
Glutarimidedioxime ^b	2.43	Cyclic Amidoxime	~ 2
	11.01		> 12
	12.37		N/A ^a

^aOutside of the experimental pH window.^bCorrected to 0.0 M ionic strength with the Davies equation.

As stated in the Introduction, the determination of the proton and metal cation affinity distributions of aqueous polymers by approximate solutions to the adsorption isotherm integral equation, such as the SAIUS algorithm, are identical with the exception of the influence of coordination number in binding affinity distributions.²² Moreover, the determination of the proton affinity distribution of poly(acrylamidoxime) fibers lays the foundation for resolving the affinity distribution of UO_2^{2+} and competing transition metal cations because the binding affinities are determined via competitive equilibria with adsorbed protons which cannot be quantitatively determined without the proton affinity distribution of the poly(acrylamidoxime) fibers.²⁸ Therefore, determination of the proton and metal cation affinity distributions can play an essential role in improving the selectivity of subsequent generations of chelating polymers used to mine uranium from seawater.

6.4. Conclusion

Poly(acrylamidoxime) fibers are the current state of the art adsorbent for mining uranium from seawater. While the acid dissociation constants of characteristic amidoxime^{11, 12} and carboxylate ligands¹³ have been reported, the protonation affinity of the grafted adsorbent containing poly(acrylamidoxime) is yet to be reported. These values are of great importance because the comparison of the acidity constants of poly(acrylamidoxime) monomer units to the acidity of their representative small ligands, is incomplete. The pK_a values of pure chemical compounds, like small ligands, are a sum of delta functions; in contrast, the acidity of polymers is more accurately described as a continuous distribution of proton affinities.¹⁴ Herein, the poly(acrylamidoxime) proton affinity distribution obtained via the SAIUS algorithm is reported. Two peaks in the proton affinity distribution of poly(acrylamidoxime) were observed: the neutral to anionic dissociation of the carboxylate monomer between pH 3.2 and pH 4.4 ($pK_a \sim 4.0$) and the protonated to neutral dissociation of the acyclic amidoxime monomer between pH 5.6 and pH 6.8 ($pK_a \sim 6.1$). The acidity constants of the carboxylate and amidoximate monomers differ from the acidity of acetic acid and acetamidoxime by ~ 0.7 pK_a units and ~ 0.5 pK_a units, respectively. This difference in acidity can be attributed to charge interaction on the poly(acrylamidoxime) fiber. Specifically, the close proximity of positively charged acyclic amidoxime monomers and neutral carboxylic acid monomers stabilize the dissociation of carboxylic acid into carboxylate. In contrast, the stabilizing interaction between the positively charged amidoxime and the negatively charged carboxylate monomers destabilized the protonated to neutral dissociation of acyclic amidoxime monomers.

This work lays the foundation for resolving the metal cation affinity distribution of the poly(acrylamidoxime) fibers, which can aid in improving the uranium selectivity of subsequent generations of chelating polymers, because the determination of the proton and metal cation

affinity distributions of aqueous polymers by approximate solutions to the adsorption isotherm integral equation, such as the SAIUS algorithm, are identical with the exception of the influence of coordination number in binding affinity distributions.²² Moreover, the poly(acrylamidoxime) binding affinity distribution of UO_2^{2+} and competing transition metal cations cannot be accurately determined without the proton affinity distribution because the binding affinity distributions are determined via competitive equilibria with adsorbed protons.²⁸

References

1. Davies, R. V.; Kennedy, J.; McIlroy, R. W.; Spence, R.; Hill, K. M. Extraction of Uranium from Sea Water. *Nature* **1964**, *203*, 1110–1115.
2. Uranium 2014: Resources, Production and Demand. OECD Nuclear Energy Agency International Atomic Energy Agency: 2014; Vol. NEA No. 7209.
3. Saito, K.; Miyauchi, T. Chemical Forms of Uranium in Artificial Seawater. *J. Nucl. Sci. Technol.* **1982**, *19*, 145–150.
4. Choppin, G. R. Soluble Rare Earth and Actinide Species in Seawater. *Mar. Chem.* **1989**, *28*, 19-26.
5. Endrizzi, F.; Rao, L. Chemical Speciation of Uranium(VI) in Marine Environments: Complexation of Calcium and Magnesium Ions with $[(\text{UO}_2)(\text{CO}_3)_3]^{4-}$ and the Effect on the Extraction of Uranium from Seawater. *Chem. Eur. J.* **2014**, *20*, 14499-14506.
6. Yue, Y.; Mayes, R. T.; Kim, J.; Fulvio, P. F.; Sun, X.-G.; Tsouris, C.; Chen, J.; Brown, S.; Dai, S. Seawater Uranium Sorbents: Preparation from a Mesoporous Copolymer Initiator by Atom-Transfer Radical Polymerization. *Angew. Chem. Int. Ed.* **2013**, *125*, 13700-13704.
7. Schenk, H. J.; Astheimer, L.; Witte, E. G.; Schwochau, K. Development of Sorbers for the Recovery of Uranium from Seawater. 1. Assessment of Key Parameters and Screening Studies of Sorber Materials. *Sep. Sci. Technol.* **1982**, *17*, 1293-1308.
8. Astheimer, L.; Schenk, H. J.; Witte, E. G.; Schwochau, K. Development of Sorbers for the Recovery of Uranium from Seawater. Part 2. The Accumulation of Uranium from Seawater

by Resins Containing Amidoxime and Imidoxime Functional Groups. *Sep. Sci. Technol.* **1983**, *18*, 307–339.

9. Kawai, T.; Saito, K.; Sugita, K.; Katakai, A.; Seko, N.; Sugo, T.; Kawakami, T.; Kanno, J. Comparison of Amidoxime Adsorbents Prepared by Cograftering Methacrylic Acid and 2-Hydroxyethyl Methacrylate with Acrylonitrile onto Polyethylene. *Ind. Eng. Res. Chem.* **2000**, *39*, 2910-2915.

10. Kawai, T.; Saito, K.; Sugita, K.; Kawakami, T.; Kanno, J.; Katakai, A.; Seko, N.; Sugo, T. Preparation of Hydrophilic Amidoxime Fibers by Cograftering Acrylonitrile and Methacrylic Acid from an Optimized Monomer Composition. *Radiat. Phys. Chem.* **2000**, *59*, 405-411.

11. Mehio, N.; Lashley, M. A.; Nugent, J. W.; Tucker, L.; Correia, B.; Do-Thanh, C.-L.; Dai, S.; Hancock, R. D.; Bryantsev, V. S. Acidity of the Amidoxime Functional Group in Aqueous Solution: A Combined Experimental and Computational Study. *J. Phys. Chem. B.* **2015**, *119*, 3567–3576.

12. Tian, G.; Teat, S. J.; Zhang, Z.; Rao, L. Sequestering Uranium from Seawater: Binding Strength and Modes of Uranyl Complexes with Glutarimidedioxime. *Dalton Trans.* **2012**, *41*, 11579-11586.

13. Smith, R. M.; Martell, A. E., *Critical Stability Constants*. Plenum Press: New York, 1981.

14. Jagiełło, J.; Bandosz, T. J.; Putyera, K.; Schwarz, J. A. Determination of Proton Affinity Distributons for Chemical Systems in Aqueous Environments Using a Stable Numerical Solution of the Adsorption Integral Equation. *J. Colloid Interface Sci.* **1995**, *172*, 341-346.

15. Mildan, E.; Gülfen, M. Equilibrium, Kinetics, and Thermodynamics of Pd(II) Adsorption onto Poly(m-aminobenzoic acid) Chelating Polymer. *J. Appl. Polym. Sci.* **2015**, *132*, 42533.
16. Gaballa, H. A.; Geever, L. M.; Killion, J. A.; Higginbotham, C. L. Synthesis and Characterization of Physically Crosslinked N-Vinylcaprolactam, Acrylic Acid, Methacrylic Acid, and N,N-Dimethylacrylamide Hydrogels. *J. Polym. Sci., Part B: Polym. Phys.* **2013**, *51*, 1555-1564.
17. Furukawa, M.; Farinato, R. S.; Kokufuta, E. Potentiometric Titration Behavior of Poly(acrylic acid) within a Cross-Linked Polymer Network Having Amide Groups. *Colloid Polym Sci.* **2008**, *286*, 1425-1434.
18. Lützenkirchen, J.; van Male, J.; Leermakers, F.; Sjöberg, S. Comparison of Various Models to Describe the Charge-pH Dependence of Poly(acrylic acid). *J. Chem. Eng. Data* **2011**, *56*, 1602-1612.
19. Hoare, T.; Pelton, R. Titrametric Characterization of pH-Induced Phase Transitions in Functionalized Microgels. *Langmuir* **2006**, *22*, 7342-7350.
20. Urry, D. W.; Peng, S. Q.; Gowda, D. C.; Parker, T. M.; Harris, R. D. Comparison of Electrostatic- and Hydrophobic-Induced pK_a Shifts in Polypentapeptides. The Lysine Residue. *Chem. Phys. Lett.* **1994**, *225*, 97-103.
21. Urry, D. W.; Gowda, D. C.; Peng, S. Q.; Parker, T. M.; Jing, N. J.; Harris, R. D. Nanometric Design of Extraordinary Hydrophobic-Induced pK_a Shifts for Aspartic Acid: Relevance to Protein Mechanisms. *Biopolymers* **1994**, *34*.

22. Ballif, J. B.; Lerf, C.; Schläpfer, C. W. The Proton Affinity Spectrum of Polyethylenimine. *Chimia* **1994**, *48*, 336-340.
23. Jagiełło, J. Stable Numerical Solution of the Adsorption Integral Equation Using Splines. *Langmuir* **1994**, *10*, 2778-2785.
24. Harris, L. B. Adsorption on a Patchwise Heterogeneous Surface; Mathematical Analysis of the Step-Function Approximation to the Local Isotherm. *Surf. Sci.* **1968**, *10*, 129-145.
25. Rudziński, W.; Jagiełło, J.; Grillet, Y. Physical Adsorption of Gases on Heterogeneous Solid Surfaces: Evaluation of the Adsorption Energy Distribution from Adsorption Isotherms and Heats of Adsorption. *J. Colloid Interface Sci.* **1982**, *87*, 478-491.
26. Nederlof, M. M.; van Riemsdijk, W. H.; Koopal, L. K. Determination of Adsorption Affinity Distributions: A General Framework for Methods Related to Local Isotherm Approximations. *J. Colloid Interface Sci.* **1990**, *135*, 410-426.
27. Jagiełło, J.; Ligner, G.; Papirer, E. Characterization of Silicas by Inverse Gas Chromatography at Finite Concentration: Determination of the Adsorption Energy Distribution Function. *J. Colloid Interface Sci.* **1990**, *137*, 128-136.
28. von Zelewsky, A.; Barbosa, L.; Schläpfer, C. W. Poly(ethylenimines) as Brønsted Bases and as Ligands for Metal Ions. *Coord. Chem. Rev.* **1993**, *123*, 229-246.
29. Schläpfer, C. W.; von Zelewsky, A. Polymeric Amines as Ligands. Polyethyleneimines as Ligands in First and Second Coordination Sphere. *Comments Inorg. Chem.* **1990**, *9*, 181-199.
30. Ballif, J. B. Thesis No. 1005,. University of Fribourg, Fribourg, Switzerland, 1991.

31. Lerf, C. Thesis No. 1054. University of Fribourg, Fribourg, Switzerland, 1993.
32. Contescu, C.; Jagiełło, J.; Schwarz, J. A. Heterogeneity of Proton Binding Sites at the Oxide/Solution Interface. *Langmuir* **1993**, *9*, 1754-1765.
33. Bandosz, T. J.; Jagiełło, J.; Contescu, C.; Schwarz, J. A. Characterization of the Surfaces of Activated Carbons in Terms of their Acidity Constant Distributions. *Carbon* **1993**, *31*, 1193–1202.
34. Nederlof, M. M.; De Wit, J. C. M.; van Riemsdijk, W. H.; Koopal, L. K. Determination of Proton Affinity Distributions for Humic Substances. *Environ. Sci. Technol.* **1993**, *27*, 846–856.
35. Contescu, C. I.; Baker, F. S.; Hunt, R. D.; Collins, J. L.; Burchell, T. D. Selection of Water-Dispersible Carbon Black for Fabrication of Uranium Oxide Microspheres. *J. Nucl. Mater.* **2008**, *375*, 38–51.
36. Laatikainen, M.; Sirola, K.; Paatero, E. Binding of Transition Metals by Soluble and Silica-Bound Branched Poly(ethyleneimine) Part I: Competitive Binding Equilibria. *Colloids Surf., A* **2007**, *296*, 191–205.
37. Ammann, L. Cation Exchange and Adsorption on Clays and Clay Minerals. Christian-Albrechts-Universität, Kiel, Germany, 2003.
38. Stumm, W.; Morgan, J. J., *Aquatic Chemistry*. Wiley: New York, 1981.
39. Tsukube, H. F.; Odani, A.; Takeda, Y.; Kudo, Y.; Inoue, Y.; Liu, Y.; Sakamoto, H.; Kimura, K., Determination of Stability Constants. In *Comprehensive Supramolecular Chemistry*,

Lehn, J. M.; Atwood, J. L.; Davis, J. E. D.; MacNicol, D. D.; Vogtle, F., Eds. Pergamon: New York, 1996; Vol. 8.

40. Contescu, C.; Popa, V. T.; Miller, J. B.; Ko, E. I.; Schwarz, J. A. Proton Affinity Distributions of $\text{TiO}_2\text{-SiO}_2$ and $\text{ZrO}_2\text{-SiO}_2$ Mixed Oxides and Their Relationship to Catalyst Activities for 1-Butene Isomerization. *J. Catal.* **1995**, *157*, 244–258.

41. Choi, S. H.; Nho, Y. C. Radiation-induced Graft Copolymerization of Binary Monomer Mixture Containing Acrylonitrile onto Polyethylene Films. *Radiation Physics and Chemistry* **2000**, *58*, 157-168.

42. Egawa, H.; Kabay, N.; Nonaka, T.; Shuto, T. Preparation of Hollow-fiber Adsorbents Containing Amidoxime Groups and Their Adsorption Ability for Uranium. *Bulletin of the Society of Sea Water Science, Japan* **1991**, *45*, 87-94.

43. Seko, N.; Katakai, A.; Tamada, M.; Sugo, T.; Yoshii, F. Fine Fibrous Amidoxime Adsorbent Synthesized by Grafting and Uranium Adsorption-elution Cyclic Test with Seawater. *Separation Science and Technology* **2004**, *39*, 3753–3767.

44. Kobuke, Y.; Tanaka, H.; Ogoshi, H. Imidedioxime As a Significant Component in So-called Amidoxime Resin for Uranyl Adsorption from Seawater. *Polymer Journal* **1990**, *22*, 179–182.

45. Eloy, F.; Lenaers, R. The Chemistry of Amidoximes and Related Compounds. *Chem. Rev.* **1962**, *62*, 155–183.

46. Tian, G. X.; Teat, S. J.; Rao, L. F. Thermodynamic Studies of U(VI) Complexation with Glutardiamidoxime for Sequestration of Uranium from Seawater. *Dalton Transactions* **2013**, 42, 5690–5696.
47. Tian, G. X.; Teat, S. J.; Zhang, Z. Y.; Rao, L. F. Sequestering Uranium from Seawater: Binding Strength and Modes of Uranyl Complexes with Glutarimidedioxime. *Dalton Transactions* **2012**, 41, 11579–11586.
48. Kang, S. O.; Vukovic, S.; Custelcean, R.; Hay, B. P. Cyclic Imide Dioximes: Formation and Hydrolytic Stability. *Ind. Eng. Res. Chem.* **2012**, 51, 6619–6624.
49. Candau, F.; Zekhnini, Z.; Heatley, F. Carbon-13 NMR Study of the Sequence Distribution of Poly(acrylamide-*co*-sodium acrylates) Prepared in Inverse Microemulsions. *Macromolecules* **1986**, 19, 1895–1902.

Chapter 7 : Conclusion

In recent years, there has been great interest in developing low-carbon emission energy sources as an alternative to the widely utilized, high-carbon emission fossil fuels. Nuclear energy is a promising alternative as there is an estimated 4.5 billion tons of uranium,¹ the primary fuel source in nuclear fission, dissolved in seawater, while only 61,600 metric tons are needed annually to meet current global energy demands.² The dominant form of the uranyl ion in seawater is the tricarbonato complex, $\text{UO}_2(\text{CO}_3)_3^{4-}$,^{1, 3-4} which associates with Ca^{2+} , a major cation in seawater, to form a $\text{Ca}_2\text{UO}_2(\text{CO}_3)_3^0$ ternary complex, the dominant uranyl species in seawater.⁵ However, there are a number of challenges associated with developing an adsorbent capable of extracting uranium from seawater that primarily stem from the fact that UO_2^{2+} is present in very low concentrations, 3.3 ppb,⁶ in the presence of competing metal cations.⁴ Therefore, the development of extremely efficient and selective adsorbents is instrumental to making this process industrially viable. Poly(acrylamidoxime) fibers are the current state of the art adsorbents for mining uranium from seawater. The poly(acrylamidoxime) fiber is a random copolymer of carboxylate and amidoxime monomers at a 40 to 60 monomer weight ratio, respectively,⁷⁻⁸ that was first identified in a screening of 200 organic polymers as the only adsorbent capable of extracting UO_2^{2+} from pH 8.3 aqueous solution, the approximate pH of seawater.⁹⁻¹⁰ However, the amidoxime functional group is not perfectly selective towards the UO_2^{2+} cation, in particular, competition with transition metal cations, such as Fe^{3+} (3.4 ppb),¹¹ Cu^{2+} (0.9 ppb),¹¹ VO^{2+} , and VO_2^+ (1.9 ppb),¹¹ remains a major challenge.^{6, 12-14}

In order for subsequent generations of chelating polymer adsorbents to be improved, the coordination chemistry of amidoxime- UO_2^{2+} and amidoxime-transition metal cation complexes needs to be better understood. The poly(acrylamidoxime) fiber is composed of two types of

amidoxime monomers: an acyclic amidoxime monomer and a cyclic imidioxime monomer. The cyclic imidioxime- and acyclic amidoxime- UO_2^{2+} binding motifs have been computationally¹⁵⁻¹⁶ and crystallographically¹⁵⁻¹⁸ elucidated in the literature. Acyclic amidoximes η^2 coordinate to UO_2^{2+} via the oxime functional group, while as cyclic imidioximes chelate to UO_2^{2+} via a tridentate chelate formed by the oxime oxygen atoms and the amine nitrogen atom. Likewise, there is consensus in the literature that cyclic imidioximes coordinate to transition metals with the UO_2^{2+} binding motif or via a similar binding motif that entails tridentate chelation of the oxime nitrogen atoms and the amine nitrogen atom. In contrast, a number of acyclic amidoxime-transition metal cation crystal structures with a variety of binding motifs have been reported in the literature. Moreover, while the log K values of cyclic imidioxime- UO_2^{2+} complexes and a number of essential cyclic imidioxime-transition metal cation complexes,^{14, 16} the UO_2^{2+} and transition metal cation log K values of acyclic amidoxime complexes remain largely unresolved due to the wide range of conflicting pK_a values that have been reported for representative acyclic amidoxime ligands in the literature.¹⁹⁻²³

Thus, an aim of our group's research was to improve the selectivity and capacity of subsequent generations of chelating polymers by further developing our understanding of the coordination chemistry of the acyclic amidoxime monomer that occurs on poly(acrylamidoxime) fibers. As stated previously, the pK_a values of oxoacids, such as cyclic imidioxime and acyclic amidoxime ligands, are used to determine the log K values of amidoxime-metal complexes, which facilitates the comparison of the strength of amidoxime- UO_2^{2+} relative to competing amidoxime-transition metal cation complexes.²⁴ Moreover, the pK_a and log K values of oxoacids are correlated by linear free energy relationships;²⁵ thus, when coupled with binding motif information, methods for predicting the pK_a values of oxoacid ligands, such as amidoximes, can

be used to design ligands that further improve the UO_2^{2+} affinity and selectivity of subsequent generations of chelating polymer adsorbents. Therefore, in **Chapter 2** we use ^1H -NMR and UV/Vis spectroscopic titrations to resolve the pK_a values of acetamidoxime and benzamidoxime. Subsequently, we use pK_a those values to develop computational protocols for predicting the pK_a values of aqueous oxoacid ligands. Density functional theory and wave-function methods were utilized in conjunction with continuum solvation calculations to develop computational protocols for predicting the pK_a values of aqueous oxoacid ligands within < 0.5 pK_a units of their experimental value.

While the computational protocols for predicting the pK_a values of oxoacids aid in the design of ligands that form more stable UO_2^{2+} complexes, they does not facilitate the design of ligands that are more selective to UO_2^{2+} than competing transition metal cations on their own because the $\log K$ value of any oxoacid-metal cation complex is related to the pK_a value of that ligand by a linear free energy relationship.¹⁸ Therefore, in order to computationally design ligands that are more selective towards UO_2^{2+} than the standard amidoxime based ligands, the coordination modes of amidoxime- UO_2^{2+} and amidoxime-transition metal cation complexes needed to be elucidated as well. In **Chapters 3** and **4**, we computationally investigate the binding motif of formamidoximate- VO_2^+ and $-\text{VO}^{2+}$ complexes, major competing ions in seawater.^{6, 12-13} Density functional theory and wave-function methods were utilized in conjunction with continuum solvation calculations to investigate potential binding motifs of formamidoximate- VO_2^+ and formamidoximate- VO^{2+} complexes. Our investigations of these formamidoximate complexes universally identified the most stable binding motif to be a tautomericly rearranged imino hydroxylamine chelate formed via coordination of the imino nitrogen and hydroxylamine oxygen. The alternative binding motifs for amidoxime chelation to VO_2^{2+} and VO^{2+} via a non-

rearranged tautomer and η^2 coordination were found to be ~ 5 kcal/mol and ~ 11 kcal/mol less stable, respectively. Thus, while η^2 -coordination of the oxime functional group is the most stable coordination mode of amidoxime- UO_2^{2+} complexes,^{15, 17-18} it is far less than the tautomeric rearranged imino hydroxylamine chelate in amidoxime- VO_2^+ and amidoxime- VO^{2+} complexes. In light of this result, an important question arose as to whether such tautomeric transformation is feasible in aqueous solution. Arshadi et al.²⁶ computationally investigated the amidoxime-imino hydroxylamine tautomerization in the absence of complexing ions and they reported that the amidoxime form is ~ 10 kcal/mol more stable than the imino hydroxylamine form. Moreover, they found a prohibitively high energy barrier for tautomerization in the gas phase (>30 kcal/mol) that could be reduced substantially in the presence of explicit solvent molecules (≤ 20 kcal/mol).²⁶ Since the relative stability of the two tautomers is reversed when bound to VO_2^+ or VO^{2+} , the reaction barrier of amidoximate- VO_2^+ and amidoximate- VO^{2+} complexes is much smaller than for a free amidoxime ligand, ~ 9 kcal/mol and ~ 3 kcal/mol, respectively. Thus, we determined that the complexation between poly(acrylamidoxime) fibers and vanadium cations can be restricted by either inhibiting the tautomeric rearrangement from the amidoxime to imino hydroxylamine via substitution of both amine hydrogen atoms with aliphatic or aromatic groups or eliminating the amine group all together.

In **Chapter 5**, we build on the design principles acquired in **Chapters 2-4** to design a ligand, salicylaldoxime that is more selective toward the UO_2^{2+} cation than competing transition metal cations. We found that the binding strength of salicylaldoxime- UO_2^{2+} complexes are $\sim 2-4$ log β_2 units greater in magnitude than their corresponding acetamidoxime- UO_2^{2+} and benzamidoxime- UO_2^{2+} complexes; moreover, the selectivity of salicylaldoxime towards the UO_2^{2+} cation over competing Cu^{2+} and Fe^{3+} cations is far greater than the selectivities reported for

glutarimidedioxime in the literature. The higher UO_2^{2+} selectivity can likely be attributed to the different coordination modes observed for salicyladoxime- UO_2^{2+} and salicylaldoxime-transition metal complexes. Density functional theory calculations show that salicylaldoxime coordinates to UO_2^{2+} as a dianion species formed by η^2 -coordination of the aldoximate and monodentate binding of the phenolate group. In contrast, salicylaldoxime coordinates to transition metal cations as a monoanion species via a chelate formed between phenolate and the oxime N; the complexes are stabilized via hydrogen bonding interactions between the oxime OH group and phenolate. Thus, by coupling the experimentally determined thermodynamic constants and the results of theoretical computations, we are able to derive a number of ligand design principles to further improve the UO_2^{2+} cation affinity, and thus further increase the selectivity, of salicylaldoxime derivatives.

Finally, in **Chapter 6** we potentiometrically determine the proton affinity distribution of the classical poly(acrylamidoxime) fiber between pH 2 and pH 10 via the Stable Numerical Solution of the Adsorption Integral Equation Using Splines (SAIUS) algorithm.²⁷⁻²⁹ These values are of great importance because the comparison of the acidity constants of poly(acrylamidoxime) monomer units to the acidity of their representative small ligands, is incomplete.²⁷⁻²⁹ The pK_a values of pure chemical compounds, like small ligands, are a sum of delta functions; in contrast, the acidity of polymers is more accurately described as a continuous distribution of proton affinities.²⁷⁻²⁹ Two peaks in the proton affinity distribution of poly(acrylamidoxime) were observed: the neutral to anionic dissociation of the carboxylate monomer between pH 3.2 and pH 4.4 ($\text{pK}_a \sim 4.0$) and the protonated to neutral dissociation of the acyclic amidoxime monomer between pH 5.6 and pH 6.8 ($\text{pK}_a \sim 6.1$). The acidity constants obtained for the carboxylate and amidoxime monomers vary from the acidity constants of acetic acid and acetamidoxime,

respectively. These variations in acidity can be attributed to charge interactions between the carboxylate ($\text{pK}_a \sim 4.76$)³⁰ and amidoxime ($\text{pK}_a \sim 5.78$) monomers. This work lays the foundation for resolving the metal cation affinity distribution of the poly(acrylamidoxime) fibers, which can aid in improving the uranium selectivity of subsequent generations of chelating polymers.²⁷⁻²⁹

References

1. Davies, R. V.; Kennedy, J.; McIlroy, R. W.; Spence, R.; Hill, K. M., Extraction of Uranium from Sea Water. *Nature* **1964**, *203*, 1110–1115.
2. Uranium 2014: Resources, Production and Demand. OECD Nuclear Energy Agency, International Atomic Energy Agency: 2014; Vol. NEA No. 7209.
3. Saito, K.; Miyauchi, T., Chemical Forms of Uranium in Artificial Seawater. *J. Nucl. Sci. Technol.* **1982**, *19*, 145–150.
4. Choppin, G. R., Soluble Rare Earth and Actinide Species in Seawater. *Mar. Chem.* **1989**, *28*, 19-26.
5. Endrizzi, F.; Rao, L., Chemical Speciation of Uranium(VI) in Marine Environments: Complexation of Calcium and Magnesium Ions with $[(\text{UO}_2)(\text{CO}_3)_3]^{4-}$ and the Effect on the Extraction of Uranium from Seawater. *Chem. Eur. J.* **2014**, *20*, 14499-14506.
6. Kim, J.; Tsouris, C.; Mayes, R. T.; Oyola, Y.; Saito, T.; Janke, C. J.; Dai, S.; Schneider, E.; Sachde, D., Recovery of Uranium from Seawater: A Review of Current Status and Future Research Needs. *Sep. Sci. Technol.* **2012**, *48*, 367–387.
7. Kawai, T.; Saito, K.; Sugita, K.; Katakai, A.; Seko, N.; Sugo, T.; Kawakami, T.; Kanno, J., Comparison of Amidoxime Adsorbents Prepared by Cograftering Methacrylic Acid and 2-Hydroxyethyl Methacrylate with Acrylonitrile onto Polyethylene. *Ind. Eng. Res. Chem.* **2000**, *39*, 2910-2915.

8. Kawai, T.; Saito, K.; Sugita, K.; Kawakami, T.; Kanno, J.; Katakai, A.; Seko, N.; Sugo, T., Preparation of Hydrophilic Amidoxime Fibers by Cograftering Acrylonitrile and Methacrylic Acid from an Optimized Monomer Composition. *Radiat. Phys. Chem.* **2000**, *59*, 405-411.
9. Schenk, H. J.; Astheimer, L.; Witte, E. G.; Schwochau, K., Development of Sorbers for the Recovery of Uranium from Seawater. 1. Assessment of Key Parameters and Screening Studies of Sorber Materials. *Sep. Sci. Technol.* **1982**, *17*, 1293-1308.
10. Astheimer, L.; Schenk, H. J.; Witte, E. G.; Schwochau, K., Development of Sorbers for the Recovery of Uranium from Seawater. Part 2. The Accumulation of Uranium from Seawater by Resins Containing Amidoxime and Imidoxime Functional Groups. *Sep. Sci. Technol.* **1983**, *18*, 307-339.
11. Turekian, K. K., *Oceans*. Prentice Hall: Englewood Cliffs, NJ 1968.
12. Wang, D. L.; Sañudo Wilhelmy, S. A., Vanadium Speciation and Cycling in Coastal Waters. *Mar. Chem.* **2009**, *117*, 52-58.
13. Suzuki, T.; Saito, K.; Sugo, T.; Ogura, H.; Oguma, K., Fractional Elution and Determination of Uranium and Vanadium Adsorbed on Amidoxime Fiber from Seawater. *Anal. Sci.* **2000**, *16*, 429-432.
14. Sun, X.; Xu, C.; Tian, G.; Rao, L., Complexation of Glutarimidedioxime with Fe(III), Cu(II), Pb(II), and Ni(II), the Competing Ions for the Sequestration of U(VI) from Seawater. *Dalton Trans.* **2013**, *42*, 14621-14627.
15. Vukovic, S.; Watson, L. A.; Kang, S. O.; Custelcean, R.; Hay, B. P., How Amidoximate Binds the Uranyl Cation. *Inorg. Chem.* **2012**, *51*, 3855-3859.

16. Tian, G.; Teat, S. J.; Zhang, Z.; Rao, L., Sequestering Uranium from Seawater: Binding Strength and Modes of Uranyl Complexes with Glutarimidedioxime. *Dalton Trans.* **2012**, *41*, 11521–11908.
17. Barber, P. S.; Kelley, S. P.; Rogers, R. D., Highly Selective Extraction of the Uranyl Ion with Hydrophobic Amidoxime-Functionalized Ionic Liquids via η^2 Coordination. *RSC Adv.* **2012**, *2*, 8526-8530.
18. Kelley, S. P.; Barber, P. S.; Mullins, P. H.; Rogers, R. D., Structural Clues to $\text{UO}_2^{2+}/\text{VO}_2^+$ Competition in Seawater Extraction Using Amidoxime-Based Extractants. *Chem. Commun.* **2014**, *50*, 12504-12507.
19. Dürüst, N.; Akay, M. A.; Dürüst, Y.; Kiliç, E., Protonation Constants of Some N-Substituted Amidoximes in a 50% Ethanol-Water Mixture (v/v). *Anal. Sci.* **2001**, *16*, 825–827.
20. Hirotsu, T.; Katoh, S.; Sugasaka, K.; Seno, M.; Itagaki, T., Binding Ability of Acetamide Oxime with Proton, Copper(II), and Dioxouranium(VI) in Aqueous Solutions *J. Chem. Soc., Dalton Trans.* **1986**, *8*, 1609–1611.
21. Bunton, C. A.; Nelson, S. E.; Quan, C., Micellar Effects Upon Dephosphorylation by Amidoximes. *J. Org. Chem.* **1982**, *47*, 1157–1160.
22. Aubort, J. D.; Hudson, R. F., Enhanced Reactivity of Nucleophiles: Orbital Symmetry and the So-Called " α -Effect" *J. Chem. Soc. D: Chem. Commun.* **1970**, *15*, 937–938.
23. Simanenko, Y. S.; Prokop'eva, T. M.; Belousova, I. A.; Popov, A. F.; Karpichev, E. A., Amidoximes as Effective Acceptors of Acyl Group. *Theor. Exp. Chem.* **2001**, *37*, 288–295.

24. Martell, A. E.; Hancock, R. D., *Metal Complexes in Aqueous Solutions*. Plenum Press: New York, 1996.
25. Hay, B. P.; Chagnes, A.; Cote, A. G., On the Metal Ion Selectivity of Oxoacid Extractants. *Solvent Extr. Ion Exch.* **2013**, *31*, 95–105.
26. Tavakol, H.; Arshadi, S., Theoretical Investigation of Tautomerism in N-Hydroxy Amidines. *J. Mol. Model.* **2009**, *15*, 807–816.
27. Jagiełło, J., Stable Numerical Solution of the Adsorption Integral Equation Using Splines. *Langmuir* **1994**, *10*, 2778-2785.
28. Jagiełło, J.; Bandosz, T. J.; Putyera, K.; Schwarz, J. A., Determination of Proton Affinity Distributons for Chemical Systems in Aqueous Environments Using a Stable Numerical Solution of the Adsorption Integral Equation. . *J. Colloid Interface Sci.* **1995**, *172*, 341-346.
29. Ballif, J. B.; Lerf, C.; Schläpfer, C. W., The Proton Affinity Spectrum of Polyethylenimine. *Chimia* **1994**, *48*, 336-340.
30. Smith, R. M.; Martell, A. E., *Critical Stability Constants*. Plenum Press: New York, 1981.

Appendix

Appendix A: Supporting Information for Acidity of the Amidoxime Functional Group in Aqueous Solution: A Combined Experimental and Computational Study

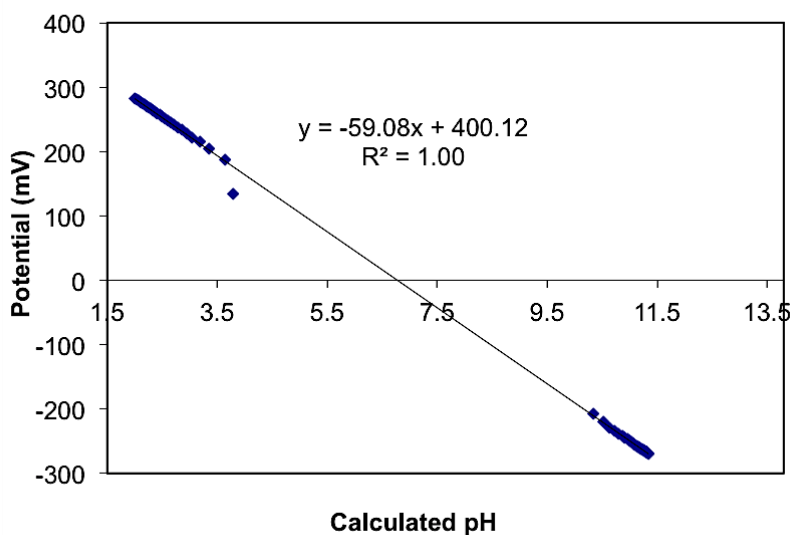
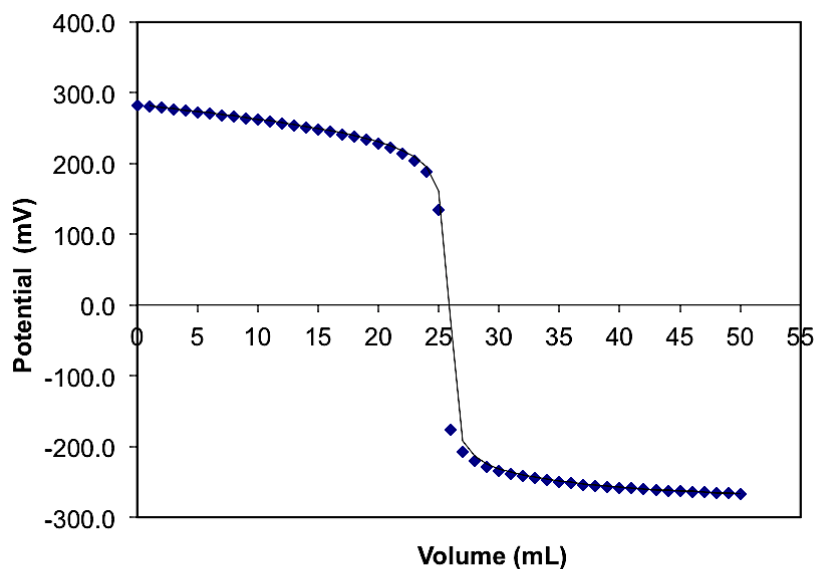


Figure A.1. (*Top*) Strong acid (0.01 M HClO_4) versus strong base (0.01 M NaOH) titration used to standardize the pH electrode. The initial solution contained 25 mL of 0.01 M HClO_4 . (*Bottom*) Calibration plot used to determine the Nernst slope (-59.08) and the E° correction factor (400.12).

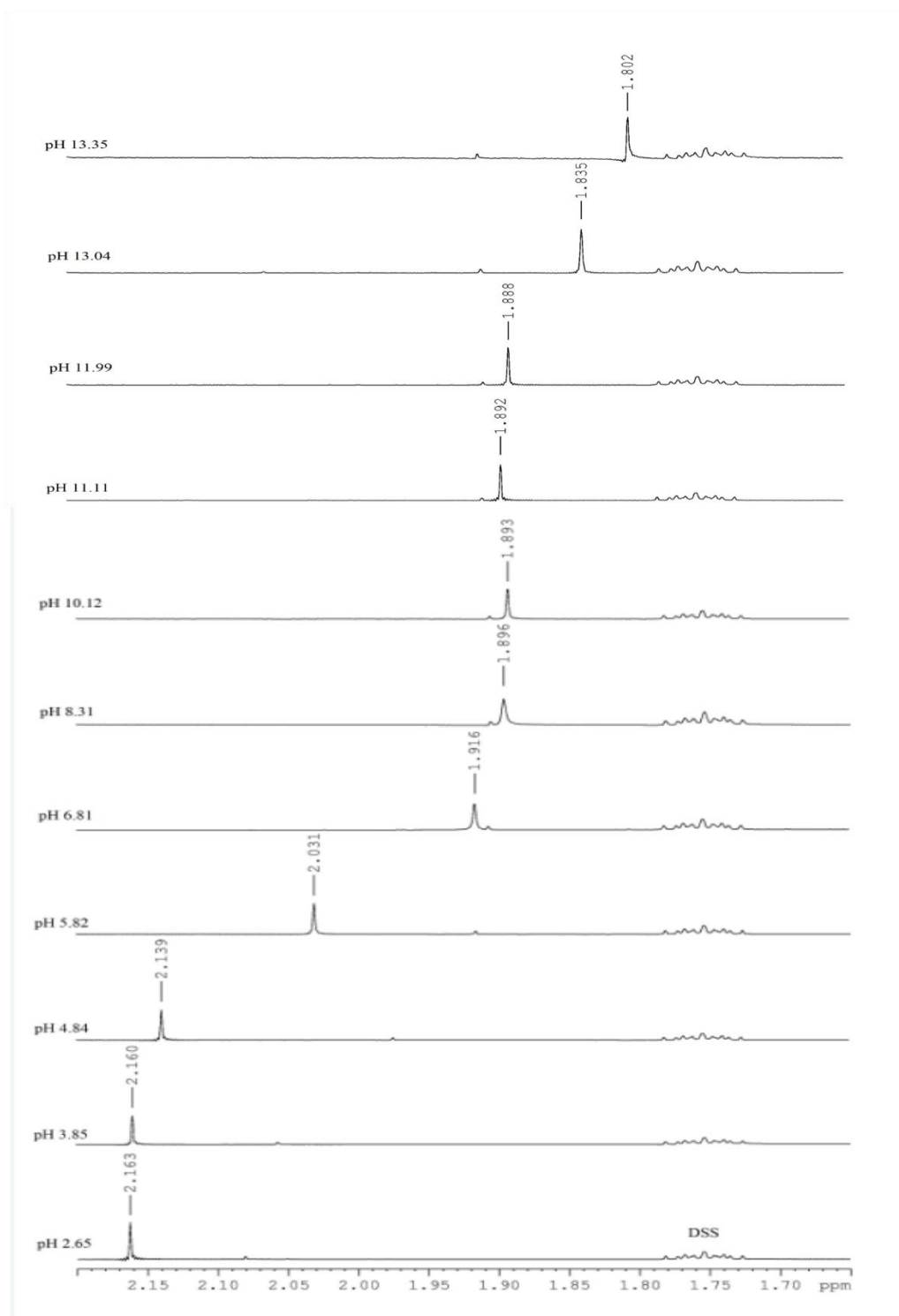


Figure A.2. ¹H-NMR spectra of aqueous acetamidoxime (2×10^{-3} M) at 25 °C and 0.0 M ionic strength by pH.

Table A. 1. pK_a values obtained by computing the solvation energies with the IEFPCM solvation model.^{a,b}

Acid	B3LYP ^g	M06 ^h	M06-2X ⁱ	MP2 ^j	CCSD(T) ^k	Exp.
1. Water ^{c,e}	16.73	17.64	16.98	16.44	16.41	15.70
2. Methanol ^c	15.33	14.99	15.31	15.96	15.52	15.54
3. Phenol ^c	9.13	8.72	8.76	9.16	8.97	9.99
4. Formic Acid ^c	4.56	4.47	4.78	4.53	4.52	3.77
5. Benzoic Acid ^c	5.51	5.33	5.13	4.92	4.86	4.20
6. Acetaldoxime ^c	11.63	11.51	11.42	11.64	11.69	11.42
7. Benzaldoxime ^c	10.12	9.87	10.07	10.49	10.76	11.30
8. Acetohydroxamic Acid ^c	9.42	9.54	9.69	9.72	9.47	8.70
9. Benzohydroxamic Acid ^c	8.87	8.96	9.42	9.30	9.17	8.81
10. Nitric Acid ^c	-0.89	-0.90	-1.22	-0.38	-0.64	-1.40
11. Sulfuric Acid ^c	-3.62	-3.46	-3.47	-3.81	-3.72	-3.00
12. Phosphoric Acid ^c	1.98	2.23	2.07	1.95	1.93	2.15
13. Carbonic Acid ^c	3.28	3.42	3.41	3.23	3.16	3.60
14. Acetamidoxime	13.24	13.21	13.00	12.94	12.83	13.21
15. Benzamidoxime	11.72	11.65	11.74	11.50	11.93	12.36
16. Azine-Amidoxime ^{d,f}	11.12	11.11	11.23	1074	11.48	11.98
Mean Absolute Error	0.61	0.68	0.63	0.67	0.53	
Root Mean Square Deviation	0.73	0.87	0.76	0.74	0.59	

^aZPE and thermal corrections are calculated in the gas phase at the B3LYP/6-311++G** level of theory.^bB3LYP and the 6-31+G* basis set was used for all solvation calculations.^cSmith, R. M.; Martell, A. E., *Critical Stability Constants*. Plenum Press: New York, 1981.^dSimanenko, Y. S.; Prokop'eva, T. M.; Belousova, I. A.; Popov, A. F.; Karpichev, E. A., Amidoximes as Effective Acceptors of Acyl Group. *Theor. Exp. Chem.* **2001**, 37, 288-295.^eThe experimental pK_a corresponds to a 55.5 M solution. However, our thermodynamic cycle calls for the conversion of an ideal gas to an ideal solution (1 M). Therefore, a correction of 1.7 pK_a units was added to all the predicted water pK_a values.^fThe full name of this structure is (Z)-N-hydroxynicotinimidamide.

$$^g pK_a[\text{Pred.}] = 0.464 \times pK_a[\text{Comp.}]; \Delta G_{\text{solv}}^*(H^+) = -268.62 \text{ kcal/mol}$$

$$^h pK_a[\text{Pred.}] = 0.465 \times pK_a[\text{Comp.}]; \Delta G_{\text{solv}}^*(H^+) = -268.59 \text{ kcal/mol}$$

$$^i pK_a[\text{Pred.}] = 0.434 \times pK_a[\text{Comp.}]; \Delta G_{\text{solv}}^*(H^+) = -269.88 \text{ kcal/mol}$$

$$^j pK_a[\text{Pred.}] = 0.492 \times pK_a[\text{Comp.}]; \Delta G_{\text{solv}}^*(H^+) = -268.78 \text{ kcal/mol}$$

$$^k pK_a[\text{Pred.}] = 0.478 \times pK_a[\text{Comp.}]; \Delta G_{\text{solv}}^*(H^+) = -272.00 \text{ kcal/mol}$$

Table A.2. pK_a values obtained by computing the solvation energies with the CPCM solvation model.^{a,b}

Acid	B3LYP ^g	M06 ^h	M06-2X ⁱ	MP2 ^j	CCSD(T) ^k	Exp.
1. Water ^{c,e}	16.94	17.65	17.00	16.45	16.42	15.70
2. Methanol ^c	15.33	15.00	15.32	15.97	15.52	15.54
3. Phenol ^c	9.13	8.72	8.74	9.16	8.96	9.99
4. Formic Acid ^c	4.56	4.48	4.79	4.54	4.52	3.77
5. Benzoic Acid ^c	5.50	5.32	5.11	4.91	4.85	4.20
6. Acetaldoxime ^c	11.62	11.51	11.42	11.63	11.69	11.42
7. Benzaldoxime ^c	10.11	9.86	10.05	10.49	10.76	11.30
8. Acetohydroxamic Acid ^c	9.40	9.52	9.68	9.70	9.26	8.70
9. Benzohydroxamic Acid ^c	8.85	8.94	9.40	9.28	9.15	8.81
10. Nitric Acid ^c	-0.88	-0.89	-1.20	-0.37	-0.63	-1.40
11. Sulfuric Acid ^c	-3.62	-3.46	-3.46	-3.81	-3.71	-3.00
12. Phosphoric Acid ^c	1.98	2.24	2.07	1.95	1.93	2.15
13. Carbonic Acid ^c	3.29	3.44	3.42	3.23	3.16	3.60
14. Acetamidoxime	13.24	13.20	13.00	12.93	12.82	13.21
15. Benzamidoxime	11.75	11.67	11.76	11.53	11.96	12.36
16. Azine-Amidoxime ^{d,f}	11.12	11.11	11.22	10.73	11.48	11.98
Mean Absolute Error	0.60	0.68	0.62	0.67	0.53	
Root Mean Square Deviation	0.73	0.86	0.76	0.74	0.59	

^aZPE and thermal corrections are calculated in the gas phase at the B3LYP/6-311++G** level of theory.^bB3LYP and the 6-31+G* basis set was used for all solvation calculations.^cSmith, R. M.; Martell, A. E., *Critical Stability Constants*. Plenum Press: New York, 1981.^dSimanenko, Y. S.; Prokop'eva, T. M.; Belousova, I. A.; Popov, A. F.; Karpichev, E. A., Amidoximes as Effective Acceptors of Acyl Group. *Theor. Exp. Chem.* **2001**, 37, 288-295.^eThe experimental pK_a corresponds to a 55.5 M solution. However, our thermodynamic cycle calls for the conversion of an ideal gas to an ideal solution (1 M). Therefore, a correction of 1.7 pK_a units was added to all the predicted water pK_a values.^fThe full name of this structure is (Z)-N-hydroxynicotinimidamide.

^g $pK_a[Pred.] = 0.464 \times pK_a[Comp.]; \Delta G_{solv}^*(H^+) = -268.60 \text{ kcal/mol}$

^h $pK_a[Pred.] = 0.465 \times pK_a[Comp.]; \Delta G_{solv}^*(H^+) = -268.57 \text{ kcal/mol}$

ⁱ $pK_a[Pred.] = 0.435 \times pK_a[Comp.]; \Delta G_{solv}^*(H^+) = -269.81 \text{ kcal/mol}$

^j $pK_a[Pred.] = 0.493 \times pK_a[Comp.]; \Delta G_{solv}^*(H^+) = -268.76 \text{ kcal/mol}$

^k $pK_a[Pred.] = 0.479 \times pK_a[Comp.]; \Delta G_{solv}^*(H^+) = -271.88 \text{ kcal/mol}$

Table A.3. pK_a values obtained by computing the solvation energies with the SMD solvation model.^{a,b}

Acid	B3LYP ^g	M06 ^h	M06-2X ⁱ	MP2 ^j	CCSD(T) ^k	Exp.
1. Water ^{c,e}	15.62	16.44	15.80	15.01	14.97	15.70
2. Methanol ^c	14.88	14.56	14.91	15.55	15.00	15.54
3. Phenol ^c	9.79	9.36	9.35	9.87	9.62	9.99
4. Formic Acid ^c	4.40	4.29	4.64	4.36	4.32	3.77
5. Benzoic Acid ^c	5.36	5.15	4.94	4.70	4.66	4.20
6. Acetaldoxime ^c	11.71	11.60	11.50	11.73	11.74	11.42
7. Benzaldoxime ^c	10.86	10.61	10.77	11.33	11.56	11.30
8. Acetohydroxamic Acid ^c	8.37	8.50	8.74	8.63	8.38	8.70
9. Benzohydroxamic Acid ^c	8.28	8.39	8.93	8.72	8.58	8.81
10. Nitric Acid ^c	-1.08	-1.15	-1.47	-0.56	-0.76	-1.40
11. Sulfuric Acid ^c	-3.89	-3.79	-3.75	-4.13	-3.90	-3.00
12. Phosphoric Acid ^c	2.42	2.66	2.46	2.41	2.43	2.15
13. Carbonic Acid ^c	3.32	3.46	3.44	3.26	3.21	3.60
14. Acetamidoxime	13.58	13.57	13.31	13.27	13.08	13.21
15. Benzamidoxime	12.55	12.50	12.54	12.37	12.89	12.36
16. Azine-Amidoxime ^{d,f}	12.15	12.17	12.21	11.80	12.53	11.98
Mean Absolute Error	0.42	0.48	0.35	0.33	0.45	
Root Mean Square Deviation	0.51	0.56	0.45	0.46	0.49	

^aZPE and thermal corrections are calculated in the gas phase at the B3LYP/6-311++G** level of theory.^bB3LYP and the 6-31+G* basis set was used for all solvation calculations.^cSmith, R. M.; Martell, A. E., *Critical Stability Constants*. Plenum Press: New York, 1981.^dSimanenko, Y. S.; Prokop'eva, T. M.; Belousova, I. A.; Popov, A. F.; Karpichev, E. A., Amidoximes as Effective Acceptors of Acyl Group. *Theor. Exp. Chem.* **2001**, 37, 288-295.^eThe experimental pK_a corresponds to a 55.5 M solution. However, our thermodynamic cycle calls for the conversion of an ideal gas to an ideal solution (1 M). Therefore, a correction of 1.7 pK_a units was added to all the predicted water pK_a values.^fThe full name of this structure is (Z)-N-hydroxynicotinimidamide.

^g $pK_a[Pred.] = 0.504 \times pK_a[Comp.]; \Delta G_{solv}^*(H^+) = -265.85 \text{ kcal/mol}$

^h $pK_a[Pred.] = 0.508 \times pK_a[Comp.]; \Delta G_{solv}^*(H^+) = -265.86 \text{ kcal/mol}$

ⁱ $pK_a[Pred.] = 0.471 \times pK_a[Comp.]; \Delta G_{solv}^*(H^+) = -267.09 \text{ kcal/mol}$

^j $pK_a[Pred.] = 0.538 \times pK_a[Comp.]; \Delta G_{solv}^*(H^+) = -266.08 \text{ kcal/mol}$

^k $pK_a[Pred.] = 0.517 \times pK_a[Comp.]; \Delta G_{solv}^*(H^+) = -269.13 \text{ kcal/mol}$

Table A.4. pK_a values obtained by computing the solvation energies with the COSMO solvation model.^{a,b}

Acid	B3LYP ^g	M06 ^h	M06-2X ⁱ	MP2 ^j	CCSD(T) ^k	Exp.
1. Water ^{c,e}	17.30	18.17	17.46	16.94	16.88	15.70
2. Methanol ^c	14.77	14.49	14.90	14.54	15.06	15.54
3. Phenol ^c	8.64	8.21	8.28	8.65	8.45	9.99
4. Formic Acid ^c	4.77	4.65	4.95	4.71	4.62	3.77
5. Benzoic Acid ^c	5.26	5.04	4.82	4.56	4.50	4.20
6. Acetaldoxime ^c	11.81	11.74	11.64	11.91	11.94	11.42
7. Benzaldoxime ^c	9.79	9.55	9.79	10.21	10.51	11.30
8. Acetohydroxamic Acid ^c	8.03	8.16	8.42	8.27	8.04	8.70
9. Benzohydroxamic Acid ^c	9.26	9.38	9.85	9.78	9.62	8.81
10. Nitric Acid ^c	-0.53	-0.64	-1.05	-0.11	-0.40	-1.40
11. Sulfuric Acid ^c	-2.43	-2.37	-2.51	-2.74	-2.67	-3.00
12. Phosphoric Acid ^c	2.78	2.99	2.74	2.71	2.68	2.15
13. Carbonic Acid ^c	2.39	2.48	2.50	2.17	2.12	3.60
14. Acetamidoxime	14.01	14.05	13.80	13.84	13.69	13.21
15. Benzamidoxime	12.90	12.88	12.92	12.83	13.37	12.36
16. Azine-Amidoxime ^{d,f}	9.55	9.56	9.80	9.05	9.90	11.98
Mean Absolute Error	0.99	1.08	0.93	0.90	0.88	
Root Mean Square Deviation	1.12	1.26	1.09	1.12	1.00	

^aZPE and thermal corrections are calculated in the gas phase at the B3LYP/6-311++G** level of theory.^bB3LYP and the 6-311++G** basis set was used for all solvation calculations.^cSmith, R. M.; Martell, A. E., *Critical Stability Constants*. Plenum Press: New York, 1981.^dSimanenko, Y. S.; Prokop'eva, T. M.; Belousova, I. A.; Popov, A. F.; Karpichev, E. A., Amidoximes as Effective Acceptors of Acyl Group. *Theor. Exp. Chem.* **2001**, 37, 288-295.^eThe experimental pK_a corresponds to a 55.5 M solution. However, our thermodynamic cycle calls for the conversion of an ideal gas to an ideal solution (1 M). Therefore, a correction of 1.7 pK_a units was added to all the predicted water pK_a values.^fThe full name of this structure is (Z)-N-hydroxynicotinimidamide.

$$^g pK_a[\text{Pred.}] = 0.500 \times pK_a[\text{Comp.}]; \Delta G_{\text{solv}}^*(H^+) = -264.04 \text{ kcal/mol}$$

$$^h pK_a[\text{Pred.}] = 0.499 \times pK_a[\text{Comp.}]; \Delta G_{\text{solv}}^*(H^+) = -263.99 \text{ kcal/mol}$$

$$^i pK_a[\text{Pred.}] = 0.467 \times pK_a[\text{Comp.}]; \Delta G_{\text{solv}}^*(H^+) = -265.26 \text{ kcal/mol}$$

$$^j pK_a[\text{Pred.}] = 0.535 \times pK_a[\text{Comp.}]; \Delta G_{\text{solv}}^*(H^+) = -264.25 \text{ kcal/mol}$$

$$^k pK_a[\text{Pred.}] = 0.518 \times pK_a[\text{Comp.}]; \Delta G_{\text{solv}}^*(H^+) = -267.36 \text{ kcal/mol}$$

Table A.5. pK_a values obtained by computing the solvation energies with the SVPE2 solvation model.^{a,b}

Acid	B3LYP ^g	M06 ^h	M06-2X ⁱ	MP2 ^j	CCSD(T) ^k	Exp.
1. Water ^{c,e}	17.79	18.48	17.78	17.38	17.30	15.70
2. Methanol ^c	15.26	14.87	15.23	15.94	15.46	15.54
3. Phenol ^c	8.68	8.27	8.33	8.69	8.50	9.99
4. Formic Acid ^c	4.27	4.21	4.53	4.21	4.16	3.77
5. Benzoic Acid ^c	5.06	4.88	4.69	4.40	4.35	4.20
6. Acetaldoxime ^c	11.32	11.18	11.13	11.33	11.38	11.42
7. Benzaldoxime ^c	9.86	9.59	9.82	10.24	10.52	11.30
8. Acetohydroxamic Acid ^c	9.17	9.29	9.47	9.48	9.22	8.70
9. Benzohydroxamic Acid ^c	8.49	8.58	9.09	8.92	8.78	8.81
10. Nitric Acid ^c	-1.32	-1.27	-1.62	-0.86	-1.10	-1.40
11. Sulfuric Acid ^c	-3.15	-2.91	-3.01	-3.36	-3.24	-3.00
12. Phosphoric Acid ^c	3.02	3.31	3.05	3.03	3.00	2.15
13. Carbonic Acid ^c	3.54	3.72	3.67	3.49	3.40	3.60
14. Acetamidoxime	13.41	13.34	13.14	13.12	12.98	13.21
15. Benzamidoxime	11.70	11.60	11.72	11.48	12.03	12.36
16. Azine-Amidoxime ^{d,f}	11.22	11.19	11.31	10.84	11.59	11.98
Mean Absolute Error	0.63	0.76	0.67	0.63	0.48	
Root Mean Square Deviation	0.84	1.05	0.89	0.79	0.66	

^aZPE and thermal corrections are calculated in the gas phase at the B3LYP/6-311++G** level of theory.^bB3LYP and the 6-311++G** basis set was used for all solvation calculations.^cSmith, R. M.; Martell, A. E., *Critical Stability Constants*. Plenum Press: New York, 1981.^dSimanenko, Y. S.; Prokop'eva, T. M.; Belousova, I. A.; Popov, A. F.; Karpichev, E. A., Amidoximes as Effective Acceptors of Acyl Group. *Theor. Exp. Chem.* **2001**, 37, 288-295.^eThe experimental pK_a corresponds to a 55.5 M solution. However, our thermodynamic cycle calls for the conversion of an ideal gas to an ideal solution (1 M). Therefore, a correction of 1.7 pK_a units was added to all the predicted water pK_a values.^fThe full name of this structure is (Z)-N-hydroxynicotinimidamide.

^g $pK_a[\text{Pred.}] = 0.477 \times pK_a[\text{Comp.}]; \Delta G_{\text{solv}}^*(H^+) = -271.37 \text{ kcal/mol}$

^h $pK_a[\text{Pred.}] = 0.476 \times pK_a[\text{Comp.}]; \Delta G_{\text{solv}}^*(H^+) = -271.32 \text{ kcal/mol}$

ⁱ $pK_a[\text{Pred.}] = 0.445 \times pK_a[\text{Comp.}]; \Delta G_{\text{solv}}^*(H^+) = -272.61 \text{ kcal/mol}$

^j $pK_a[\text{Pred.}] = 0.510 \times pK_a[\text{Comp.}]; \Delta G_{\text{solv}}^*(H^+) = -271.58 \text{ kcal/mol}$

^k $pK_a[\text{Pred.}] = 0.494 \times pK_a[\text{Comp.}]; \Delta G_{\text{solv}}^*(H^+) = -274.68 \text{ kcal/mol}$

Optimized Geometries and Absolute Energies Obtained at the M06-2X/6-31++G Level of Theory**

Water

Absolute Energy = -76.260910 Hartrees

Cartesian Coordinates

O	-0.002070	0.118692	0.027223
H	-0.755183	-0.460698	-0.123510
H	0.771323	-0.442694	-0.083683

Hydroxide

Absolute Energy = -75.637018 Hartrees

Cartesian Coordinates

O	0.086253	0.065079	0.016970
H	-0.673320	-0.508023	-0.132470

Methanol

Absolute Energy = -115.421921 Hartrees

Cartesian Coordinates

C	-0.004417	0.666808	0.000000
H	1.013745	1.052714	0.000000
H	-0.516876	1.041817	-0.891571
H	-0.516876	1.041817	0.891571
O	0.093056	-0.744870	0.000000
H	-0.790535	-1.116847	0.000000

Methoxide

Absolute Energy = -114.806259 Hartrees

Cartesian Coordinates

C	-0.000001	-0.000005	0.511879
H	-0.264377	0.987138	1.002755
H	-0.722684	-0.722677	1.002545
H	0.987142	-0.264373	1.002750

O -0.000080 -0.000083 -0.822497

Phenol

Absolute Energy = -306.610690 Hartrees

Cartesian Coordinates

O 1.780544 1.407647 0.365075

H 2.612854 0.932108 0.275292

C -1.481646 -1.094909 -0.286233

C -1.653795 0.256031 0.020157

C -0.555524 1.082101 0.235642

C 0.732869 0.552799 0.144157

C 0.916540 -0.796757 -0.161654

C -0.192368 -1.614414 -0.375449

H -2.341308 -1.732774 -0.452889

H -2.652524 0.672076 0.092390

H -0.676317 2.131886 0.474021

H 1.920087 -1.206507 -0.232324

H -0.042050 -2.661709 -0.612566

Phenoxide

Absolute Energy = -306.049409 Hartrees

Cartesian Coordinates

O 1.842702 1.390086 0.363266

C -1.439535 -1.085890 -0.282880

C -1.600988 0.270589 0.024812

C -0.516816 1.103607 0.241499

C 0.847742 0.639338 0.167063

C 0.968700 -0.762722 -0.152793

C -0.130615 -1.576751 -0.365385

H -2.294058 -1.731184 -0.451547

H	-2.605735	0.683535	0.096273
H	-0.664852	2.153327	0.478405
H	1.975872	-1.163694	-0.221881
H	0.029855	-2.627028	-0.602697

Formic Acid

Absolute Energy = -189.326673 Hartrees

Cartesian Coordinates

C	-0.136317	-0.108695	-0.407864
O	0.224313	-0.831287	0.659702
O	-0.151270	1.083758	-0.450146
H	0.462637	-0.215204	1.367117
H	-0.414901	-0.772751	-1.234114

Formate

Absolute Energy = -188.773483 Hartrees

Cartesian Coordinates

C	-0.087547	-0.169565	-0.261618
O	0.237487	-0.882707	0.707668
O	-0.126261	1.071123	-0.375262
H	-0.397914	-0.741847	-1.189584

Benzoic Acid

Absolute Energy = -419.706869 Hartrees

Cartesian Coordinates

C	0.838409	-1.034650	-0.081107
C	0.139670	0.165717	0.043336
C	-1.253442	0.167908	0.111038
C	-1.945095	-1.036004	0.053863
C	-1.248397	-2.234486	-0.069964
C	0.142874	-2.234458	-0.137563

H	1.920165	-1.005792	-0.131378
H	-1.783111	1.106825	0.207995
H	-3.027037	-1.039839	0.105993
H	-1.791131	-3.171522	-0.113999
H	0.682081	-3.168892	-0.234184
C	0.928304	1.426136	0.101618
O	0.155524	2.523785	0.223785
O	2.127235	1.488707	0.048154
O	0.749438	3.284974	0.255857

Benzoate

Absolute Energy = -419.159978 Hartrees

Cartesian Coordinates

C	0.843014	-0.965085	0.000034
C	0.140960	0.239783	-0.000018
C	-1.253107	0.202258	-0.000207
C	-1.934207	-1.012536	-0.000350
C	-1.224218	-2.211870	-0.000306
C	0.169277	-2.183927	-0.000111
H	1.925906	-0.909070	0.000194
H	-1.775934	1.152287	-0.000242
H	-3.019936	-1.028011	-0.000505
H	-1.752750	-3.159857	-0.000421
H	0.728136	-3.114918	-0.000065
C	0.897875	1.597530	0.000157
O	0.168215	2.607034	0.000371
O	2.140248	1.507495	0.000068

Acetaldoxime

Absolute Energy = -208.585009 Hartrees

Cartesian Coordinates

N	0.686724	-0.728843	0.002752
C	-0.581279	-0.674224	0.000467
H	-1.061148	-1.647737	-0.000901
O	1.241033	0.547628	0.004323
C	-1.392532	0.584379	-0.000422
H	-2.457756	0.362452	-0.001966
H	-1.147874	1.187679	0.876704
H	-1.145442	1.188043	-0.876622
H	2.186711	0.380520	0.006088

Acetaldoximate

Absolute Energy = -207.997904 Hartrees

Cartesian Coordinates

N	0.737456	-0.690969	-0.001334
C	-0.564140	-0.684695	-0.001031
H	-1.056918	-1.653456	-0.002228
O	1.324279	0.472454	0.000080
C	-1.361975	0.589153	0.000775
H	-2.437843	0.386611	0.000625
H	-1.108754	1.203844	0.873865
H	-1.108912	1.206119	-0.870752

Benzaldoxime

Absolute Energy = -399.769457 Hartrees

Cartesian Coordinates

C	0.927972	-1.268983	0.000000
C	0.192118	-0.083527	0.000000
C	-1.205732	-0.144059	0.000000
C	-1.847028	-1.373138	0.000000

C	-1.106276	-2.555064	0.000000
C	0.282106	-2.501043	0.000000
H	2.012036	-1.224945	0.000000
H	-1.773186	0.778551	0.000000
H	-2.929834	-1.413881	0.000000
H	-1.613209	-3.512629	0.000000
H	0.863411	-3.415264	0.000000
N	0.296260	2.304677	0.000000
C	0.914854	1.196655	0.000000
H	2.006059	1.181709	0.000000
O	1.179111	3.371485	0.000000
H	0.606188	4.142606	0.000000

Benzaldoximate

Absolute Energy = -399.202209 Hartrees

Cartesian Coordinates

C	0.944513	-1.246115	0.000000
C	0.262999	-0.009448	0.000000
C	-1.151514	-0.068769	0.000000
C	-1.820939	-1.280475	0.000000
C	-1.127283	-2.495514	0.000000
C	0.265793	-2.457866	0.000000
C	2.030514	-1.238561	0.000000
C	-1.695766	0.867709	0.000000
C	-2.907250	-1.284049	0.000000
C	-1.659393	-3.439974	0.000000
H	0.831838	-3.384951	0.000000
N	0.375568	2.391261	0.000000
C	0.997653	1.230724	0.000000

H	2.090348	1.212293	0.000000
O	1.086150	3.446430	0.000000

Acetohydroxamic Acid

Absolute Energy = -283.673446 Hartrees

Cartesian Coordinates

C	-1.294687	-0.707244	1.176792
H	-2.238918	-0.163753	1.147685
H	-1.439785	-1.704036	0.760207
H	-0.981172	-0.784483	2.218357
C	-0.265060	0.092465	0.425830
N	0.331685	-0.545318	-0.621339
O	0.013476	1.251607	0.671603
O	1.404949	0.107846	-1.208259
H	1.415539	0.960753	-0.737958
H	0.475597	-1.544612	-0.605370

Acetohydroxamate (Gas Phase Structure)

Absolute Energy = -283.101532 Hartrees

Cartesian Coordinates

C	-1.004435	-0.341391	1.004440
H	-1.619118	0.315884	1.619130
H	-1.622706	-0.999278	0.388771
H	-0.388753	-0.999272	1.622706
C	-0.117361	0.504727	0.117348
N	0.673572	-0.205301	-0.673595
O	-0.141278	1.758617	0.141261
H	1.282223	0.335329	-1.282261
O	0.739541	-1.553853	-0.739562

Acetohydroxamate (Aqueous Phase Structure)

Absolute Energy = -283.093560 Hartrees

Cartesian Coordinates

C	-1.262103	-0.697403	1.039835
H	-2.239960	-0.221847	0.926279
H	-1.325256	-1.725959	0.672676
H	-1.029698	-0.717496	2.107884
C	-0.214243	0.158939	0.325460
N	0.451288	-0.485034	-0.633450
O	-0.064128	1.339468	0.673141
O	1.412679	-0.008200	-1.421753
H	0.190136	-1.456391	-0.777626

Benzohydroxamic Acid

Absolute Energy = -474.856058 Hartrees

Cartesian Coordinates

C	0.728937	1.407288	-0.055360
C	0.084591	2.634031	-0.141889
C	-1.303130	2.700003	-0.048674
C	-2.047398	1.538986	0.137474
C	-1.407171	0.308021	0.220389
C	-0.017309	0.241892	0.113525
H	1.807963	1.330371	-0.114180
H	0.662766	3.539761	-0.278585
H	-1.804912	3.658237	-0.112805
H	-3.125286	1.593062	0.230041
H	-1.983626	-0.591905	0.402427
C	0.726449	-1.047698	0.182445
N	0.001010	-2.170843	-0.122369
O	1.897134	-1.143199	0.502903

H	-0.675850	-2.113841	-0.872218
O	0.736270	-3.343835	-0.216595
H	1.644823	-3.050218	-0.023687

Benzohydroxamate (Gas Phase Structure)

Absolute Energy = -474.292107 Hartrees

Cartesian Coordinates

C	0.933117	1.229820	0.000000
C	0.315352	2.473393	0.000000
C	-1.076163	2.561257	0.000000
C	-1.832114	1.393224	0.000000
C	-1.218650	0.141008	0.000000
C	0.180041	0.048714	0.000000
H	2.011977	1.128804	0.000000
H	0.917020	3.376796	0.000000
H	-1.564175	3.530726	0.000000
H	-2.915962	1.452766	0.000000
H	-1.785138	-0.781486	0.000000
C	0.968137	-1.232390	0.000000
N	0.315738	-2.391561	0.000000
O	2.225017	-1.188635	0.000000
H	0.949515	-3.188677	0.000000
O	-0.994345	-2.664359	0.000000

Benzohydroxamate (Aqueous Phase Structure)

Absolute Energy = -474.284840 Hartrees

Cartesian Coordinates

C	0.768662	1.353072	-0.099691
C	0.122816	2.579770	-0.183235
C	-1.267010	2.651667	-0.100873

C	-1.996527	1.479667	0.080683
C	-1.347200	0.251414	0.164352
C	0.046076	0.163826	0.048981
H	1.849026	1.273569	-0.135852
H	0.703645	3.488014	-0.307800
H	-1.773320	3.608907	-0.160103
H	-3.076509	1.522911	0.177302
H	-1.930212	-0.643300	0.353837
C	0.844625	-1.117147	0.132655
N	0.180221	-2.189953	-0.301690
O	2.015640	-1.084631	0.542699
H	-0.738188	-2.018065	-0.700347
O	0.617859	-3.433770	-0.352909

Nitric Acid

Absolute Energy = -280.284885 Hartrees

Cartesian Coordinates

N	0.038941	0.117074	-0.000034
O	-0.642162	1.087997	0.000021
O	1.236473	0.016657	0.000006
O	-0.666306	-1.070789	-0.000010
H	0.020873	-1.754911	0.000017

Nitrate

Absolute Energy = -279.761750 Hartrees

Cartesian Coordinates

N	0.001478	0.002438	0.000000
O	-0.634180	1.075278	0.000000
O	1.248331	0.016288	0.000000
O	-0.610168	-1.084304	0.000000

Sulfuric Acid

Absolute Energy = -699.064742 Hartrees

Cartesian Coordinates

S	0.045633	0.449242	0.055119
O	-0.991603	1.141916	0.749092
O	0.583822	-0.658677	1.076750
O	1.165390	1.082956	-0.562837
O	-0.618094	-0.460504	-1.081859
H	1.435275	-1.005538	0.773913
H	-1.505608	-0.736325	-0.811230

Bisulfate

Absolute Energy = -698.561665 Hartrees

Cartesian Coordinates

S	0.100733	0.109572	0.146027
O	-0.849236	0.905403	0.911804
O	0.899996	-0.845173	0.921279
O	0.874190	0.843166	-0.860502
O	-0.918278	-0.866235	-0.757408
H	-0.340279	-1.451497	-1.257580

Phosphoric Acid

Absolute Energy = -643.018956 Hartrees

Cartesian Coordinates

P	-0.021144	0.012880	0.013506
O	-1.133927	0.773483	0.862446
O	0.708526	-0.865861	1.123830
O	0.848722	0.858765	-0.810853
O	-0.880164	-1.077022	-0.768749
H	-0.410308	-1.469222	-1.512078

H -1.513045 1.529201 0.401726

H 1.455892 -0.417536 1.533225

Dihydrogen Phosphate

Absolute Energy = -642.493173 Hartrees

Cartesian Coordinates

P 0.002496 0.070034 -0.182411

O -0.925754 1.171461 0.647076

O 0.557422 -0.875201 1.066857

O 1.182427 0.810387 -0.715074

O -0.939697 -0.769930 -0.976717

H -1.814567 0.810112 0.689621

H 1.381246 -0.483378 1.367176

Carbonic Acid

Absolute Energy = -264.419360 Hartrees

Cartesian Coordinates

C -0.005039 0.116488 -0.018850

O 0.349237 -0.617736 1.034173

O -0.019979 1.314549 -0.059235

H 0.585834 -0.003418 1.738744

O -0.340531 -0.695779 -1.019451

H -0.593466 -0.136855 -1.763387

Bicarbonate

Absolute Energy = -263.875351 Hartrees

Cartesian Coordinates

C -0.052041 0.052022 -0.155281

O 0.348414 -0.645241 1.031325

O -0.013386 1.291658 -0.039125

H 0.553910 0.067896 1.640927

O -0.365548 -0.684602 -1.088017

Acetamidoxime

Absolute Energy = -263.821470 Hartrees

Cartesian Coordinates

N 0.969231 0.175408 0.314078

C -0.277010 0.273611 0.040149

O 1.339772 -1.184601 0.345171

H -1.966564 -0.646163 -0.642489

H -0.668532 -1.695431 -0.262432

H 2.279100 -1.150508 0.535204

N -1.114922 -0.800403 -0.128967

C -0.876117 1.642278 -0.041878

H -1.669089 1.751258 0.701138

H -0.103798 2.385700 0.141949

H -1.307248 1.811713 -1.031967

Acetamidoximate

Absolute Energy = -263.230765 Hartrees

Cartesian Coordinates

N 1.028821 0.176839 -0.326347

C -0.227238 0.244171 -0.033711

O 1.544449 -1.045411 -0.383267

H -1.784547 -1.024089 -0.321393

H -0.303324 -1.682820 0.075545

N -0.971123 -0.930552 0.281210

C -0.931867 1.557629 0.055871

H -1.774301 1.625855 -0.650208

H -1.344898 1.730014 1.058848

H -0.219178 2.349870 -0.180817

Benzamidoxime

Absolute Energy = -455.004504 Hartrees

Cartesian Coordinates

C	2.404463	1.044401	-0.254464
C	1.019449	1.172058	-0.229303
C	0.216156	0.057311	0.016058
C	0.812392	-1.186527	0.233680
C	2.194661	-1.309917	0.205478
C	2.994546	-0.195116	-0.035412
H	3.020815	1.912874	-0.454053
H	0.560371	2.133264	-0.430218
H	0.179145	-2.043760	0.424503
H	2.651359	-2.277320	0.377664
H	4.073420	-0.294136	-0.053658
C	-1.260759	0.190010	0.044524
N	-1.960698	-0.826468	-0.301521
N	-1.791766	1.413772	0.384310
H	-2.788938	1.410704	0.543698
H	-1.255177	1.962156	1.038174
O	-3.327045	-0.525673	-0.183395
H	-3.756344	-1.330703	-0.479984

Benzamidoximate

Absolute Energy = -454.435093 Hartrees

Cartesian Coordinates

C	2.300588	1.030122	-0.068219
C	0.928298	1.265714	-0.093835
C	0.002737	0.205511	-0.027771
C	0.527690	-1.103958	0.064546

C	1.891972	-1.327851	0.081563
C	2.801298	-0.263959	0.019674
H	2.985092	1.871452	-0.124408
H	0.554218	2.278117	-0.191391
H	-0.176163	-1.925162	0.118538
H	2.261729	-2.346619	0.150543
H	3.869914	-0.446295	0.039672
C	-1.423821	0.457667	-0.028720
N	-2.267669	-0.543892	-0.107203
N	-1.895013	1.801879	-0.006217
H	-2.912150	1.700662	0.020977
H	-1.592648	2.281578	0.837728
O	-3.525213	-0.235086	-0.094318

Azine-Amidoxime

Absolute Energy = -471.027322 Hartrees

Cartesian Coordinates

N	1.763149	-1.178783	0.315001
C	0.533231	-1.148052	-0.045113
O	2.256287	-2.486478	0.209069
H	-0.955114	-2.114929	-1.043468
H	0.339849	-3.097976	-0.530916
H	3.161556	-2.409004	0.517576
N	-0.201502	-2.257425	-0.389660
C	-1.509172	2.522652	0.019632
N	-2.204738	1.400741	0.188063
C	-1.530882	0.252078	0.169097
C	-0.151585	0.164415	-0.025510
C	0.562255	1.350374	-0.194452

C	-0.128401	2.550354	-0.167100
H	-2.080572	3.445548	0.035072
H	-2.116154	-0.646944	0.338730
H	1.634277	1.310362	-0.343632
H	0.384769	3.494838	-0.296517

Azine-Amidoximate

Absolute Energy = -470.465311 Hartrees

Cartesian Coordinates

N	1.840272	-1.248504	-0.045363
C	0.530234	-1.173928	-0.089066
O	2.346959	-2.436697	-0.095350
H	-0.855531	-2.386487	-0.939770
H	0.418297	-3.108886	-0.165998
N	-0.267224	-2.352774	-0.111550
O	-1.465369	2.528144	0.017711
N	-2.176707	1.404254	0.080356
C	-1.514347	0.245577	0.053867
C	-0.112355	0.119798	-0.041157
C	0.608985	1.328240	-0.111466
C	-0.070462	2.530290	-0.073428
H	-2.024201	3.459829	0.041775
H	-2.119374	-0.652177	0.128367
H	1.688222	1.279023	-0.189391
H	0.466493	3.471780	-0.122926

Imidazole-Oxime

Absolute Energy = -356.695798 Hartrees

Cartesian Coordinates

N	-0.739233	-0.682356	-0.000062
---	-----------	-----------	-----------

C	-0.051895	-1.898883	0.016710
C	1.260939	-1.618468	0.023158
N	1.396834	-0.228744	0.009619
C	0.152294	0.361707	-0.006214
H	-0.561655	-2.845373	0.023736
H	2.112942	-2.274015	0.036409
H	2.251610	0.298721	0.008048
N	-0.076574	1.628639	-0.023504
O	-1.497199	1.778601	-0.037390
H	-1.607919	2.730529	-0.043790
H	-1.732521	-0.525274	-0.014551

Imidazole-Oximate

Absolute Energy = -356.088503 Hartrees

Cartesian Coordinates

N	-0.796924	-0.694062	0.332411
C	-0.067217	-1.843963	-0.001557
C	1.244973	-1.558479	-0.008038
N	1.430707	-0.191346	0.324352
C	0.118147	0.387105	0.219234
H	-0.538904	-2.810397	-0.098992
H	2.082223	-2.234546	-0.087570
H	2.116170	0.320409	-0.216122
N	-0.182911	1.582743	-0.076413
O	-1.520170	1.780810	-0.213445
H	-1.670492	-0.426456	-0.121205

Imidazolidine-Oxime

Absolute Energy = -357.912078 Hartrees

Cartesian Coordinates

C	0.647774	0.027430	1.744563
C	-0.845660	-0.305950	1.819013
N	-1.289640	0.122616	0.493092
C	-0.228310	-0.062382	-0.389224
N	0.918455	-0.276425	0.344100
C	0.815941	1.085020	1.977414
H	1.248118	-0.591966	2.410040
H	-1.359993	0.245468	2.605024
H	-0.983816	-1.382351	1.974946
H	-2.185076	-0.199619	0.156074
H	1.788928	-0.018930	-0.097338
N	-0.357736	-0.027335	-1.659820
O	0.930997	-0.184296	-2.235018
H	0.756343	-0.093406	-3.173252

Imidazolidine-Oximate

Absolute Energy = -357.302496 Hartrees

Cartesian Coordinates

C	0.664262	0.094323	1.704988
C	-0.815778	-0.348638	1.679721
N	-1.315561	0.353568	0.490221
C	-0.220704	0.219675	-0.427381
N	0.970399	0.423830	0.310923
H	0.784132	0.979810	2.339404
H	1.309436	-0.696131	2.102183
H	-1.359179	-0.057695	2.582523
H	-0.870065	-1.442147	1.563041
H	-2.125658	-0.097214	0.079463
H	1.694059	-0.112065	-0.167079

N	-0.296155	-0.201646	-1.625106
O	0.893893	-0.363605	-2.237044

N-Methyl Acetamidoxime

Absolute Energy = -303.766466 Hartrees

Cartesian Coordinates

N	1.390059	0.265676	0.422175
C	0.148302	0.387629	0.120009
O	1.745170	-1.101519	0.422095
H	-0.211072	-1.557889	-0.189182
H	2.681155	-1.081641	0.628918
C	-0.688532	-0.672006	-0.109060
C	-0.410655	1.776363	0.073470
H	-1.216901	1.889735	0.802016
H	0.385545	2.479154	0.307831
H	-0.811636	2.004834	-0.916718
C	-1.947362	-0.531431	-0.815432
H	-2.479476	-1.480634	-0.766447
H	-2.573191	0.221346	-0.334609
H	-1.821381	-0.258472	-1.869654

N-Methyl Acetamidoximate

Absolute Energy = -303.167643 Hartrees

Cartesian Coordinates

N	1.380047	0.130555	0.116544
C	0.115474	0.407426	0.140513
O	1.692332	-1.157040	0.090954
H	-0.251628	-1.471547	0.183413
N	-0.848479	-0.636737	0.219457
C	-0.356031	1.825229	0.202910

H	-0.952807	2.011421	1.106650
H	0.522786	2.472331	0.214928
H	-0.979795	2.109203	-0.656308
C	-1.820354	-0.644603	-0.862193
H	-2.439662	-1.544528	-0.794043
H	-2.490466	0.217693	-0.777689
H	-1.362861	-0.613733	-1.864886

N,N-Dimethyl Acetamidoxime

Absolute Energy = -343.056628 Hartrees

Cartesian Coordinates

N	1.333980	0.147893	0.122927
C	0.067472	0.338274	0.121667
O	2.035486	1.345917	0.327595
H	2.946657	1.049498	0.375453
N	-0.757129	-0.779858	0.021962
C	-0.583030	1.683886	0.280347
H	-1.542296	1.583188	0.786316
H	0.069584	2.331776	0.860886
H	-0.741711	2.153955	-0.693527
C	-1.899174	-0.665060	-0.875397
H	-2.583954	-1.491371	-0.680525
H	-2.436873	0.265577	-0.703855
H	-1.595967	-0.705155	-1.931766
C	-0.078089	-2.060916	-0.091622
H	-0.825506	-2.852067	-0.019973
H	0.462903	-2.157083	-1.042614
H	0.642497	-2.165917	0.717023

N,N-Dimethyl Acetamidoximate

Absolute Energy = -342.457363 Hartrees

Cartesian Coordinates

N	1.348194	0.226297	-0.210018
C	0.094510	0.377318	0.054078
O	2.105611	1.303016	-0.179542
N	-0.782365	-0.769923	0.086771
C	-0.514086	1.700496	0.414473
H	-1.440322	1.562106	0.980100
H	0.223140	2.251419	1.005511
H	-0.723349	2.321122	-0.466592
C	-1.804121	-0.695817	-0.944129
H	-2.538871	-1.497021	-0.802602
H	-2.325983	0.261633	-0.881778
H	-1.374163	-0.785740	-1.959071
C	-0.084852	-2.037959	0.009105
H	-0.812537	-2.847307	0.141296
H	0.436828	-2.173668	-0.951942
H	0.670348	-2.083863	0.793126

N-Phenyl Acetamidoxime

Absolute Energy = -495.478248 Hartrees

Cartesian Coordinates

N	2.799156	0.125619	1.181432
C	1.695406	0.437424	0.605306
O	2.648300	-1.080038	1.894562
H	0.753145	-1.259572	1.109333
H	3.531384	-1.248817	2.228302
N	0.571778	-0.352201	0.701290
C	1.692570	1.696829	-0.206154

H	1.155845	2.497881	0.303908
H	2.726436	2.006061	-0.343852
H	1.222118	1.534206	-1.177297
C	-3.075056	-0.011210	-1.368814
C	-2.397475	-1.225144	-1.314655
C	-1.183689	-1.322283	-0.647047
C	-0.637992	-0.207109	-0.005444
C	-1.335416	1.002390	-0.033043
C	-2.536087	1.098493	-0.726320
H	-4.016766	0.066960	-1.897674
H	-2.808126	-2.100021	-1.804603
H	-0.641542	-2.261281	-0.626077
H	-0.952884	1.855577	0.511062
H	-3.065034	2.044120	-0.742735

N-Phenyl Acetamidoximate

Absolute Energy = -494.895724 Hartrees

Cartesian Coordinates

N	2.845384	-0.110795	1.047056
C	1.756469	0.464533	0.632444
O	2.795800	-1.425320	1.151473
H	1.009247	-1.325939	0.670964
N	0.657373	-0.389494	0.416736
C	1.685203	1.954783	0.551382
H	0.855251	2.364120	1.139783
H	2.624952	2.327259	0.962129
H	1.588369	2.335795	-0.472140
C	-3.147049	-0.128562	-1.353423
C	-2.668713	-1.315630	-0.790051

C	-1.414794	-1.380897	-0.214598
C	-0.553114	-0.252173	-0.172122
C	-1.045612	0.940236	-0.756222
C	-2.312208	0.985617	-1.323286
H	-4.131756	-0.078269	-1.801408
H	-3.289120	-2.206685	-0.798234
H	-1.061212	-2.308682	0.222855
H	-0.431412	1.827797	-0.767087
H	-2.650368	1.921296	-1.758616

Optimized Geometries and Absolute Energies Obtained at the MP2/aug-cc-pVDZ Level of Theory

Water

Absolute Energy = -76.260910 Hartrees

Cartesian Coordinates

O	-0.00214645	0.12073129	0.02769000
H	-0.75202088	-0.46860328	-0.12525219
H	0.76836379	-0.45067121	-0.08558558

Hydroxide

Absolute Energy = -75.637018 Hartrees

Cartesian Coordinates

O	0.08735202	0.06590749	0.01718571
H	-0.68018515	-0.51320276	-0.13382021

Methanol

Absolute Energy = -115.421931 Hartrees

Cartesian Coordinates

C	0.00001900	0.67076701	0.00002124
H	1.02805587	1.05470922	-0.00007246
H	-0.51718564	1.04508230	-0.89940822
H	-0.51726655	1.04501166	0.89942734

O	0.10415596	-0.76032144	0.00004157
H	-0.79127271	-1.12246589	-0.00000948

Methoxide

Absolute Energy = -114.806259 Hartrees

Cartesian Coordinates

C	0.00000000	0.00000000	0.55431594
H	-0.26660810	0.99499498	1.03764490
H	-0.72838688	-0.72838688	1.03764491
H	0.99499498	-0.26660810	1.03764491
O	-0.00000000	0.00000000	-0.80662754

Phenol

Absolute Energy = -306.610690 Hartrees

Cartesian Coordinates

O	1.79931340	1.43077009	0.37082772
H	2.62859651	0.94022995	0.27752668
C	-1.48526541	-1.09620969	-0.28661135
C	-1.66016518	0.26662253	0.02244155
C	-0.54984250	1.09987845	0.23986173
C	0.74706813	0.56357320	0.14696520
C	0.93501743	-0.79657164	-0.16116956
C	-0.18416778	-1.62238968	-0.37708510
H	-2.35271967	-1.73988340	-0.45478886
H	-2.66750671	0.68710544	0.09549616
H	-0.66973649	2.15955063	0.48053765
H	1.94762950	-1.20935694	-0.23233077
H	-0.03286271	-2.67913510	-0.61635561

Phenoxide

Absolute Energy = -306.049409 Hartrees

Cartesian Coordinates

O	1.87418678	1.41408112	0.36876289
C	-1.45214436	-1.09565095	-0.28571228
C	-1.61883164	0.27357167	0.02500204
C	-0.51384682	1.11359395	0.24384831
C	0.85976433	0.64869673	0.16916146
C	0.97945154	-0.76228867	-0.15225732
C	-0.13180268	-1.59443576	-0.36943878
H	-2.31608935	-1.74750601	-0.45567627
H	-2.63206697	0.69348880	0.09778578
H	-0.66783981	2.17383695	0.48386073
H	1.99562524	-1.17201229	-0.22263054
H	0.03306340	-2.65445152	-0.60914600

Formic Acid

Absolute Energy = -189.326673 Hartrees

Cartesian Coordinates

C	-0.12892097	-0.12708401	-0.38230007
O	0.23597823	-0.86611567	0.69785767
O	-0.14420033	1.08748324	-0.42563851
H	0.47205842	-0.23018680	1.39848863
H	-0.40851840	-0.79786631	-1.21176548

Formate

Absolute Energy = -188.773483 Hartrees

Cartesian Coordinates

C	-0.08795325	-0.16208997	-0.26283524
O	0.24365354	-0.88553910	0.72607684
O	-0.12635359	1.10169192	-0.37548830
H	-0.39923541	-0.73587629	-1.19351251

Benzoic Acid

Absolute Energy = -419.706869 Hartrees

Cartesian Coordinates

C	0.84204472	-1.03124883	-0.11914222
C	0.13507899	0.18273352	0.00735824
C	-1.27423268	0.18526242	0.07573810
C	-1.97166104	-1.03368632	0.01680167
C	-1.27049313	-2.24804411	-0.10944087
C	0.13654856	-2.24378884	-0.17718709
H	1.93354159	-1.00502022	-0.16996205
H	-1.81320353	1.12990724	0.17363454
H	-3.06424842	-1.03694314	0.06940899
H	-1.81824731	-3.19397493	-0.15485746
H	0.68211419	-3.18674558	-0.27526510
C	0.92607177	1.44669515	0.06516339
O	0.13536220	2.55656536	0.18802687
O	2.14581522	1.51519794	0.01116445
H	0.75318657	3.30869798	0.21526472

Benzoate

Absolute Energy = -419.159978 Hartrees

Cartesian Coordinates

C	0.85033714	-0.96740784	-0.00001252
C	0.14096053	0.25306249	0.00002963
C	-1.27014441	0.21375536	-0.00008150
C	-1.95840839	-1.01489631	-0.00020983
C	-1.24199568	-2.22968989	-0.00027471
C	0.16798662	-2.19935320	-0.00019035
H	1.94321426	-0.91371335	0.00011687

H	-1.79977341	1.17122942	-0.00008711
H	-3.05495296	-1.03080735	-0.00026836
H	-1.77536379	-3.18721876	-0.00039320
H	0.73167240	-3.14005593	-0.00024705
C	0.89511015	1.60695073	0.00019926
O	0.15610302	2.63837193	-0.00042699
O	2.16107497	1.52154800	0.00094372

Acetaldoxime

Absolute Energy = -208.585022 Hartrees

Cartesian Coordinates

N	0.71918372	-0.75444241	0.00084021
C	-0.57444777	-0.68698524	-0.00143207
H	-1.05160940	-1.67120261	-0.00260418
O	1.26835500	0.55596075	0.00234391
C	-1.38243414	0.58025768	-0.00224959
H	-2.45735180	0.35554857	-0.00370603
H	-1.13803637	1.18816479	0.88346520
H	-1.13579302	1.18859840	-0.88703615
H	2.21874447	0.37004685	0.00464879

Acetaldoximate

Absolute Energy = -207.997932 Hartrees

Cartesian Coordinates

N	0.79460632	-0.68435926	-0.00115476
C	-0.53727323	-0.66984462	-0.00052693
H	-1.02465207	-1.65212866	-0.00149165
O	1.36667950	0.51109028	-0.00015025
C	-1.32741129	0.61192803	0.00117106
H	-2.41450588	0.41284000	0.00046948

H	-1.06817874	1.23135353	0.88187221
H	-1.06721183	1.23401170	-0.87736460

Benzaldoxime

Absolute Energy = -399.769457 Hartrees

Cartesian Coordinates

C	0.94722322	-1.26786147	-0.00000178
C	0.20214935	-0.06750318	0.00000631
C	-1.21180540	-0.12824906	0.00000139
C	-1.85961928	-1.37269494	-0.00000042
C	-1.11224295	-2.56895264	-0.00000145
C	0.29321302	-2.51280950	0.00000023
H	2.04151262	-1.22297122	0.00000101
H	-1.78706212	0.80143203	0.00000129
H	-2.95299289	-1.41374339	-0.00000099
H	-1.62356766	-3.53604513	-0.00000124
H	0.87960425	-3.43634212	-0.00000351
N	0.28674099	2.33906342	0.00000388
C	0.92870199	1.21238231	0.00000522
H	2.02897668	1.20718539	0.00000087
O	1.20637921	3.41324653	-0.00000594
H	0.61965941	4.18375190	-0.00000462

Benzaldoximate

Absolute Energy = -399.202209 Hartrees

Cartesian Coordinates

C	0.95064757	-1.24073220	-0.00000009
C	0.26148672	0.00825979	-0.00000064
C	-1.16609428	-0.05005502	0.00000086
C	-1.84708559	-1.27651670	-0.00000333

C	-1.14363606	-2.50314669	0.00000048
C	0.26618377	-2.46866359	0.00000106
H	2.04760778	-1.23404946	0.00000299
H	-1.71529767	0.89589349	0.00000019
H	-2.94391947	-1.28007266	0.00000153
H	-1.68056498	-3.45780818	-0.00000210
H	0.83659974	-3.40545033	0.00000038
N	0.35932081	2.43320065	0.00000456
C	0.99801134	1.25364846	0.00000060
H	2.10238471	1.24153424	-0.00000455
O	1.10416950	3.49826800	-0.00000206

Acetohydroxamic Acid

Absolute Energy = -283.673446 Hartrees

Cartesian Coordinates

C	-1.34351545	-0.70860809	1.08267145
H	-2.29787884	-0.16418418	1.04757983
H	-1.48648584	-1.71494538	0.66273563
H	-1.03030293	-0.78544552	2.13402165
C	-0.30684337	0.08493951	0.32496088
N	0.25864484	-0.55684167	-0.75544989
O	0.00344830	1.25783478	0.57546992
O	1.35599999	0.11787359	-1.32718115
H	1.35270679	0.94938267	-0.79908482
H	0.46111269	-1.55095918	-0.67700931

Acetohydroxamate (Gas Phase Structure)

Absolute Energy = -283.101532 Hartrees

Cartesian Coordinates

C	-1.02497736	-0.33821135	1.02510425
---	-------------	-------------	------------

H	-1.64447904	0.32566944	1.64482879
H	-1.65314829	-1.00123628	0.40689890
H	-0.40753323	-1.00216755	1.65294137
C	-0.13631555	0.51191471	0.13675581
N	0.66441229	-0.20420933	-0.66384176
O	-0.15536888	1.78964665	0.15513093
H	1.27486869	0.34259982	-1.27612206
O	0.73493510	-1.55669063	-0.73405425

Acetohydroxamate (Aqueous Phase Structure)

Absolute Energy = -283.093600 Hartrees

Cartesian Coordinates

C	-1.28395361	-0.69682331	1.02559036
H	-2.27565311	-0.22557187	0.91491836
H	-1.33861860	-1.73193665	0.64364386
H	-1.05253176	-0.72896701	2.10411046
C	-0.23744103	0.16748225	0.31508366
N	0.43662395	-0.48650243	-0.65497134
O	-0.07839122	1.37239364	0.66148089
O	1.40075851	-0.02018986	-1.44918399
H	0.16669818	-1.46369060	-0.79095332

Benzohydroxamic Acid

Absolute Energy = -475.856058 Hartrees

Cartesian Coordinates

C	0.76618047	1.41029596	-0.10232336
C	0.11284845	2.65025875	-0.19235136
C	-1.29031713	2.72175879	-0.08867576
C	-2.04079903	1.54778197	0.11187392
C	-1.39557157	0.30160314	0.20022696

C	0.01016915	0.23420642	0.08474939
H	1.85454492	1.33393839	-0.17272921
H	0.69676935	3.56307433	-0.34166459
H	-1.79584579	3.68952678	-0.15513423
H	-3.12856720	1.60434971	0.21212602
H	-1.97559757	-0.60532719	0.39454524
C	0.74358157	-1.06310901	0.15281114
N	0.00041593	-2.18605811	-0.17089569
O	1.92704090	-1.18284628	0.50350338
H	-0.60656154	-2.10595803	-0.98574756
O	0.77391810	-3.36276203	-0.27347985
H	1.66603007	-3.02183556	-0.03157946

Benzohydroxamate (Gas Phase Structure)

Absolute Energy = -474.292107 Hartrees

Cartesian Coordinates

C	0.96273606	1.27718676	-0.00000074
C	0.33063433	2.53108204	-0.00000549
C	-1.07766307	2.61897908	0.00000045
C	-1.83591775	1.43202754	0.00000191
C	-1.21237565	0.16819360	-0.00000146
C	0.20306137	0.08031291	-0.00000245
H	2.05209208	1.18010203	-0.00000107
H	0.93477871	3.44592075	-0.00000108
H	-1.57321946	3.59662516	0.00000268
H	-2.93079672	1.48833249	0.00000461
H	-1.77555607	-0.76914935	-0.00000095
C	0.98257518	-1.20208081	0.00000225
N	0.31353312	-2.37213494	0.00000013

O	2.26493260	-1.18079532	0.00000507
H	0.95394158	-3.17356204	0.00000351
O	-0.99768164	-2.64940070	-0.00000742

Benzohydroxamate (Aqueous Phase Structure)

Absolute Energy = -474.284840 Hartrees

Cartesian Coordinates

C	0.77461030	1.36189408	-0.06806162
C	0.11719419	2.60066383	-0.15339736
C	-1.28946996	2.67205056	-0.08149957
C	-2.02304543	1.48187946	0.09464386
C	-1.36395341	0.24160762	0.18602787
C	0.04850313	0.15313513	0.07525711
H	1.86545562	1.28540727	-0.10081388
H	0.70290618	3.51959871	-0.27189146
H	-1.80323282	3.63731898	-0.14290446
H	-3.11459103	1.52168813	0.18591960
H	-1.95471974	-0.65989936	0.38060441
C	0.85205976	-1.11937075	0.15203906
N	0.16566388	-2.20829233	-0.26891068
O	2.05829787	-1.09936785	0.54125994
H	-0.77039630	-2.02109146	-0.63869698
O	0.58912325	-3.45203242	-0.34355764

Nitric Acid

Absolute Energy = -280.284885 Hartrees

Cartesian Coordinates

N	0.05250094	0.14129308	0.00000330
O	-0.64946923	1.12842324	-0.00000134
O	1.26896086	0.03049217	-0.00000088

O	-0.67801143	-1.07288606	-0.00000013
H	0.03592643	-1.73999501	-0.00000045

Nitrate

Absolute Energy = -279.761750 Hartrees

Cartesian Coordinates

N	-0.00001470	-0.00001054	-0.00000000
O	-0.64651706	1.09162348	-0.00000000
O	1.26861625	0.01411084	-0.00000000
O	-0.62208476	-1.10572431	-0.00000000

Sulfuric Acid

Absolute Energy = -699.064742 Hartrees

Cartesian Coordinates

S	0.01035268	0.16687378	0.00938006
O	-1.06185917	0.86760676	0.72446364
O	0.55085220	-0.97360565	1.06858450
O	1.16483216	0.80773827	-0.62974398
O	-0.65822828	-0.77258893	-1.16750366
H	1.40054518	-1.29768299	0.71414582
H	-1.54376561	-1.02743884	-0.84563014

Bisulfate

Absolute Energy = -699.104805 Hartrees

Cartesian Coordinates

S	0.07906382	0.10075456	0.09206449
O	-0.90523215	0.91741022	0.86822435
O	0.89828990	-0.87674586	0.89263873
O	0.86737491	0.84233637	-0.95488389
O	-0.98598931	-0.90972428	-0.82978910
H	-0.36347617	-1.45256015	-1.34280161

Phosphoric Acid

Absolute Energy = -643.018955 Hartrees

Cartesian Coordinates

P	0.06651569	0.06524232	-0.06349137
O	-1.09333464	0.81710028	0.80849025
O	0.78742827	-0.83803145	1.09206721
O	0.95975765	0.93437525	-0.90881358
O	-0.81706122	-1.07068551	-0.83814310
H	-0.31922092	-1.40412302	-1.60202968
H	-1.40989105	1.59649810	0.32372993
H	1.55717381	-0.36172263	1.44280722

Dihydrogen Phosphate

Absolute Energy = -642.493173 Hartrees

Cartesian Coordinates

P	0.02834739	-0.01162887	-0.15679148
O	-0.92701499	1.11290735	0.69672575
O	0.59695963	-0.97342554	1.13075566
O	1.24383919	0.75413706	-0.69215071
O	-0.94529360	-0.87947256	-0.96267272
H	-1.82163068	0.74438634	0.64347514
H	1.46468111	-0.59536895	1.33750783

Carbonic Acid

Absolute Energy = -264.419360 Hartrees

Cartesian Coordinates

C	-0.00124006	0.10335302	-0.00352380
O	0.35659876	-0.65178130	1.05773882
O	-0.01629071	1.32050597	-0.04483552
H	0.59161429	-0.02141831	1.75821986

O	-0.33950703	-0.73051610	-1.01087740
H	-0.58968195	-0.15487334	-1.75209939

Bicarbonate

Absolute Energy = -263.875351 Hartrees

Cartesian Coordinates

C	-0.05224516	0.05148841	-0.15502704
O	0.35414541	-0.66458063	1.04923959
O	-0.01192713	1.30976332	-0.03304767
H	0.55469189	0.07256657	1.64586851
O	-0.37089577	-0.69882841	-1.10144465

Acetamidoxime

Absolute Energy = -263.821470 Hartrees

Cartesian Coordinates

N	0.99842239	0.18395781	0.22943833
C	-0.27098500	0.27609358	-0.04528052
O	1.35684395	-1.21041248	0.26811062
H	-1.94636887	-0.65997908	-0.74705910
H	-0.64473628	-1.69943829	-0.35480930
H	2.30703473	-1.15743854	0.43961458
N	-1.11257894	-0.81295378	-0.19249748
C	-0.86638275	1.65164058	-0.12876367
H	-1.66591214	1.76790781	0.62019838
H	-0.08248312	2.39709379	0.05642534
H	-1.30067597	1.82683244	-1.12708052

Acetamidoximate

Absolute Energy = -263.230765 Hartrees

Cartesian Coordinates

N	1.02713516	0.16972122	-0.23941896
---	------------	------------	-------------

C	-0.26486852	0.24377341	0.05203783
O	1.50547102	-1.09202615	-0.28450209
H	-1.79675067	-1.06459787	-0.23530780
H	-0.25604575	-1.66245818	0.12702952
N	-0.97893048	-0.94775985	0.36917626
C	-0.95165775	1.56970097	0.14115174
H	-1.80255815	1.65134841	-0.56809593
H	-1.36229969	1.75629521	1.15361687
H	-0.21935931	2.35610448	-0.10295101

Benzamidoxime

Absolute Energy = -455.004504 Hartrees

Cartesian Coordinates

N	1.77444040	-1.18423319	0.37929645
C	0.53968372	-1.16221885	-0.04356438
O	2.27848672	-2.52106566	0.25121163
H	-0.86819438	-2.11953551	-1.15548588
H	0.41293187	-3.10077861	-0.60913170
H	3.18212277	-2.41812230	0.58098907
N	-0.17220794	-2.28776930	-0.43608364
C	-1.51214025	2.62223941	0.02982468
C	-2.22701749	1.42749475	0.23311318
C	-1.55913571	0.18974977	0.21175176
C	-0.16593679	0.14142207	-0.01885749
C	0.55013357	1.34112332	-0.22744003
C	-0.12229296	2.57375436	-0.19651551
H	-2.03317105	3.58398222	0.04674031
H	-3.30479456	1.45921985	0.41874719
H	-2.11113235	-0.73541496	0.40222002

H	1.62621266	1.29116487	-0.41252854
H	0.43671743	3.49996837	-0.36009140

Benzamidoximate

Absolute Energy = -454.435093 Hartrees

Cartesian Coordinates

N	1.92960599	1.58808602	0.03540147
C	0.59686001	1.36572143	0.03768720
O	2.75089197	0.57556686	-0.08984831
H	-0.66447672	2.66905863	0.97706129
H	0.49581324	3.33674575	0.03513922
N	-0.19653115	2.58217118	0.06710650
C	-1.62772426	-2.33444273	-0.03326636
C	-2.28918996	-1.08709078	-0.05834816
C	-1.55788707	0.11087279	-0.04559990
C	-0.12664534	0.11252717	-0.01020917
C	0.53045234	-1.15898696	0.00516905
C	-0.21754057	-2.34989739	-0.00272493
H	-2.19908657	-3.26947091	-0.04308918
H	-3.38488639	-1.05036764	-0.09290531
H	-2.08459437	1.06851258	-0.08987511
H	1.62267528	-1.15227580	0.01784762
H	0.31303016	-3.30977009	0.01176986

Azine-Amidoxime

Absolute Energy = -471.027322 Hartrees

Cartesian Coordinates

N	1.75712831	-1.18780522	0.37583080
C	0.52211132	-1.15529256	-0.04389020
O	2.24287083	-2.52962614	0.26333468

H	-0.91652106	-2.10244435	-1.13223041
H	0.35742994	-3.09795743	-0.58814714
H	3.14763337	-2.43759375	0.59368970
N	-0.20873826	-2.26995818	-0.42467310
C	-1.53071493	2.54573119	0.04658089
N	-2.23591443	1.41046169	0.24650475
C	-1.54880322	0.24683544	0.21562785
C	-0.15914740	0.16086619	-0.02018567
C	0.55966926	1.35505030	-0.22761087
C	-0.14211356	2.56715285	-0.18548895
H	-2.10478567	3.47750032	0.07255721
H	-2.13140205	-0.65985522	0.40871937
H	1.63559790	1.31609702	-0.41570018
H	0.37171348	3.51986294	-0.34106241

Azine-Amidoximate

Absolute Energy = -470.465311 Hartrees

Cartesian Coordinates

N	1.86820652	-1.26623113	-0.00412772
C	0.51900290	-1.18747456	-0.03026092
O	2.33717893	-2.49343070	-0.05820649
H	-0.89670807	-2.41838374	-0.81673767
H	0.48495458	-3.10594720	-0.15535155
N	-0.24827088	-2.38464904	-0.02621612
C	-1.47985640	2.54496450	0.06816696
N	-2.21421103	1.40859442	0.12373415
C	-1.53785382	0.23518275	0.09972695
C	-0.11721730	0.10538498	0.01510725
C	0.61954260	1.32473136	-0.04255519

C	-0.06927536	2.54046246	-0.01080632
H	-2.03963400	3.48748047	0.08741363
H	-2.15282844	-0.66820793	0.17011712
H	1.70957736	1.27440085	-0.11058588
H	0.47554692	3.49064409	-0.05205240

Imidazole-Oxime

Absolute Energy = -355.814900 Hartrees

Cartesian Coordinates

N	-0.75592563	-0.64034405	0.00498574
C	-0.07577658	-1.86659071	0.01993769
C	1.26284935	-1.58363442	0.02560958
N	1.39539026	-0.18971617	0.01182384
C	0.14400863	0.40952308	-0.00305553
H	-0.58989538	-2.82220400	0.02783530
H	2.12004953	-2.24904387	0.03909085
H	2.25689855	0.33786170	0.01298129
N	-0.07904323	1.69982002	-0.02074224
O	-1.53806946	1.82310488	-0.03126794
H	-1.63791296	2.78441803	-0.04348175
H	-1.75410168	-0.48004039	-0.01317256

Imidazole-Oximate

Absolute Energy = -355.216642 Hartrees

Cartesian Coordinates

N	-0.81100274	-0.60201373	0.29528258
C	-0.09159361	-1.75877821	-0.07206986
C	1.24718508	-1.47510659	-0.08228915
N	1.43721314	-0.10660980	0.28243245
C	0.11771237	0.46910020	0.18434769

H	-0.56902936	-2.73441149	-0.16853631
H	2.08710623	-2.16595722	-0.15608282
H	2.11706579	0.41316216	-0.27176917
N	-0.20356651	1.68434250	-0.15793319
O	-1.57060743	1.81307773	-0.29412255
H	-1.67394685	-0.27164906	-0.17196946

Imidazolidine-Oxime

Absolute Energy = -357.020447 Hartrees

Cartesian Coordinates

C	0.65075899	0.13567731	1.72837972
C	-0.84471299	-0.20409644	1.80288331
N	-1.29576578	0.26378240	0.47967791
C	-0.22893248	0.04906901	-0.41083729
N	0.92446788	-0.20136615	0.32426082
H	0.81355212	1.20744719	1.94260546
H	1.25967907	-0.47546802	2.40881222
H	-1.36423256	0.33477217	2.60694893
H	-0.98001060	-1.29337120	1.93442028
H	-2.18753400	-0.09165618	0.14385462
H	1.79090999	0.09699183	-0.11577106
N	-0.36880296	0.09586318	-1.70039706
O	0.95291174	-0.09738673	-2.26900510
H	0.76356649	0.00807428	-3.21142361

Imidazolidine-Oximate

Absolute Energy = -356.420248 Hartrees

Cartesian Coordinates

C	0.66746325	0.11409115	1.64761026
C	-0.81038403	-0.35119639	1.61005047

N	-1.32830791	0.41488067	0.44755023
C	-0.22811509	0.28469618	-0.47540639
N	0.97888753	0.48517180	0.24733204
H	0.77671608	0.99582529	2.30391449
H	1.33404143	-0.68173964	2.02369351
H	-1.36060193	-0.10993391	2.53522380
H	-0.85174963	-1.44523087	1.42948666
H	-2.13173063	-0.05149057	0.01921537
H	1.65887386	-0.10493721	-0.26091649
N	-0.30263060	-0.23860105	-1.67195088
O	0.92062786	-0.43977486	-2.23808287

N-Methyl Acetamidoxime

Absolute Energy = -302.995861 Hartrees

Cartesian Coordinates

N	1.41842225	0.27106256	0.41144459
C	0.14727692	0.38857285	0.13440913
O	1.75810006	-1.13118068	0.41467251
H	-0.19923282	-1.56195453	-0.16584040
H	2.70716613	-1.09412217	0.59602691
N	-0.70158683	-0.68655307	-0.04394825
C	-0.40514803	1.78513482	0.08890044
H	-1.21980439	1.90522651	0.82124265
H	0.40350294	2.48708218	0.33013341
H	-0.80264228	2.02504328	-0.91030637
C	-1.93499594	-0.54673489	-0.81433831
H	-2.48542949	-1.49604504	-0.76089936
H	-2.57116957	0.23286417	-0.37281172
H	-1.76086438	-0.30117450	-1.87774457

N-Methyl Acetamidoximate

Absolute Energy = -302.407046 Hartrees

Cartesian Coordinates

N	1.44390365	0.12080883	0.15952083
C	0.14783053	0.42394673	0.18935874
O	1.69755528	-1.20153055	0.13427630
H	-0.14377643	-1.44180684	0.23293042
N	-0.80221048	-0.63047537	0.29014459
C	-0.29032283	1.85376750	0.27490732
H	-0.84336138	2.05542917	1.21461526
H	0.61065740	2.48745007	0.24501715
H	-0.95430491	2.15539162	-0.55977925
C	-1.75592186	-0.67005403	-0.82216801
H	-2.37794903	-1.57894277	-0.74304733
H	-2.43482303	0.19925609	-0.77622374
H	-1.26819088	-0.66595866	-1.82087370

N,N-Dimethyl Acetamidoxime

Absolute Energy = -342.169960 Hartrees

Cartesian Coordinates

N	1.34713188	0.12598301	0.14462571
C	0.05961449	0.33753527	0.16423053
O	2.05149224	1.36046839	0.33639829
H	2.96660682	1.04679369	0.34820831
N	-0.77470157	-0.78856157	0.09619219
C	-0.58138262	1.69137499	0.32868423
H	-1.55430638	1.59126628	0.82937131
H	0.07547166	2.33146808	0.93144626
H	-0.72684232	2.18259826	-0.64711823

C	-1.88998478	-0.67088551	-0.85007258
H	-2.58597164	-1.50540206	-0.67953894
H	-2.43490491	0.26828830	-0.69164916
H	-1.54346021	-0.70798845	-1.90320231
C	-0.07583538	-2.06713428	-0.04081353
H	-0.82536969	-2.87081472	0.00626169
H	0.48002891	-2.13799109	-0.99629613
H	0.64261545	-2.18185951	0.78095351

N,N-Dimethyl Acetamidoximate

Absolute Energy = -341.577891 Hartrees

Cartesian Coordinates

N	1.38562288	0.21214541	-0.07209325
C	0.09408142	0.38573693	0.17260753
O	2.13149339	1.31995282	-0.04119762
N	-0.77823558	-0.76623540	0.24030587
C	-0.49370702	1.72114749	0.52963883
H	-1.45465614	1.59972338	1.05932909
H	0.24365906	2.24304715	1.16695223
H	-0.64373195	2.37273008	-0.35264429
C	-1.80607773	-0.70152293	-0.80203446
H	-2.53609949	-1.52005231	-0.66130305
H	-2.34242657	0.25760184	-0.73766514
H	-1.36567536	-0.78575265	-1.82343439
C	-0.05839749	-2.03231421	0.12934030
H	-0.78669892	-2.85576966	0.24617250
H	0.46466245	-2.14022174	-0.84495822
H	0.70597429	-2.08665606	0.91669250

N-Phenyl Acetamidoxime

Absolute Energy = -494.180571 Hartrees

Cartesian Coordinates

N	2.85678825	0.10942988	1.17188100
C	1.76491181	0.43857711	0.56561369
O	2.68856916	-1.14345605	1.84159557
H	0.83111147	-1.28048975	0.98023586
H	3.56941415	-1.31417755	2.18681341
N	0.64816285	-0.36845483	0.58279835
C	1.79752014	1.73400039	-0.19130665
H	1.22355575	2.51409491	0.31410577
H	2.83427603	2.06069920	-0.25557686
H	1.39105327	1.61363846	-1.19803822
C	-3.07035740	-0.05907420	-1.38750114
C	-2.39269419	-1.27547849	-1.31434767
C	-1.15653135	-1.35605801	-0.68214597
C	-0.58003557	-0.22093650	-0.09305521
C	-1.27744113	0.99278526	-0.14308798
C	-2.50385232	1.06962680	-0.79890800
H	-4.02914831	0.00583083	-1.88799070
H	-2.82083797	-2.16521815	-1.76234141
H	-0.62355802	-2.30040893	-0.64692059
H	-0.87973861	1.86803320	0.35167247
H	-3.02845870	2.01816630	-0.82904654

N-Phenyl Acetamidoximate

Absolute Energy = -493.609671 Hartrees

Cartesian Coordinates

N	2.90818194	-0.10140302	1.15117750
C	1.81730864	0.51796626	0.68153373

O	2.74500015	-1.43453383	1.27711136
H	1.16862012	-1.27541897	0.75600297
N	0.73496478	-0.34033463	0.47293870
C	1.81669201	2.00745106	0.53873996
H	1.01873677	2.48966459	1.13497677
H	2.79451082	2.35215399	0.91235464
H	1.70587493	2.34808200	-0.50793282
C	-3.09645198	-0.10840201	-1.33335599
C	-2.59077501	-1.31613889	-0.80241263
C	-1.32092591	-1.36825109	-0.21419839
C	-0.48184766	-0.21228802	-0.12731267
C	-1.00530570	1.00016233	-0.67367197
C	-2.28358945	1.03994535	-1.25762103
H	-4.08914701	-0.06637508	-1.79180862
H	-3.19465836	-2.23000999	-0.84624705
H	-0.94171606	-2.31095434	0.19599922
H	-0.40808293	1.91174534	-0.63859716
H	-2.64590638	1.99144237	-1.66431454

Appendix B: Electronic Supplementary Information for Theoretical Study of the Coordination Behavior of Formate and Formamidoximate with Dioxovanadium (V) Cation: Implications for Selectivity towards Uranyl

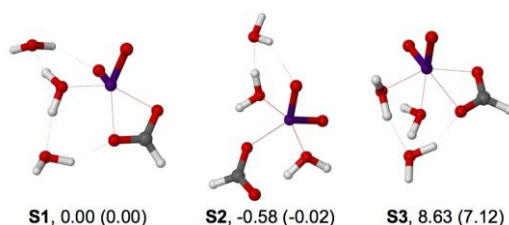


Figure A.3. Structures of $\text{VO}_2(\text{HCOO})(\text{H}_2\text{O})_3$ complexes and relative energies in the gas phase and in aqueous solution (in parentheses) in units of kcal/mol.

Table A.6. Relative gas phase electronic energies of five- and six-coordinate $\text{VO}_2(\text{HCOO})(\text{H}_2\text{O})_3$ in kcal/mol.^{a,b} All energies are given relative to complex S1 in Figure 9.1.

Theory	S2 (c.n. = 5)	S3 (c.n. = 6)
MP2	-0.73	-1.53
MP2/aug-qz//MP2	-0.32	-1.46
CCSD(T)//MP2	-2.38	4.53
CCSD(T) + δ MP2	-1.97	4.60
B3LYP	-1.74	7.49
CCSD(T)//B3LYP	-2.52	2.75
M06		3.53
M06-L		2.03
ω B97XD		5.17
B97D3		5.98
PBE-D3		6.32
TPSS-D3		5.50
M06-L-D3		2.02
B3LYP-D3		5.15

^aThe aug-cc-pVDZ basis set was employed in all calculations unless otherwise specified.

^bc.n. denotes coordination number.

^caug-qz denotes the aug-cc-pVQZ basis set.

Optimized Geometries and Absolute Energies Obtained at the MP2/aug-cc-pVDZ Level of Theory

VO₂⁺

Absolute Energy = -1093.236200 Hartrees

Cartesian Coordinates

V 0.0000 0.0000 0.4169

O 0.0000 1.2479 -0.5994

O 0.0000 -1.2479 -0.5994

VO₂(H₂O)₃⁺

Absolute Energy = -1322.251842 Hartrees

Cartesian Coordinates

V 0.9128 -0.2490 -2.6596

O 1.0976 1.1110 -1.6697

O 0.3804 -1.4041 -1.5435

O -1.0200 0.2633 -3.4321

H -1.7418 -0.3186 -3.1468

H -1.3199 1.1614 -3.2214

O 2.9741 -0.8371 -2.6660

H 3.1632 -1.6701 -2.2063

H 3.5853 -0.1901 -2.2802

O 1.2600 -0.4533 -4.7634

H 0.6120 -0.3039 -5.4668

H 2.0933 -0.7117 -5.1828

H₂VO₃(H₂O)₂⁺

Absolute Energy = -1322.218646 Hartrees

Cartesian Coordinates

V 2.0964 1.4268 0.8837

O 0.9126 2.2224 1.9232

O 1.4237 1.1868 -0.5742

O	3.5550	2.6244	0.2892
H	3.7139	2.9152	-0.6698
H	0.0277	2.5616	1.6993
O	3.7736	3.2285	-2.1682
H	4.4759	2.8811	-2.7372
H	3.5601	4.1060	-2.5176
O	2.6675	-0.1254	1.4998
H	4.2200	3.0163	0.8749
H	2.6848	-0.9931	1.0582

H₄VO₄(H₂O)⁺

Absolute Energy = -1322.166880 Hartrees

Cartesian Coordinates

V	0.2769	0.7656	-0.9472
O	-0.9595	0.9964	-2.1769
O	0.0584	-0.6376	-0.1056
O	0.1799	-2.9404	0.6734
H	1.0681	-3.3237	0.5448
H	-1.6165	0.3852	-2.5526
O	0.2475	2.1818	0.0973
H	0.2857	2.2621	1.0660
O	1.8848	0.5272	-1.6773
H	-0.0845	-3.0626	1.6045
H	2.2328	1.2477	-2.2388
H	0.1327	-1.8927	0.3552

VO₂(AO)(H₂O)₃⁺

Absolute Energy = -1546.562308 Hartrees

Cartesian Coordinates

V	0.1324	1.0252	-0.4016
---	--------	--------	---------

O	-0.5392	1.0493	-1.9465
O	-0.8109	-0.8847	2.7738
O	-1.6651	0.3958	0.5191
N	2.2334	-0.7161	0.6384
C	2.8588	-0.0133	-0.3119
N	2.1653	0.8959	-0.9561
H	2.7120	1.4392	-1.6198
O	0.0763	2.6251	0.0840
H	-0.6663	-0.2906	3.5218
H	0.0097	-0.8182	2.2286
H	3.9223	-0.2286	-0.4625
H	2.5784	-1.6144	0.9632
O	0.8746	-0.5209	0.7497
H	-2.1129	-0.2092	-0.1126
H	-1.5319	-0.0966	1.3639
O	-2.5302	-0.9602	-1.7097
H	-1.8887	-0.4097	-2.1954
H	-3.3848	-0.7529	-2.1099

H₂VO₃(AO)(H₂O)₂⁺

Absolute Energy = -1546.539677 Hartrees

Cartesian Coordinates

V	1.4532	-1.8187	0.3581
O	1.9410	-0.1711	0.9352
O	1.4508	-1.4682	-1.2535
C	-1.0003	-2.5549	1.6917
N	-0.5267	-2.2037	0.4939
H	-1.2482	-2.0833	-0.2133
N	-0.1168	-2.7343	2.6557

O	1.1863	-2.5548	2.3650
O	1.8879	-2.2564	4.9041
H	1.9525	-0.4692	4.3057
H	1.8561	-2.4770	3.9407
O	2.8299	-3.0582	0.2319
H	2.9149	-3.4388	1.1250
H	2.6386	-2.7476	5.2606
O	1.8009	0.2749	3.6907
H	2.3699	0.9887	4.0037
H	1.9385	-0.1452	1.9264
H	-2.0548	-2.7122	1.9336
H	-0.3546	-2.9847	3.6138

Complex 1

Absolute Energy = -1398.545356 Hartrees

Cartesian Coordinates

O	0.3604	-2.6448	-0.7723
O	-1.5204	-3.6351	0.7574
O	-1.9947	-3.8756	-1.9453
O	0.8976	-4.9453	0.9184
O	-1.1631	-6.3140	-0.6033
O	0.7302	-5.1609	-2.0823
V	-0.4627	-4.1004	-0.4843
H	0.6016	-6.0947	-2.3027
H	1.4267	-4.8203	-2.6605
H	0.8333	-4.5267	1.7918
H	1.8381	-4.9171	0.6822
H	-2.6714	-3.2356	-1.6721
H	-1.0404	-6.8271	0.2097

H -2.0954 -6.4380 -0.8376

H -1.7129 -3.5977 -2.8310

Complex 2

Absolute Energy = -1398.541208 Hartrees

Cartesian Coordinates

O 0.2344 -4.0508 1.2520

O -1.9503 -3.4037 -0.0313

O 0.4409 -2.3565 -1.1153

O -1.1524 -6.1414 -0.1739

O 0.3930 -4.9437 -2.0790

V -0.4368 -4.1142 -0.2962

H 0.2818 -5.8616 -2.3607

H 1.0119 -4.4966 -2.6917

H -2.1205 -6.2032 -0.1656

H -0.8634 -6.6209 0.6178

H 0.6336 -1.6202 -0.5191

H 1.1733 -2.4132 -1.7597

O 2.0663 -3.1105 -3.2573

H 1.8573 -2.6801 -4.1008

H 3.0298 -3.2165 -3.2700

Complex 3

Absolute Energy = -1358.697173 Hartrees

Cartesian Coordinates

V 0.1482 -0.3605 0.2816

O 0.4640 0.7467 1.5104

O 1.0607 0.2100 -1.0092

O -1.7674 0.3620 -0.3385

C 0.0691 -2.7459 0.7624

O 1.1530 -2.0972 0.9161
O -1.0028 -2.1641 0.3548
H -2.2730 -0.4602 -0.4581
H -1.7442 0.7910 -1.2058
H 0.0457 -3.8266 0.9827

Complex 4

Absolute Energy = -1358.682407 sHartrees

Cartesian Coordinates

V -1.0412 0.6254 0.5267
O -1.6884 1.0175 2.0104
O -1.3013 -1.3900 0.2864
O -2.0086 1.4156 -0.5714
O 0.9345 0.6732 0.2769
O 1.1858 -1.5272 -0.2595
C 1.6246 -0.3651 -0.0807
H -0.3203 -1.6208 0.0540
H -1.5322 -1.8788 1.0894
H 2.7015 -0.1728 -0.2316

Complex 5

Absolute Energy = -1434.979157 Hartrees

Cartesian Coordinates

V 2.2016 9.6200 12.1816
O 0.4678 8.5264 12.6333
O 1.5059 9.7164 14.2020
O 3.7651 10.7849 12.9994
O 3.7483 12.6687 11.0781
O 1.7460 10.6456 10.9409
O 3.1425 8.4530 11.4161

C	0.5553	8.9355	13.8371
H	-0.1966	8.6121	14.5770
H	2.9653	12.3242	10.6160
H	3.6364	13.6280	11.0927
H	3.8509	11.5959	12.4400
H	3.4340	11.0716	13.8652

Complex 6

Absolute Energy = -1434.981796 Hartrees

Cartesian Coordinates

V	2.2164	9.6024	12.2670
O	0.3634	8.6425	12.6844
O	1.3847	9.8438	14.2491
O	3.7834	10.8521	12.9654
O	1.8526	10.4634	10.8717
O	3.1369	8.3206	11.6976
C	0.3996	9.1079	13.8608
H	-0.4175	8.8863	14.5682
H	3.6110	11.1868	13.8858
H	3.8877	11.6350	12.4086
H	2.2907	10.9979	15.3898
O	3.0493	11.6139	15.4242
H	3.5478	11.3691	16.2144

Complex 7

Absolute Energy = -1434.982087 Hartrees

Cartesian Coordinates

V	-1.2912	0.5534	0.5708
O	-1.1993	-1.5364	0.2383
O	0.7501	0.5665	0.1775

O 1.3540 -1.6036 -0.1432
C 1.6036 -0.3819 -0.0702
H -0.2161 -1.7266 0.0945
H -1.4671 -2.0428 1.0165
H 2.6437 -0.0377 -0.2274
O -0.6303 2.6056 0.8077
H 0.2840 2.4682 0.4936
H -1.0474 3.2018 0.1702
O -2.5339 0.8852 -0.5117
O -2.1046 0.4697 2.0459

Complex 8

Absolute Energy = -1434.978050 Hartrees

Cartesian Coordinates

V 2.6312 9.6650 12.0025
O 0.5409 9.6862 12.1563
O 1.6660 10.5968 13.8643
O 4.4977 10.4210 12.7276
O 2.5302 12.0248 11.6760
O 2.9527 9.5354 10.3426
O 2.8957 8.0757 12.5356
C 0.5798 10.2032 13.3287
H -0.3718 10.3051 13.8820
H 2.1980 12.1261 10.7719
H 1.8172 12.3133 12.2661
H 4.5076 10.2475 13.6823
H 4.3773 11.3823 12.6435

Complex 9

Absolute Energy = -1393.999430 Hartrees

Cartesian Coordinates

V 0.0922 1.0227 -0.4501
O -0.6263 1.0165 -1.9751
O -1.6361 0.2584 0.5978
N 2.0705 -0.8641 0.4704
C 2.7726 -0.0644 -0.3276
N 2.1349 0.9208 -0.9300
H 2.7301 1.4888 -1.5272
O -0.0549 2.6243 0.0567
H 3.8400 -0.2873 -0.4305
H 2.4624 -1.6265 1.0106
O 0.7396 -0.6035 0.6264
H -2.2598 -0.0708 -0.0658
H -1.2324 -0.5367 0.9929

Complex 10

Absolute Energy = -1393.984783 Hartrees

Cartesian Coordinates

V -2.1842 -1.1767 0.1110
O -3.1290 -2.2611 -0.7429
O -2.2679 -0.8376 1.9813
O -1.8981 0.1089 -0.9239
O 0.3097 -1.6836 1.4804
N -0.3317 -2.1122 0.2945
C 0.4157 -2.9114 -0.4007
N 1.6695 -3.2785 -0.0423
H 2.0133 -3.0013 0.8693
H 2.1466 -4.0049 -0.5544
H -2.8144 -1.3836 2.5642

H -0.4585 -1.3033 1.9776

H -0.0000 -3.2716 -1.3423

Complex 11

Absolute Energy = -1393.983631 Hartrees

Cartesian Coordinates

V 0.2862 -0.0973 -0.1309

O 0.9661 1.3911 -0.4753

O -0.0426 0.3226 1.9472

O -1.3259 0.0123 -0.5605

O 1.1909 -1.5301 -1.1350

N 1.3115 -1.8502 0.2160

C 1.9464 -2.9498 0.4807

N 2.5279 -3.7148 -0.5004

H 2.2145 -3.4932 -1.4426

H 2.6958 -4.6907 -0.2931

H 0.3302 1.2080 2.0795

H -1.0019 0.4454 2.0194

H 2.0646 -3.2322 1.5275

Complex 12

Absolute Energy = -1393.989084 Hartrees

Cartesian Coordinates

V -0.3341 0.3614 -0.9335

O -0.2779 0.5638 -2.6056

O -1.7827 1.0569 -0.4146

O 0.8691 -0.8493 0.1496

N -0.1855 -1.5742 -0.3988

C -0.2205 -2.8434 -0.1482

N 0.6914 -3.4528 0.6823

H	1.5261	-2.8969	0.8526
H	0.8355	-4.4462	0.5505
O	0.9861	1.8935	-0.2759
H	-1.0434	-3.4219	-0.5688
H	0.4813	2.5334	0.2485
H	1.5311	1.4034	0.3635

Complex 13

Absolute Energy = -1393.988844 Hartrees

Cartesian Coordinates

V	0.0559	1.0320	-0.4447
O	-0.6036	1.0557	-2.0034
O	-1.6414	0.2373	0.5935
N	2.0612	-0.8921	0.5127
C	2.7652	-0.1273	-0.2621
O	-0.0082	2.6337	0.0918
H	3.8332	-0.3292	-0.3633
O	0.7366	-0.5578	0.5675
H	-2.2729	-0.1383	-0.0372
H	-1.1761	-0.5268	0.9919
N	2.1443	0.9746	-0.9863
H	2.5985	1.8617	-0.7560
H	2.2436	0.8454	-1.9964

Complex 14

Absolute Energy = -1393.970530 Hartrees

Cartesian Coordinates

V	-0.0489	0.9050	-0.1102
O	-0.2718	1.3873	-1.7150
O	-1.5886	-0.5829	-0.1615

N	0.9841	-0.8183	0.7460
C	2.0365	-0.3395	0.0524
N	2.0694	0.9901	0.0314
H	2.8261	1.3784	-0.5282
O	-0.8177	2.0792	0.8041
H	2.7308	-1.0180	-0.4668
O	0.6823	-2.1905	0.3622
H	-1.0956	-1.4024	0.0579
H	-2.1899	-0.4293	0.5821
H	0.7131	-2.6565	1.2137

Complex 15

Absolute Energy = -1393.972482 Hartrees

Cartesian Coordinates

V	-0.1737	0.8829	-0.1771
O	-0.3814	1.5320	-1.7189
O	-1.6384	-0.6264	-0.0436
N	0.8732	-0.8873	0.3365
C	2.1003	-0.4172	0.3810
N	2.0164	1.0022	0.0469
H	2.5230	1.2464	-0.8058
O	-0.7026	2.0599	0.9095
H	3.0228	-0.9529	0.6254
O	0.4408	-2.0705	0.5690
H	-1.0684	-1.4160	0.2485
H	-2.3144	-0.4967	0.6354
H	2.3411	1.6114	0.7996

Complex 16

Absolute Energy = -1470.282922 Hartrees

Cartesian Coordinates

V 0.0385 0.9331 -0.3814
O -0.5396 1.3089 -1.9218
O -0.7049 -0.3735 2.7246
O -1.7939 0.0782 0.3027
N 2.0839 -0.9914 0.4157
C 2.7652 -0.0914 -0.3016
N 2.1116 0.9397 -0.7847
H 2.7038 1.6093 -1.2702
O -0.1307 2.3679 0.4781
H -0.4495 0.4620 3.1400
H 0.0368 -0.5807 2.1056
H 3.8410 -0.2689 -0.4102
H 2.4319 -1.9296 0.5863
O 0.7161 -0.8360 0.4811
H -1.8920 -0.8026 -0.0891
H -1.6210 -0.0919 1.2657

Complex 17

Absolute Energy = -1470.277878 Hartrees

Cartesian Coordinates

V -2.2756 -1.1028 0.0391
O -2.9869 -2.3132 -0.8846
O -2.1521 -0.8215 2.0474
O -1.7294 0.0169 -1.0848
O -4.0824 -0.0048 0.5571
O 0.2414 -1.6793 1.5457
N -0.4106 -2.0890 0.3716
C 0.3032 -2.9119 -0.3271

N	1.5237	-3.3849	0.0631
H	1.9736	-2.9077	0.8364
H	2.1159	-3.8125	-0.6345
H	-2.5199	-1.5300	2.5977
H	-0.5323	-1.2255	1.9977
H	-0.1318	-3.2654	-1.2627
H	-3.6838	0.1353	1.4462
H	-4.0926	0.8590	0.1209

Complex 18

Absolute Energy = -1470.275822 Hartrees

Cartesian Coordinates

V	-0.2477	0.3612	-0.8106
O	-0.3348	0.5826	-2.4768
O	1.2178	0.8345	2.1906
O	-1.6749	1.0006	-0.1892
O	0.9662	-0.9520	0.1865
N	-0.1637	-1.6011	-0.3201
C	-0.2269	-2.8796	-0.1294
N	0.7138	-3.5603	0.6061
H	1.5874	-3.0530	0.7281
H	0.7952	-4.5546	0.4341
O	1.1029	1.8789	-0.2614
H	0.4524	0.9336	2.7729
H	1.0547	-0.0095	1.7045
H	-1.0949	-3.4096	-0.5230
H	0.7114	2.7586	-0.3548
H	1.2054	1.7190	0.7165

Complex 19

Absolute Energy = -1470.275291 Hartrees

Cartesian Coordinates

V	0.0922	1.0434	-0.4524
O	-0.6022	0.7590	-1.9654
O	-0.9112	-1.1538	2.4887
O	-1.6669	0.6018	0.6571
N	2.2736	-0.4882	0.8450
C	2.8874	0.0772	-0.1458
O	0.0723	2.7176	-0.2862
H	-0.8085	-0.8894	3.4119
H	-0.0288	-0.9828	2.0639
H	3.9652	-0.0695	-0.2381
O	0.9221	-0.2477	0.8709
H	-2.3268	0.1867	0.0856
H	-1.5102	-0.0388	1.4083
N	2.1542	0.8734	-1.1143
H	2.5807	1.7957	-1.2256
H	2.1712	0.4270	-2.0351

Complex 20

Absolute Energy = -1470.262919 Hartrees

Cartesian Coordinates

V	0.4284	0.5952	-0.3818
O	0.9263	1.0703	-1.9171
O	0.2976	0.3788	1.9355
O	0.7845	2.5189	0.4548
O	-1.2161	0.3618	-0.5399
O	1.5061	-1.0144	-0.2559

N	1.2648	-1.7769	0.9005
C	1.6689	-3.0055	0.7439
N	2.2871	-3.4702	-0.3900
H	2.1942	-2.8544	-1.1938
H	2.2561	-4.4658	-0.5653
H	-0.6527	0.1922	1.9888
H	0.6997	-0.5459	1.8624
H	0.3686	3.2921	0.0510
H	0.4975	2.4683	1.3810
H	1.5530	-3.6799	1.5946

Complex 21

Absolute Energy = -1546.562308 Hartrees

Cartesian Coordinates

V	0.1324	1.0252	-0.4016
O	-0.5392	1.0493	-1.9465
O	-0.8109	-0.8847	2.7738
O	-1.6651	0.3958	0.5191
N	2.2334	-0.7161	0.6384
C	2.8588	-0.0133	-0.3119
N	2.1653	0.8959	-0.9561
H	2.7120	1.4392	-1.6198
O	0.0763	2.6251	0.0840
H	-0.6663	-0.2906	3.5218
H	0.0097	-0.8182	2.2286
H	3.9223	-0.2286	-0.4625
H	2.5784	-1.6144	0.9632
O	0.8746	-0.5209	0.7497
H	-2.1129	-0.2092	-0.1126

H -1.5319 -0.0966 1.3639

O -2.5302 -0.9602 -1.7097

H -1.8887 -0.4097 -2.1954

H -3.3848 -0.7529 -2.1099

Complex 22

Absolute Energy = -1546.563673 Hartrees

Cartesian Coordinates

V -2.0823 -0.5941 0.0231

O -2.7079 -0.6087 -1.5400

O -1.3896 1.4750 2.7171

O -2.2910 1.5321 0.2193

O -3.3635 -1.0535 0.9889

O -0.0793 -2.7566 0.6970

N -1.1547 -2.5170 -0.1693

C -1.4499 -3.5526 -0.8881

N -0.8222 -4.7616 -0.7765

H 0.0483 -4.7693 -0.2551

H -0.9138 -5.4153 -1.5416

H -1.9042 1.0126 3.3918

H -0.8603 0.7631 2.2679

H -3.1991 1.8143 0.0452

H -2.1202 1.6963 1.1864

H -2.2885 -3.4473 -1.5776

O -0.3087 -0.2239 0.9559

H 0.0917 -1.8073 0.9834

H 0.3243 0.3152 0.4585

Complex 23

Absolute Energy = -1546.556854 Hartrees

Cartesian Coordinates

V -0.1585 0.4500 -0.6771
O -0.2321 0.7318 -2.3303
O 1.4759 0.7222 2.3282
O -1.5644 1.1053 -0.0307
O 1.0152 -0.9461 0.2281
N -0.1343 -1.5333 -0.3019
C -0.2306 -2.8197 -0.1959
N 0.6993 -3.5705 0.4822
H 1.5877 -3.0960 0.6273
H 0.7506 -4.5542 0.2487
O 1.2092 1.9189 -0.1036
H 0.7629 0.8392 2.9701
H 1.2275 -0.0833 1.8213
H -1.1170 -3.2995 -0.6119
H 0.6948 2.7596 -0.0968
H 1.3981 1.7042 0.8438
O -0.7199 3.8634 -0.1361
H -1.3908 3.1644 -0.2345
H -0.8448 4.4334 -0.9066

Complex 24

Absolute Energy = -1546.554129 Hartrees

Cartesian Coordinates

V 0.1701 0.9200 -0.5032
O -0.4134 0.5316 -2.0368
O -0.8060 -1.2193 2.5221
O -1.5878 0.4063 0.5281
N 2.3963 -0.3600 0.9729

C	3.0149	0.1889	-0.0239
O	0.0587	2.5902	-0.4098
H	-0.7708	-0.8836	3.4268
H	0.0726	-0.9911	2.1258
H	4.1038	0.1233	-0.0611
O	1.0320	-0.2242	0.9186
H	-2.1880	-0.0604	-0.0954
H	-1.4422	-0.1926	1.3060
O	-2.9380	-0.6925	-1.5996
H	-2.2267	-0.4070	-2.1987
H	-3.7289	-0.2427	-1.9252
N	2.2663	0.8591	-1.0720
H	2.6328	1.7981	-1.2411
H	2.3444	0.3476	-1.9550

Complex 25

Absolute Energy = -1546.549250 Hartrees

Cartesian Coordinates

V	-0.3424	0.5467	-0.3443
O	-0.2937	0.5714	-2.0364
O	-0.2222	0.6725	2.0502
O	-1.9321	1.0415	-0.0244
O	1.3515	-0.7284	0.0978
N	0.1411	-1.3956	0.0314
C	0.1627	-2.6787	0.2070
N	1.3207	-3.3542	0.5354
H	2.1579	-2.8170	0.3163
H	1.3530	-4.3308	0.2668
O	0.8374	2.3109	-0.0988

H	-0.9685	1.2530	2.2553
H	0.5614	1.0513	2.4809
H	-0.7829	-3.2179	0.1460
H	1.2409	2.5135	-0.9549
H	1.5798	2.0221	0.4887
O	2.4336	1.0231	1.6800
H	3.3783	0.9009	1.8324
H	2.1021	0.1880	1.2380

Complex S1

Absolute Energy = -1511.261465 Hartrees

Cartesian Coordinates

V	2.1353	9.6790	12.2772
O	0.3723	8.5914	12.7249
O	1.4332	9.7085	14.3236
O	3.8002	10.7254	13.0077
O	3.9885	12.3891	10.8491
O	1.6300	10.7481	11.0997
O	2.9800	8.5112	11.4086
C	0.4584	8.9645	13.9337
H	-0.3067	8.6484	14.6630
H	3.1327	12.1160	10.4784
H	3.9716	13.3549	10.8315
H	3.5803	11.1827	13.8556
H	4.0038	11.4273	12.3477
H	2.2283	11.0522	15.3787
O	2.9070	11.7541	15.3651
H	3.4020	11.6476	16.1874

Complex S2

Absolute Energy = -1511.262636 Hartrees

Cartesian Coordinates

V -1.2331 0.4792 0.6384

O -1.1165 -1.6140 0.3712

O 0.7906 0.4839 0.2037

O 1.3943 -1.6806 -0.1608

C 1.6367 -0.4554 -0.0874

H -0.1406 -1.7997 0.1624

H -1.3257 -2.1055 1.1764

H 2.6673 -0.1039 -0.2852

O -0.6414 2.5245 0.8742

H 0.2639 2.4818 0.5210

H -1.1673 3.0553 0.2305

O -2.4434 0.7830 -0.4732

O -2.0742 0.3926 2.0956

O -2.2899 3.5771 -1.0253

H -2.7492 2.7412 -1.2121

H -2.9931 4.2138 -0.8416

Complex S3

Absolute Energy = -1511.263902 Hartrees

Cartesian Coordinates

V -0.4585 0.5784 -0.3167

O -0.3108 0.5745 -2.0087

O -0.2472 0.6006 1.9880

O -1.9906 1.2798 -0.1217

O 1.3500 -0.7847 0.1684

C 0.4676 -1.7112 0.1933

O	0.7869	2.3171	-0.0615
H	-0.9215	1.2115	2.3166
H	0.6057	0.9089	2.3394
H	1.1399	2.5778	-0.9235
H	1.5638	2.0392	0.4780
O	2.4929	1.0540	1.6431
H	3.4136	1.0612	1.9309
H	2.3418	0.1957	1.1791
O	-0.7589	-1.4868	-0.0554
H	0.7770	-2.7469	0.4215

Optimized Geometries and Absolute Energies Obtained at the B3LYP/aug-cc-pVDZ Level of Theory

VO₂⁺

Absolute Energy = -1094.198446 Hartrees

Cartesian Coordinates

V	0.010592	0.000000	0.008000
O	0.009996	0.000000	1.558220
O	1.501554	0.000000	-0.416515

Complex 1

Absolute Energy = -1400.211579 Hartrees

Cartesian Coordinates

O	0.379485	-2.745090	-0.830609
O	-1.465735	-3.640096	0.701711
O	-1.953706	-3.900414	-1.955501
O	0.901174	-4.956031	0.870030
O	-1.191209	-6.278038	-0.561911
O	0.713230	-5.143943	-2.056998
V	-0.461233	-4.039570	-0.463068

H	0.625811	-6.070566	-2.316494
H	1.398748	-4.731445	-2.599033
H	0.788398	-4.626840	1.775779
H	1.844072	-4.879571	0.660189
H	-2.694223	-3.344405	-1.665681
H	-1.060484	-6.798621	0.243289
H	-2.117570	-6.408802	-0.809267
H	-1.679856	-3.569867	-2.824237

Complex 2

Absolute Energy = -1400.217767 Hartrees

Cartesian Coordinates

O	0.615404	-4.247902	0.926937
O	-1.740188	-3.436919	0.245346
O	0.282589	-2.393399	-1.246156
O	-1.162574	-6.075436	-0.195001
O	0.209088	-4.884744	-2.172252
V	-0.396017	-4.093906	-0.280854
H	0.083957	-5.804695	-2.438585
H	0.917355	-4.473826	-2.711412
H	-2.115342	-6.092571	-0.010329
H	-0.742067	-6.605322	0.500826
H	0.157894	-1.541269	-0.805991
H	1.099231	-2.380284	-1.787937
O	2.158181	-3.150727	-3.094259
H	2.136388	-2.735788	-3.969347
H	3.095101	-3.316111	-2.911987

Complex 3

Absolute Energy = -1360.301270 Hartrees

Cartesian Coordinates

V	0.196334	-0.335346	0.298439
O	0.420268	0.676524	1.502307
O	0.962095	0.177703	-1.004582
O	-1.719799	0.302753	-0.347714
C	0.061038	-2.725671	0.765169
O	1.137612	-2.060532	0.857572
O	-0.998977	-2.122464	0.409197
H	-2.279184	-0.472171	-0.509582
H	-1.679474	0.818052	-1.165387
H	0.053387	-3.803647	0.991181

Complex 4

Absolute Energy = -1360.301193 Hartrees

Cartesian Coordinates

V	-1.101894	0.617275	0.529732
O	-1.550277	1.033081	1.996711
O	-1.246172	-1.365675	0.288622
O	-1.930489	1.435495	-0.548463
O	0.812308	0.635892	0.224801
O	1.193858	-1.549629	-0.188109
C	1.570016	-0.369834	-0.070025
H	-0.243434	-1.629352	0.075515
H	-1.582183	-1.909377	1.013373
H	2.632667	-0.120875	-0.221557

Complex 5

Absolute Energy = -1436.768243 Hartrees

Cartesian Coordinates

V	2.250554	9.574710	12.101873
---	----------	----------	-----------

O	0.456199	8.720614	12.577831
O	1.622167	9.668291	14.158649
O	3.717094	10.778897	12.931635
O	3.687434	12.688349	11.137987
O	1.897841	10.605477	10.913050
O	3.110899	8.367745	11.543760
C	0.584088	9.031944	13.801891
H	-0.193059	8.751569	14.530519
H	2.968394	12.181882	10.707529
H	3.374029	13.597503	11.209815
H	3.813220	11.626252	12.407698
H	3.533441	10.989068	13.857262

Complex 6

Absolute Energy = -1436.766267 Hartrees

Cartesian Coordinates

V	2.241368	9.558049	12.212201
O	0.407852	8.716718	12.638706
O	1.382091	9.857572	14.220952
O	3.601423	10.939215	12.942459
O	1.958359	10.341864	10.851816
O	3.165701	8.297919	11.930235
C	0.398429	9.156028	13.822739
H	-0.447762	8.933291	14.492037
H	3.530405	11.236085	13.894177
H	3.699172	11.712395	12.373596
H	2.351715	10.952661	15.463990
O	3.123058	11.549714	15.459328
H	3.694189	11.270189	16.184864

Complex 7

Absolute Energy = -1436.767201 Hartrees

Cartesian Coordinates

V	-1.284791	0.532032	0.575229
O	-1.166014	-1.490446	0.226392
O	0.710811	0.524946	0.149055
O	1.337297	-1.632058	-0.066065
C	1.576923	-0.416797	-0.040482
H	-0.179355	-1.746373	0.122135
H	-1.566997	-2.021562	0.925450
H	2.614262	-0.066780	-0.191993
O	-0.626585	2.580570	0.775267
H	0.255596	2.601506	0.371471
H	-1.201568	3.167871	0.265553
O	-2.402671	0.955315	-0.483907
O	-1.921308	0.433376	2.034295

Four-Coordinate VO₂(HCOO)(H₂O)₂ Complex

Absolute Energy = -1436.766288 Hartrees

Cartesian Coordinates

V	1.751693	8.675161	12.238341
O	0.412477	8.831187	13.568829
O	1.266658	8.891759	15.661442
O	3.061388	10.132656	12.612263
O	1.182805	8.897184	10.768314
O	2.531447	7.291944	12.341841
C	0.373857	8.631217	14.859810
H	-0.585497	8.212191	15.211569
H	3.371509	10.202525	13.600002

H	2.966525	11.004509	12.210350
H	4.306469	9.659910	15.419131
O	3.546782	10.141523	15.069702
H	2.730187	9.663435	15.384207

Complex 9

Absolute Energy = -1395.740582 Hartrees

Cartesian Coordinates

V	0.115968	1.052107	-0.444132
O	-0.604067	0.964757	-1.880703
O	-1.608485	0.229875	0.560467
N	2.084562	-0.827141	0.499025
C	2.769797	-0.060840	-0.332825
N	2.104342	0.891860	-0.941320
H	2.631721	1.474661	-1.578549
O	0.045996	2.544863	0.126251
H	3.833844	-0.268446	-0.460632
H	2.465404	-1.582723	1.051419
O	0.758724	-0.553021	0.642584
H	-2.258111	0.026226	-0.126751
H	-1.306995	-0.614177	0.933566

Complex 10

Absolute Energy = -1395.741404 Hartrees

Cartesian Coordinates

V	-2.136784	-1.189736	0.070467
O	-3.099718	-2.264446	-0.627765
O	-2.349950	-0.831977	1.866563
O	-1.918682	0.104668	-0.845542
O	0.360890	-1.691129	1.527913

N	-0.302879	-2.103762	0.360249
C	0.406740	-2.911739	-0.361308
N	1.639981	-3.335341	-0.041753
H	2.078133	-3.012441	0.809317
H	2.135162	-3.972043	-0.643886
H	-2.939007	-1.379555	2.400433
H	-0.356936	-1.271306	2.045314
H	-0.046050	-3.258194	-1.288302

Complex 11

Absolute Energy = -1395.733252 Hartrees

Cartesian Coordinates

V	0.055457	1.049748	-0.432735
O	-0.538727	0.977084	-1.928280
O	-1.631024	0.218438	0.562479
N	2.064827	-0.842180	0.513937
C	2.768772	-0.111460	-0.261708
O	0.113181	2.549166	0.133138
H	3.834397	-0.303449	-0.371151
O	0.752346	-0.502250	0.555846
H	-2.307673	-0.068462	-0.066005
H	-1.260734	-0.578339	0.983246
N	2.130457	0.970729	-0.994829
H	2.554992	1.874111	-0.781496
H	2.199829	0.835863	-2.004539

Complex 12

Absolute Energy = -1395.733252 Hartrees

Cartesian Coordinates

V	-0.345890	0.339344	-0.939562
---	-----------	----------	-----------

O	-0.254246	0.474853	-2.532130
O	-1.687847	0.995296	-0.339476
O	0.895931	-0.803697	0.121334
N	-0.150061	-1.543359	-0.378786
C	-0.206557	-2.808961	-0.160990
N	0.705473	-3.473266	0.597104
H	1.547222	-2.975039	0.854562
H	0.737507	-4.479479	0.565392
O	0.958156	1.870147	-0.267264
H	-1.047849	-3.356534	-0.579984
H	0.428287	2.585964	0.112129
H	1.496375	1.502332	0.449371

Complex 13

Absolute Energy = -1395.727057 Hartrees

Cartesian Coordinates

V	0.2935	0.3275	-0.4283
O	0.7283	1.5664	-1.3326
O	0.3787	0.5041	1.6239
O	-1.2027	-0.1438	-0.7583
O	1.5853	-1.0163	-0.3021
N	1.2904	-1.7748	0.8525
C	1.6182	-3.0193	0.7155
N	2.1500	-3.5681	-0.3972
H	2.2783	-2.9850	-1.2123
H	2.3497	-4.5526	-0.4475
H	-0.4673	0.5985	2.0819
H	0.7023	-0.4515	1.7578
H	1.4589	-3.6640	1.5793

Complex 14

Absolute Energy = -1395.704388 Hartrees

Cartesian Coordinates

V	-0.045643	0.921272	-0.161637
O	-0.240843	1.305859	-1.701388
O	-1.603684	-0.538405	-0.098822
N	0.977463	-0.845730	0.638759
C	2.070065	-0.348136	0.055864
N	2.014160	0.971374	0.007096
H	2.751012	1.448346	-0.497514
O	-0.741728	1.997616	0.796100
H	2.855528	-0.984886	-0.371947
O	0.733100	-2.221873	0.322890
H	-1.217371	-1.411945	0.093754
H	-2.240763	-0.331542	0.598204
H	0.718402	-2.659451	1.186741

Complex 15

Absolute Energy = -1395.709269 Hartrees

Cartesian Coordinates

V	-0.201170	0.892330	-0.182218
O	-0.283156	1.447956	-1.680005
O	-1.597082	-0.609665	-0.011577
N	0.868110	-0.854346	0.327095
C	2.075221	-0.405679	0.369564
N	1.997688	1.008913	0.048898
H	2.477705	1.272706	-0.810719
O	-0.629114	1.980211	0.914740
H	2.992428	-0.948223	0.602973

O	0.400665	-2.030654	0.547495
H	-1.039012	-1.431961	0.272390
H	-2.326282	-0.479071	0.606857
H	2.302700	1.625384	0.801007

Complex 16

Absolute Energy = -1472.203027 Hartrees

Cartesian Coordinates

V	0.135064	1.052678	-0.483787
O	-0.567201	0.890058	-1.920452
O	-0.931333	-1.020202	2.639665
O	-1.613907	0.440393	0.527825
N	2.232691	-0.642426	0.638105
C	2.827309	-0.028604	-0.377913
N	2.102027	0.806058	-1.071821
H	2.571650	1.301543	-1.818989
O	0.171630	2.592703	-0.056295
H	-0.872415	-0.544514	3.476956
H	-0.059614	-0.908452	2.194177
H	3.881345	-0.250775	-0.556550
H	2.608832	-1.456587	1.105570
O	0.891227	-0.409674	0.786096
H	-2.236049	0.032811	-0.086110
H	-1.544157	-0.121709	1.344423

Complex 17

Absolute Energy = -1472.200707 Hartrees

Cartesian Coordinates

V	-2.193113	-1.079742	0.130545
O	-2.843768	-2.263261	-0.740663

O	-2.127662	-0.879946	2.048333
O	-1.705161	0.147091	-0.788935
O	-4.121065	-0.068127	0.513196
O	0.351736	-1.694721	1.591301
N	-0.350066	-2.046706	0.435400
C	0.300466	-2.853799	-0.334610
N	1.534142	-3.331070	-0.071770
H	2.009526	-3.047392	0.772459
H	1.985080	-3.966516	-0.707776
H	-2.562341	-1.551350	2.588912
H	-0.369113	-1.256389	2.108027
H	-0.200750	-3.154746	-1.252024
H	-3.904996	0.419708	1.323057
H	-4.242514	0.589767	-0.186152

Complex 18

Absolute Energy = -1472.198576 Hartrees

Cartesian Coordinates

V	-0.316064	0.326026	-0.845738
O	-0.268944	0.471304	-2.440152
O	1.319439	0.935225	2.239345
O	-1.682751	0.905429	-0.231917
O	0.892301	-0.888282	0.234737
N	-0.163792	-1.581454	-0.316474
C	-0.214022	-2.860892	-0.202027
N	0.692942	-3.580704	0.510840
H	1.548130	-3.109569	0.777271
H	0.724406	-4.581073	0.393799
O	1.007275	1.812775	-0.238948

H	0.622214	1.097528	2.886866
H	1.110632	0.064817	1.837694
H	-1.049794	-3.376237	-0.670438
H	0.678270	2.705850	-0.402236
H	1.164160	1.708557	0.741378

Complex 19

Absolute Energy = -1472.197307 Hartrees

Cartesian Coordinates

V	0.4809	0.5694	-0.9697
O	0.8750	1.1169	-2.4192
O	0.3655	0.4828	2.4567
O	0.7875	1.9983	0.4450
O	-1.0746	0.1877	-0.8894
O	1.6167	-0.7619	-0.3761
N	1.2496	-1.4625	0.7867
C	1.5433	-2.7200	0.6881
N	2.0921	-3.3201	-0.3906
H	2.2935	-2.7632	-1.2090
H	2.2868	-4.3067	-0.3946
H	-0.5619	0.3253	2.6744
H	0.6742	-0.3511	1.9890
H	0.3381	2.8492	0.3750
H	0.5705	1.5580	1.3432
H	1.3268	-3.3378	1.5592

Complex 20

Absolute Energy = -1472.192635 Hartrees

Cartesian Coordinates

V	0.0751	1.0538	-0.4499
---	--------	--------	---------

O	-0.5058	0.6976	-1.9085
O	-0.9234	-1.0980	2.5194
O	-1.6393	0.5360	0.6170
N	2.2535	-0.5000	0.7872
C	2.8725	0.0603	-0.1783
O	0.1821	2.6361	-0.2210
H	-0.8438	-0.8132	3.4374
H	-0.0355	-0.9667	2.1055
H	3.9430	-0.0995	-0.2945
O	0.9182	-0.2294	0.8224
H	-2.3153	0.1601	0.0398
H	-1.5240	-0.0702	1.4095
N	2.1382	0.8946	-1.1069
H	2.5218	1.8386	-1.1573
H	2.1471	0.5117	-2.0531

Complex 21

Absolute Energy = -1548.668264 Hartrees

Cartesian Coordinates

V	0.163038	0.937158	-0.486461
O	-0.483931	0.722657	-1.962446
O	-0.839831	-1.058608	2.730425
O	-1.534546	0.216641	0.451738
N	2.355881	-0.518503	0.769037
C	2.921675	0.053410	-0.284738
N	2.142814	0.770604	-1.050483
H	2.580414	1.236547	-1.835079
O	0.124044	2.481547	-0.094747
H	-0.864432	-0.504997	3.520098

H	0.029177	-0.888886	2.305320
H	3.991320	-0.102463	-0.437300
H	2.783924	-1.251064	1.319383
O	1.000637	-0.372172	0.880139
H	-2.140822	-0.228683	-0.192734
H	-1.474892	-0.292505	1.294918
O	-2.767109	-0.734031	-1.723045
H	-2.003341	-0.277955	-2.141669
H	-3.550717	-0.273495	-2.045955

Complex 22

Absolute Energy = -1548.666049 Hartrees

Cartesian Coordinates

V	-2.0884	-0.6701	0.0672
O	-2.6011	-0.6710	-1.4606
O	-1.3719	1.6328	2.6976
O	-2.3515	1.4460	0.2394
O	-3.2575	-1.1018	1.0745
O	-0.0798	-2.8274	0.7424
N	-1.1095	-2.5288	-0.1525
C	-1.3969	-3.5049	-0.9482
N	-0.7768	-4.7025	-0.9411
H	-0.0389	-4.8787	-0.2751
H	-1.0393	-5.4203	-1.5950
H	-1.8706	1.2526	3.4310
H	-0.8609	0.8840	2.3077
H	-3.2452	1.7148	-0.0068
H	-2.1859	1.7076	1.1845
H	-2.1970	-3.3232	-1.6625

O -0.3825 -0.2296 0.9531

H 0.1054 -1.9223 1.0985

H 0.2780 0.2443 0.4323

Complex 23

Absolute Energy = -1548.664163 Hartrees

Cartesian Coordinates

V -0.095822 0.436709 -0.902649

O 0.204145 0.515865 -2.467487

O 1.745260 0.813882 2.289002

O -1.528982 1.109467 -0.536229

O 0.919122 -0.844467 0.278812

N -0.127088 -1.468842 -0.359807

C -0.263814 -2.744156 -0.271577

N 0.537808 -3.526901 0.498559

H 1.399713 -3.115982 0.834085

H 0.513489 -4.526153 0.370550

O 1.087225 1.910587 -0.099852

H 1.218165 1.026015 3.068660

H 1.362857 -0.005390 1.917340

H -1.090217 -3.200816 -0.811844

H 0.529529 2.728281 -0.016314

H 1.405630 1.673493 0.807701

O -0.890307 3.711776 0.082912

H -1.446098 2.935476 -0.145745

H -1.051815 4.360955 -0.612118

Complex 24

Absolute Energy = -1548.656813 Hartrees

Cartesian Coordinates

V	0.1255	0.9275	-0.4831
O	-0.3892	0.5091	-1.9690
O	-0.8391	-1.1228	2.5871
O	-1.5694	0.3341	0.4963
N	2.3644	-0.4027	0.8841
C	2.9762	0.1441	-0.0934
O	0.1623	2.5143	-0.2934
H	-0.8098	-0.7569	3.4788
H	0.0487	-0.9628	2.1935
H	4.0590	0.0597	-0.1661
O	1.0129	-0.2352	0.8561
H	-2.1977	-0.1105	-0.1290
H	-1.4715	-0.2033	1.3286
O	-2.8469	-0.7000	-1.6155
H	-2.0563	-0.3711	-2.0914
H	-3.5966	-0.2295	-1.9991
N	2.2131	0.8600	-1.0939
H	2.5320	1.8229	-1.2014
H	2.2725	0.4151	-2.0107

Figure 3.11, reactant

Absolute Energy = -454.595311445 Hartrees

Cartesian Coordinates

N	-0.8180	-1.5483	0.0757
C	-0.2680	-1.4795	-1.0963
H	0.2683	-2.3811	-1.3967
O	-1.5130	-0.3258	0.3504
N	-0.3102	-0.4497	-1.9733
H	-0.5179	0.4986	-1.6431

H	0.2850	-0.5110	-2.7850
O	-0.2304	2.3209	-1.0678
H	0.2968	2.1343	-0.2596
O	1.2991	1.7224	1.1980
H	2.2234	1.9945	1.1830
H	1.3084	0.7834	1.4855
H	-1.0401	2.7295	-0.7413
H	0.6060	-1.3848	1.3434
O	1.3245	-0.9925	1.8880
H	1.1798	-1.3099	2.7863
H	-1.9858	-0.5317	1.1651

Figure 3.11, transition state

Absolute Energy = -454.549629140 Hartrees

Cartesian Coordinates

N	2.2915	-0.5455	0.6658
C	2.8815	-0.4352	-0.5225
H	3.6606	-1.1846	-0.6829
O	1.3106	0.4317	0.9307
N	2.5875	0.4517	-1.4404
H	2.3530	1.4878	-1.0801
H	3.1431	0.3915	-2.2850
O	2.5970	2.7835	-0.4683
H	3.3523	2.4643	0.2897
O	4.2445	1.9274	1.1332
H	5.0667	2.4275	1.1452
H	4.2547	0.7599	1.9506
H	1.8441	3.1304	0.0238
H	2.9753	-0.6272	1.5035

O 4.1452 -0.1916 2.4288
H 3.9968 -0.0245 3.3657
H 0.5740 -0.0783 1.2966

Figure 3.11, product

Absolute Energy = -454.583306000 Hartrees

Cartesian Coordinates

N -0.7500 -1.3440 0.1420
C -0.1067 -1.2667 -1.0683
H 0.7131 -1.9988 -1.1097
O -1.6946 -0.3243 0.4017
N -0.4450 -0.4845 -2.0301
H -0.5205 1.2725 -1.3983
H 0.1372 -0.6604 -2.8478
O -0.3508 2.1366 -0.9504
H 0.8758 1.8152 0.2606
O 1.5461 1.5898 0.9529
H 2.3727 1.9837 0.6548
H 1.4802 -0.0053 1.7023
H -1.1701 2.3119 -0.4716
H -0.1208 -1.4225 0.9537
O 1.3519 -0.9252 2.0335
H 1.3425 -0.8568 2.9944
H -2.5498 -0.7508 0.2539

Figure 3.12, reactant

Absolute Energy = -1701.56628149 Hartrees

Cartesian Coordinates

V -1.3462 -0.3894 -0.6491
O -1.9510 -1.0907 -1.9582

N	0.9005	-1.7244	0.6227
C	1.4462	-1.2163	-0.4140
O	-1.6296	1.2039	-0.6279
H	2.5040	-1.3919	-0.6035
O	-0.4237	-1.4174	0.7536
N	0.6869	-0.3230	-1.2480
H	1.0798	0.6552	-1.0817
H	0.8034	-0.5375	-2.2384
O	1.8512	2.0389	-0.5964
H	2.3684	1.8632	0.2163
O	3.2916	1.2385	1.6720
H	4.2155	1.4347	1.8583
H	3.0869	0.4062	2.1511
H	1.1792	2.7160	-0.3647
H	1.9968	-1.5886	2.2088
O	2.6299	-1.2043	2.8515
H	2.1768	-1.2180	3.7024
O	-0.3758	3.5933	-0.0354
H	-0.9682	2.8307	-0.2093
H	-0.6767	4.2933	-0.6256
O	-2.8693	-1.0575	0.6943
H	-3.5380	-1.5745	0.2244
H	-2.3783	-1.6687	1.2724

Figure 3.11, transition state 1

Absolute Energy = -1701.55792713 Hartrees

Cartesian Coordinates

V	-1.2429	-0.3415	-0.6726
O	-1.9605	-1.1591	-1.8504

N	1.0052	-1.7109	0.5571
C	1.4613	-1.2724	-0.5628
O	-1.5684	1.2590	-0.7595
H	2.4657	-1.5744	-0.8657
O	-0.2917	-1.2678	0.7732
N	0.7245	-0.3361	-1.2938
H	1.2465	0.9227	-0.8336
H	0.9123	-0.3801	-2.2934
O	1.7084	1.8642	-0.4406
H	2.2077	1.6745	0.4171
O	2.9935	1.3376	1.7644
H	3.9387	1.5165	1.8172
H	2.8520	0.4498	2.1884
H	0.9849	2.5600	-0.2749
H	2.0195	-1.5336	2.0454
O	2.5941	-1.1346	2.7480
H	2.1175	-1.2542	3.5774
O	-0.2994	3.4310	-0.0411
H	-0.9486	2.7093	-0.2731
H	-0.4854	4.1656	-0.6371
O	-2.7089	-0.8670	0.8241
H	-3.3882	-1.4145	0.4070
H	-2.1565	-1.4569	1.3710

Figure 3.11, intermediate

Absolute Energy = -1701.55812653 Hartrees

Cartesian Coordinates

V	-1.2262	-0.3433	-0.6988
O	-1.9891	-1.1878	-1.8282

N	1.0319	-1.6868	0.5495
C	1.4667	-1.2838	-0.5960
O	-1.5470	1.2620	-0.8217
H	2.4650	-1.5990	-0.9070
O	-0.2668	-1.2297	0.7610
N	0.7168	-0.3887	-1.3417
H	1.2897	1.0092	-0.7902
H	0.9287	-0.4112	-2.3360
O	1.7059	1.8836	-0.3881
H	2.2018	1.6679	0.4796
O	2.9568	1.3501	1.7873
H	3.9042	1.5224	1.8230
H	2.8162	0.4532	2.2034
H	0.9469	2.5688	-0.2239
H	2.0147	-1.5016	2.0101
O	2.5816	-1.1104	2.7300
H	2.1000	-1.2511	3.5531
O	-0.3025	3.3733	-0.0136
H	-0.9439	2.6484	-0.2898
H	-0.4691	4.1253	-0.5938
O	-2.6740	-0.8071	0.8421
H	-3.3572	-1.3666	0.4478
H	-2.1095	-1.3834	1.3917

Figure 3.11, transition state 2

Absolute Energy = -1701.55148707 Hartrees

Cartesian Coordinates

V	0.1654	0.5355	-0.9477
O	-0.7239	-0.3468	-1.9529

N	2.5005	-0.6880	0.3052
C	2.8637	-0.3965	-0.9103
O	-0.1179	2.1347	-1.1491
H	3.8595	-0.7090	-1.2338
O	1.1972	-0.2445	0.5388
N	2.0360	0.3290	-1.6991
H	2.7714	2.0533	-0.9095
H	2.2821	0.3582	-2.6823
O	3.1593	2.8113	-0.4175
H	3.6910	2.4751	0.7332
O	4.1864	2.2173	1.7078
H	5.1242	2.4423	1.6656
H	4.0568	1.1532	2.0413
H	2.4200	3.4898	-0.3513
H	3.3327	-0.4987	1.5187
O	3.9061	-0.1167	2.3389
H	3.3989	-0.2666	3.1463
O	1.0344	4.3341	-0.2652
H	0.4561	3.5852	-0.5820
H	0.8767	5.0657	-0.8725
O	-1.2034	0.2047	0.7015
H	-1.8996	-0.3767	0.3656
H	-0.6172	-0.3393	1.2601

Figure 3.11, product

Absolute Energy = -1701.58206042 Hartrees

Cartesian Coordinates

V	-1.5381	-0.6618	-0.8354
O	-2.6368	-1.6383	-1.4788

N	0.9651	-1.4151	0.3392
C	1.1923	-1.4926	-0.9522
O	-1.7168	0.8539	-1.3899
H	2.1991	-1.7540	-1.2805
O	-0.3145	-1.0832	0.6876
N	0.1719	-1.2552	-1.7567
H	2.7870	2.9542	-0.3137
H	0.3430	-1.3509	-2.7491
O	2.1661	2.8944	0.4202
H	2.5892	1.9623	1.7996
O	2.8792	1.4451	2.5906
H	3.5159	2.0025	3.0497
H	2.9849	-0.2613	2.4490
H	1.2701	2.9327	0.0027
H	1.6729	-1.4394	1.0958
O	2.9425	-1.2352	2.2794
H	2.8544	-1.6495	3.1448
O	-0.1889	3.0468	-0.8859
H	-0.7455	2.2519	-1.0725
H	-0.8099	3.7644	-0.7218
O	-2.6860	-0.4784	0.9836
H	-3.4160	-1.1109	0.9330
H	-2.0769	-0.7892	1.6746

Complex S1

Absolute Energy = -1513.230730 Hartrees

Cartesian Coordinates

V	2.298649	9.569206	12.238981
O	0.404562	8.835654	12.575136

O	1.378086	9.880853	14.220310
O	3.620293	10.923347	12.964298
O	3.756400	12.553923	10.878925
O	2.113916	10.307843	10.819722
O	3.160702	8.253082	12.054246
C	0.375497	9.243589	13.771820
H	-0.504680	9.046356	14.404398
H	3.132474	11.922560	10.468670
H	3.346379	13.422887	10.795687
H	3.575196	11.216893	13.910383
H	3.768011	11.686184	12.345867
H	2.388369	10.931344	15.512651
O	3.168166	11.514745	15.530055
H	3.734982	11.191934	16.240749

Complex S2

Absolute Energy = -1513.233497 Hartrees

Cartesian Coordinates

V	-1.206642	0.513868	0.560514
O	-1.107426	-1.524236	0.252912
O	0.784945	0.439194	0.164409
O	1.396377	-1.731358	0.063294
C	1.645885	-0.517417	0.043888
H	-0.123170	-1.805565	0.198953
H	-1.549698	-2.028313	0.946997
H	2.690515	-0.182395	-0.090388
O	-0.590366	2.526283	0.666158
H	0.311452	2.585571	0.320249
H	-1.188371	3.098209	0.109724

O	-2.362890	0.866093	-0.507223
O	-1.829352	0.421887	2.021768
O	-2.410615	3.577487	-0.942397
H	-2.726038	2.654511	-1.030076
H	-3.155906	4.079381	-0.590682

Complex S3

Absolute Energy = -1513.218789 Hartrees

Cartesian Coordinates

V	-0.553966	0.596639	-0.376712
O	-0.321587	0.691419	-1.953707
O	-0.259843	0.651189	1.986457
O	-1.994439	1.203531	-0.064929
O	1.395137	-0.820188	0.192076
C	0.492631	-1.692706	0.164818
O	0.803267	2.197874	-0.077219
H	-0.992171	1.198187	2.298541
H	0.556572	0.981417	2.391405
H	1.150093	2.422447	-0.951305
H	1.568949	1.960131	0.500128
O	2.532610	1.069490	1.659882
H	3.458798	1.152339	1.911143
H	2.414773	0.196584	1.222867
O	-0.720118	-1.383034	-0.080785
H	0.721094	-2.756618	0.348339

Appendix C: Supporting Information for Theoretical Study of Oxovanadium(IV) Complexation with Formamidoximate: Implications for the Design of Uranyl-Selective Adsorbents

Table A.7. The absolute electronic energies and relative electronic energies of R/R-CCSD(T)/aug-cc-pVDZ//B3LYP/aug-cc-pVDZ (R/R-CCSD(T)//B3LYP) calculations carried out in the restricted formalism in which only valence and valence together with sub-valence 3s and 3p electrons on vanadium are correlated

Complex	Valence ^a	Relative Energy ^b	Valence and Sub-valence ^a	Relative Energy ^b
1	-1399.105282	0.0	-1399.364345	0.0
2	-1399.099763	3.5	-1399.357539	4.3
3	-1399.060298	28.2	-1399.325690	24.2
4	-1394.720459	0.0	-1394.981632	0.0
5	-1394.691347	18.3	-1394.952842	18.1
6	-1394.700297	12.6	-1394.960551	13.2
7	-1394.676550	27.6	-1394.937176	27.9
8	-1471.025469	0.0	-1471.287559	0.0
9	-1471.023134	1.5	-1471.285994	1.0
10	-1471.014219	7.0	-1471.275375	7.6
11	-1470.995553	18.8	-1471.257677	18.8
12	-1471.004862	12.9	-1471.265855	13.6
13	-1470.998022	17.2	-1471.261229	16.5
14	-1471.003603	13.7	-1471.268447	12.0
15	-1471.005850	12.3	-1471.265343	13.9

^aThese energies are given in units of Hartrees.

^bThese energies are given in units of kcal/mol.

Table A.8. The relative Gibbs free energies of 1-15 in aqueous solution computed at the R/R-CCSD(T)//B3LYP level of theory using the IEF-PCM and SMD solvation models in units of kcal/mol.^a

Complex	SMD	IEF-PCM
1	-1.4	0.0
2	0.0	2.9
3	32.9	27.4
4	0.0	0.0
5	6.9	10.5
6	8.4	11.5
7	23.9	24.4
8	0.0	0.0
9	5.6	3.1
10	5.6	7.6
11	8.0	10.5
12	9.5	11.6
13	10.2	11.6
14	12.0	12.3
15	15.6	16.8

^aSolvent corrections are obtained at the B3LYP/6-31+G**//B3LYP/aug-cc-pVDZ level.

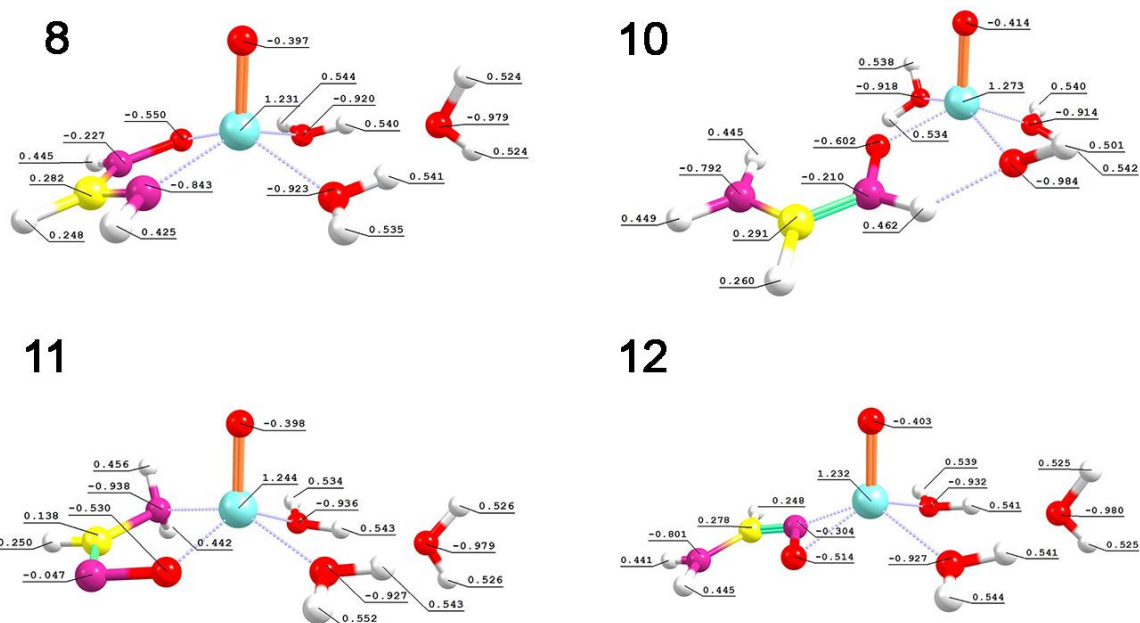


Figure A.6. Natural charge distribution in complexes 8, 10, 11, and 12 obtained via natural population analysis (NPA) at the B3LYP/6-31G(d) level of theory.

Table A.9. The zero-point energies (ZPE) with thermal corrections and the solvation free energies obtained with the IEF-PCM and SMD solvation models for all 15 VO²⁺ complexes discussed in the manuscript.^a

Complex	ZPE with Thermal Corrections (Hartrees)	IEF-PCM (kcal/mol)	SMD (kcal/mol)
1	0.091533	-185.2	-223.4
2	0.092149	-187.0	-229.4
3	0.086767	-179.0	-211.8
4	0.070572	-58.4	-80.5
5	0.070319	-65.7	-91.5
6	0.067637	-58.2	-83.4
7	0.067708	-60.0	-82.8
8	0.093142	-56.4	-78.6
9	0.092963	-54.1	-73.9
10	0.091592	-55.5	-79.7
11	0.092269	-64.1	-88.8
12	0.090250	-56.6	-81.0
13	0.091723	-60.4	-84.1
14	0.090095	-54.2	-76.7
15	0.092370	-53.0	-76.4

^aZPE with thermal corrections are obtained at the B3LYP/6-311++G** level. Solvent corrections are obtained at the B3LYP/6-31+G*//B3LYP/aug-cc-pVDZ level.

Table A.10. The complexation free energies for reactions (1) UO₂²⁺ and (2) UO₂²⁺ obtained with the B3LYP//B3LYP//IEF-PCM(UFF), MO6//B3LYP//IEF-PCM(UFF) , and CCSD(T)//B3LYP//IEF-PCM(UFF) levels of theory.

Method	$\Delta G_{\text{aq}}(1) \text{ UO}_2^{2+}$, kcal/mol	$\Delta G_{\text{aq}}(2) \text{ UO}_2^{2+}$, kcal/mol
B3LYP	-54.7	-49.0
M06	-51.2	-50.2
CCSD(T)	-38.0	-38.7

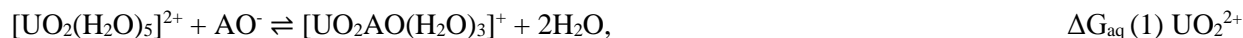


Table A.11. The complexation free energies for reactions (1) VO^{2+} , (2) VO^{2+} , (3) VO^{2+} , and (4) VO^{2+} obtained with the B3LYP//B3LYP//IEF-PCM(UFF), MO6//B3LYP//IEF-PCM(UFF) , and R/R-CCSD(T)//B3LYP//IEF-PCM(UFF) levels of theory.

Method	$\Delta G_{\text{aq}}(1) \text{VO}^{2+}$, kcal/mol	$\Delta G_{\text{aq}}(2) \text{VO}^{2+}$, kcal/mol	$\Delta G_{\text{aq}}(3) \text{VO}^{2+}$, kcal/mol	$\Delta G_{\text{aq}}(4) \text{VO}^{2+}$, kcal/mol
B3LYP	-68.5	-66.2	-68.6	-66.3
M06	-67.4	-62.7	-72.3	-67.6
R/R-CCSD(T)	-61.4	-56.9	-68.8	-64.3

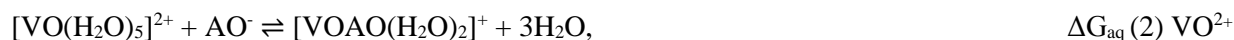


Table A.12. The complexation free energies for reactions (1) VO_2^+ , (2) VO_2^+ , (3) VO_2^+ , and (4) VO_2^+ obtained with the B3LYP//B3LYP//IEF-PCM(UFF), MO6//B3LYP//IEF-PCM(UFF) , and CCSD(T)//B3LYP//IEF-PCM(UFF) levels of theory.

Method	$\Delta G_{\text{aq}}(1) \text{VO}_2^+$, kcal/mol	$\Delta G_{\text{aq}}(2) \text{VO}_2^+$, kcal/mol	$\Delta G_{\text{aq}}(3) \text{VO}_2^+$, kcal/mol	$\Delta G_{\text{aq}}(4) \text{VO}_2^+$, kcal/mol
B3LYP	-60.4	-61.5	-54.9	-56.0
M06	-58.1	-58.2	-53.7	-53.8
CCSD(T)	-54.4	-53.4	-55.6	-54.6



Optimized Geometries and Absolute Energies Obtained at the B3LYP/aug-cc-pVDZ Level of Theory

Complex 1

Electronic Energy = -1401.063525 Hartrees

Cartesian Coordinates

V	-0.000008	0.000416	-0.005745
O	1.821254	1.027347	-0.126543
H	2.353603	1.258909	0.652244
H	2.279992	1.351502	-0.917303

O	0.011326	-0.125530	1.537418
O	-1.824046	-0.995793	-0.264737
H	-2.294574	-1.188240	-1.090806
H	-2.345695	-1.350377	0.473963
O	1.000959	-1.766603	-0.513770
H	0.589104	-2.635588	-0.373499
H	1.946829	-1.880814	-0.322140
O	-1.005795	1.825399	-0.206577
H	-1.948608	1.906093	0.014872
H	-0.590855	2.660859	0.065937
O	-0.017071	0.184812	-2.268690
H	0.356080	-0.444343	-2.905561
H	-0.399130	0.908173	-2.789699

Complex 2

Electronic Energy = -1401.066715 Hartrees

Cartesian Coordinates

V	0.001246	-0.002922	0.012698
O	-0.369325	0.072688	-1.479382
O	1.476042	-1.419216	0.101817
H	1.432999	-2.244224	-0.409311
H	2.428482	-1.132958	0.140263
O	-1.339832	1.453099	0.703099
H	-1.577223	1.706886	1.609676
H	-1.896034	1.967801	0.094395
O	1.492560	1.283790	0.468588
H	1.414602	2.250711	0.488958
H	2.451909	1.025152	0.401878
O	-1.194716	-1.371019	0.975644

H	-2.166582	-1.355859	0.958706
H	-0.922693	-2.242913	1.306962
O	3.792682	-0.055979	0.272007
H	4.383390	-0.153683	1.037915
H	4.384366	0.036888	-0.493851

Complex 3

Electronic Energy = -1401.044666 Hartrees

Cartesian Coordinates

V	0.015476	0.000075	-0.000041
O	0.038575	-1.729017	-0.000319
H	0.055015	-2.698851	0.000355
O	-0.007257	1.729160	0.000725
H	-0.016584	2.699089	0.001990
O	0.027602	0.000872	-2.082190
H	0.020234	0.788335	-2.647000
H	0.032610	-0.786197	-2.647571
O	0.007906	-0.000622	2.082337
H	-0.018426	0.786140	2.647546
H	0.012312	-0.788108	2.647135
O	-2.066461	-0.027671	-0.009712
H	-2.620701	-0.822647	-0.009175
H	-2.642044	0.751926	-0.019801
O	2.097732	0.027740	0.009556
H	2.652152	0.822476	0.020612
H	2.673156	-0.751999	0.008355

Complex 4

Electronic Energy = -1396.734134 Hartrees

Cartesian Coordinates

V	0.008130	0.002186	0.000611
O	0.949824	1.762340	-0.649072
H	1.868932	1.996514	-0.457999
H	0.409152	2.563243	-0.565591
N	-1.441369	-1.289524	-0.568224
C	-2.653471	-0.756044	-0.500088
N	-2.708279	0.531264	-0.236521
H	-3.546986	1.092232	-0.142541
O	-1.518691	1.176434	-0.069967
H	-3.588795	-1.298131	-0.646544
H	-1.425422	-2.289138	-0.739435
O	0.463703	-0.333108	1.462554
O	1.532552	-1.011446	-1.095830
H	2.086982	-1.640625	-0.611763
H	1.479268	-1.313290	-2.013131

Complex 5

Electronic Energy = -1396.700184 Hartrees

Cartesian Coordinates

V	0.001373	-0.006043	0.008932
O	-0.373880	0.101322	-1.509421
O	-1.243931	-1.546220	0.760637
H	-1.961445	-1.894181	0.209250
H	-0.678701	-2.302193	0.999901
O	1.310085	-1.250087	0.465283
N	2.643039	-0.917266	0.512493
C	2.875400	0.317866	0.318614
H	3.897974	0.691120	0.336644
N	1.760816	1.241753	0.074496

H	1.800502	2.007060	0.753517
H	1.876622	1.683481	-0.843153
O	-1.154069	1.261529	1.230921
H	-1.397174	2.176276	1.027661
H	-1.852079	0.894969	1.794828

Complex 6

Electronic Energy = -1396.718978 Hartrees

Cartesian Coordinates

V	0.005406	-0.011851	0.023235
O	-0.466127	-0.025148	-1.470470
O	1.583037	-0.920461	0.489531
N	1.893078	0.446338	0.367084
C	3.141563	0.773459	0.226459
N	4.155671	-0.094058	0.288898
H	3.968970	-1.082134	0.401643
H	5.109637	0.218766	0.191837
H	3.362094	1.828945	0.072920
O	-1.234106	-1.480981	0.911695
H	-1.845321	-1.947412	0.320808
H	-0.772168	-2.160241	1.427995
O	-1.013954	1.416820	1.158716
H	-0.784127	2.356436	1.178944
H	-1.926817	1.328051	1.467788

Complex 7

Electronic Energy = -1396.688553 Hartrees

Cartesian Coordinates

V	-0.004272	-0.001830	0.002360
O	-0.400062	0.038422	-1.503277

O	0.029454	-1.957906	0.740915
H	0.789829	-2.546484	0.634106
H	-0.751588	-2.503816	0.910161
N	2.053476	0.189964	0.214366
C	1.860774	1.503401	0.290083
N	0.620843	1.781120	0.702912
H	0.346961	2.757518	0.696202
H	2.617422	2.229635	-0.029215
O	3.141795	-0.173482	-0.589369
H	3.635937	-0.829318	-0.074361
O	-1.920631	0.077457	0.951825
H	-2.693352	0.176933	0.374913
H	-2.057357	0.668904	1.707351

Complex 8

Electronic Energy = -1473.207345 Hartrees

Cartesian Coordinates

V	0.049705	-0.105520	-0.262763
O	-1.118815	0.658972	-1.820547
O	-1.533301	-1.463127	-0.139751
N	2.406403	-1.570128	-0.167761
C	2.756833	-0.535626	-0.901725
N	1.795699	0.321823	-1.210645
H	2.105352	1.122893	-1.749746
O	-0.107789	0.892569	0.938951
H	3.800184	-0.447005	-1.207885
H	3.015773	-2.313593	0.151371
O	1.093161	-1.661474	0.187282
H	-1.436456	-2.243055	0.423844

H	-2.084023	0.697022	-1.640647
H	-0.870993	1.426774	-2.350988
H	-2.453897	-1.140672	-0.117747
O	-3.639797	0.239116	-0.785924
H	-3.984933	0.867757	-0.134829
H	-4.405204	-0.029327	-1.314490

Complex 9

Electronic Energy = -1473.198148 Hartrees

Cartesian Coordinates

V	0.047198	0.020637	-0.142574
O	1.084373	1.895060	-0.385668
H	1.879467	2.010625	0.155218
H	0.488464	2.625653	-0.154598
N	-1.440046	-1.313634	-0.569685
C	-2.639123	-0.776655	-0.417286
N	-2.684271	0.524048	-0.207632
H	-3.519964	1.074391	-0.051541
O	-1.492861	1.189929	-0.151564
H	-3.582911	-1.323245	-0.456209
H	-1.436074	-2.319962	-0.693095
O	0.452630	-0.291321	1.344870
O	1.744486	-1.102269	-0.852229
H	2.192158	-1.743709	-0.285275
H	1.859059	-1.352388	-1.778255
O	0.251686	0.262494	-2.547140
H	0.600756	1.099321	-2.883926
H	-0.531526	0.065426	-3.077909

Complex 10

Electronic Energy = -1473.200351 Hartrees

Cartesian Coordinates

V	0.225299	-0.199028	0.162584
O	0.008070	1.217700	1.402733
H	0.440978	2.068879	1.266709
O	0.549324	0.329590	-1.278078
O	-1.679938	-0.598712	0.422282
N	-2.393187	0.360720	1.067767
C	-3.692597	0.363411	1.032703
N	-4.406119	-0.552879	0.380798
H	-3.937077	-1.269685	-0.156549
H	-5.413559	-0.506033	0.366544
H	-4.201244	1.156936	1.576559
O	1.981190	-0.589837	1.238906
H	2.730822	-1.160563	1.025183
H	2.255020	0.077102	1.884070
O	0.309906	-2.327035	-0.222011
H	0.502954	-2.560303	-1.142037
H	-0.485633	-2.819749	0.028126
H	-1.787310	1.073190	1.513412

Complex 11

Electronic Energy = -1473.173030 Hartrees

Cartesian Coordinates

V	-0.032103	-0.045633	0.323779
O	-0.622584	0.062573	-1.125817
O	-1.052377	-1.519813	1.366362
H	-0.705672	-2.423295	1.340411
O	1.361537	-1.281270	0.488878

N	2.656696	-0.928369	0.218870
C	2.834421	0.319149	0.043202
H	3.828654	0.708396	-0.167939
N	1.690884	1.237282	0.133242
H	1.869205	1.930269	0.865612
H	1.609723	1.768988	-0.738222
O	-1.091708	1.245175	1.594975
H	-1.216530	2.186488	1.415467
H	-1.941436	0.892903	1.953884
H	-1.973899	-1.498297	1.677113
O	-3.296684	-0.187802	2.367558
H	-4.133019	-0.095658	1.887580
H	-3.545407	-0.272187	3.299845

Complex 12

Electronic Energy = -1469.163298 Hartrees

Cartesian Coordinates

V	-0.216816	-0.102063	0.158265
O	0.491034	1.683054	-0.659483
H	0.130821	2.551921	-0.438989
O	0.222655	-0.169612	1.661854
O	1.294367	-0.970196	-0.976559
O	-1.536238	-1.329162	-0.399350
N	-2.163628	-0.098153	-0.161856
C	-3.457116	-0.075908	-0.092721
N	-4.235026	-1.144938	-0.306487
H	-3.927601	0.879375	0.134680
H	-5.238782	-1.074274	-0.246801
H	-3.811667	-2.045443	-0.488455

H	1.387416	-1.928856	-1.056751
H	2.171378	-0.542912	-1.039302
H	1.459777	1.762117	-0.796270
O	3.163877	1.081692	-1.008014
H	3.785789	1.203719	-0.275355
H	3.657258	1.322938	-1.805605

Complex 13

Electronic Energy = -1473.167667 Hartrees

Cartesian Coordinates

V	0.085216	0.008245	0.216257
O	-0.443075	0.242406	-1.249330
O	-1.186767	-1.623200	0.755524
H	-1.856694	-1.854339	0.094623
H	-0.635233	-2.416302	0.864140
O	1.417652	-1.314778	0.307622
N	2.744538	-0.980111	0.200487
C	2.970105	0.267149	0.072149
H	3.995414	0.620098	-0.027464
N	1.860254	1.222598	0.049304
H	2.001362	1.937184	0.767032
H	1.849808	1.719342	-0.845760
O	-1.283861	1.484838	1.055451
H	-1.785605	1.957547	0.374864
H	-1.915729	1.251747	1.750268
O	0.592854	0.065083	2.520819
H	0.393525	0.583826	3.310578
H	1.199035	-0.639532	2.789833

Complex 14

Electronic Energy = -1473.183367 Hartrees

Cartesian Coordinates

V	-0.398213	-0.004451	0.004421
O	0.423859	1.974773	-0.300323
H	1.368139	2.055253	-0.097502
H	-0.008914	2.697160	0.178127
O	-0.141715	-0.106919	1.550822
O	1.492797	-0.871483	-0.486583
O	-0.115574	0.110402	-2.385080
H	-0.008968	0.904922	-2.924630
H	-0.842794	-0.398408	-2.771656
O	-1.695458	-1.258959	-0.600414
N	-2.344216	-0.036979	-0.372214
C	-3.626818	-0.065111	-0.176598
N	-4.375288	-1.169592	-0.286215
H	-4.116247	0.878727	0.058945
H	-5.370229	-1.138148	-0.126140
H	-3.926949	-2.062948	-0.443710
H	1.613081	-1.201258	-1.388640
H	1.887609	-1.503080	0.131090

Complex 15

Electronic Energy = -1473.189867 Hartrees

Cartesian Coordinates

V	-0.278468	0.251391	0.296537
O	0.857132	0.934432	-0.964376
H	1.803086	1.119442	-0.970286
O	0.110684	-0.176336	1.761809

N	-2.307192	0.070391	-0.127639
O	-3.210530	1.110866	0.173250
H	-2.652550	1.865522	0.417704
C	-2.954013	-0.969362	-0.588773
N	-4.272451	-1.026477	-0.761440
H	-4.855843	-0.233264	-0.528266
H	-4.705840	-1.860797	-1.127535
H	-2.355852	-1.840001	-0.846751
O	0.072740	-1.678301	-0.564563
H	0.700257	-1.595863	-1.300247
H	0.443118	-2.326088	0.054276
H	-0.197277	2.906693	0.267999
O	-0.724264	2.310356	0.824311
H	-0.532339	2.533995	1.748490

Optimized Geometries and Absolute Energies Obtained at the M06/aug-cc-pVDZ Level of Theory

Complex 1

Electronic Energy = -1400.785971 Hartrees

Cartesian Coordinates

V	0.013274	-0.006523	0.033112
O	-0.337311	0.068807	-1.454320
O	1.470919	-1.413545	0.138850
H	1.419680	-2.253064	-0.343662
H	2.423595	-1.136214	0.162578
O	-1.319258	1.440158	0.712324
H	-1.580040	1.683104	1.613691
H	-1.861845	1.959739	0.097713
O	1.485338	1.284093	0.470358
H	1.390971	2.247566	0.505980

H	2.445147	1.044598	0.392609
O	-1.201833	-1.366826	0.946348
H	-2.171647	-1.334694	0.920202
H	-0.950050	-2.246453	1.268740
O	3.793599	-0.049437	0.249931
H	4.400956	-0.132939	1.001395
H	4.370379	0.029871	-0.525784

Complex 2

Electronic Energy = -1400.783378 Hartrees

Cartesian Coordinates

V	-0.000063	0.000550	-0.009274
O	1.808638	1.018367	-0.133102
H	2.340549	1.252458	0.643404
H	2.265263	1.340841	-0.923779
O	0.009721	-0.123309	1.526796
O	-1.810396	-0.988441	-0.271541
H	-2.277922	-1.179088	-1.097805
H	-2.333834	-1.342988	0.463963
O	0.992792	-1.749423	-0.511401
H	0.582971	-2.617908	-0.372764
H	1.937506	-1.862895	-0.321434
O	-0.996082	1.809211	-0.208814
H	-1.937187	1.890346	0.012989
H	-0.581743	2.643833	0.061705
O	-0.018500	0.183173	-2.248102
H	0.352656	-0.444321	-2.885020
H	-0.401006	0.905817	-2.766458

Complex 3

Electronic Energy = -1400.768933 Hartrees

Cartesian Coordinates

V	0.015673	0.000065	0.000078
O	0.038937	-1.723813	-0.000330
H	0.055155	-2.692364	-0.000186
O	-0.007304	1.723938	0.000739
H	-0.016797	2.692579	0.001475
O	0.026933	0.000849	-2.062841
H	0.020626	0.787798	-2.625794
H	0.032022	-0.785710	-2.626352
O	0.007698	-0.000646	2.063107
H	-0.016905	0.785647	2.626476
H	0.011336	-0.787616	2.626049
O	-2.047196	-0.027576	-0.009505
H	-2.599896	-0.821787	-0.009825
H	-2.620770	0.751649	-0.019010
O	2.078479	0.027651	0.009575
H	2.631304	0.821680	0.019895
H	2.652000	-0.751643	0.009252

Complex 4

Electronic Energy = -1396.425562 Hartrees

Cartesian Coordinates

V	0.002889	0.008940	-0.016122
O	0.944274	1.756064	-0.630574
H	1.875337	1.970280	-0.492894
H	0.424884	2.565695	-0.520872
N	-1.430263	-1.283779	-0.579369
C	-2.639101	-0.757124	-0.500133

N	-2.697002	0.526237	-0.233529
H	-3.538558	1.084979	-0.139353
O	-1.519430	1.169431	-0.081035
H	-3.576469	-1.299916	-0.640335
H	-1.414245	-2.283727	-0.751983
O	0.440000	-0.326958	1.441481
O	1.519430	-0.991642	-1.102571
H	2.090067	-1.585057	-0.595850
H	1.433714	-1.360518	-1.990406

Complex 5

Electronic Energy = -1396.390106 Hartrees

Cartesian Coordinates

V	0.007346	-0.006169	0.020701
O	-0.356465	0.083096	-1.491709
O	-1.232579	-1.530717	0.759034
H	-1.945455	-1.871829	0.200752
H	-0.674579	-2.290656	0.996720
O	1.314481	-1.247237	0.470453
N	2.629203	-0.913749	0.510646
C	2.858925	0.318750	0.317986
H	3.880318	0.698197	0.333848
N	1.744037	1.233434	0.079064
H	1.792929	2.009205	0.745106
H	1.848174	1.663874	-0.845732
O	-1.149738	1.247049	1.219209
H	-1.341893	2.181968	1.070871
H	-1.870174	0.884170	1.753654

Complex 6

Electronic Energy = -1396.408494 Hartrees

Cartesian Coordinates

V	0.020296	-0.005797	0.036625
O	-0.411146	-0.019690	-1.459096
O	1.589033	-0.907523	0.507831
N	1.889908	0.440979	0.378598
C	3.133077	0.768232	0.224102
N	4.139940	-0.099108	0.287820
H	3.942958	-1.085553	0.407973
H	5.096213	0.205097	0.182024
H	3.351059	1.823528	0.058831
O	-1.218138	-1.456871	0.917858
H	-1.855081	-1.893246	0.334236
H	-0.748729	-2.160335	1.389928
O	-1.020127	1.406306	1.137573
H	-0.832284	2.353383	1.138308
H	-1.900145	1.277127	1.514473

Complex 7

Electronic Energy = -1396.382969 Hartrees

Cartesian Coordinates

V	0.009069	0.001787	0.026997
O	-0.354809	0.061430	-1.477432
O	0.030855	-1.958034	0.701985
H	0.774865	-2.556400	0.557490
H	-0.746150	-2.490373	0.915890
N	2.044583	0.186281	0.253165
C	1.839250	1.497576	0.287341
N	0.614581	1.778053	0.726719

H	0.334114	2.752335	0.677217
H	2.580135	2.213747	-0.094014
O	3.105140	-0.185122	-0.555851
H	3.617450	-0.823333	-0.039223
O	-1.887244	0.081328	0.971929
H	-2.666755	0.121724	0.400229
H	-2.025857	0.729519	1.676531

Complex 8

Electronic Energy = -1472.864718 Hartrees

Cartesian Coordinates

V	-0.095300	-0.215700	-0.432500
O	-1.135900	0.455200	-2.089700
O	-1.565300	-1.670000	-0.419400
N	2.335100	-1.458600	-0.045200
C	2.675500	-0.405200	-0.750400
N	1.688100	0.358600	-1.178300
H	1.986500	1.179700	-1.694400
O	-0.493400	0.764900	0.721500
H	3.737200	-0.229800	-0.937600
H	2.966500	-2.146500	0.350800
O	1.014700	-1.659000	0.155400
H	-1.430700	-2.450300	0.133800
H	-2.076900	0.612000	-1.866600
H	-0.837400	1.134100	-2.704700
H	-2.468300	-1.322800	-0.298000
O	-3.385800	0.374200	-0.551700
H	-3.191800	0.941400	0.207900
H	-4.335000	0.455000	-0.704800

Complex 9

Electronic Energy = -1472.859209 Hartrees

Cartesian Coordinates

V	0.044400	0.030100	-0.173900
O	1.086600	1.878600	-0.396500
H	1.905300	1.964400	0.110000
H	0.516700	2.611500	-0.119700
N	-1.427500	-1.305200	-0.600200
C	-2.621200	-0.773400	-0.433300
N	-2.669000	0.524000	-0.221800
H	-3.506900	1.068700	-0.050700
O	-1.491100	1.188200	-0.177600
H	-3.566800	-1.320400	-0.462700
H	-1.424800	-2.311800	-0.725800
O	0.427900	-0.286000	1.311000
O	1.759600	-1.073400	-0.840600
H	2.180100	-1.702100	-0.242200
H	1.881100	-1.368700	-1.750300
O	0.217600	0.259100	-2.513500
H	0.545800	1.099800	-2.855200
H	-0.584100	0.060900	-3.011500

Complex 10

Electronic Energy = -1472.845063 Hartrees

Cartesian Coordinates

V	-0.293296	0.250433	0.294525
O	0.846187	0.929024	-0.950718
H	1.786970	1.122518	-0.971764
O	0.082516	-0.188055	1.751486

N	-2.300748	0.082230	-0.133804
O	-3.199169	1.109847	0.148598
H	-2.649742	1.871966	0.386780
C	-2.939584	-0.964809	-0.579667
N	-4.252411	-1.028409	-0.748852
H	-4.833628	-0.230129	-0.521726
H	-4.687056	-1.867056	-1.104861
H	-2.332870	-1.835625	-0.827197
O	0.050837	-1.655420	-0.571360
H	0.684394	-1.568085	-1.299091
H	0.419664	-2.298621	0.050389
H	-0.176914	2.877638	0.276609
O	-0.723959	2.289058	0.818986
H	-0.540793	2.500094	1.746167

Complex 11

Electronic Energy = -1472.827644 Hartrees

Cartesian Coordinates

V	-0.031028	-0.037467	0.376343
O	-0.651539	0.056889	-1.051315
O	-1.020615	-1.492530	1.433297
H	-0.678885	-2.395713	1.387976
O	1.355409	-1.281265	0.494192
N	2.624634	-0.933777	0.185049
C	2.802987	0.310016	0.006914
H	3.791421	0.699120	-0.234857
N	1.670072	1.226708	0.135951
H	1.879640	1.928650	0.850916
H	1.554360	1.749842	-0.737203

O	-1.054595	1.253611	1.646038
H	-1.137947	2.204550	1.511790
H	-1.916685	0.919983	1.982176
H	-1.949607	-1.469935	1.720213
O	-3.292680	-0.207025	2.293797
H	-4.084963	-0.134025	1.745560
H	-3.620278	-0.298734	3.197964

Complex 12

Electronic Energy = -1472.846567 Hartrees

Cartesian Coordinates

V	-0.143000	-0.023300	-0.162900
O	0.442600	1.728600	-1.094500
H	0.013500	2.584400	-0.980100
O	0.495800	-0.003500	1.263700
O	1.245700	-0.928600	-1.389400
O	-1.485100	-1.291700	-0.478300
N	-2.093500	-0.074800	-0.224200
C	-3.363600	-0.069900	0.015800
N	-4.128400	-1.159900	-0.042000
H	-3.822300	0.888800	0.257200
H	-5.118700	-1.111900	0.143300
H	-3.700900	-2.057600	-0.235100
H	1.276900	-1.886600	-1.501700
H	2.150300	-0.575300	-1.285100
H	1.413000	1.846800	-1.042900
O	3.019000	0.974000	-0.567300
H	3.089600	0.893100	0.394200
H	3.886800	1.270700	-0.868000

Complex 13

Electronic Energy = -1472.828114 Hartrees

Cartesian Coordinates

V	0.087500	0.011200	0.217300
O	-0.445900	0.236300	-1.239300
O	-1.183300	-1.594600	0.764500
H	-1.851800	-1.821000	0.103300
H	-0.640900	-2.391600	0.875500
O	1.414200	-1.315400	0.292700
N	2.724200	-0.975300	0.233600
C	2.949700	0.269900	0.112300
H	3.976900	0.629400	0.049200
N	1.841600	1.214500	0.045600
H	1.968100	1.950500	0.744200
H	1.841800	1.687200	-0.862700
O	-1.265700	1.469600	1.065600
H	-1.763700	1.952500	0.392100
H	-1.902300	1.215700	1.746000
O	0.612600	0.059900	2.472200
H	0.415900	0.574400	3.262300
H	1.224100	-0.641500	2.731800

Complex 14

Electronic Energy = -1472.842396 Hartrees

Cartesian Coordinates

V	-0.424000	0.011100	-0.044200
O	0.461600	1.951900	-0.330100
H	1.406300	1.976800	-0.123500
H	0.067400	2.678400	0.170500

O	-0.203100	-0.070000	1.501800
O	1.471400	-0.860000	-0.473600
O	-0.140500	0.150500	-2.363400
H	-0.017300	0.970200	-2.855600
H	-0.856400	-0.333800	-2.794600
O	-1.709100	-1.253300	-0.618300
N	-2.351500	-0.045100	-0.415800
C	-3.626200	-0.080000	-0.191800
N	-4.355500	-1.193300	-0.263400
H	-4.121400	0.865100	0.031400
H	-5.348500	-1.178600	-0.087200
H	-3.887400	-2.080600	-0.405400
H	1.615700	-1.232600	-1.352900
H	1.832600	-1.472800	0.180000

Complex 15

Electronic Energy = -1472.845063 Hartrees

Cartesian Coordinates

V	-0.293296	0.250433	0.294525
O	0.846187	0.929024	-0.950718
H	1.786970	1.122518	-0.971764
O	0.082516	-0.188055	1.751486
N	-2.300748	0.082230	-0.133804
O	-3.199169	1.109847	0.148598
H	-2.649742	1.871966	0.386780
C	-2.939584	-0.964809	-0.579667
N	-4.252411	-1.028409	-0.748852
H	-4.833628	-0.230129	-0.521726
H	-4.687056	-1.867056	-1.104861

H	-2.332870	-1.835625	-0.827197
O	0.050837	-1.655420	-0.571360
H	0.684394	-1.568085	-1.299091
H	0.419664	-2.298621	0.050389
H	-0.176914	2.877638	0.276609
O	-0.723959	2.289058	0.818986
H	-0.540793	2.500094	1.746167

Appendix D: Electronic Supplementary Information for Quantifying the Binding Strength of Salicylaldoxime-Uranyl Complexes Relative to Competing Salicylaldoxime-Transition Metal Ion Complexes in Aqueous Solution: A Combined Experimental and Computational Study

Table A.13. Acid dissociation and formation constants of the ligands and complexes discussed in this manuscript. The ligands ($L^{(I)}$) tabulated correspond to the ligands illustrated in **Figure 5.2**. The constants were obtained in aqueous solution at 25 °C and, unless otherwise noted, $I = 0.0$ M ionic strength.

Equilibrium	$\log \beta$	References
$H_2O \rightleftharpoons H^+ + OH^-$	14.00	29
$UO_2^{2+} + OH^- \rightleftharpoons UO_2(OH)^+$	8.75	49
$UO_2^{2+} + 2 OH^- \rightleftharpoons UO_2(OH)_2$	15.85	49
$UO_2^{2+} + 3 OH^- \rightleftharpoons UO_2(OH)_3^-$	21.8	49
$UO_2^{2+} + 4 OH^- \rightleftharpoons UO_2(OH)_4^{2-}$	23.6	49
$2 UO_2^{2+} + OH^- \rightleftharpoons (UO_2)_2(OH)^{3+}$	11.3	49
$2 UO_2^{2+} + 2 OH^- \rightleftharpoons (UO_2)_2(OH)_2^{2+}$	22.4	49
$3 UO_2^{2+} + 5 OH^- \rightleftharpoons (UO_2)_3(OH)_5^+$	54.4	49
$UO_2^{2+} + CO_3^{2-} \rightleftharpoons (UO_2)(CO_3)$	9.94	51
$UO_2^{2+} + 2 CO_3^{2-} \rightleftharpoons (UO_2)(CO_3)_2^{2-}$	16.61	51
$UO_2^{2+} + 3 CO_3^{2-} \rightleftharpoons (UO_2)(CO_3)_3^{4-}$	21.84	51
$L^{(I)}H_2 \rightleftharpoons H^+ + L^{(I)}H^-$	8.07	44 ^b and this work
$L^{(I)}H_2 \rightleftharpoons 2 H^+ + L^{(I)2-}$	19.35	44 ^b and this work
$UO_2^{2+} + L^{(I)2-} \rightleftharpoons UO_2 L^{(I)}$	16.1	This work
$UO_2^{2+} + 2 L^{(I)2-} \rightleftharpoons UO_2 L_2^{(I)2-}$	25.5	This work
$Cu^{2+} + HL^{(I)-} \rightleftharpoons Cu(HL^{(I)})^+$	10.12	57
$Cu^{2+} + 2 HL^{(I)-} \rightleftharpoons Cu(HL^{(I)})_2$	15.78	57
$Fe^{3+} + HL^{(I)-} \rightleftharpoons Fe(HL^{(I)})^{2+}$	9.38	58
$Fe^{3+} + 2 HL^{(I)-} \rightleftharpoons Fe(HL^{(I)})_2^+$	16.73	58
$L^{(II)}H_2 \rightleftharpoons H^+ + L^{(II)}H^-$	2.97	29
$L^{(II)}H_2 \rightleftharpoons 2 H^+ + L^{(II)2-}$	16.7	29

Table A.13. Continued

Equilibrium	$\log \beta$	References
$\text{UO}_2^{2+} + \text{L}^{(\text{II})2-} \rightleftharpoons \text{UO}_2 \text{L}^{(\text{II})}$	13.1	29
$\text{UO}_2^{2+} + 2 \text{L}^{(\text{II})2-} \rightleftharpoons \text{UO}_2 \text{L}_2^{(\text{II})2-}$	21.8	29
$\text{Cu}^{2+} + \text{L}^{(\text{II})2-} \rightleftharpoons \text{CuL}^{(\text{II})}$	10.60	29
$\text{Cu}^{2+} + 2 \text{L}^{(\text{II})2-} \rightleftharpoons \text{CuL}_2^{(\text{II})2-}$	18.45	29
$\text{Fe}^{3+} + \text{L}^{(\text{II})2-} \rightleftharpoons \text{FeL}^{(\text{II})+}$	28.25	29
$\text{Fe}^{3+} + 2 \text{L}^{(\text{II})2-} \rightleftharpoons \text{FeL}_2^{(\text{II})2-}$	11.90	29
$\text{L}^{(\text{III})}\text{H} \rightleftharpoons \text{H}^+ + \text{L}^{(\text{III})-}$	11.30	29
$\text{L}^{(\text{IV})}\text{H} \rightleftharpoons \text{H}^+ + \text{L}^{(\text{IV})-}$	10.0	29
$\text{UO}_2^{2+} + \text{L}^{(\text{IV})-} \rightleftharpoons \text{UO}_2 \text{L}^{(\text{IV})+}$	5.9	29
$\text{L}^{(\text{V})}\text{H} \rightleftharpoons \text{H}^+ + \text{L}^{(\text{V})-}$	4.20	29
$\text{UO}_2^{2+} + \text{L}^{(\text{V})-} \rightleftharpoons \text{UO}_2 \text{L}^{(\text{V})+}$	2.68	29
$\text{L}^{(\text{VI})}\text{H} \rightleftharpoons \text{H}^+ + \text{L}^{(\text{VI})-}$	12.36	46 ^a
$\text{UO}_2^{2+} + \text{L}^{(\text{VI})-} \rightleftharpoons \text{UO}_2 \text{L}^{(\text{VI})+}$	12.4	30
$\text{UO}_2^{2+} + 2 \text{L}^{(\text{VI})-} \rightleftharpoons \text{UO}_2 \text{L}_2^{(\text{VI})}$	22.3	30
$\text{L}^{(\text{VII})}\text{H} \rightleftharpoons \text{H}^+ + \text{L}^{(\text{VII})-}$	13.21	46 ^a
$\text{UO}_2^{2+} + \text{L}^{(\text{VII})-} \rightleftharpoons \text{UO}_2 \text{L}^{(\text{VII})+}$	13.6	30
$\text{UO}_2^{2+} + 2 \text{L}^{(\text{VII})-} \rightleftharpoons \text{UO}_2 \text{L}_2^{(\text{VII})}$	23.7	30
$\text{L}^{(\text{VIII})}\text{H}_2 \rightleftharpoons \text{H}^+ + \text{L}^{(\text{VIII})}\text{H}^-$	12.06	48 ^b
$\text{L}^{(\text{VIII})}\text{H}_2 \rightleftharpoons 2 \text{H}^+ + \text{L}^{(\text{VIII})2-}$	24.19	48 ^b
$\text{UO}_2^{2+} + \text{L}^{(\text{VIII})2-} \rightleftharpoons \text{UO}_2 \text{L}^{(\text{VIII})}$	17.3	48 ^b
$\text{UO}_2^{2+} + 2 \text{L}^{(\text{VIII})2-} \rightleftharpoons \text{UO}_2 \text{L}_2^{(\text{VIII})2-}$	26.1	48 ^b
$\text{L}^{(\text{IX})}\text{H}_2 \rightleftharpoons \text{H}^+ + \text{L}^{(\text{IX})}\text{H}^-$	10.70	47 ^b
$\text{L}^{(\text{IX})}\text{H}_2 \rightleftharpoons 2 \text{H}^+ + \text{L}^{(\text{IX})2-}$	22.76	47 ^b
$\text{UO}_2^{2+} + \text{L}^{(\text{IX})2-} \rightleftharpoons \text{UO}_2 \text{L}^{(\text{IX})}$	17.8	47 ^b
$\text{UO}_2 \text{L}^{(\text{IX})} + 2 \text{L}^{(\text{IX})2-} \rightleftharpoons \text{UO}_2 \text{L}_2^{(\text{IX})2-}$	27.5	47 ^b
$\text{Cu}^{2+} + \text{L}^{(\text{IX})2-} \rightleftharpoons \text{CuL}^{(\text{IX})}$	18.94	15 ^b

Table A.13. Continued

Equilibrium	log β	References
$\text{Cu}^{2+} + 2 \text{L}^{(\text{IX})2-} \rightleftharpoons \text{CuL}_2^{(\text{IX})2-}$	24.45	15 ^b
$\text{Fe}^{3+} + \text{HL}^{(\text{IX})-} \rightleftharpoons \text{Fe}(\text{HL}^{(\text{IX})})^{2+}$	25.66	15 ^b
$\text{Fe}^{3+} + \text{HL}^{(\text{IX})-} + \text{L}^{(\text{IX})2-} \rightleftharpoons \text{Fe}(\text{L}^{(\text{IX})})(\text{HL}^{(\text{IX})})$	43.94	15 ^b

^aIonic strength 0.3 M NaClO₄.^bIonic strength 0.5 M NaCl.**Table A.14.** Comparison of experimental, calculated, and predicted stability constant (log β) values for UO₂²⁺-ligand complexes.

Ligand	<i>exp log β^a</i>	<i>calc log β^b</i>	<i>pred log β^c</i>	<i>abs. error</i>
1 acetate	3.1	9.9	5.3	2.2
2 acetylacetonate	7.7	15.6	8.5	0.8
3 phenolate	8.8	18.4	10.1	1.3
4 OH ⁻	0	1.0	0.2	0.2
5 NO ₃ ⁻	0.5	-1.9	-1.4	1.9
6 ClO ₃ ⁻	3.3	6.3	3.2	0.1
7 H ₂ PO ₄ ⁻	13.6	24.3	13.4	0.2
8 acetamidoxime	12.4	22.1	12.2	0.2
9 benzamidoxime	23.7	41.2	23.1	0.6
10 2acetamidoxime	22.3	37.7	21.1	1.2
11 2benzamidoxime	11.3	23.4	12.9	1.6
12 glutarimidedioxime (HL ⁻)	6.4	13.6	7.4	1.0
13 oxalate	7.3	11.7	6.3	1.0
14 phthalate	5.6	9.4	5.0	0.6
15 salicylate	13.0	20.2	11.1	1.9
16 catecholate	16.8	24.7	13.7	3.1
17 glutarimidedioxime (L ²⁻)	19.1	35.2	19.6	0.5
18 CO ₃ ²⁻	9.7	17.5	9.6	0.1

Table A.14. Continued

Ligand	$\exp \log \beta^a$	$\text{calc} \log \beta^b$	$\text{pred} \log \beta^c$	abs. error
19 SO_4^{2-}	3.0	5.2	2.6	0.4
20 HPO_4^{2-}	7.2	14.7	8.0	0.8
21 phthalimidedioxime	16.8	25.5	14.1	2.7

^aCorrected to zero ionic strength with the Davies equation. ^bCalculated using the methodology described in ref 40. ^cPredicted from the correlation [$\text{pred} \log \beta = 0.5692 \times \text{calc} \log \beta$] shown in **Figure 5.1.2**.

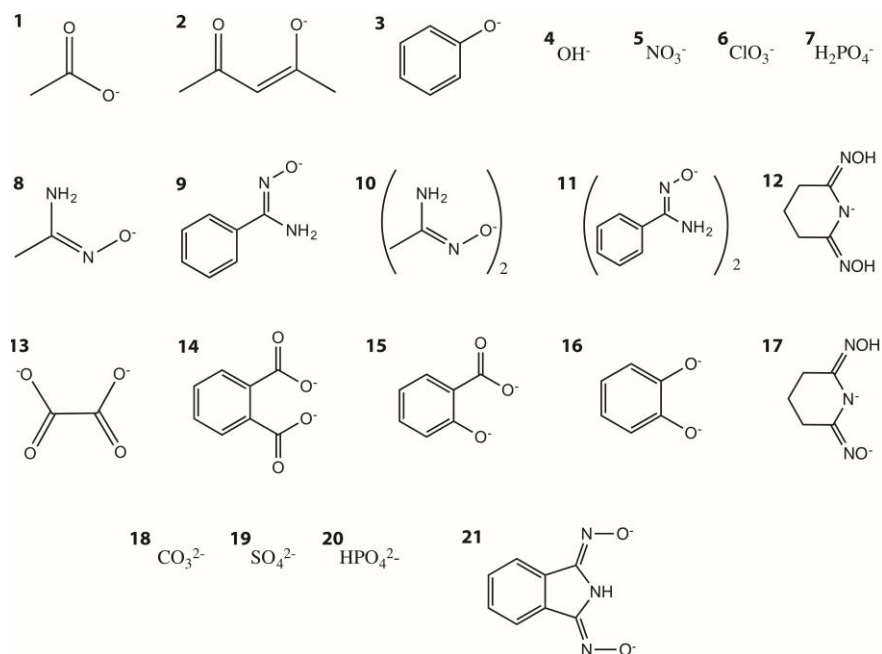


Table A.15. Full chemical formulas of the CSD crystal structures depicted in **Figures 5.1, A.11, and A.12** by CSD reference code.

Figure	Ref. Code	Chemical Formula
1	ACOXNI10	bis(2,2'-Imino-bis(Acetamidoxime)) copper(II) chloride
1	AICOCU10	bis(4-Aminoimidazole-5-carboxamidoxime) copper(II) perchlorate
1	YOHFEI	bis(Acetato-O)-bis(N'-hydroxypyridine-2-carboximidamide) cadmium(II) ethanol solvate
1	CUHJUK	Disodium bis(adenine-N ¹ -oxide) copper(II) octahydrate
1	ORUTIF	(N'-(oxy)-N-methylbenzenecarboximidamido)-(N-(oxy)-N'-methylbenzenecarboximidamide) oxo-technetium(IV)
1	CIMMIW	tris(N ¹ , N ² -dihydroxyethanediimidamide) nickel(II) ditetrafluoroborate
1	WOBHUS	Aqua-(N ¹ , N ² -dihydroxyethanediimidamide)-oxolato copper(II)
1	TEKYUD	bis(N-(2,6-Dimethylphenyl)aminoglyoximato-N,N') nickel(II)
1	RASBIW	Oxo-(2-thienylamidoximato-N,O)-(2-thienylamidoximato-N',O)-acetylacetonato molybdenum(VI)
1	FOWJAC	bis(Acetylacetonato-O,O')-(acetamidoximato-N,O)-nitrosyl molybdenum(VI)
S2	GIQBUE	bis(Triethylammonium) bis(m2-2-oxybenzoato)-bis(nitrato-O,O')-tetraoxo-di-uranium(VI)
S2	BIDVUF	bis(2-Amino-2-methyl-1-propanol)-copper(II) bis(salicylato)-copper(II) 2-propanol solvate
S2	PIMSUB	bis(Oxonium) chloride diaqua-bis(2-oxy-5-nitrobenzoato) iron(III)
S2	TEVWAU	dioxo-bis(2,6-bis(N-oxidoiminio)piperidinato) uranium(VI) monohydrate
S2	Ref. 15	Glutarimidedioxime iron(III) dichloride
S3	BOCCOL	tetrakis((μ ₃ -Salicylidenealdoximato)-(salicylidenealdoxime) iron(III)) salicylidenealdoxime xylene solvate
S3	CSALCU	bis(5-Chlorosalicylaldoximato) copper(II)

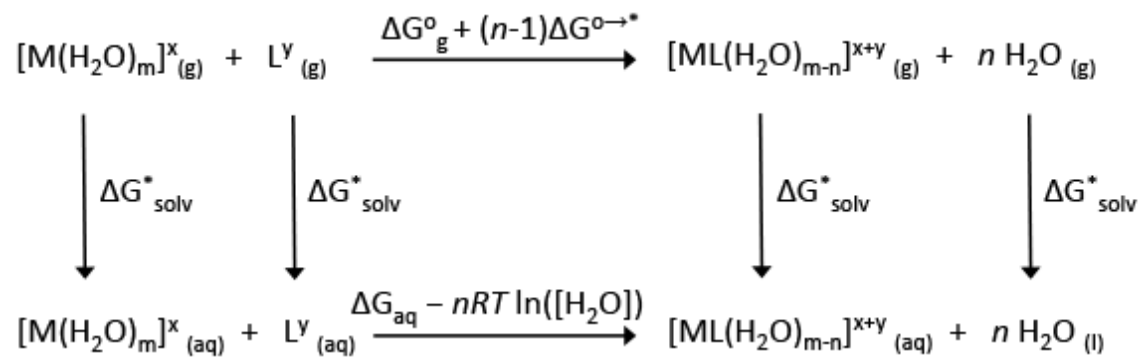


Figure A.7. Thermodynamic cycle used to calculate $\Delta\Delta G_{aq}$.

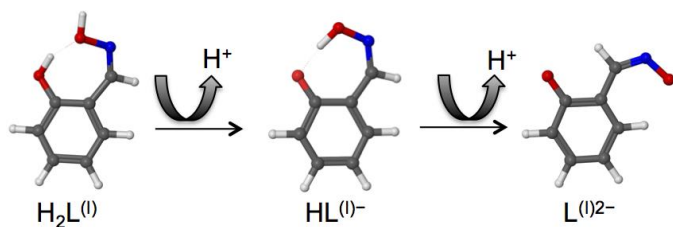


Figure A.8. Stepwise dissociation of salicylaldoxime used to fit UV/Vis titration data. Color legend: red represents oxygen, blue represents nitrogen, grey represents carbon, and white represents hydrogen.

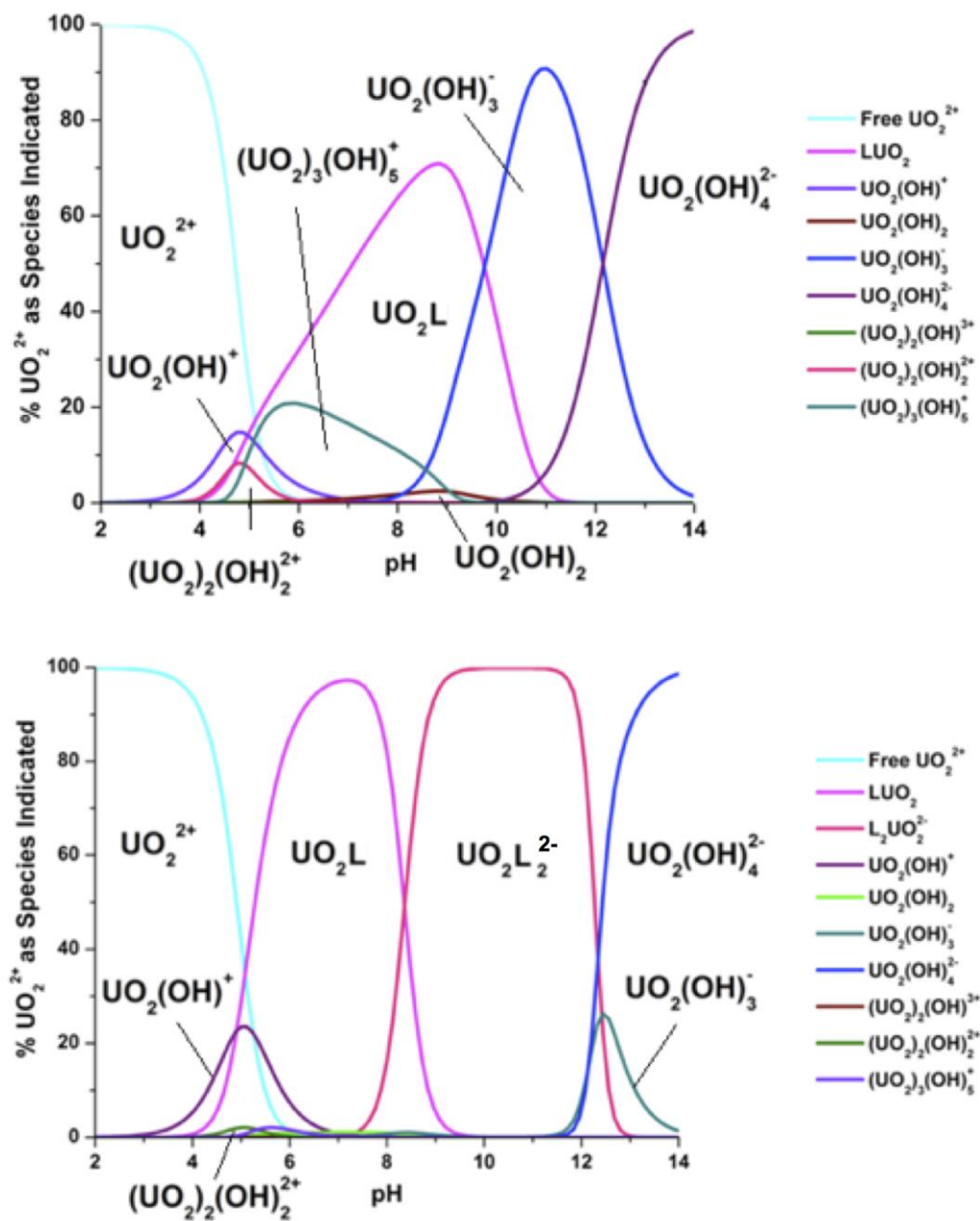


Figure A.9. Species distribution diagrams of the 1:1 (*top*) and the 10:1 (*bottom*) salicylaldoxime to uranyl titration solutions as a function of pH. Distribution diagrams were generated with the HYSS⁵² software using the uranyl hydrolysis constants in ref. 51 and the uranyl-salicylaldoxime formation constants from this work.

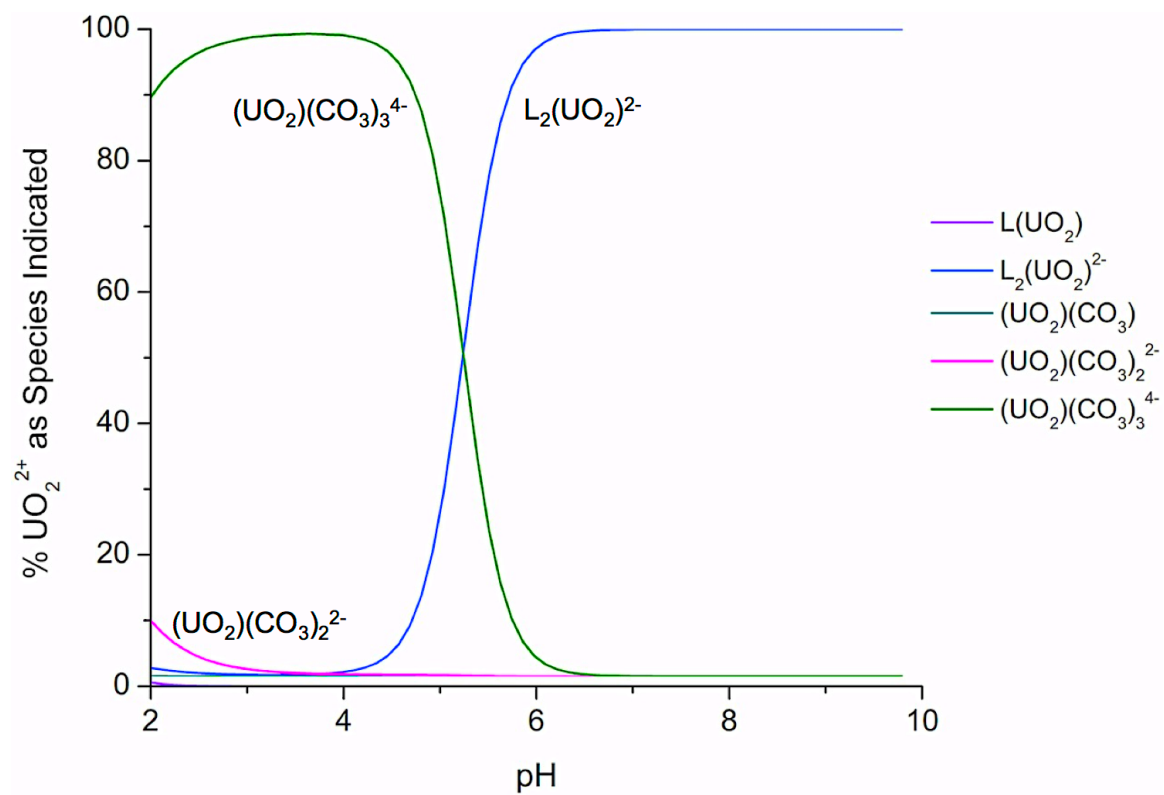


Figure A.10. Species distribution diagrams of 0.001 M salicylaldoxime, 1.3×10^{-8} M uranyl, and 0.0025 M carbonate calculated using the HYSS⁵² software. The uranyl carbonate constants were taken from ref. 53 and the uranyl-salicylaldoxime formation constants from this work.

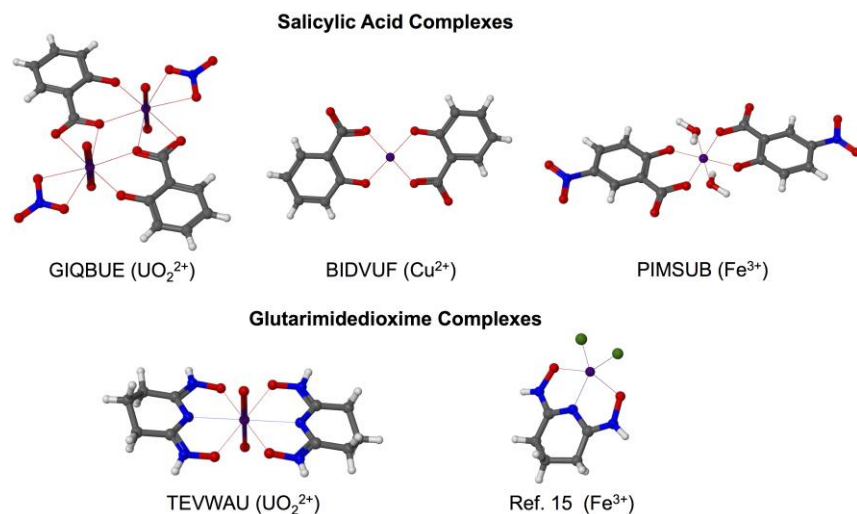


Figure A.11. Crystal structures of salicylic acid and glutarimidedioxime complexes. GIQBUE⁵⁹ ($\text{C}_{30}\text{H}_{32}\text{Cu}_2\text{N}_4\text{O}_{10} \cdot 2(\text{H}_3\text{BO}_3 \cdot 4(\text{H}_2\text{O}))$): phenolate- UO_2^{2+} bond = 2.23(1) Å and carboxylate- UO_2^{2+} bond = 2.42(1) Å. BIDVUF⁶⁰ ($\text{C}_{14}\text{H}_8\text{CuO}_6^{2-} \cdot \text{C}_8\text{H}_{22}\text{CuN}_2\text{O}_2^{2+} \cdot 4(\text{C}_3\text{H}_8\text{O})$): phenolate- Cu^{2+} bond = 1.900 Å and carboxylate- Cu^{2+} bond = 1.903 Å. PIMSUB⁶¹ ($\text{C}_{14}\text{H}_{10}\text{FeN}_2\text{O}_{12}^- \cdot 2(\text{H}_3\text{O}^+) \cdot \text{Cl}^-$): phenolate- Fe^{3+} bond = 1.973 Å and carboxylate- Fe^{3+} bond = 1.944 Å. TEVWAU⁴⁹ ($\text{C}_{10}\text{H}_{16}\text{N}_6\text{O}_6\text{U} \cdot \text{H}_2\text{O}$): oximate- UO_2^{2+} bond 1 = 2.430 Å, oximate- UO_2^{2+} bond 2 = 2.535 Å, and piperidine- UO_2^{2+} bond = 2.563 Å. Ref. 15 ($\text{C}_{10}\text{H}_{16}\text{N}_6\text{O}_6\text{FeCl}_2^+$): oximate- UO_2^{2+} bond 1 = 2.019(7) Å, oximate- UO_2^{2+} bond 1 = 2.027(7) Å, and piperidine- UO_2^{2+} bond = 2.009(8) Å. Color legend: O, red; N, blue; C, grey; H, white; S, yellow; metal ion, purple.

Salicylaldoxime Complexes

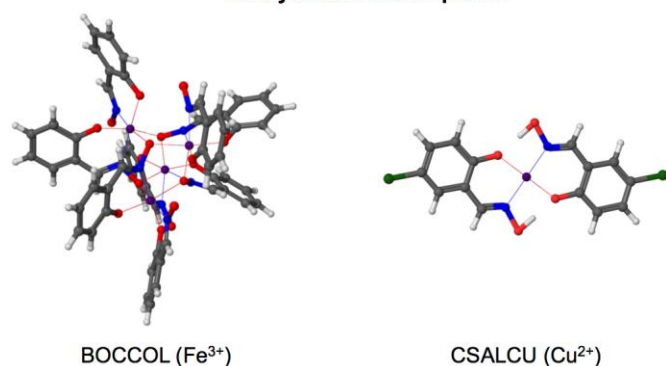


Figure A.12. Crystal structures of salicylaldoxime- Fe^{3+} and $-\text{Cu}^{2+}$ complexes. BOCCOL⁶⁵ ($\text{C}_{56}\text{H}_{44}\text{Fe}_4\text{N}_8\text{O}_{16} \cdot \text{C}_7\text{H}_7\text{NO}_2 \cdot \text{C}_8\text{H}_{10} \cdot \text{C}_8\text{H}_{10}$): phenolate- Fe^{3+} bond = 1.889(8) Å and oximate- Fe^{3+} bond = 2.14(1) Å. CSALCU⁶⁴ ($\text{C}_{14}\text{H}_{10}\text{Cl}_2\text{CuN}_2\text{O}_4$): phenolate- Cu^{2+} bond = 1.9082 Å and oximate- Cu^{2+} bond = 1.9579 Å. Color legend: O, red; N, blue; C, grey; H, white; S, yellow; metal ion, purple.

Optimized Geometries of Salicylaldoxime Ligands, UO_2^{2+} , and Cu^{2+} Complexes Discussed in the Main Text and Their Total Energies at the M06/SSC/6-311++G** Level of Theory

Salicylaldoxime:

1) $\text{H}_2\text{L}^{(1)}$; Total Energy: - 475.9163087 Hartrees

Symmetry C_1

N	2.457273000	-1.030157000	0.023359000
C	1.246482000	-1.286549000	-0.286277000
C	-2.594349000	0.507900000	0.118076000
C	-2.420764000	-0.872432000	0.183089000
C	-1.150571000	-1.389886000	0.047146000
C	-0.022129000	-0.572103000	-0.122601000
C	-0.217849000	0.820702000	-0.197748000
C	-1.509067000	1.337221000	-0.074011000
H	-3.586918000	0.938229000	0.210625000

H	-3.269822000	-1.531693000	0.326187000
H	-1.001650000	-2.466701000	0.077200000
O	0.752779000	1.709894000	-0.453666000
H	-1.622779000	2.414158000	-0.143087000
O	2.606182000	0.207013000	0.664980000
H	1.162998000	-2.279580000	-0.730274000
H	3.549636000	0.252571000	0.848890000
H	1.613867000	1.351606000	-0.174843000

2) HL⁽¹⁾⁻; Total Energy: -475.376987 Hartrees

Symmetry C₁

N	2.464990000	-0.948622000	0.070220000
C	1.238101000	-1.255691000	-0.158932000
C	-2.645004000	0.495463000	0.073156000
C	-2.469543000	-0.892308000	0.104222000
C	-1.178271000	-1.383386000	0.016686000
C	-0.050342000	-0.560425000	-0.082050000
C	-0.219194000	0.869909000	-0.156224000
C	-1.565277000	1.340329000	-0.046852000
H	-3.648537000	0.915267000	0.137965000
H	-3.318565000	-1.564566000	0.189052000
H	-1.016838000	-2.462218000	0.032265000
O	0.744772000	1.679510000	-0.332066000
H	-1.698748000	2.419161000	-0.089150000
O	2.764083000	0.319869000	0.485292000
H	1.149906000	-2.312491000	-0.432036000
H	2.022018000	0.943274000	0.197891000

3) L⁽¹⁾²⁻; Total Energy: -474.658113 Hartrees

Symmetry C₁

N	1.622994000	-2.512728000	-0.155315000
C	1.203245000	-1.263496000	-0.161247000
C	-2.682090000	0.535910000	0.057551000
C	-2.573980000	-0.851588000	0.078304000
C	-1.298495000	-1.429761000	0.005822000
C	-0.125178000	-0.674239000	-0.087036000
C	-0.213452000	0.792587000	-0.112849000
C	-1.542199000	1.326410000	-0.034267000
H	-3.666768000	1.011513000	0.113376000
H	-3.461656000	-1.481496000	0.150637000
H	-1.162631000	-2.507947000	0.020552000
O	0.798465000	1.552335000	-0.197643000
H	-1.619989000	2.415834000	-0.052217000
O	0.761835000	-3.494371000	-0.070777000
H	2.012689000	-0.537448000	-0.234415000

Uranyl Complexes with Salicylaldoxime:

1) [UO₂(HL^(O))(H₂O)₃]⁺; Total Energy: -1331.951756 Hartrees

Symmetry C₁

N	1.620771000	1.495598000	1.914273000
C	0.398930000	1.205690000	1.611566000
C	-1.110834000	-2.570435000	0.547856000
C	-1.924970000	-1.438528000	0.464480000
C	-1.399042000	-0.213799000	0.801037000
C	-0.056005000	-0.084763000	1.198792000
C	0.768383000	-1.239713000	1.271542000

C	0.206265000	-2.478752000	0.952691000
H	-1.519852000	-3.543690000	0.294532000
H	-2.958565000	-1.527251000	0.151622000
H	-2.020056000	0.677526000	0.763106000
O	2.021806000	-1.148893000	1.658024000
H	0.830669000	-3.362957000	1.025457000
O	1.763847000	2.841490000	2.339092000
U	3.735671000	0.204816000	1.409351000
O	4.142083000	0.451781000	3.091157000
O	3.515355000	0.107103000	-0.318795000
O	4.089110000	2.677959000	0.993729000
H	3.371993000	3.169314000	1.440093000
H	4.194959000	3.052327000	0.113961000
O	4.700672000	-2.155052000	1.554024000
H	4.015820000	-2.828691000	1.635535000
H	5.482308000	-2.475505000	2.013669000
H	-0.342171000	2.004006000	1.704791000
H	1.875786000	2.794633000	3.299725000
O	6.245778000	0.409819000	0.947830000
H	6.680021000	0.278296000	0.098556000
H	6.882899000	0.823674000	1.539662000

2) [UO₂(HL^(O))₂(H₂O)]; Total Energy: -1654.6585449 Hartrees

Symmetry C₁

N	-1.149985000	1.238379000	0.668627000
C	-2.334548000	1.714920000	0.545601000
H	-2.466642000	2.768579000	0.808107000
C	-5.859978000	-0.221589000	-0.757961000

C	-5.877839000	1.130234000	-0.416689000
C	-4.705918000	1.724127000	0.004935000
C	-3.507487000	1.004196000	0.096161000
C	-3.495660000	-0.371890000	-0.247708000
C	-4.695482000	-0.958908000	-0.675514000
H	-6.773179000	-0.705002000	-1.093892000
H	-6.794905000	1.705211000	-0.481468000
H	-4.697497000	2.777735000	0.275456000
O	-2.401183000	-1.076829000	-0.165699000
H	-4.676259000	-2.011211000	-0.941438000
O	-0.254557000	2.176931000	1.136003000
U	-0.217138000	-1.135117000	0.253976000
O	-0.497203000	-1.558171000	1.937894000
O	0.180649000	-0.812511000	-1.419824000
O	1.611825000	0.229001000	0.752901000
N	1.973456000	-2.484599000	0.602892000
O	1.875116000	-3.852016000	0.968716000
C	3.173676000	-2.156769000	0.281363000
C	3.588499000	-0.828349000	-0.067667000
C	2.792424000	0.320880000	0.210618000
C	3.348934000	1.579552000	-0.085178000
C	4.603112000	1.695635000	-0.641466000
C	5.384665000	0.567487000	-0.911872000
C	4.876342000	-0.673129000	-0.610153000
H	3.934599000	-2.942585000	0.298251000
H	5.470106000	-1.565553000	-0.795495000
H	6.374258000	0.671376000	-1.342117000
H	4.991673000	2.684341000	-0.869127000

H	2.749634000	2.460487000	0.126639000
H	0.596974000	1.692400000	1.135841000
H	1.488634000	-3.814272000	1.854991000
O	-0.501032000	-3.606141000	-0.416615000
H	-1.335878000	-4.073646000	-0.340278000
H	0.213532000	-4.166145000	-0.072927000

3) $[\text{UO}_2(\text{L}^{(1)})(\text{H}_2\text{O})_2]$; Total Energy: -1255.1180818 Hartrees

Symmetry C_1

N	1.418780000	1.472192000	0.833286000
C	0.198387000	1.387873000	0.462221000
H	-0.455528000	2.262199000	0.498521000
C	-1.353103000	-2.297229000	-0.934728000
C	-2.169511000	-1.170077000	-0.875476000
C	-1.631999000	0.015328000	-0.413942000
C	-0.297377000	0.111719000	-0.007974000
C	0.541085000	-1.041055000	-0.068256000
C	-0.030358000	-2.233106000	-0.540310000
H	-1.756513000	-3.239741000	-1.294653000
H	-3.207756000	-1.221112000	-1.185086000
H	-2.251608000	0.908265000	-0.359302000
O	1.802747000	-1.026433000	0.293746000
H	0.609186000	-3.109821000	-0.585268000
O	2.129057000	2.464426000	1.286400000
U	3.369900000	0.386249000	1.102404000
O	3.053655000	-0.041416000	2.785887000
O	3.983463000	0.798953000	-0.501098000
O	4.722505000	-1.812573000	0.942540000

O	4.919492000	2.260433000	1.997405000
H	4.732408000	-2.170098000	0.048520000
H	4.357762000	-2.501357000	1.507951000
H	4.927724000	2.945786000	1.319582000
H	4.446802000	2.648697000	2.742830000

4) $[\text{UO}_2(\text{L}^{(1)})_2]^{2-}$; Total Energy: -1577.0735695 Hartrees

Symmetry C_1

N	0.921845000	1.089174000	0.748487000
C	-0.165602000	1.193887000	0.075684000
H	-0.630633000	2.179567000	-0.058286000
C	-2.072829000	-2.174767000	-1.684633000
C	-2.623279000	-0.901199000	-1.830513000
C	-1.961649000	0.166994000	-1.236211000
C	-0.781532000	0.017881000	-0.508050000
C	-0.196488000	-1.295744000	-0.348818000
C	-0.903964000	-2.362012000	-0.970246000
H	-2.566363000	-3.034986000	-2.137565000
H	-3.541832000	-0.745414000	-2.391346000
H	-2.370512000	1.174540000	-1.333878000
O	0.880241000	-1.530032000	0.297281000
H	-0.470601000	-3.352953000	-0.854069000
O	1.595177000	2.024576000	1.327738000
U	2.605789000	-0.343148000	1.572982000
O	1.674088000	-0.589665000	3.061122000
O	3.537493000	-0.096644000	0.084837000
O	4.331331000	0.843759000	2.848649000
N	4.289715000	-1.775457000	2.397556000

O	3.616402000	-2.710862000	1.818285000
C	5.377108000	-1.880170000	3.070445000
C	5.993005000	-0.704152000	3.654190000
C	5.407984000	0.609474000	3.494873000
C	6.115434000	1.675757000	4.116306000
C	7.284236000	1.488522000	4.830799000
C	7.834656000	0.214952000	4.976774000
C	7.173059000	-0.853253000	4.382455000
H	5.842119000	-2.865851000	3.204481000
H	7.581901000	-1.860801000	4.480193000
H	8.753157000	0.059175000	5.537692000
H	7.777745000	2.348753000	5.283735000
H	5.682100000	2.666701000	4.000051000

Copper Complexes with Salicylaldoxime:

1) $[\text{Cu}(\text{HL})^{\text{(I)}}(\text{H}_2\text{O})_2]^+$; Total Energy: -825.3637068 Hartrees

Symmetry C_1

N	1.880590000	1.162398000	0.904042000
C	0.595168000	1.032131000	0.740641000
H	-0.024435000	1.857073000	1.098865000
C	-1.407019000	-2.092587000	-1.199477000
C	-2.115025000	-0.965400000	-0.751902000
C	-1.434135000	0.029272000	-0.107746000
C	-0.038379000	-0.063077000	0.115029000
C	0.670525000	-1.223598000	-0.320828000
C	-0.053239000	-2.219660000	-0.999404000
H	-1.939274000	-2.886097000	-1.715324000

H	-3.182217000	-0.886092000	-0.920674000
H	-1.955997000	0.917284000	0.238757000
O	1.942715000	-1.418325000	-0.106210000
H	0.488004000	-3.095914000	-1.338804000
O	2.264199000	2.294539000	1.638183000
Cu	3.140939000	-0.265296000	0.736189000
O	4.513070000	-1.707036000	0.368959000
H	5.377328000	-1.577982000	-0.035527000
H	4.057124000	-2.414428000	-0.107803000
O	4.444879000	0.700484000	1.930760000
H	3.995233000	1.464498000	2.329547000
H	4.978203000	0.259150000	2.600304000
H	2.496741000	2.969365000	0.983666000

2) [Cu(HL⁽¹⁾)₂]; Total Energy: -1148.103999 Hartrees

Symmetry C_{2h}

N	0.819874000	1.773927000	0.000000000
C	2.074882000	2.045812000	0.000000000
H	2.346880000	3.103966000	0.000000000
C	5.306615000	-0.664251000	0.000000000
C	5.535332000	0.714568000	0.000000000
C	4.451775000	1.561168000	0.000000000
C	3.131887000	1.075882000	0.000000000
C	2.900928000	-0.326043000	0.000000000
C	4.026435000	-1.171130000	0.000000000
H	6.149213000	-1.350080000	0.000000000
H	6.545352000	1.108635000	0.000000000
H	4.602363000	2.638464000	0.000000000

O	1.709229000	-0.862301000	0.000000000
H	3.849064000	-2.242279000	0.000000000
O	-0.004559000	2.864272000	0.000000000
Cu	0.000000000	0.000000000	0.000000000
O	-1.709229000	0.862301000	0.000000000
N	-0.819874000	-1.773927000	0.000000000
O	0.004559000	-2.864272000	0.000000000
C	-2.074882000	-2.045812000	0.000000000
C	-3.131887000	-1.075882000	0.000000000
C	-2.900928000	0.326043000	0.000000000
C	-4.026435000	1.171130000	0.000000000
C	-5.306615000	0.664251000	0.000000000
C	-5.535332000	-0.714568000	0.000000000
C	-4.451775000	-1.561168000	0.000000000
H	-2.346880000	-3.103966000	0.000000000
H	-4.602363000	-2.638464000	0.000000000
H	-6.545352000	-1.108635000	0.000000000
H	-6.149213000	1.350080000	0.000000000
H	-3.849064000	2.242279000	0.000000000
H	-0.897451000	2.455605000	0.000000000
H	0.897451000	-2.455605000	0.000000000

Vita

Nada Mehio was born in 1991 in New Jersey to Mrs. Rola Mehio and Dr. Mohamad Mehio. She grew up in Naperville, IL and graduated from Neuqua Valley High School in 2009. She subsequently attended Loyola University Chicago and graduated in December 2011 with a Bachelors of Science in Molecular Biology and a minor in Chemistry. After graduating from LUC, Nada enrolled in advanced courses at the University of Illinois at Chicago from January 2012 to May 2012. Subsequently, she joined the University of Tennessee-Knoxville's Chemistry PhD program in August 2012. During her time in the PhD program, Nada authored six peer-reviewed papers and two book chapters, co-authored seven peer-reviewed papers, and attended two national ACS conferences.